**Formation and Passivation of Sub-Nanoliter Droplets for High Throughput Biological Assay Platforms**

by

Cheryl Janay DeJournette

A dissertation submitted to the Graduate Faculty of
Auburn University
in partial fulfillment of the
requirements for the Degree of
Doctor of Philosophy

Auburn, Alabama
August 2, 2014

Keywords: emulsion PCR, droplet microfluidics, aptamer selection, bead, digital detection, surfactant



Approved by

Christopher J. Easley, Knowles Associate Professor of Chemistry & Biochemistry
Vince Cammarata, Associate Professor of Chemistry & Biochemistry and Associate Chairman
Curtis Shannon, Andrew T. Hunt Professor of Chemistry & Biochemistry
Wei Zhan, Associate Professor of Chemistry & Biochemistry

Abstract

In Vitro Compartmentalization (IVC) is a technique that utilizes water-in-oil emulsion droplets of fL – nL volume to compartmentalize and perform biological reactions and assays in parallel. At its highest capacity it has the capability to create $>10^{10}$ droplets in just 1 mL of sample volume, meaning that $10^{10}$ reactions can be performed in a single microcentrifuge tube. This saves time and material cost in comparison to conventional microtiter plate techniques. This has made IVC ideal for use in a variety of areas requiring analysis of large libraries of samples, including directed evolution of proteins and RNAs, amplification of complex gene libraries using PCR, and screening of large libraries for rare mutations. Our research focuses on the use of IVC to perform assays within droplets generated by microfluidics. Biocompatible surfactants must be developed alongside droplet generation techniques in order to ensure droplet stability and optimal assay performance. When combined, the chapters presented in this work provide a platform for the formation and passivation of sub-nanoliter droplets for the performance of several high-throughput biological assays. Chapter 1 provides information on the principles of IVC, droplet microfluidics, surfactants, and PCR amplification. In Chapter 2, we introduce two passively-controlled emulsion generator devices for rapid formation of monodisperse emulsion droplet populations. Single-channel and multi-channel emulsion generators are operated using only a handheld, glass syringe to pull a vacuum at the outlet of each microfluidic device. In addition, wide-field and single-droplet imaging techniques are introduced for obtaining data from emulsion droplets. Chapter 3 details a technique for the formation of a biocompatible surfactant without synthesis, exploiting the direct interaction between commercially-available primary

amines and carboxylated perfluorocarbon surfactants. This interaction was confirmed using the analytical techniques of FT-IR, Mass Spectrometry, and NMR, as well as with qualitative observations of emulsion formation under various physical and chemical stressors. Droplets formed using this surfactant were tested for assay biocompatibility with DNA amplification using both PCR and RPA, and with a novel proximity FRET assay for the detection of insulin. These results showed that the interaction is sufficient for performance of these assays in emulsion droplets, and compares well in efficiency to other synthesized surfactants. Chapter 4 discusses the use of bead-based assays as complements to droplet compartmentalization. Micro-beads modified with DNA have been used by other researchers to capture and detect various targets, including cancerous cells in the blood, DNA for sequencing, and for aptamer selection. PCR is often used to amplify DNA onto the surface, and the beads can be rapidly analyzed and sorted into discrete populations using FACS technology. Compartmentalizing beads into emulsion droplets ensures parallel and efficient amplification of a single DNA sequence onto a single bead, forming clonal bead populations. We have developed several methods for attachment of DNA to micro-beads and successfully amplified them using PCR to cover the beads with many copies of a single DNA sequence. Finally, Chapter 5 provides conclusions and future applications for this work, including a high-throughput aptamer selection method using beads and droplet microfluidics, surface-based proximity assays that exploit the surfactant interactions discussed in chapter 3, and multi-islet secretion measurements using the pFRET assay in droplets and previously-developed microfluidic techniques for measuring murine pancreatic islet secretions.

Acknowledgments

I would first like to thank my research advisor and principal investigator Dr. Christopher Easley for allowing me to work in your lab during my graduate career. You have challenged me and pushed me to accomplish goals I never thought were possible. Your enthusiasm and determination have inspired me and helped me to recognize and cultivate qualities within myself that I can carry with me for the rest of my life, and for that I am grateful. Next, I would like to thank Dr. Vince Cammarata, Dr. Curtis Shannon, and Dr. Wei Zhan for serving as my advisory committee. Thank you for giving of your time and expertise in helping me to complete my research projects. Also, thank you to Dr. Leonardo De La Fuente for agreeing to serve as the University Reader in the completion of this dissertation. Next, I would like to thank Michael Meadows, Yonnie Wu, Krishan Raghuveer, Allison Bird, and Dr. Curtis Bird for their training and assistance in the areas of NMR, mass spectrometry, FT-IR, and flow cytometry, respectively, which were essential to this work. Many thanks also go to the current and former members of the Easley research group. I have learned a tremendous amount of information from you all, received encouragement, and even shared a few laughs. Good luck to all of you in your current and future endeavors and War Eagle! Last but certainly not least, I must thank my family and friends. Thank you for your constant support, prayers, and guidance throughout this journey, without which none of this would be possible.

Table of Contents

List of Figures

List of Abbreviations

| | |
|---|---|
| *E. coli* | *Escherichia coli* |
| IVC | In Vitro Compartmentalization |
| FACS | Fluorescence-activated Cell Sorting |
| PCR | Polymerase Chain Reaction |
| GSIS | Glucose-stimulated Insulin Secretion |
| DOD | Department of Defense |
| PDMS | Polydimethylsiloxane |
| IFT | Interfacial Tension |
| CMC | Critical Micelle Concentration |
| PEG | Polyethylene Glycol |
| PFPE | Perfluoropolyether |
| dNTP | Deoxynucleotide Triphosphate |
| qPCR | Real-time PCR |
| ddPCR | Droplet Digital PCR |
| SVM | Syringe-vacuum Microfluidics |
| PBS | Phosphate Buffered Saline |
| PMT | Photomultiplier Tube |
| RPA | Recombinase Polymerase Amplification |
| ROI | Region of Interest |

| | |
|---|---|
| PED | Polyetherdiamine |
| ESI-MS | Electrospray Ionization-Mass Spectrometry |
| EDTA | Ethylenediaminetetraacetic Acid |
| HEPES | 4-(2-hydroxyethyl)piperazine-1-ethanesulfonic acid |
| IDT | Integrated DNA Technologies |
| FT-IR | Fourier Transform Infrared Spectroscopy |
| D.I. | Deionized |
| pFRET | Proximity Förster Resonance Energy Transfer |
| NC | Negative Control |
| PEA | Polyetheramine |
| $C_t$ | Threshold Cycle |
| PC | Positive Control |
| EDC | 1-ethyl-3-[3-dimethylaminopropyl]carbodiimide |
| DIPEA | N,N-Diisopropylethylamine |
| DMAP | 4-dimethylaminopyridine |
| Cu-TBTA | Copper (II) - Tris(benzyltriazolylmethyl)amine |
| NHS | N-hydroxysuccinimide |
| ss | Single-stranded |
| ds | Double-stranded |
| DIPEA | 1% N,N-Diisopropylethylamine |
| CuAAC | Huisgen copper(I)-catalyzed azide-alkyne 1,3-dipolar cycloaddition |
| $T_M$ | Melting Temperature |
| $K_d$ | Dissociation Constant |

| | |
|---|---|
| PPG | Polypropylene Glycol |
| ECPA | Electrochemical Proximity Assay |
| ELISA | Enzyme-linked Immunosorbent Assay |

# CHAPTER 1

# INTRODUCTION

## 1.1 Miniaturization of Laboratory Techniques

### 1.1.1 A Brief History

Miniaturization has often been viewed as an indicator of scientific progress. No area paints a truer picture of this observation than the field of microelectronics. In recent history, the miniaturization of electronic devices has exploded more rapidly than ever before. Richard Feynman opened the eyes of many to this possibility when he discussed how virtually limitless miniaturization could be in his well-known 1959 talk at Caltech, "There's Plenty of Room at the Bottom". Based on the laws of physics it could be possible in principle, he stated, to "write all 24 volumes of the Encyclopedia Britannica on the head of a pin" [1]. In the April 1965 issue of *Electronics* magazine, the director of R&D Laboratories at Fairchild Semiconductor, and later President and CEO of Intel, Gordon E. Moore, made a prediction that "by 1975 it would be possible to cram as many as 65,000 components onto a single silicon chip about 6 millimeters square" [2]. Based on past trends and future projections on production advancements, mainly the creation of larger chips with finer dimensions to use more of the total space available, he speculated that the density and performance of integrated circuits would double yearly. In 1975 he amended this to every 18 months. His prediction, now dubbed "Moore's Law," held true for nearly 40 years [2-4]. Since its development, through the end of the last century, microelectronics has followed Moore's Law and doubled integration density every 18 months [4].

Biology and chemistry have also made advancements toward miniaturization. Although the development has been much slower than the microelectronics industry, they have gone from using milliliter-volume test tubes, to using microliter-volume centrifuge tubes and microtiter plates, and even smaller microarrays and bead-based assays. Figure 1.1 illustrates this reduction in assay volume. With these advancements came increased experimental throughput and cost effectiveness due to the smaller sample volumes required and faster analysis times [5]. One example of this is seen in the use of DNA microarray technology, which allows researchers to study the gene expression and genetic variation of thousands of cells at one time by robotically arranging the DNA sequences encoding each gene onto a single glass slide [6-8]. Samples can then simply be mixed with each spot, and a fluorescent readout provides quantitative measurements of gene expression for that particular sample. Multiple samples can even be analyzed at one time, provided they have different fluorescent probes, making this technique attractive for use in complex matrices [6].This is helpful when studying the human genome, which contains 20,000 – 30,000 different genes [9], as well as the genomes of other complex eukaryotes and bacterial species [6]. Understanding and measuring individual gene expression can provide insight into evolution, predict disease, and help diagnose certain hereditary genomic disorders [9]. Microarrays have provided a method to analyze samples quickly, but as we will discuss in the next section of this chapter, they do have spatial limitations that limit the number of samples that can be analyzed at one time; this has led to even greater advancements in miniaturization through the use of water-in-oil emulsion droplets, often coupled with droplet microfluidics, to perform biological assays.

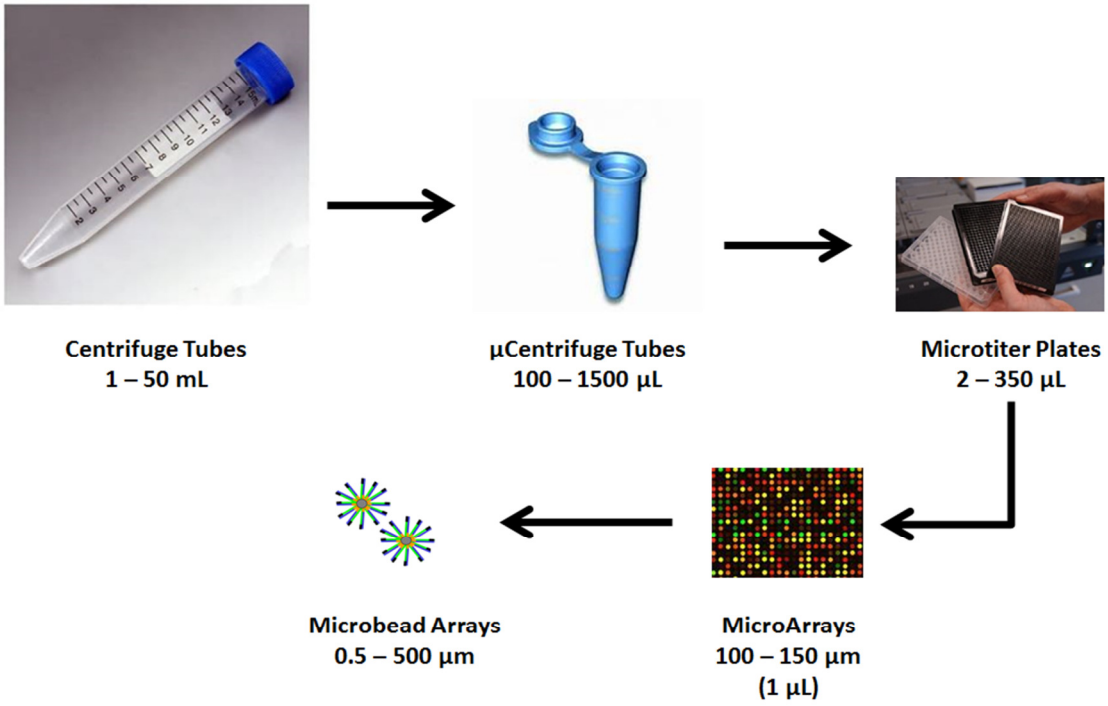


**Figure 1.1** Miniaturization of laboratory techniques in chemistry and biology. Assays have gone from being performed in centrifuge tubes of 1-50 mL volume, down to Micro Arrays, which can require as little as 1 µL of sample.

Figures were compiled into this illustration from the following sources: http://www.katsci.com/products/15ml-centrifuge-tube-non-sterile-polypropylene-pp.aspx ; http://astralscientific.com.au/1-5ml-graduated-microcentrifuge-tube-with-attached-flat-cap-natural-500-per-bag.html ; http://en.wikipedia.org/wiki/Microtiter_plate; and http://www.agilent.com/labs/features/2011_101_microarray.pdf.

### 1.1.2 Limitations of Conventional Techniques

As mentioned previously, there are limitations to microarrays when analyzing large numbers of reactions in the "study of biological and macromolecular systems" [10]. For example, scientists who work on the human genome, which has approximately 30,000 genes in it, could have to analyze up to 30,000 × 30,000 ($10^9$) different combinations in order to find any two proteins, or proteins and nucleic acids that work together to perform a cellular process. Another limitation is in the area of designing and creating new molecules. These could be novel proteins, drug compounds, or nucleic acids, to name a few. When thinking of all of the variations a protein has, one realizes that a polypeptide chain could contain thousands of amino acids, which could be any of 20 different molecules [11]. This does not include man-made variations of these amino acids or post-translationally modified versions. If a protein has, for example, 100 amino acids, it could have ~$20^{100}$ different sequences. This is approximately $10^{130}$ different variations that must be selected and analyzed for the desired properties/effects [5, 10].

Analyzing organic compounds for drug design or even designing novel nucleic acid sequences, though less complex than the protein, would still present a similar problem. A library of "drug-like" molecules (less than 500 Da) could contain $10^{60}$ different molecules [10, 12]. Current advancements in technology allow for the analysis of 100,000 compounds per day using robotics for lab automation [13-14], but any further increase in throughput is limited by the evaporation that is likely to occur with sample volume reduction [15]. For example, high throughput robotic systems remain insufficient for aptamer selection, which involves screening ligand-binding members from a large oligonucleotide library of $10^{12} – 10^{15}$ different sequences [16]. These sequences are often made synthetically by changing the order of nucleotides and the length of the resulting DNA or RNA chains. When coupled with chemically- modified

nucleotides that many research groups are incorporating now [17-18], the number of possible combinations to achieve desired binding effects is virtually endless. Improvements in selection methods for aptamer selection will be discussed in future sections of this work, as it is a major goal of the research presented herein. A typical microtiter plate setup can only feasibly handle $10^6 – 10^7$ reactions [5]. Under the aforementioned scenarios, there is a need for quick and efficient analyses of all possible aptamer variations that is unmet by conventional techniques. .

### 1.1.3 Emulsion Droplets as Miniature Reaction Compartments

When we observe biological reactions in nature, we find that most of the processes take place in the cell. Plant and animal cells are even further divided into organelles and compartments where separate processes take place simultaneously. Simpler cells, like bacteria, may not have as many organelles, but they usually exist as individual cells and contain a nucleoid and thousands of ribosomes, which are the sites for protein synthesis from RNA. For example, *Escherichia coli* (*E. coli*), the most studied bacterium, is about 2 µm long, has a diameter of less than 1 µm, and can have more than $10^8$ cells in just 1 mL of cell culture [11]. *E. coli* has about 15,000 ribosomes in the cytoplasm. This means any given culture can have more than $10^8$ cells of fL-volume, performing 15,000 independent reactions in parallel. Furthermore, each cell behaves as its own compartment, preventing crosstalk or interference from surrounding cells [5, 11].

Andrew Griffiths realized that harnessing this power for the laboratory setting could allow the performance of the larger, more complex assays mentioned above [5], so he developed In Vitro Compartmentalization (IVC) in 1998 [19]. Inspired by the cellular compartmentalization observed in plant and animal cells, IVC has the capability to perform $>10^{10}$ reactions

simultaneously in just 1 mL of sample volume by employing water-in-oil emulsion droplets of fL–nL volume [19-20]. As a result, assay cost and time are reduced, and higher-throughput experiments like directed evolution of proteins and RNAs [15, 19, 21], screening large libraries for rare mutations [15, 20], or fluorescence-activated cell sorting (FACS) of emulsion-induced products [15, 22-23] can be performed. Figure 1.2 is a comparison of the miniaturization and parallelization found in nature (e.g. a typical bacterial cell) to that of the smallest available conventional technique. A typical w/o emulsion used in IVC can be $10^9$ times smaller than a microtiter plate well [15]. In order to run $10^8$ reactions in parallel with a standard microtiter plate, it would take approximately one hundred thousand 1536-well plates (10 µL assay). At a cost of $3 - $4 per plate, the overall expense would be $350,000 [5]. One must also consider the time it would take to run 100,000 assays. For high-throughput experiments like the aforementioned studies for testing libraries of molecules, the microtiter plate proves to be ineffective in both time and cost, and demonstrates why a technique like IVC is ideal for miniaturization and parallelization of biochemical processes.

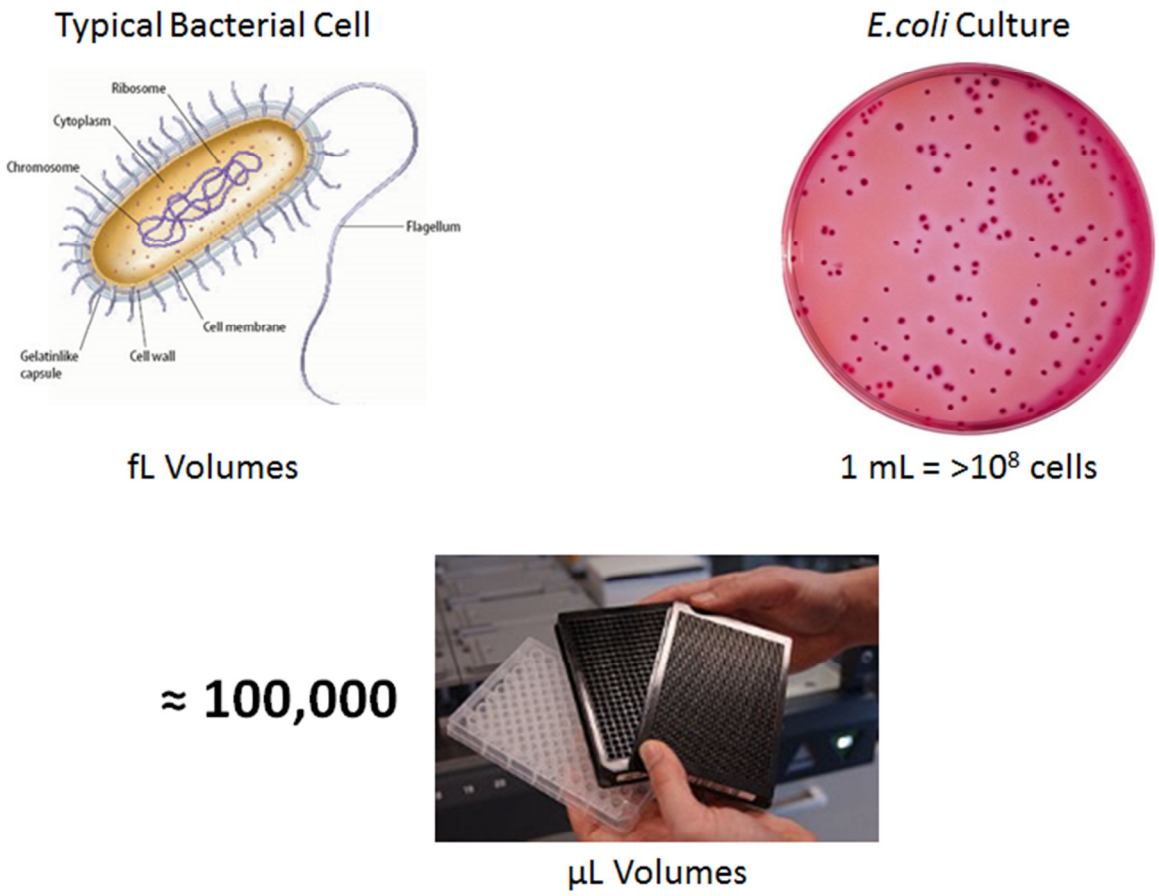


**Figure 1.2** Miniaturization in nature compared to conventional techniques. A typical bacterial cell is just femtoliters in volume (Top Left), while a typical *E.coli* cell culture can contain as many as $10^8$ cells in just 1 mL (Top Right). In order to run $10^8$ reactions in parallel with a standard microtiter plate, it would take approximately one hundred thousand 1536-well plates (10 µL assay). The time and cost ($350,000 at $3-$4 per plate) associated makes microtiter plates unfit for experiments at this level of throughput.

### 1.1.4 Applications of In Vitro Compartmentalization (IVC)

IVC has been used for a wide variety of applications, which is possible for several reasons, including that the droplets are easy to make and that they remain stable under a variety of physical and chemical stressors like changing temperature, pH, and salt concentration [5]. Figure 1.3 illustrates several of these physical and chemical methods used to alter or control droplet content without breaking them [5]. Changing temperature, for example can be used to facilitate the polymerase chain reaction (PCR) within droplets [20]. Also, reagents can be made to enter or exit droplets by exploiting their hydrophobic or hydrophilic nature, which determines a reagent's affinity for the oil or water phase. By tailoring reagent properties, these reagents can even be designed to leave one droplet, travel through the oil, and into a neighboring droplet to start a reaction [5, 21, 24].

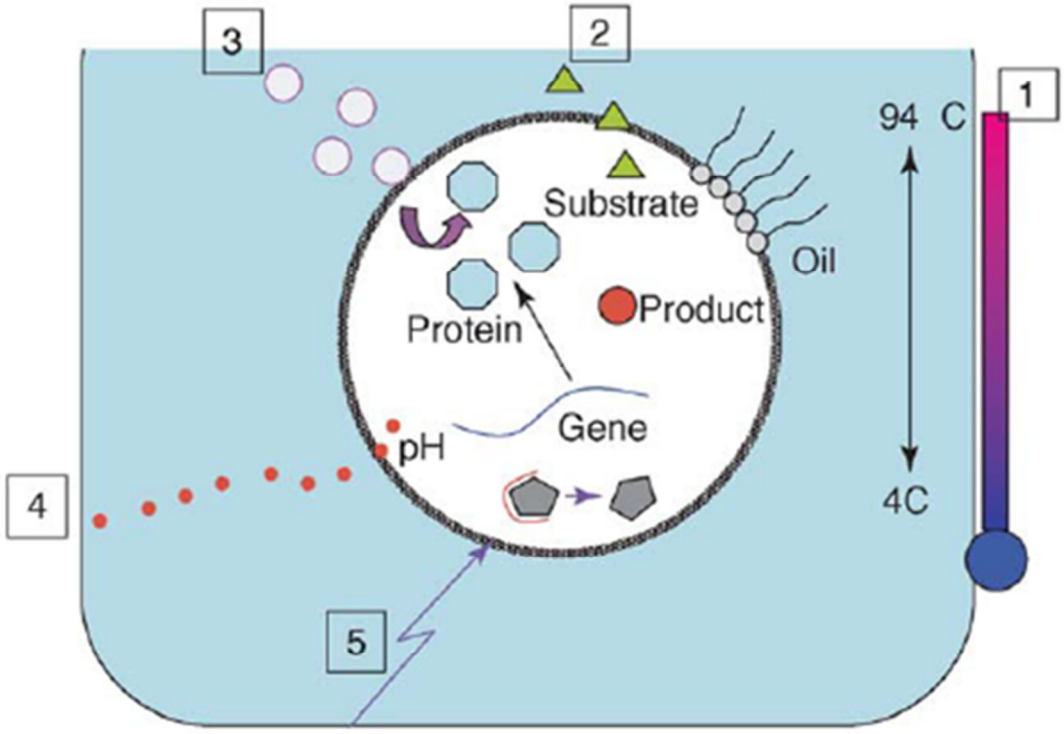


**Figure 1.3** Physical and chemical manipulation of the content of emulsion droplets. Various means of 'communicating' with droplets or changing their composition without compromising their integrity have been developed. (1) The temperature can be readily altered over a wide range, as demonstrated by the application of PCR in emulsions. (2) Hydrophobic substrates or ligands can be delivered through the oil phase into the water droplets. (3) Water-soluble components can be delivered through nanodroplets or swollen micelles, thereby providing a general means of regulating biochemical processes within the water droplets. The delivery of water-soluble ligands can be used to regulate enzyme activities or gene expression. Other nanodroplet compositions might enable high-molecular weight molecules, for example, DNA and proteins, to be delivered, provided that delivery does not promote the exchange of DNA or proteins between the emulsion droplets. (4) The pH can be altered, for example, by the delivery of acetic acid. (5) Substrates or ligands can be photocaged, introduced into the droplets during emulsification and remain inert until irradiated. (6) Droplets from two water-in-oil emulsions can be fused, thus combining reagents contained in the different emulsions (not shown).

Reprinted from [5] with permission from Elsevier.

An early application of IVC demonstrated by Griffiths et al. was the use of water-in-oil emulsion droplets for the enrichment of genes encoding enzymes for a specific activity [5]. As shown in Figure 1.4 A, a library of genes, each physically attached to a substrate, is emulsified with transcription or translation reagents at a concentration of no more than 1 gene per droplet. After transcription and translation takes place inside each droplet, if the resulting protein has enzymatic activity, it converts the substrate to a product that is still physically attached to the original gene sequence. Once droplets are broken, all genes can be pooled together and then separated into substrates and products using technology like flow cytometry (Figure 1.4 B). The genes attached to products can now be enriched via PCR, re-linked to substrates, and introduced into another round of enrichment. After several rounds, a pool only containing the desired genes should be left. This technique has been applied to the enrichment of genes encoding enzymes for DNA methylation [19]. In Chapter 5 we will discuss the use of a similar in vitro selection method for the enrichment of DNA aptamer sequences from a complex pool, that bind to targets with high affinity (Section 5.2.1.).

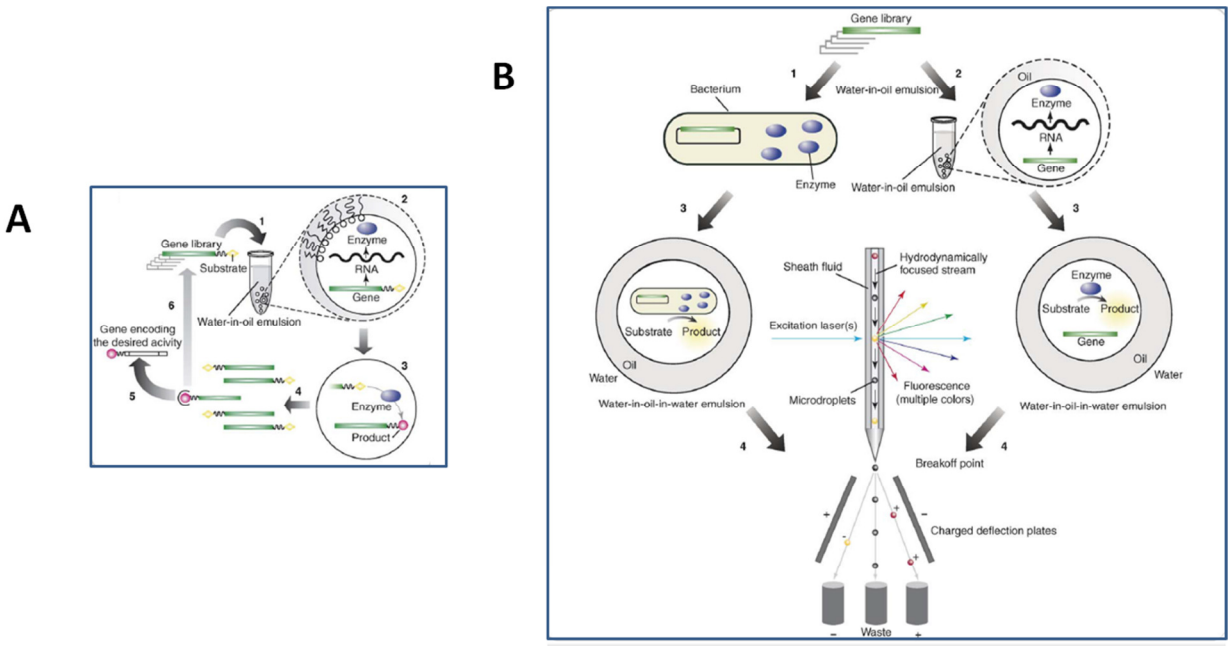


**Figure 1.4** Compartmentalization and enzyme selections in emulsions. (A) Schematic representation of IVC selection by physical gene-product linkage. An in vitro transcription and/or translation reaction mixture containing a library of genes linked to a substrate for the reaction being selected is dispersed to form a water-in-oil emulsion with typically one gene per aqueous compartment (1). The genes are transcribed and translated within their compartments (2). Subsequently, proteins (or RNAs) with enzymatic activities convert the substrate into a product that remains linked to the gene (3). Compartmentalization prevents the modification of genes in other compartments. Next, the emulsion is broken, all reactions are stopped, and the aqueous compartments combined (4). Genes linked to the product are selectively enriched, then amplified and either characterized (5) or linked to the substrate and compartmentalized for further rounds of selection (6). (B) Selections by fluorescence-activated cell sorter (FACS) sorting of double emulsion droplets. A gene library is transformed into bacteria, and the encoded proteins expressed in the cytoplasm, periplasm or the surface of the cells (1). The bacteria are dispersed to form a water-in-oil emulsion, with typically one cell per aqueous microdroplet. Alternatively, an in vitro transcription and/or translation reaction mixture containing a library of genes is dispersed to form a water-in-oil emulsion, with typically one gene per aqueous microdroplet, and the genes are transcribed and translated within the microdroplets (2). Proteins with enzymatic activity convert the non-fluorescent substrate into a fluorescent product, and the water-in-oil emulsion is converted into a water-in-oil-in-water emulsion (3). Fluorescent microdroplets are separated from non-fluorescent microdroplets using FACS (4). Bacteria or genes from fluorescent microdroplets, which encode active enzymes, are recovered and the bacteria propagated or the DNA amplified using the polymerase chain reaction. These bacteria or genes can be re-compartmentalized for further rounds of selection.

Reprinted from [5] with permission from Elsevier.

Emulsion PCR is another useful application of IVC. Certain biological applications, such as the in vitro selection of DNA sequences with a desired property from a large pool, require the use of PCR amplification to enrich selected DNA sequences. Segregating oligonucleotides during this step has proven to be necessary in order to prevent formation of unwanted products, as illustrated in Figure 1.5. To simplify amplification of a complex pool of sequences, DNA strands are usually linked to the same PCR primer sequence, so that amplification can take place with a minimal number of reagents. Because of this, if sequences are allowed to amplify in free solution (Left), DNA sequences can overlap and form recombinant products that are different from and shorter than the correct sequences. PCR preferentially amplifies shorter sequences, which will lead to a build-up of unwanted DNA in the reaction. Conversely, when sequences are amplified within water-in-oil emulsion droplets (Right), each DNA strand is segregated and can amplify in its own compartment, preventing the overlap and formation of unwanted products [20]. Griffiths et al. demonstrated the unbiased enrichment of DNA sequences through emulsion PCR done with droplets generated by the dropwise addition of an aqueous solution to a stirring mixture of oil/surfactant [20].

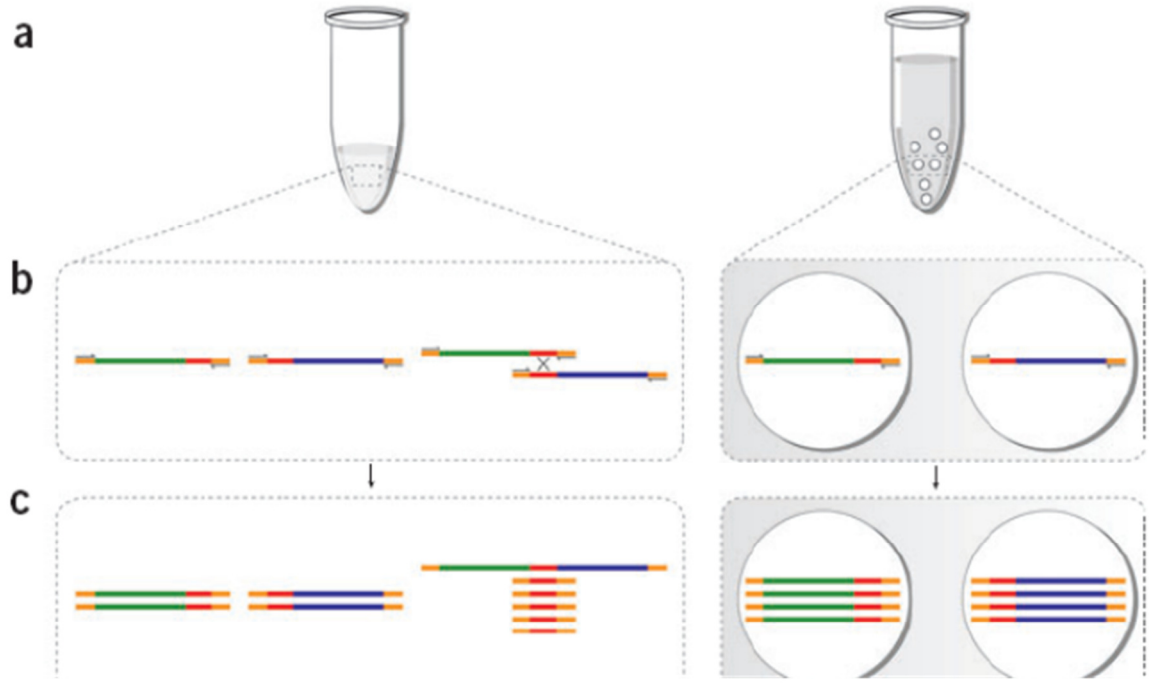


**Figure 1.5** Amplification of complex gene libraries by conventional PCR and emulsion PCR. (A) DNA fragments from a complex gene library are pooled together for amplification in a conventional PCR (left) or compartmentalized in the aqueous droplets of a w/o emulsion such that each droplet contains a single, or at most a few, template DNA molecules (right). (B) Each DNA molecule has an identical linker (orange) ligated at each end to allow amplification with a single PCR primer. If two template DNA molecules containing nonhomologous regions (green and blue) and homologous regions (red) are amplified in a conventional PCR, recombination events can occur, leading to the formation of chimeric products. In contrast, when the same fragments are amplified in an emulsion, the segregation of template DNA molecules prevents the formation of chimeric products. (C) In a conventional PCR, the short, chimeric products are amplified more efficiently than the template DNA molecules, leading to a buildup of artifactual DNA. The absence of chimeric products in the emulsion PCR prevents this from happening.

IVC has also been coupled with microfluidics to perform assays within monodisperse droplets of picoliter size. The measurement of glucose-stimulated insulin secretions (GSIS) within aqueous droplets has been demonstrated by our research group using a handheld microfluidic device and fluorescence microscopy [25-26]. Murine islets were trapped on the microfluidic device (Figure 1.6 A) and stimulated with glucose to induce insulin secretion. Secretions became encapsulated in aqueous droplets along with necessary reagents for the assay at the droplet formation region on the device, and fluorescent intensity was measured downstream via microscopy. Because zinc ($Zn^{2+}$) is co-secreted with insulin, an assay for zinc was chosen, and the results were used to calculate corresponding insulin concentration. With this method, unprecedented temporal resolution in quantitative sampling of secretions from small numbers of living cells was achieved. As shown in Figure 1.6 B, long bursts of secretions on the order of 5-10 min were observed, which is believed to represent insulin secretion in the bloodstream. In addition, shorter pulses (20-60 sec; median period 38.7 sec) were observed, which represent calcium oscillations that occur among the β-cells of intact islets. [25-26]. The Easley research group is broadly interested in using droplet microfluidics, along with aptamer and antibody-based hormone assays to understand secretions of various kinds from primary tissues that are associated with diabetes, obesity, and metabolic syndrome. Based on its importance to our group and to the possibility of using IVC for aptamer selection, the next section will discuss the role of microfluidics in monodisperse droplet formation.

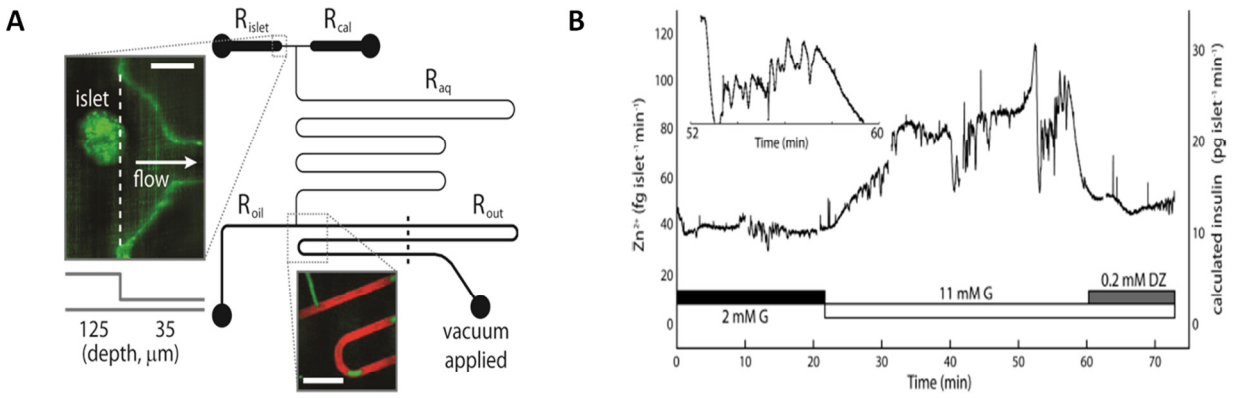


**Figure 1.6** Insulin secretion sampling from a passively-controlled microfluidic device. (A) Channel layout with viewpoint from the top of device, with five categories of channels: islet loading/trapping ($R_{islet}$), calibration ($R_{cal}$), aqueous ($R_{aq}$), oil ($R_{oil}$), and outlet ($R_{out}$). Upper inset shows a confocal fluorescence image of an islet in the trapping region (scale bar 100 $\mu$m). Lower inset shows an image during droplet formation (scale bar 500 $\mu$m). Aqueous phase contains fluorescein (green) and oil phase DiI (red). The device is operated by simply applying vacuum to the outlet with a hand-held syringe. (B) Quantitative $Zn^{2+}$ secretion measurements from live murine islets using the microfluidic droplet sampler. Islets were starved in 2 mM glucose for 2 h prior to analysis. Upon stimulation from 2 to 11 mM glucose (G), $Zn^{2+}$ secretion from islet Z1 rose from a basal level of ~40 fg islet-1 min-1 to ~90 fg islet-1 min-1, then returned to basal levels upon treatment with the potassium channel activator diazoxide (DZ). Observed slow oscillations (9.9 ( 2.0 min spacing, 8.7 ( 2.3 min plateau width) resembled well-characterized slow insulin pulses. Inset data highlights rapid Zn2+ bursts, with median period of 38.7 s. Calculated insulin levels, based on the 2:6 (Zn2+/insulin) crystallization ratio are shown on the secondary *y*-axes (right).

## 1.2 Microfluidics for Droplet Generation

### 1.2.1 Microfluidics Defined

Microfluidics is defined as "the science and engineering of systems in which fluid behavior differs from conventional flow theory primarily due to the small length scale of the system" [4]. These systems utilize $10^{-9}$ – $10^{-18}$ liters of fluid within channels of sizes on the order of only tens to hundreds of micrometers [27].

The microfluidics field finds its origins in meeting needs expressed by science and government in four specific areas, a few of which were mentioned in section 1.1. These are microelectronics (mentioned in section 1.1.1), molecular analysis, biodefense, and molecular biology (mentioned in section 1.1.2.).The microelectronics industry provided motivation for miniaturization and for the use of techniques, such as photolithography and fabrication with silicon and glass materials. Analytical techniques like HPLC and CE were the first to be translated to the microfluidic level, because they had already made significant advancements in achieving low limits of detection and high resolution separations, but the sensors lacked in areas of selectivity and lifetime. This opened the door for microfluidic devices to make these improvements. The biodefense aspect came from the US Department of Defense's (DOD) support of research in the 1990s to develop portable devices to detect chemical and biological threats in the field. Finally, molecular biology provided motivation through the explosion of genomics research, which required high throughput analysis techniques beginning in the 1980s [27]. All of these areas paved the way for modern microfluidics, and have contributed to the explosion and continuously-growing interest in this field (Figure 1.7). Microfluidics has proven to be applicable to an even wider variety of scientific disciplines, including electrical and

mechanical engineering, fluid mechanics, and analytical and computational chemistry; and the capabilities are constantly leading to new applications. The amount of worldwide sales of microfluidic systems and devices has increased linearly since 1998, and it continues to grow. In addition, many professional conferences now have sessions for microfluidics [4]. All of this demonstrates that microfluidics is a field that is sure to develop into a mainstream technology in the future.

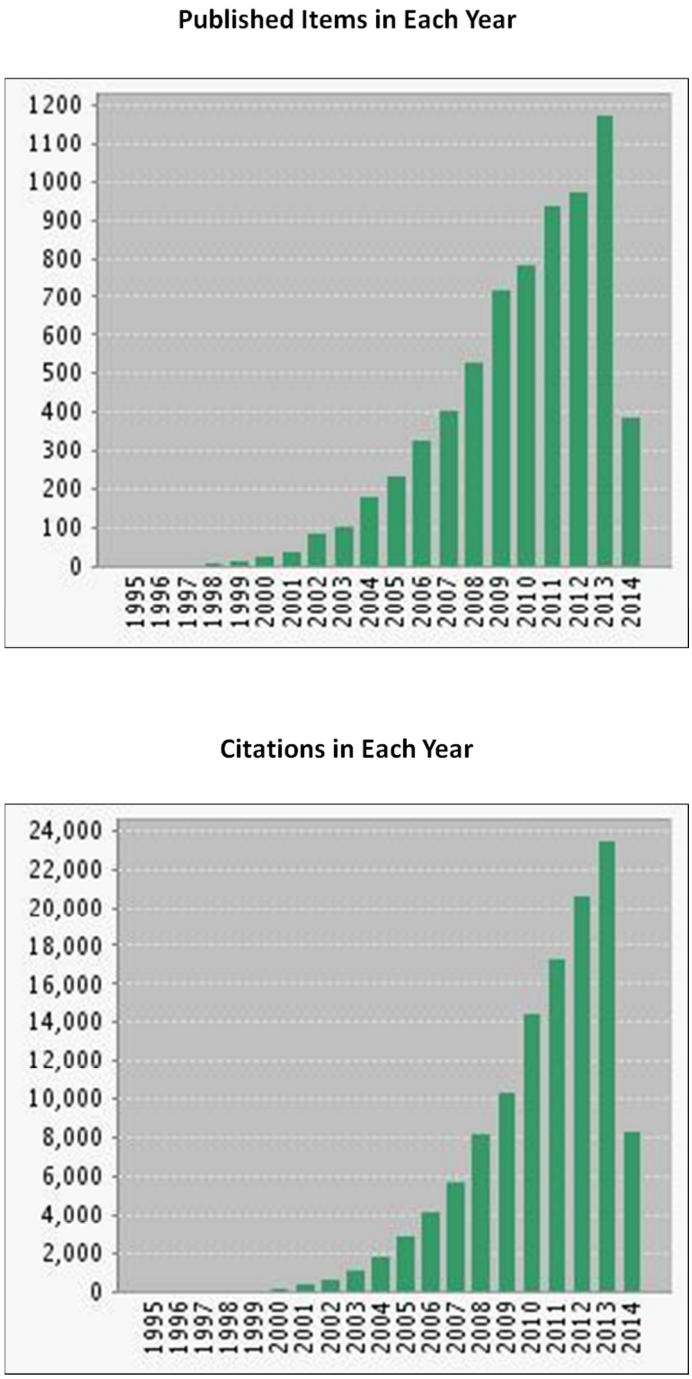


**Figure 1.7** Approximate number of publications and citations on the topic of microfluidics from the year 1995-2014. Calculations based on published articles only.

Results compiled from Thomson Reuters™ Web of Science™ database. Accessed June 4, 2014.

### 1.2.2 Device Fabrication

Most microfluidic devices require four basic components to complete analysis on the chip. The device must be able to provide a means for sample introduction, fluid movement through the channels, reagent combining and mixing, and analyte detection [27-28]. After the first silicon and glass devices used for gas chromatography [28], liquid chromatography [29-30], and capillary electrophoresis [31], there were several major advancements that improved the device fabrication process, allowing them to be used in a larger number and wider variety of experiments. The areas of particular importance were in the selection of better materials, the development of soft lithography for fabrication, and the use of soft lithography to create active valves, mixers, and pumps on the chip.

#### 1.2.2.1 Polydimethylsiloxane (PDMS)

Over time, the original device materials of glass and silicon proved to be disadvantageous for certain applications. Glass and silicon provide advantages in situations where chemical, thermal, or mechanical stability are required, but for a lot of biological applications that are performed in buffers of physiological pH or water, and other "exploratory" research in its beginning stages like that encountered in academia, the use of expensive materials that were difficult to work with was simply undesirable and unnecessary. [27]. Silicon was abundant and inexpensive, but it was also an opaque material, which prevented use of the devices with certain optical detection methods [27, 32]. Glass provided mechanical rigidity, but took a lot of time to create usable devices that once created, were prone to clogging and difficult to clean [32]. The solution to these problems has been found in the use of polymers, particularly

poly(dimethylsiloxane) (PDMS), a material championed by George Whitesides in the early 2000s [27, 33-34].

PDMS is an optically transparent, soft elastomer that can easily be manipulated for fabrication of small parts [27]. It also has good biocompatibility [35]. It is usually made using the 'Sylgard 184' kit from Dow Corning and mixing the elastomer and curing agent at a ratio of 10:1 [35]. The mixture can then be poured over a silicon master for molding of microfluidic devices. The properties of the PDMS can also be tailored once mixed. For instance, if one desires to decrease the amount of UV light scattered by the polymer, fluorescent dyes can be mixed into the material before molding into a device [35]. These advantages, along with the ease of making the elastomer, have allowed PDMS to emerge as one of the main materials used in the fabrication of microfluidic devices for research requiring optically transparent, gas permeable devices to test new ideas and concepts, especially in the area of biological applications [27].

#### 1.2.2.2 Soft Lithography from a Silicon Master

The development of soft lithography in PDMS as a method for fabricating prototype devices has made it possible to test new ideas in a time period much shorter (typically less than 2 days from design to working device) than what could be achieved using silicon technology (typically, for nonspecialists, a month or more) [27]. The process starts with a silicon master. The channel design is drawn in a program like Adobe Illustrator then sent to a company to create a photo-mask. This design can then be etched onto a silicon wafer using photolithography as illustrated in Figure 1.8 A [31, 36-37], but more commonly, positive relief features are patterned onto silicon wafers for PDMS molding, as described below.

The master is usually made via contact photolithography in which the most commonly used photoresist is SU-8 (Microchem), which is a negative resist that can be ordered at different viscosities and spin coated onto the wafer to make a layer of material of varying thicknesses. In this manner the channel depth can be controlled within a range of 1 μm to hundreds of micrometers [35]. This means that after the mask design is placed of the silicon wafer and exposed to UV light. The exposed channels will polymerize and become more difficult to dissolve, leaving the surrounding space to be more soluble and wash away [31, 36-37]. The polymerized channel design will be left behind with a positive surface relief.

The micromachining process described above was used to create silicon wafers with positive surface relief. These wafers are then in turn used to make the polymeric chips as illustrated in Figure 1.8 B. A mixture of PDMS elastomer and curing agent is poured over the wafer and allowed to cure for 2-4 h at 65 °C. After curing, the PDMS is removed, the chip is cut, and access holes for channels, vacuum, and reservoirs are created. After this, the PDMS is attached to another solid surface (e.g. glass or another piece of PDMS) to form closed channels. The length, width, and depth of these channels are dictated by the original mask design and the spin coating process used in preparing the silicon wafer [38].

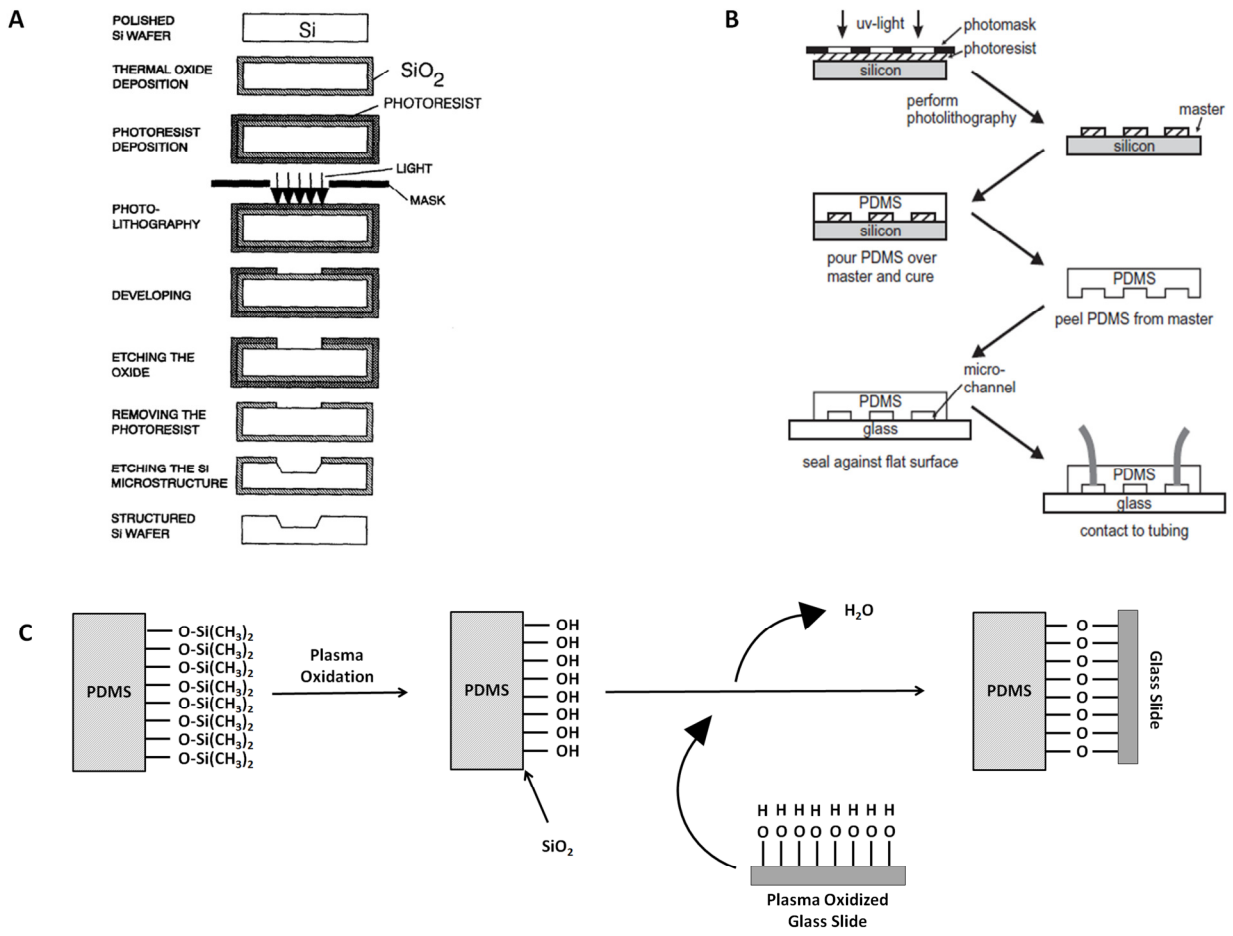


**Figure 1.8** Overview of microfluidic device fabrication using PDMS. (A) Process steps of a standard one-mask micromachining procedure to etch a channel structure into silicon. (1) - Clean the wafer (purchased from a company) to remove particulate matter. (2) - Add a layer of $SiO_2$ to serve as a barrier. (3) - Add a layer of photoresist (positive or negative) by spin coating to form a uniform layer. (4) - Soft baking to remove solvents from photoresist. (5) - Cover with the mask. (6) - Add UV light. If positive photoresist was used, the exposed resist becomes more soluble and washes away. If negative, the exposed resist becomes polymerized and more difficult to dissolve. (7) - Image projected onto silicon wafer. (8) –Develop. (9) - Hard bake to harden the developed photoresist. (10) - Remove photoresist residues with solvents and also etch the oxide to remove polymer debris. (11) - Etching removes unwanted material. (B) Schematic of a typical device fabrication using contact photolithography for structuring and PDMS as the device material. (C) Schematic procedure for the modification and bonding of PDMS to a glass surface. Plasma oxidation changes the PDMS polymer units (–O-Si(CH3)2-) into silanol groups (-OH). When brought into contact with a glass slide that has also undergone treatment, an irreversible bond forms due to the loss of a water molecule [39].

Figure 1.8 A Reprinted from [31] with permission from Elsevier.; Figure 1.8 B Reprinted by permission from IOP Publishing Ltd: Reports on Progress in Physics [35], Copyright 2012.

#### 1.2.2.3 Bonding via Plasma Oxidation

Bonding is usually performed by using an oxygen plasma to covalently bond the PDMS and glass –OH bonds [35]. More specifically, this well-studied process exploits that PDMS is a polymer made up of repeating units of $–O\text{-}Si(CH_3)_2\text{-}$ (Figure 1.8 C). After exposing these to the oxygen plasma, they briefly turn into oxygen radicals of silanol groups (-OH), as the oxidation removes the methyl groups. It is believed that this increase in hydroxyl concentration at the surface helps the material to form strong intermolecular bonds [39]. This radical hydroxyl group remains stable for less than 1 min, so bonding to a second surface must be done quickly. When brought in contact with another plasma-treated surface, such as glass, the silanol groups on both surfaces will condense, forming Si-O-Si bonds after loss of a water molecule. This bond is covalent, irreversible, and usually strong enough to withstand 30–50 psi of air pressure [39]. After bonding to a second surface, tubing is used to interface the device to necessary vacuum and pump apparatuses [35] (Figure 1.8 B).

### 1.2.3 Droplet Microfluidics

#### 1.2.3.1 Droplet Microfluidics Defined

Droplet Microfluidics is a sub-field of microfluidics that focuses on making droplets of a controlled size at high frequency by either pulling a vacuum, or applying pressure [35]. In recent years it has emerged to reinvigorate the area of In Vitro Compartmentalization (IVC) by providing a number of avenues for high-throughput, robust droplet generation and manipulation. This technique uses microfluidic devices to generate, manipulate, and perform chemical and biological reactions within droplets of femtoliter to nanoliter volume [40], which has led to more flexibility, lab portability, and increased likelihood of automation [25, 41-44].

In IVC droplets can serve as individual microreactors, preventing reagents and assays from interacting with the surrounding droplets, because they are spatially separated by an immiscible carrier fluid [40]. This fluid, which will be discussed in greater detail in the next section of this chapter, consists of one of many different types of oil and surfactants. The earliest methods for forming these emulsions involved either vortexing mixtures of oil/surfactant and aqueous solution to create microfine solutions of droplets, or adding an aqueous solution dropwise to a mixture of oil and surfactant as it was simultaneously agitated by a magnetic stirrer [20]. These methods, though simple and effective, created droplets of varying size, with many of them being too small to carry all of the assay components. This polydispersity increases droplet-to-droplet variation in reagent concentration and can negatively impact assay performance. One major advantage gained by using droplet microfluidics is the ability to quickly produce highly monodisperse emulsions. By controlling the flow rates of the aqueous and oil phases within microfluidic channels of specific dimensions and orientations, droplet size can become highly uniform with as little as 1-3% size variation [40]. We have developed devices for rapid droplet formation (Chapter 2) that have been used to perform biological assays.

#### 1.2.3.2 Channel Geometries for Droplet Formation

Channel geometry is an element of microfluidic device design that must be controlled for proper droplet formation. Two popular techniques are flow focusing, which is also called co-flow, and t-junction geometries. Flow focusing is a technique that allows for the production of small droplets at high frequency ($\leq$ 1 000 Hz) by focusing a stream of dispersed phase, surrounded by continuous phase, through a small opening in the device and relying on viscous stress to form droplets. If the flow rate for each phase is varied, droplet size can even be changed to form a variety of sizes on a single device. However, complex fabrication and operation

demands can make this design undesirable [35]. An attractive alternative, if higher production rates and variable control of droplet size can be sacrificed, is the use of t-junction geometries, which are easier to fabricate and operate, and still have the ability to produce droplets at rates of up to several hundred droplets per second [35].

The t-junction channel geometry was the first used to produce monodisperse droplets with microfluidic devices. It involves flowing a constant stream of the continuous phase, usually oil/surfactant, perpendicular to a constant stream of the dispersed phase (Figure 1.9 A). This creates a shear that breaks the dispersed phase into individual droplets [35]. Figure 1.9 A shows several t-junction arrangements that can be used to form droplets. Variations of this design have also been used to alter droplet content and to increase the speed and volume of droplet production. As seen in Figure 1.9 B, opposing and parallel t-junctions can allow for the production of two different kinds of droplets on a single chip [35]. Even higher throughput has been realized by the parallelization of eight or more t-junctions onto a single device [42, 45-46]. We frequently use t-junction geometries for rapid droplet generation in our passively-controlled devices (See Chapter 2).

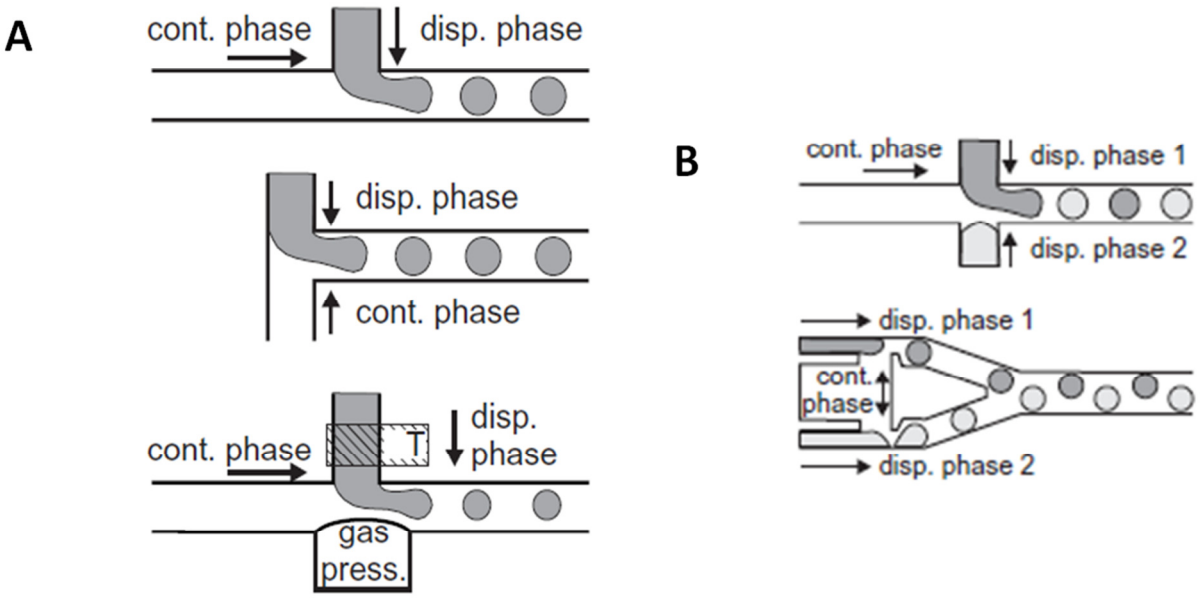


**Figure 1.9** (A) Schematic of various T-junction geometries. (Top) 'regular T-junction' geometry where the dispersed phase is injected perpendicular into a stream of continuous fluid. (Middle) 'Head on' geometry where the dispersed and the continuous phases are injected from opposite sides. (Bottom) 'Active T-junction' allowing variations of the geometry by air pressure and temperature control of the dispersed phase. (B) Schematic of various double T-junction geometries for the synchronized production of two kinds of droplets. Combination of two T-junctions as demonstrated.

#### 1.2.3.3 Channel Wettability

Knowing and understanding the characteristics of the channels and walls of a microfluidic device is also important for droplet formation. For example, to form water-in-oil emulsion droplets where the oil acts as the carrier phase, channels must be hydrophobic. The opposite is true when forming oil-in-water droplets [35]. The selection of fluids is also important, as many organic reagents and oils can cause PDMS to swell or even dissolve. PDMS is mainly compatible with polar fluids like water or ethanol, as well as fluorocarbon oils. Of course, the material is not impenetrable. Many components have been shown to diffuse through the PDMS to some extent, and PDMS material can leach into the fluid [35]. Therefore, tailoring the surface properties of the device is critical to successful droplet formation and long-term assay stability.

There are a variety of methods for modifying the PDMS/glass surface to achieve these desired properties. Some may soak the device in the continuous phase with a high surfactant concentration before using it to make droplets [35]. Other examples take it a step further and include using sol-gel to form a thin glass coating, acrylic acid coatings, plasma polymerization, and deposition of electrolytes [35]. In our research we use Aquapel, which is a perfluorocarbon coating that matches the properties of our selected carrier oil. How this is used to create hydrophobic surfaces within the microfluidic device will be discussed in more detail in Chapter 2. Regardless of the technique used, the wettability of the channels must be tailored to match that of the continuous phase.

#### 1.2.3.4 Carrier Fluids

Emulsion systems using commercially-available silicone and hydrocarbon oils have been successfully applied to many different areas, such as PCR and directed evolution in droplets [46,

76-77]. However, silicone oil is not compatible with PDMS, resulting in the need for glass device fabrication, which can be both time-consuming and expensive. Some hydrocarbon oils are compatible with PDMS, but they have been shown to cause problems with reagent diffusion into the oil and transfer between droplets [47]. Organic oils like mineral oil and hexadecane are often used, along with Tween 20 or Span 80 surfactants. As mentioned previously, these types of oils also have a history of swelling PDMS, which should lead the investigator to either use a different material, a surface coating, or a different continuous phase [35].

A popular solution is to use fluorinated oils and surfactants, such as FC40 or FC70 oils with pentadecafluoro-1-octanol or Krytox perfluoropolyether (DuPont) surfactants [35]. Fluorocarbon oils are repellent to both oil and water, which makes them less likely to promote droplet coalescence. In addition, fewer reagents are soluble in this oil, preventing transfer of materials between droplets through diffusion. They are also denser than water, have low viscosity, and the electronegativity of fluorine gives them low polarizability. Another attractive feature is their ability to allow gases to diffuse through them, making them attractive for use with live cells [47-48]. But these oil/surfactant combinations are not without problems. Because fluorinated oils allow gas and vapor to diffuse through them, contamination between droplets and loss of encapsulated material becomes a real possibility. However, this property can be harnessed and used to enhance experiments requiring selective exchange of ions or materials between droplets, such as delivery of oxygen to live cells [35]. In summary, factors like channel wettability and properties of the carrier fluid should be considered and carefully selected for each droplet microfluidics application.

#### 1.2.3.5 Applications of Droplet Microfluidics

Andrew Griffiths, the founder of IVC, has partnered with several researchers to combine IVC with high-throughput droplet microfluidics technology for a variety of biological applications. These include encapsulating individual cells in droplets ≤33 pL in size that ensures that cells remain viable and that secretions remain at detectable levels [66], performing directed evolution to screen and sort a library of $10^8$ enzyme variants in just 10 h [67], and to perform digital quantification of DNA templates amplified isothermally in 2 pL droplets on a single device [68].

One particularly interesting technique is the microfluidic generation of double emulsions. Water-in-oil-in-water droplets have been made using a microcapillary device (Figure 1.10). These droplets can be produced at a rate of 100-5 000 Hz and have the advantage of completely separating encapsulated material from the carrier fluid [69]. Droplets are so stable that they can even be directly analyzed and sorted using flow cytometry [70-72]. Double emulsions find application in experiments requiring control over the release and separation of reagents or materials, such as in food additives or personal care products to name a few and are traditionally made via a two-step emulsification process that results in polydispersity. Incorporating droplet microfluidics allows control over droplet size and rate of production, opening the door to a wider variety of experiments requiring precision [69].

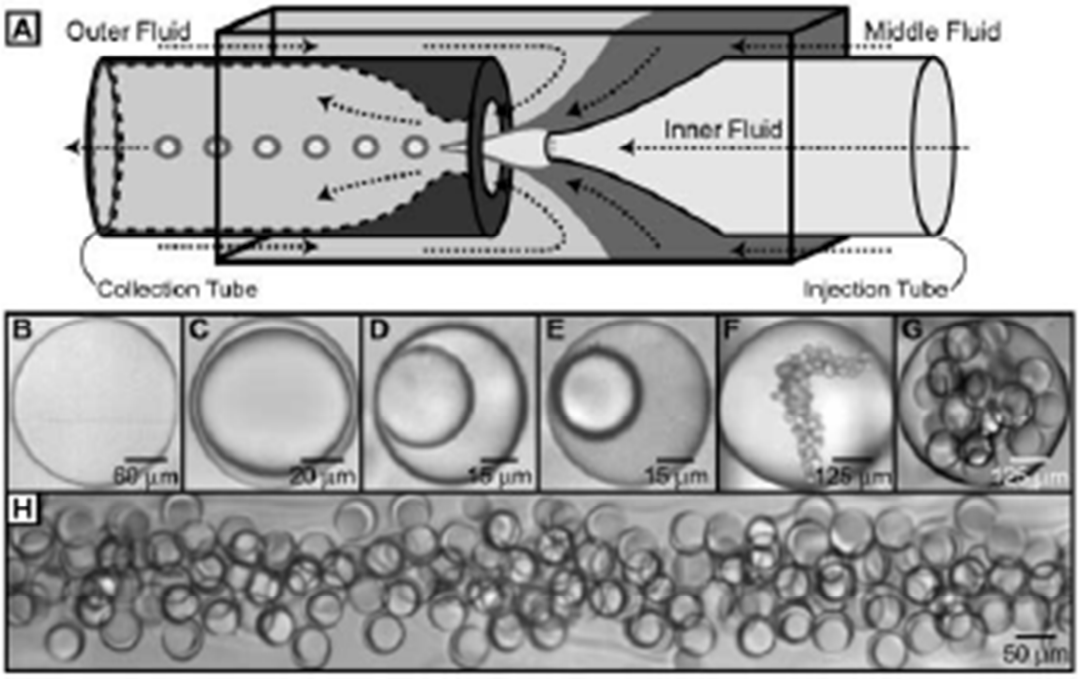


**Figure 1.10** Microcapillary geometry for generating double emulsions from coaxial jets. (A) Schematic of the coaxial microcapillary fluidic device. The geometry requires the outer fluid to be immiscible with the middle fluid and the middle fluid to be in turn immiscible with the inner fluid. The geometry of the collection tube (round tube on the left) can be a simple cylindrical tube with a constriction, as shown here, or it can be tapered into a fine point (not shown). The typical inner dimension of the square tube is 1 mm; this matches the outer diameter of the untapered regions of the collection tube and the injection tube. Typical inner diameters of the tapered end of the injection tube range from 10 to 50 mm. Typical diameters of the orifice in the collection tube vary from 50 to 500 mm. (B to E) Double emulsions containing only one internal droplet. The thickness of the coating fluid on each drop can vary from extremely thin (less than 3 mm) as in (B) to significantly thicker. (F and G) Double emulsions containing many internal drops with different size and number distributions. (H) Double emulsion drops, each containing a single internal droplet, flowing in the collection tube. The devices used to generate these double emulsions had different geometries.

Reprinted from [69] with permission from AAAS.

Darren Link, a frequent collaborator of Andrew Griffiths, went on to co-found Raindance Technologies, which is a company that specializes in digital droplet technology for a variety of biological applications. With their patented technology and surfactants, researchers can encapsulate single DNA templates into millions of picoliter-sized droplets at speeds of up to 10,000 droplets per second [73]. These droplets are then combined with another droplet containing PCR reagents, and the reaction takes place through thermal cycling. This DNA enrichment technology has already been applied to DNA sequencing and digital PCR (See Section 1.4) [68, 74-75], and could also allow for rapid analysis of content from single cells and proteins [73] for detection of rare mutations or directed evolution. Overall, technologies like this are allowing researchers to obtain unprecedented levels of throughput with high sensitivity (i.e. Detection of 1 rare event out of 1 000 000 total) and precision [73].

## 1.3 The Role of Surfactants in Droplet-Based Microfluidics

### 1.3.1 Surfactants and Their Properties

#### 1.3.1.1 Surfactants Defined

Surfactants, or surface active agents, are amphipathic molecules that play a major role in the chemical industry. As mentioned previously, droplets generated using microfluidics consist of two fluids called a dispersed phase and a continuous phase. Surfactants are generally added to the carrier phase (i.e. continuous phase) in order to prevent coalescence of droplets after generation and to ensure monodispersity. They do this by assembling at the oil/water interface, which lowers the interfacial surface tension [35, 49].

Surfactants can also be found in a variety of products from detergents to cosmetics and plastics, and they are also used to prepare emulsions and suspensions. Surfactants can also find

use in environmental industries, such as in the cleaning up of oil spills. Surfactants are typically not pure when purchased from companies. They are instead prepared from petrochemicals, natural vegetable oils, and natural animal fats. Both hydrophobic and polar/ionic groups are usually a mixture of different chain lengths. One can contact manufacturers for properties, suitability for your purposes, batch to batch variation, toxicity, and other additional information needed [49].

Amphipathic molecules like surfactants contain a non-polar, hydrophobic region and a polar/ionic, hydrophilic region (Figure 1.11). The non-polar region is typically a straight or branched hydrocarbon or fluorocarbon chain that becomes hydrophobic as a result of being squeezed out of the water by dispersion and hydrogen bonding that occurs between water molecules. Conversely, the polar region can be nonionic, ionic, or zwitterionic, and it interacts with water via dipole or ion-dipole interactions, making it hydrophilic. The length and geometry of each oil-soluble or water-soluble portion of the surfactant molecule can be tuned to give the surfactant a variety of different properties [49].

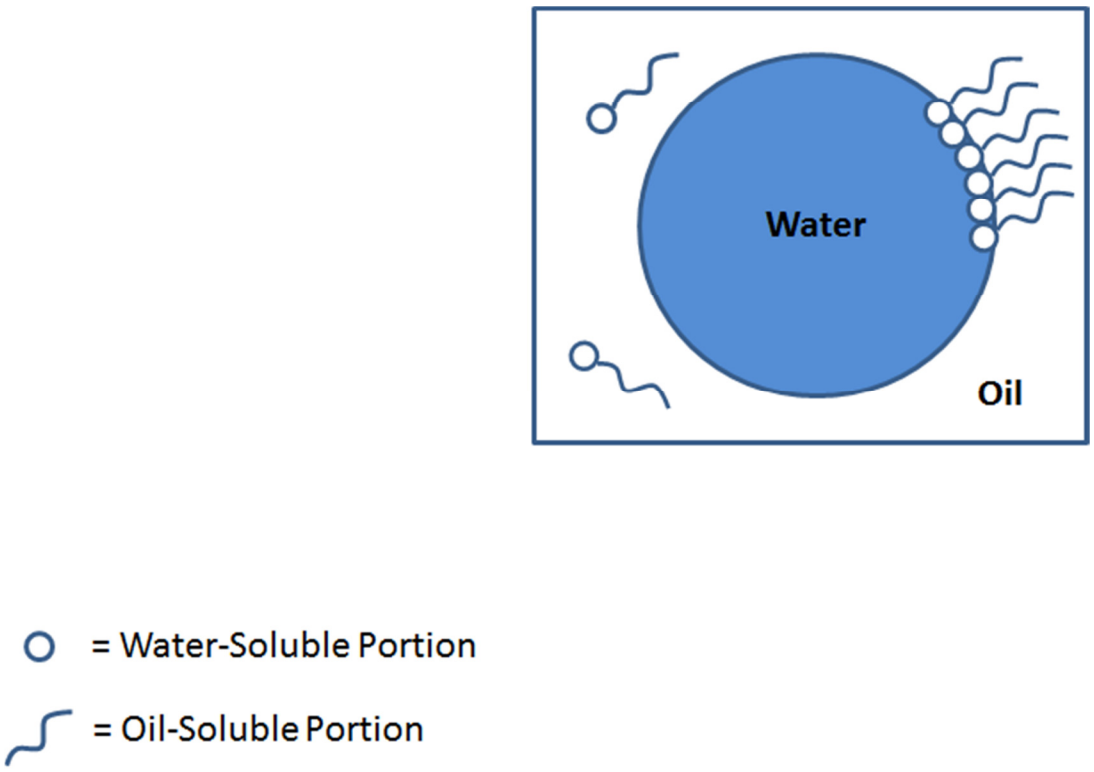


**Figure 1.11** Surfactants are amphipathic molecules that assemble at the oil-water interface of emulsion droplets. Comprised of oil-soluble (non-polar/hydrophobic) and water-soluble (polar/hydrophilic) portions, these molecules act to prevent droplet coalescence through steric and electrostatic repulsion between droplets. They can also be used to provide biocompatibility by making the inner interface inert to effects from the oil or surfactant itself. Changes in length (i.e. molecular weight) and geometry (e.g. diblock or triblock surfactants [48]) of each portion can result in a variety of different properties for the emulsion system [49].

The different classes of surfactants are named according to the properties of the polar region of the molecule. Anionic, cationic, amphoteric, nonionic, polymeric, and fluorocarbon/silicone surfactants are all available. Anionic surfactants are the most widely used, because they are inexpensive to produce. Carboxylates, sulphates, sulphonates, and phosphates have all been used as anionic headgroups, but carboxylates provide several advantages. Mainly they are inexpensive, biodegradable, and have low toxicity. Fluorocarbon surfactants also provide several advantages over the other classes in that they have ability to lower the surface tension to below 20 mN/m, while most surfactants can only reach 25-27 mN/m. The ability to lower the surface tension between two liquids is an important property of surfactants, as this is the driving force for droplet formation [49].

#### 1.3.1.2 Adsorption at the Liquid/Liquid Interface

Surface formation is thermodynamically unfavorable, because molecules experience fewer interactions at the surface than in bulk solution. Surfactants work by lowering the surface tension (the amount of energy required to create a surface per unit area) of the phase boundary between two states of matter (Figure 1.12). With more surfactant molecules adsorbed at the interface, surface tension is lowered, which eases surface formation. Without surfactants, surface tension can remain fairly high at the boundary between two phases, because the few molecules at the surface will exert stronger forces upon the surrounding molecules to compensate for the lack of interactions as compared to bulk solution [47, 49]. The degree of surfactant adsorption to the interface, which is inversely proportional to the surface tension, is dependent on the structure of the surfactant and the properties of the two phases at the boundary. [47, 49].

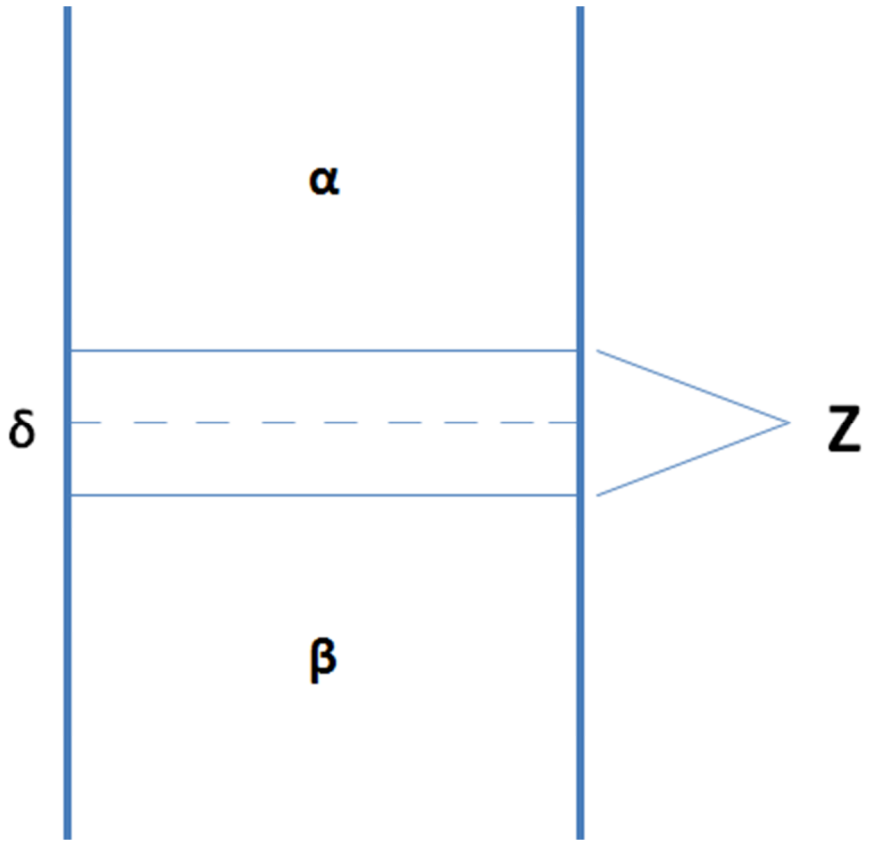


**Figure 1.12** The surface of a liquid is the boundary between two bulk phases. Two immiscible liquids must have a dividing line. The interface has a thickness (δ) with properties that differ from the bulk phases (α & β). α & β are uniform in properties until Z [49].

Adapted from [49] without permissions.

The Gibbs adsorption isotherm for dilute solutions uses the relationship between surfactant concentration and surface tension to calculate the concentration of surfactant at the surface with the following equation [47]:

$$\Gamma = \frac{-c}{RT}\frac{d\gamma}{dc}$$

In this equation Γ is the surface concentration, *c* is the surfactant concentration in bulk solution, γ is the surface tension, T is the temperature, and R is the gas constant [47]. Generally, surfactant concentration is in excess at the interface, or surface. A true measure of total surfactant concentration would combine the surface concentration and the concentration in bulk solution, but it is generally accepted that the concentration at the surface is so much greater for most surfactant solutions that bulk concentration can be neglected [47, 49]. Therefore, this equation can be used to obtain an accurate determination of surfactant concentration at the interface. This will be an important concept to remember when we discuss the role of surfactants in emulsion formation and stabilization for in vitro compartmentalization (IVC).

### 1.3.2 Emulsion Formation and Stability

Governed by the second law of thermodynamics, the free energy of emulsification is positive and can be found using the following equation [49]:

$$\Delta G_{form} = \Delta A_{\gamma 12} - T\Delta S_{conf}$$

Where, A2 = Area of many small droplets, $A_1$ = Area of original large droplet, γ12 = Interfacial Tension (IFT) of $A_1$ and $A_2$, $\Delta A_{\gamma 12}$ = Surface Energy Term, where ($\Delta A = A_2 - A_1$), and $T\Delta S_{conf}$

= Entropy of Dispersion Term. The interfacial tension of $A_1$ and $A_2$ ($\gamma 12$) can combine into a single term, because IFT is generally the same for larger and smaller droplets, as we are often dealing with droplets from just 0.1 to a few micrometers in size. Therefore, $\Delta A_{\gamma 12}$ >> - $T\Delta S_{conf}$ , and $\Delta G_{form}$ becomes positive (Figure 1.13) [49].

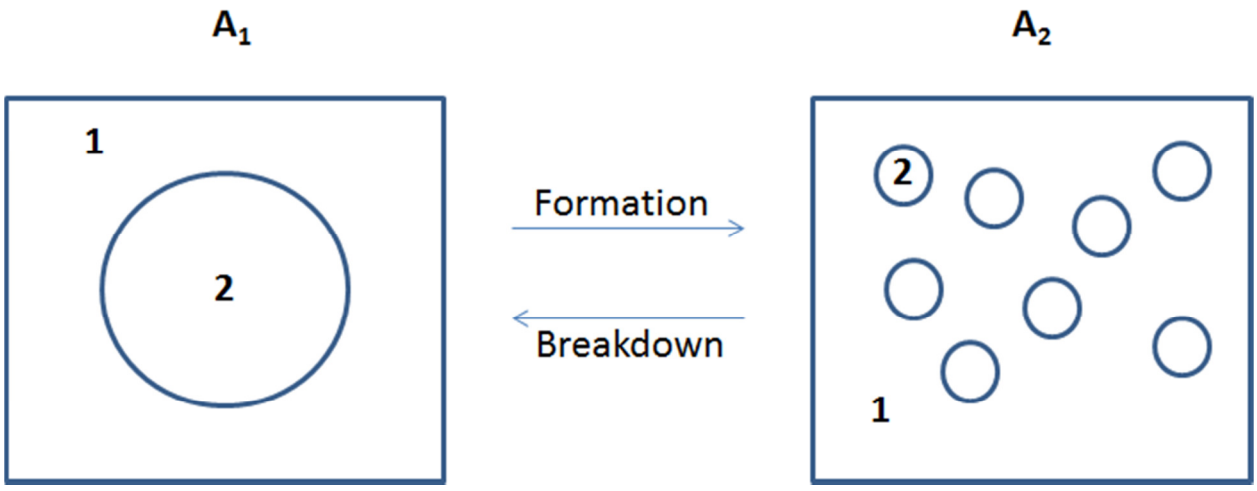


**Figure 1.13** Formation and breakdown of emulsion droplets. Water is represented by a large drop (2) of area A1 immersed in an oil (1). Now subdivided into smaller drops of total area A2. Area 2 is larger than Area 1 [49]. The breakdown of emulsion droplets from many surfaces back to one surface is thermodynamically favorable. Therefore, surfactants must be used in order to prevent this process.

Adapted from [49] without permissions.

In order to prevent the return of emulsion solutions to a state of minimal energy separation into two phases (Figure 1.13), surfactants are employed. They serve this purpose by creating an energy barrier that uses electrostatic and/or steric repulsion to combat the van der waals attraction between droplets. The energy barrier causes the process of emulsion breakdown (e.g. coalescence) in Figure 1.13 to become non-continuous by making the system kinetically stable [47, 49].

There are several properties that must be considered when trying to achieve droplet stability. First, the interfacial tension (IFT) is the amount of force needed to break a surface per unit area. Therefore, it is important not to lower interfacial tension too much, or droplets will break and/or become incapable of forming in microfluidic devices, making the two phases miscible [47-49]. As more surfactant molecules migrate to the interface, the surface tension will quickly decrease until the critical micelle concentration (CMC) is reached. After this point, the surface tension will be largely unaffected by changes in surfactant concentration [48].

The second property to consider is the CMC itself. The driving force for micelle formation is the decrease of contact between the hydrocarbon chain and water, along with the decrease in the free energy of the system [49]. Unlike surface formation, this is an exergonic process that occurs in the bulk solution [50]. The CMC will dictate how many available molecules are in solution. Only molecules that exist as monomers can move to the interface, so once micelles begin to form, the number of available molecules has decreased [48]. CMC can be determined from a plot of surface tension versus the natural log of the concentration. Two lines should be extrapolated in this plot, one over the area where the interfacial tension is dependent on surfactant concentration, and a second over the area where IFT becomes constant. The intersection of these two lines should be the point at which IFT ceases to change with increasing

surfactant concentration, denoting that this is the CMC [50]. Determining CMC for each surfactant solution and balancing this property with molecular weight and geometry should provide a means for achieving maximum droplet stability.

Molecular weight and geometry play a large role in adsorption at the oil-water interface and resultant droplet stability. In the case of molecular weight, the molecules should remain at a size where they can diffuse through solution and move to the interface before droplets have a chance to collide and coalesce [48].

The geometry of these molecules can be studied through the use of diblock or triblock surfactants. For an accurate determination, droplet stability could be compared between surfactants with one or two oil-soluble portions for every one water-soluble portion. David Weitz' group studied this using polyethylene glycol (PEG) and perfluoropolyether (PFPE) surfactants to make diblock (PEG-PFPE) and triblock (PFPE-PEG-PFPE) copolymer surfactants [48]. They found that the triblock surfactant provided a denser layer on the outside of each droplet interface, resulting in better repulsion between droplets and fewer cases of coalescence. After combining information obtained about the critical micelle concentration (CMC), molecular weight, and geometry of their surfactant solution, the group was able to determine that a longer PEG chain, shorter PFPE chain, and triblock geometry provided them with a higher CMC [48]. We have also studied the properties of surfactants for biological applications and demonstrated their use in our microfluidic systems (Chapter 3).

### 1.3.3 Biocompatibility

A major factor to consider when selecting oil/surfactant combinations is biocompatibility. When assays are reduced from bulk solution to encapsulation in droplets of micrometer size, any

interaction at the oil-water interface will become greater than interactions found in the bulk solution. This is especially important when working with biological materials whose interaction with the selected oil or surfactant can cause a decrease in assay performance. Interaction could include reagent attraction and adsorption to the interface, and crashing of proteins out of solution. Therefore, it is important to choose surfactants that will help minimize any negative effects that the interfacial properties may have on the assay [47]. A surfactant is considered biocompatible if it can fulfill this role of minimizing surface effects, allowing assays and reactions to occur at the same level of efficiency that they would in bulk solution [47].

Emulsion-generating devices typically employ hydrocarbon or fluorocarbon oils for aqueous droplet encapsulation, and one solution used for providing biocompatibility is to use polyethyleneglycol (PEG) in combination with fluorinated oils and surfactants [35, 48]. If organic oils are used, solutions include using squalane with a lipid like monoolein [35]. We have published a study on biocompatible surfactants, in which we used the fluorinated oil HFE 7500 (Novec 7500 Engineered Fluid by 3M), Krytox 157 FSH surfactant, and a polyetherdiamine (Jeffamine ED900) that is PEG-like in nature [51]. This successfully prevented swelling of PDMS and provided a biocompatible droplet environment for biological assays using droplet microfluidics.

## 1.4 DNA Amplification Using PCR

### 1.4.1 Defining PCR

The polymerase chain reaction (PCR) is a method for exponentially amplifying DNA, first described in 1987 by Nobel Prize winner Kary Mullis [52-53]. It is so sensitive that even a single DNA molecule can be amplified [53]. As a result, this technique is routinely used for

applications where enrichment of DNA is required, such as in the detection of rare mutations from a pool of sequences, or obtaining DNA evidence from crime scenes. PCR relies on efficient heating and cooling and precise temperature control to denature and anneal complementary strands of DNA, and it creates additional sequences by using DNA polymerase enzymes along with free deoxynucleotide triphosphate (dNTP) bases – A, T, G, and C – in solution. Although PCR conditions must be optimized for each new application, there are basic components that are necessary for the reaction to take place. These include a template sequence, an excess of forward and reverse primers, deoxynucleotide triphosphates (dNTPs), buffer with necessary ions (e.g. $Mg^{2+}$) , and DNA polymerase enzyme [53].

Typical PCR consists of 20-35 cycles of 3 distinct steps, and takes 1-2 hours (Figure 1.14 A). Step 1 is the initial denaturation of the double-stranded DNA template, in which the temperature is raised to 94-95 °C. In step 2 the temperature is lowered to just below the melting temperature of the primer/template complex (approximately 50-60 °C), allowing the primers to hybridize at the 5' ends of each template strand. Step 3, optimally performed at 72 °C, is the polymerase-catalyzed extension of the primer sequences in the 5' to 3' direction on each strand until the complementary strands are formed. After repeating steps 1-3 for 20-35 cycles, the reaction is concluded by performing a final extension at 72 °C for 5-10 min, and then stopped by dropping the temperature to 4 °C until samples are ready for further analysis [53]. The full-length desired template is not actually formed until about the third cycle. From there, exponential amplification takes place, resulting in 8 target copies after the fourth cycle, 22 target copies after the fifth cycle, and so on. This process continues until a plateau phase is reached due to depletion of reagents and loss of enzymatic activity. In addition, a buildup of DNA template can cause them to hybridize instead of primers, resulting in unwanted PCR products.

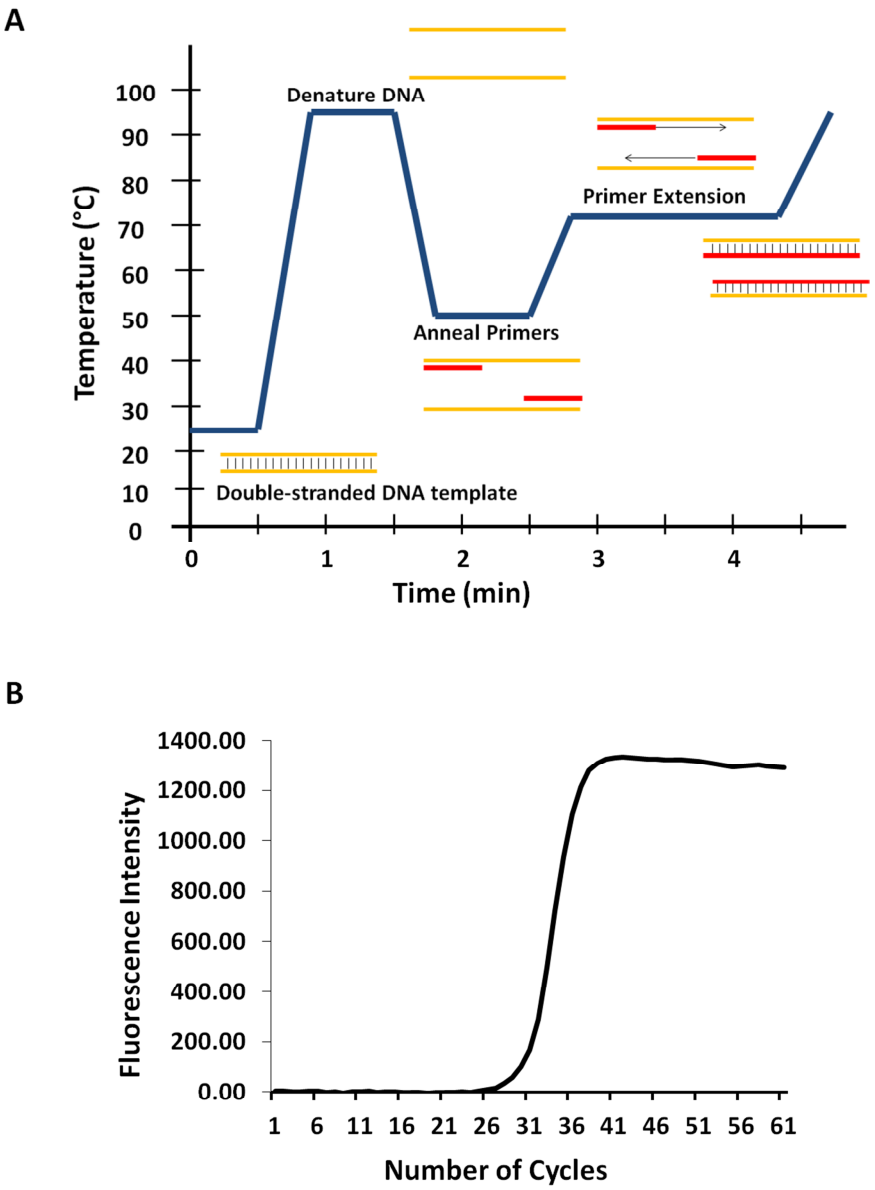


**Figure 1.14** DNA amplification with the polymerase chain reaction (PCR). (A) PCR thermal cycling results in DNA replication. PCR begins with a single-tube reaction in a thermal cycler containing a double-stranded (ds) DNA template, excess of two primer sequences, DNA polymerase, excess of the four deoxynucleotide triphosphates (dNTPs) A,C,G, and T, and buffer containing necessary ions like $Mg^{2+}$. DNA denaturation takes place when the temperature is raised to approximately 94 C. The temperature is then lowered to below the melting temperature ($T_M$) of the primers to induce primer annealing. This is usually between 50-60 C. Finally, the temperature is raised to approximately 72 C to allow for optimal enzyme extension of the primer sequences, effectively replicating the original template strand. (B) Real-time PCR (qPCR) trace of DNA amplification. Fluorescence probes (e.g. DNA intercalating dye or Taqman Probe) are used to monitor amplification after each cycle of PCR by indicating the amount of DNA present. In PCR, target DNA of correct length is not produced until the third cycle, and cycle 4 begins true exponential amplification (i.e. After 4 cycles, 8 target copies should exist. After 5 cycles, 22 target copies should exist). Amplification continues until a plateau is reached due to depletion of reagents and deterioration of the enzyme.

### 1.4.2 Types of PCR

In the beginning, qualitative evidence of PCR amplification could be found using gel electrophoresis for end-point analysis. With the introduction of DNA intercalating dyes and template-specific probes, it is possible to monitor PCR amplification in real time (Figure 1.14 B). Real-time PCR (qPCR) provides quantitative information on DNA concentration by defining a cycle threshold ($C_T$) for each sample, which is the cycle number at which the fluorescence signal increases above background on a log scale [54]. Quantitative information for samples of unknown concentration can be obtained by first generating a standard curve using samples of known DNA concentration and plotting their $C_T$ values vs. concentration.

PCR analysis was taken a step further with the advent of Digital PCR in the early 1990's [55-56]. Digital PCR takes DNA and dilutes it into multiple reactions of equal volume, usually chambers or droplets, to an extent where some reactions have no template copies and other have at least one or more copies. Amplification is then allowed to take place until the plateau phase, at which point the reactions that had template in them will register as positive, while those containing no template will remain negative [54]. The following equation can then be used to calculate the average number of DNA molecules ($\lambda$) per reaction: $\lambda = - \ln (1 - p)$, where p is the fraction of positive reactions. Combining this information with the reaction volume and the total number of reactions performed can provide an estimate of the absolute DNA concentration [54].

One benefit of digital PCR is that the number of reactions performed is proportional to the dynamic range of detection. For instance, increasing the number of replicates by an order of magnitude will lead to the same increase in dynamic range. Another benefit of increasing the number of reactions is achieving greater precision, which allows for easier detection of differences between sample concentrations, no matter how minor. This resolution could be

compared to the relationship between the number of pixels in an image and its resultant resolution. Finally, variations in PCR efficiency have essentially no effect on obtaining an accurate DNA concentration. This is because analysis is done at the end-point once the plateau phase is reached for each reaction [54]. How quickly the reactions reach this end point or variation in efficiency between reactions is negligible.

Chamber-based digital PCR has been made commercially available using micro-wells [57] and microfluidic chambers [58-59, 78] to dilute DNA samples over hundreds of chambers of nanoliter volume, but an alternative called droplet digital PCR (ddPCR) has recently been established to improve the throughput, dynamic range, and the ease of handling the assays that were once limited to microfluidic chambers and wells [54]. Harnessing the power of droplet microfluidics, ddPCR disperses DNA samples into approximately 20,000 monodisperse droplets that simultaneously perform PCR reactions with fluorescent probes. The system then automatically feeds the droplets into a droplet flow cytometer that reads the end-point of each droplet at 32 wells per hour [54]. Bio-Rad Laboratories, Inc. has made this technology commercially available for sample-in/answer-out quantification of DNA copy number [60] (Figure 1.15).

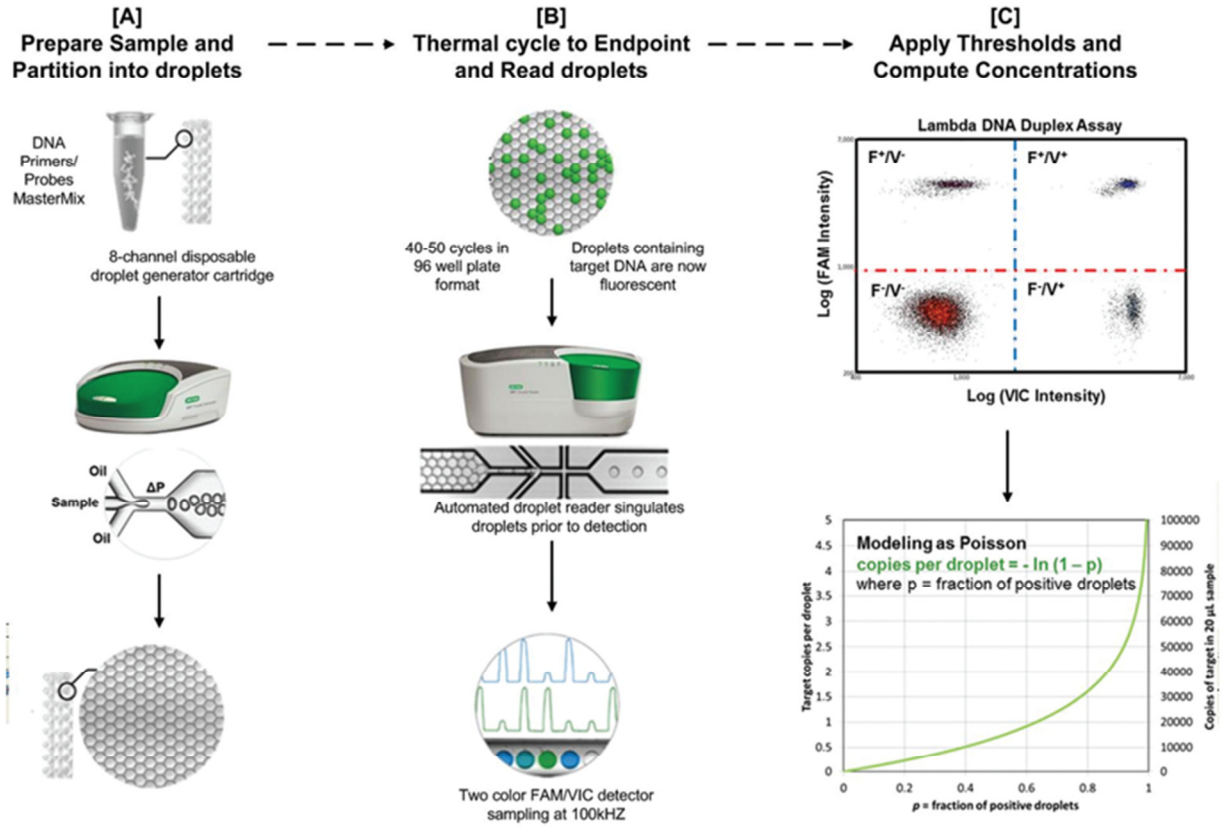


**Figure 1.15** Schematic showing the ddPCR workflow. (A) Each 20 µL sample containing the Master Mix, primers, TaqMan probes, and DNA target is loaded in the middle wells of a disposable eight channel droplet generator cartridge (pictured). Droplet generation oil (8 × 60 µL) containing the emulsion stabilizing surfactant is then loaded into the left-hand wells of the droplet generator cartridge. A vacuum is automatically applied to the outlet well (right) creating a pressure difference that, together with the geometry of the microfluidic circuit, converts the aqueous sample into stable, monodisperse, water-in-oil droplet emulsions which concentrate due to density differences from the oil phase and accumulate in the droplet collection wells of the cartridge. The droplets from each well are then transferred to one well of a 96-well plate, foil sealed, and thermal-cycled to the end-point. (B) After amplification, the plate is then loaded to a droplet reader where an autosampler aspirates the droplets and, using a microfluidic singulator, streams them single file (~1500 droplets/s) past a FAM/VIC two color fluorescence detector which samples at a rate of 100 kHz. (C) The difference in fluorescence amplitudes for droplets where amplification has or has not occurred (positive and negatives, respectively) divides the entire droplet population into four discrete clusters for a typical Fam/Vic duplex assay. These four populations are droplets containing either no target (F–/V–), one of the targets (F–/V+, F+,V–), or both targets (F+,V+). Setting a fluorescence threshold for each detection channel affords a digital method of droplet classification and computing the average number of copies per droplet based on the fraction of positive droplets and Poisson modeling.

### 1.4.3 Amplifying onto Solid Surfaces and Analysis

Amplification of DNA onto solid surfaces has been found to be useful for a variety of applications. A PCR primer is attached to the solid surface, the surface is placed in solution with PCR reagents, and amplification results in the surface being covered with copies of the template sequence. DNA-covered micro-beads have been used for detection of cancerous cells [61-62], finding genetic variations [22], and aptamer selection [63]. One specific application that couples DNA-covered micro-beads with IVC is a technique called BEAMing [23]. BEAMing combines beads, emulsions, and magnetics by amplifying DNA onto magnetic beads that are compartmentalized via water-in-oil emulsion droplets. After PCR, the beads are recovered and then analyzed with conventional flow cytometry [54]. We have started development on a technique that simplifies the BEAMing method by ligating DNA templates directly to micro-beads, thereby ensuring efficient encapsulation of template DNA and beads and preventing interaction of DNA with the oil-water interface. These details can be found in Chapter 4.

Flow cytometry is often used for rapid analysis of these particles. The basis of flow Cytometry is that single particles suspended in a liquid stream are analyzed individually in a very short amount of time by a light source, usually a laser, focused on a very small region [64]. During analysis, several detectors are pointed at the place where the stream of liquid passes through the laser beam. One detector is in line with the light beam (Called Forward Scatter, or FSC), and several detectors are perpendicular to the light beam (Called Side Scatter, or SSC). One or more of the side scatter detectors can detect fluorescence [65]. As each particle passes through the light beam, it scatters the light away and any fluorescence in or on the particle becomes excited and emits light at a longer wavelength than the light source. These changes are passed on to the detector, which analyzes changes in brightness to obtain information about the

physical and chemical makeup of each particle [65]. The results can be plotted in a histogram, which gives information of Count vs. Fluorescence Intensity.

The particles can then be separated based on statistical differences of 10-20 variables [64]. Flow Cytometry can be used to analyze particles within a wide range of sizes (e.g. 0.2 to several thousand micrometers) and can evaluate up to 100,000 particles per second [64]. Fluorescence Activated Cell Sorting (FACS) is often used to sort cells for diagnosis of health disorders, especially blood cancers, but it has many other research and clinical applications. The principle of cell sorting in flow cytometry allows this technology to separate single particles/cells physically from mixed populations. This technology allows individual particles to be physically placed into a defined location for further analysis and, if necessary, this process can be performed under sterile conditions. This capability makes flow cytometry a valuable tool for rare event (1:100,000 or even 1:1,000,000) analysis [64].

### 1.5 Concluding Remarks

The topics introduced in Chapter 1 provide the foundation for the work discussed herein, which is for the formation and passivation of sub-nanoliter droplets for high-throughput biological assay platforms. In Vitro Compartmentalization (IVC) is a robust method for the performance of high-throughput biological assays. This technology allows for the performance of as many as $10^{10}$ reactions in parallel in just 1 mL of sample volume by utilizing water-in-oil emulsion droplets. The use of small sample volumes in droplets of just femtoliters to nanoliters in size carries several advantages, such as a decrease in assay cost and time compared to assays employing microcentrifuge tubes and microtiter plates that require microliter volumes of sample. In addition, the parallelization provided by IVC allows performance of processes requiring

analysis of large amounts of samples, such as emulsion PCR [20], directed evolution and selection of genes encoding for a specific activity [5], and continuous monitoring of hormone secretions from primary tissues [25]. These are applications that would have been limited in throughput by conventional techniques like microtiter plates, which have a defined number of reservoirs per plate. Finally, the environment within emulsion droplets can be controlled and manipulated through changes in temperature, pH, salinity, and physical properties of reagents in order to perform reactions and assays of various kinds, making this technique applicable to a wide array of experiments. Performance of various reactions and assays using IVC is the major focus of this work.

Droplet microfluidics has enhanced the IVC field by providing a platform for the rapid generation of emulsion droplets of uniform size. Using standard techniques for device design and fabrication, prototypes for exploratory research can be created quickly and easily. Channel design and wettability are important properties of microfluidic devices that can control the speed, size, and effectiveness of droplet production. The t-junction channel is one of the most popular for its ease of fabrication and operation. Several hundred droplets per second can be produced using this method, and incorporation of several junctions onto a single microfluidic device can increase the rate even further. Channels must also be wetting to the carrier fluid. If water-in-oil droplets are being produced, the channels must be hydrophobic in order for droplets to form properly. Devices for rapid droplet generation, as well as methods for creating hydrophobic device channels are discussed in Chapter 2.

Selection of appropriate carrier oils and surfactants for droplet formation and stability is important. Certain types of organic oils are not compatible with the PDMS material that is used to fabricate many micro devices. As a result, fluorocarbon oils and surfactants provide a viable

alternative for use with many biological applications. Surfactants are utilized to prevent droplet coalescence and to impart biocompatibility to the inner droplet interface. These surfactants are comprised of oil and water soluble portions that assemble at the oil-water interface. The size and configuration of each portion can be changed in order to increase droplet stability and decrease negative interactions of reagents with the interface. A biocompatible surfactant system that also imparts droplet stability is introduced in Chapter 3. This system has been used for the performance of PCR and recombinase polymerase amplification (RPA) in droplets generated using droplet microfluidics.

Coupling IVC with micro-beads opens the door for a variety of applications that when coupled with flow cytometry, allow for rapid sample analysis. The polymerase chain reaction (PCR) can be used in emulsion droplets to amplify single DNA strands simultaneously without interference [20] and is often presented as droplet digital PCR (ddPCR) for quantification of absolute DNA concentration [54]. If beads modified with one of the PCR primer sequences are also encapsulated, amplification will result in the covalent attachment of many copies of the template DNA sequence onto a single bead [23]. These beads can then be analyzed rapidly via flow cytometry. Chapter 4 presents work done toward the development of high-throughput micro-bead assays for binding affinity measurements and digital PCR detection.

## 1.6 References


1. Available on the Web with the permission of Caltech's Engineering and Science Journal: http://www.zyvex.com/nanotech/feynman.html, Accessed June 5, 2014.
2. Schaller, R.R. *IEEE Spectrum* **1997**, 53-59.
3. Thompson, S.E., Parthasarathy, S. *Materials Today* **2006**, 9(6), 20-25.
4. Nguyen, N.; Wereley S.T. *Fundamentals and Applications of Microfluidics*, 2nd ed. ; Artech House, Inc.: Massachusetts, **2006**.

5. Griffiths, A.D.; Tawfik D.S. *TRENDS in Biotechnol.* **2006**, 24 (9), 395-402.

6. Brown, P.O.; Botstein, D. *Nature Genetics Supplement* **1999**, 21, 33-37.

7. http://www.ncbi.nlm.nih.gov/projects/genome/probe/doc/TechMicroarray.shtml, Accessed May 1, 2014.

8. http://www.genome.gov/10000533, Accessed May 1, 2014.

9. Check, E. *Nature* **2005**, 437, 1084-1086.

10. Kelly, B. T.; Baret, J. C.; Taly, V.; Griffiths, A. D. *Chem. Commun.* **2007**, 1773–1788.

11. Nelson, D. L.; Cox, M.M. *Lehninger Principles of Biochemistry*, 5th ed.; W.H. Freeman and Company: New York, **2008**.

12. Bohacek, R.S.; McMartin, C.; Guida, W.C. *Med. Res. Rev.* **1996**, 16, 3-50.

13. Dove, A. *Nat. Biotechnol.* **1999**, 17, 859-863.

14. Chapman, T. *Nature* **2004**, 430, 109-115.

15. Kelly, B. T.; Baret, J. C.; Taly, V.; Griffiths, A. D. *Chem. Commun.* **2007**, 1773–1788.

16. Cho, E.J.; Lee, J-W.; Ellington, A.D. *Annu. Rev. Anal. Chem.* **2009**, 2, 241-264.

17. Stoltenburg, R.; Reinemann, C.; Strehlitz, B. *Biomolecular Eng* **2007**, 24, 381-403.

18. Vaught, J.D.; Bock, C.; Carter, J.; Fitzwater, T.; Otis, M.; Schneider, D.; Rolando, J.; Waugh, S.; Wilcox, S.K.; Eaton, B.E. *J. Am. Chem. Soc.* **2010**, 132, 4141-4151.

19. Tawfik, D. S.; Griffiths, A. D. *Nat. Biotechnol.* **1998**, 16, 652– 656.

20. Williams, R.; Peisajovich, S. G.; Miller, O. J.; Magdassi, S.; Tawfik, D. S.; Griffiths, A. D. *Nature Methods* **2006**, 3 ( 7) 545– 550.

21. Griffiths, A. D.; Tawfik, D. S. *EMBO* **2003**, 22 ( 1) 24– 35.

22. Dressman, D.; Yan, H.; Traverso, G.; Kinzler, K. W.; Vogelstein, B. *Proc. Natl. Acad. Sci. U.S.A.* **2003**, 100 ( 15) 8817– 8822.

23. Diehl, F.; Li, M.; He, Y.; Kinzler, K. W.; Vogelstein, B.; Dresman, D. *Nature Methods* **2006**, 3 (7) 551– 559.

24. Bernath, K.; Magdassi, S.; Tawfik, D.S. *J. Mol. Biol.* **2005**, 345, 1015–1026.

25. Easley, C. J.; Rocheleau, J. V.; Head, W. S.; Piston, D. W. *Anal. Chem.* **2009**, 81, 9086–9095.

26. Dishinger, J.F.; Reid, K.R.; Kennedy, R.T. *Anal. Chem.* **2009**, 81, 3119-3127.

27. Whitesides, G.M. *NATURE* **2006**, 442, 368-373.

28. Reyes, D.R.; Iossifidis, D.; Auroux, P-A.; Manz, A. *Anal. Chem.* **2002**, 74, 2623-2636.

29. Manz, A.; Miyahara, Y.; Miura, J.; Watanabe, Y.; Miyagi, H.; Sato, K. *Sensors and Actuators B* **1990**, 249-255.

30. Manz, A.; Graber, N.; Widmer, H.M. *Sensors and Actuators B* **1990**, 244-248.

31. Manz, A.; Harrison, D.J.; Verpoorte, E.M.J.; Fettinger, J.C.; Paulus, A.; Ludi, H.; Widmer, H.M. *Journal of Chromatography A* **1992**, 593, 253-258.

32. Li, Paul C.H. *Microfluidic Lab-on-a-Chip for Chem and Bio Analysis and Discovery* CRC Press: Boca Raton, **2006**.

33. McDonald, J.C.; Duffy, D.C.; Anderson, J.R.; Chiu, D.T.; Wu, H.; Schueller, O.J.A.; Whitesides G.M. *Electrophoresis* **2000**, 21, 27-40.

34. McDonald, J.C.; Whitesides, G.M. *Acc. Chem. Res.* **2002**, 35(7), 491-499.

35. Seemann, R.; Brinkmann, M.; Pfohl, T.; Herminghaus, S. *Rep Prog Phys* **2012**, 75, 1-41.

36. http://www.ece.gatech.edu/research/labs/vc/theory/photolith.html, accessed April 10, 2014.

37. Manz, A.; Fettinger, J.C.; Verpoorte, E.; Ludi, H.; Widmer, H.M.; Harrison, D.J. *TrAC Trends in Anal. Chem.* **1991**, 10(5), 144-149.

38. Effenhauser, C.S.; Bruin, G.J.M.; Paulus, A.; Ehrat, M. *Anal. Chem.* **1997**, 69, 3451-3457.

39. Bhattacharya, S.; Datta, A.; Berg, J.M.; Gangopadhyay, S. *Journ Microelectromech Sys* **2005**, 14(3), 590-597.

40. Lin, B. editor, *Topics in Current Chemistry vol. 304: Microfluidics Technologies and Applications*; Springer-Verlag: Heidelberg, **2011**.

41. Sun, S.; Slaney, T. R.; Kennedy, R. T. *Anal. Chem.* **2012**, 84, 5794– 5800.

42. Abate, A. R.; Weitz, D. A. *Biomicrofluidics 5* **2011**, 014107, 1– 8.

43. Zeng, Y.; Shin, M. M.; Wang, T. Y. *Lab Chip* **2013**, 13, 267– 273.

44. Matosevic, S.; Paegel, B. M. *J. Am. Chem. Soc.* **2011**, 133, 2798– 2800.

45. Nisisako, T.; Torii, T. *Lab Chip* **2008**, 8, 287-293.

46. Zeng, Y.; Novak, R.; Shuga, J.; Smith, M.T.; Mathies, R.A. *Anal. Chem.* **2010**, 82, 3183-3190.

47. Baret, J-C. *Lab Chip* **2012**, 12, 422-433.

48. Holtze, C.; Rowat, A. C.; Agresti, J. J.; Hutchison, J. B.; Angilé, F. E.; Schmitz, C. H. J.; Köster, S.; Duan, H.; Humphry, K. J.; Scanga, R. A. *Lab Chip* **2008**, 8, 1632–1639.

49. Tadros, T. F. *Applied Surfactants-Principles and Applications*; Wiley-VCH: Weinheim,**2005**.

50. http://chemweb.calpoly.edu/jhagen/CMC_Surface_Tens.pdf, Accessed May 2, 2014.

51. DeJournette, C.J.; Kim, J.; Medlen, H.; Li, X.; Vincent, L.J.; Easley, C.J., *Anal. Chem.* **2013**, 85, 10556-10564.

52. Mullis, K.; Faloona, F.A. *Methods Enzymol.* **1987**, 155, 335-350.

53. *PCR Protocols: A Guide to Methods and Applications*, ed. Innis, M.A.; Gelfand, D.H.; Sninsky, J.J.; White, T.J., Academic Press: **1990**.

54. Hindson, B.J. et. al. *Anal. Chem.* **2011**, 83(22), 8604-8610.

55. Sykes, P.J.; Neoh, S.H.; Brisco, M.J.; Hughes, E.; Condon, J.; Morley, A.A. *Biotechniques* **1992**, 13, 444-449.

56. Vogelstein, B.; Kinzler, K.W. *Proc. Natl. Acad. Sci. USA* **1999**, 96, 9236-9241.

57. Morrison, T.; Hurley, J.; Garcia, J.; Yoder, K.; Katz, A.; Roberts, D.; Cho, J.; Kanigan, T.; Ilyin, S.E.; Horowitz, D.; Dixon, J.M.; Brenan, C.J.H. *Nucleic Acids Res* **2006**, 34, e123.

58. Warren, L.; Bryder, D.; Weissman, I.L.; Quake, S.R. *Proc Natl Acad Sci USA* **2006**, 103, 17807-17812.

59. Ottesen, E.A.; Hong, J.W.; Quake, S.R.; Leadbetter, J.R. *Science* **2006**, 314, 1464-1467.

60. Pinheiro, L.B.; Coleman, V.A.; Hindson, C.M.; Herrmann, J.; Hindson, B.J.; Bhat, S.; Emslie, K.R. *Anal. Chem* **2012**, 84, 1003-1011.

61. Herr, J.K.; Smith, J.E.; Medley, C.D.; Shangguan, D.; Tan, W. *Anal. Chem.* **2006**, 78(9), 2918-2924.

62. Medley, C.D.; Smith, J.E.; Tang, Z.; Wu, Y.; Bamrungsap, S.; Tan, W. *Anal. Chem.* **2008**, 80(4), 1067-1072.

63. Wang, J.; Gong, Q.; Maheshwari, N.; Eisenstein, M.; Arcila, M.L.; Kosik, K.S.; Soh, H.T. *Angew. Chem. Int. Ed.* **2014**, 53, 1-6.

64. Robinson, P.J. "Flow Cytometry" *Encyclopedia of Biomaterials and Biomedical Engineering* **2004**, 630-640.

65. Nolla, H., "Basic Principles in Flow Cytometry", UC Berkeley CRL Flow Cytometry Lab, http://flowcytometry.berkeley.edu/pdfs/Basic%20Flow%20Cytometry.pdf, Accessed April 23, 2014.

66. Koster, S.; Angile`, F.E.; Duan, H.; Agresti, J.J.; Wintner, A.; Schmitz, C.; Rowat, A.C.; Merten, C.A.; Pisignano, D.; Griffiths, A.D.; Weitz, D.A. *Lab Chip* **2008**, 8, 1110-1115.

67. Agresti, J.J.; Antipov, E.; Abate, A.R.; Ahn, K.; Rowat, A.C.; Baret, J-C.; Marquez, M.; Klibanov, A.M.; Griffiths, A.D.; Weitz, D.A. *PNAS* **2010**, 107(9), 4004-4009.

68. Mazutis, L.; Araghi, A.F.; Miller, O.J.; Baret, J-C.; Frenz, L.; Janoshazi, A.; Taly, V.; Miller, B.J.; Hutchison, B.; Link, D.; Griffiths, A.D.; Ryckelynck, M. *Anal. Chem.* **2009**, 81, 4813-4821.

69. Utada, A.S.; Lorenceau, E.; Link, D.R.; Kaplan, P.D.; Stone, H.A.; Weitz, D.A. *SCIENCE* **2005**, 308, 537-541.

70. Hai, M.; Bernath, K.; Tawfik, D.; Magdassi, S. *Langmuir* **2004**, 20(6), 2081-2085.

71. Bernath, K.; Hai, M.; Mastrobattista, E.; Griffiths, A.D.; Magdassi, S.; Tawfik, D.S. *Anal. Biochem.* **2004**, 325(1), 151-157.

72. Mastrobattista, E.; Taly, V.; Chanudet, E.; Treacy, P.; Kelly, B.T.; Griffiths, A.D. *Chemistry & Biology* **2005**, 12(12), 1291-1300.

73. http://www.raindancetech.com Accessed June 6, 2014.

74. Baret, J-C.; Miller, O.J.; Taly, V.; Ryckelynck, M.; El-Harrak, A.; Frenz, L.; Rick, C.; Samuels, M.L.; Hutchison, J.B.; Agresti, J.J.; Link, D.R.; Weitz, D.A.; Griffiths, A.D. *Lab Chip* **2009**, 9, 1850-1858.

75. Kiss, M.M.; Ortoleva-Donnelly, L.; Beer, N.R.; Warner, J.; Bailey, C.G.; Colston, B.W.; Rothberg, J.M.; Link, D.R.; Leamon, J.H. *Anal. Chem.* **2008**, 80(23), 8975-8981.

76. Schaerli, Y.; Stein, V.; Spiering, M.M.: Benkovic, S.J.; Abell, C.; Hollfelder, F. *Nucleic Acids Res* **2010**, 38, e201.

77. Paegel, B.M.; Joyce, G.F. *Chem. Biol.* **2010**, 17, 717-724.

78. Fan, H.C.; Quake, S.R. *Anal. Chem.* **2007**, 79, 7576-7579.

# CHAPTER 2

# PASSIVELY-CONTROLLED EMULSION GENERATORS FOR RAPID DROPLET FORMATION

## 2.1 Introduction

Droplet microfluidics combines the efficiency of in vitro compartmentalization (IVC) with the speed and precision of microfluidics to carry out a variety of biological reactions with high throughput. IVC with droplet microfluidics is efficient because of the small amount of reagents required to carry out reactions within droplets of just picoliter volume, and because of the fact that microfluidics can produce droplets at speeds greater than hundreds of kilohertz [1]. Many microfluidic devices require the use of mechanical pumps to push fluid through the channels and computer programs to control the flow rates [1]. These machines can be costly and challenging to operate without expertise, making them undesirable for use as portable devices for applications outside of the laboratory and undesirable for novices who simply need to perform exploratory research [1].

Portable microfluidic devices can be used for a variety of applications, including point-of-care testing in rural or underprivileged areas, or even for military testing for chemical and biological weapons in the field. These applications require fast results often while using only a small amount of available materials and samples, but they are not amenable to interfacing with pumps and computer programs for operation. To address this problem, Easley et al. developed a vacuum-driven microfluidic droplet generator that used only a handheld syringe for operation [20-21]. Later, Abate and Weitz described a similar system, referring to the technique as "syringe-vacuum microfluidics" (SVM). This concept involves the use of a syringe (plastic or

glass) to create a vacuum at the outlet of the microfluidic device, pulling the reagents that were previously loaded into the inlets of the device through the microfluidic channels [1]. The flow rate can be controlled by simply adjusting the strength of the vacuum, adding hydrodynamic resistors to change channel resistances, or adding "single-layer membrane valves". In this manner, the device can be passively controlled, eliminating the need for pumps, computers, and electricity [1]. We have used SVM to control the devices described in this work to form monodisperse droplet populations, which are required for many biological applications in which the number of components compartmentalized depends on droplet volume (e.g. encapsulating cells or molecules like DNA) [1-3].

Achieving monodispersity requires continuous and controlled flow of reagents, along with distinct channel geometries of which there are many available (e.g. T-junctions, flow focusing, and step emulsification) [1, 4-5]. These are described in greater detail in Chapter 1 (Section 1.2.2.). Our work utilizes a T-junction geometry in which a stream of aqueous solution is broken up into individual droplets by shear force when it comes into contact with a perpendicular flow of oil/surfactant at the droplet formation region [5, 22]. We utilize a single-channel emulsion generator with three aqueous inlets that merge into a single channel before reaching the droplet formation junction [28-29]. This provides great assay flexibility by allowing for the combination of different reagents/materials into a single droplet. We have also developed a multi-channel emulsion generator to increase the speed of droplet production. In short, we have incorporated eight alternating T-junctions onto a single microfluidic device by arranging them in a circular fashion. In this manner, droplet production can become much faster. Abate and Weitz demonstrated this concept by designing a chip with eight T-junction droplet formation regions on a single device. These junctions shared an oil inlet and an outlet for the droplets, but they each

had their own aqueous inlet, allowing for the production of droplets of different composition [1]. Others have explored parallelization as well, although their devices were not passively controlled [6, 19].

One of the attractive qualities of microfluidic devices is their potential to be used as total analysis systems that combine all aspects of an experiment, from preparing the sample to detecting assay/reaction results, onto a single device [7-8, 23]. Therefore, when using microfluidics, the detection method that will be used to analyze the assay or reaction results is an important aspect that must be considered beforehand. There are many detection methods available, including electrochemical detection, mass spectrometry, and even NMR, but optical detection is often preferred for droplet microfluidics applications, because it can be done on or off chip, does not disturb the droplets, and it gives fast and sensitive results [9]. Off-chip techniques are defined as those where light travels through air before and after hitting the droplet sample. This means that the detector and all of its parts, such as mirrors and light sources, are separate from the chip itself. These include absorption, fluorescence, luminescence, and scattering methods. There are published techniques, such as megapixel digital PCR, that maximize the benefits of this type of optical detection by allowing quantitative detection of rare PCR products from an array of up to 1,000,000 chambers at once. These chambers are arranged onto a single device, captured in a single image, illuminated via fluorescence microscopy, and then counted to get an accurate measure of DNA concentration [10]. On-chip techniques integrate the optical parts of the detector onto the microfluidic device and allow for detection using waveguides, micro lenses, mirrors, filters, and light sources directly on the chip. These methods define a sub-field called “optofluidics” [9]. This type of device is one of the closest to being a stand-alone total analysis system, since it doesn’t require manual control or interfacing of

outside devices for detection. One recent example of the power of integration of optical components onto a single device comes from Jean-Christophe Baret and colleagues. They designed devices to include micro lens arrays and mirrored surfaces, resulting in greater sensitivity in fluorescence detection of droplets and better resolution between droplets, which allowed them to achieve throughputs of 2,000 droplets per second per lens over 625 measurement points [11]. In this chapter, we will discuss two passively-controlled devices developed for rapid droplet formation, as well as droplet imaging techniques used for analyzing assays that take place within these droplets.

## 2.2 Experimental

### 2.2.1 Materials

SU-8 2035 photoresist was obtained from Microchem. Silicon wafers were purchased from Silicon Inc. 0.02-in I.D. Tygon tubing (TGY-020-5C; 0.02 in. ID, 0.06 in. OD, 0.02 in. wall) and blunt needles (NE-223PL-C 22G) were obtained from Small Parts. Aquapel was obtained from Pittsburgh Glass Works. Polydimethylsiloxane (PDMS) precursors were obtained from Dow Corning (Sylgard 184 elastomer and curing agent). Chlorotrimethylsilane was obtained from Sigma. Methanol, mineral oil, plastic weigh boats, 100 mL glass syringe (SGE), and glass slides were obtained from VWR. Novec 7500 Engineered Fluid (HFE-7500) was obtained from 3M. Krytox 157 FSH was obtained from DuPont

### 2.2.2 Hydrophobicity Studies

PDMS elastomer base and curing agent were mixed in a 10:1 ratio, poured into a plastic weigh boat, and left to cure for 35 min at 65 °C. PDMS was cut into 1 cm squares, placed on glass slides, and treated with the following conditions: Slide 1 – Three PDMS squares were exposed to

an air plasma for 45 s (Harrick Plasma), then either analyzed immediately, after 2 hours, or after sitting overnight at room temperature.; Slide 2 – Two PDMS squares were exposed to an air plasma for 45 s (Harrick Plasma), then either analyzed after 2 hours, or after sitting overnight in an oven at 65 °C.; Slide 3 – As a control for slide 1, three PDMS squares were analyzed immediately, after 2 hours, or after sitting overnight at room temperature.; Slide 4 – As a control for slide 2, Two PDMS squares were analyzed after 2 hours, or after sitting overnight in an oven at 65 °C. Analysis for each PDMS square involved pipetting 10 µL of deionized water onto the PDMS surface and visually observing the behavior of the water droplet on the surface as a simple determination of wetting capabilities.

### 2.2.3 Microchip Fabrication for Passively-Controlled Devices

#### 2.2.3.1 Single-Channel Emulsion Generator

PDMS microchips for emulsion generation were fabricated using standard soft lithography. The microfluidic channel layout was designed in Adobe Illustrator software and sent to Fineline Imaging (Colorado Springs, CO) for photomask printing at 50 800 DPI resolution (negative image). The SU-8/silicon master was fabricated using standard photolithography with channels that varied in length and depth. PDMS elastomer base and curing agent were mixed in a 10:1 ratio, poured over the master defined by photoresist (SU-8, Microchem) on a silicon wafer, and cured overnight at 65 °C. Patterned PDMS was removed from the silicon master, and holes were punched for channel access. The device was then cleaned with methanol, air dried with a nitrogen stream, then bonded immediately to a no.1 glass slide after exposure to an air plasma for 45 s (Harrick Plasma). Microchannels were then treated with Aquapel (Pittsburgh Glass Works), rinsed with methanol, and placed in an oven at 65 °C overnight prior to use. Flow control in the

microfluidic emulsion generating devices was achieved passively using a handheld, 100-mL glass syringe (SGE Analytical Science) connected to 0.02-in I.D. Tygon tubing (Small Parts). The tubing was interfaced to the device via a PDMS plug. This plug was constructed by simply punching out a large hole from a blank piece of PDMS. This hole was approximately 2 mm larger than the size of the outlet. A blunt needle was used to punch a hole for the tubing in the center of the plug. When the device was ready for use, the plug was inserted into the outlet opening on the device, and a vacuum was applied using the handheld syringe.

#### 2.2.3.2 Multi-Channel Emulsion Generator

PDMS microchips for multi-channel emulsion generation were fabricated as described in the previous section, through the bonding to a no. 1 glass slide. Next, an O-ring interface was created by using a brass cork borer of 1.8 cm diameter to punch a hole into a blank piece of PDMS, resulting in a solid, circular plug. A second hole was punched into the center of this plug with a brass cork borer of 0.5 cm diameter. The resulting plug was removed, leaving a PDMS ring behind. A small amount of PDMS elastomer base and curing agent were mixed at a 10:1 ratio, and a standard wooden tongue depressor was used to carefully smear the mixture over one side of the O-ring. The ring was then carefully placed on top of the device, with the outlet hole in the center of the ring. The entire device was cured overnight at 65 °C.

Microchannels were then treated with Aquapel coating as previously described through PDMS plug interfacing, and the device was ready to use.

### 2.2.4 Methods for Droplet Imaging

#### 2.2.4.1 PDMS Reservoirs for Droplet Segregation

Imaging chips were made by cutting an approximately 1 inch thick piece of cured, blank PDMS into dimensions of 25 x 75 mm, which is the length and width of the glass slide (VWR) to which it was bonded. The PDMS was made using the same procedure for fabricating microfluidic devices on a plain, untreated silicon wafer. Two rows of 4 holes were punched into the PDMS using a brass cork borer (1.8 cm diameter). The punched PDMS was then cleaned with methanol, air dried with a nitrogen stream, then bonded immediately to a glass slide after exposure to an air plasma for 45 s (Harrick Plasma). Each circular reservoir then treated with Aquapel (Pittsburgh Glass Works), rinsed with methanol, and placed in an oven at 65 °C overnight prior to use.

#### 2.2.4.2 Exploiting Density to Form Droplet Monolayers for Imaging

To create a monolayer of droplets for imaging, a small, plastic petri dish was filled halfway with an oil/surfactant mixture (1.8% w/w Krytox 157 FSH in HFE 7500 oil). Mineral oil was carefully layered on top of the fluorocarbon oil using a plastic transfer pipette. A single-channel microfluidic emulsion generator (Section 2.2.2.1) was used to generate droplets with phosphate buffered saline (PBS) as the aqueous phase. After 30 min, the aqueous wells were replaced with ~10 μM fluorescein, and droplets were generated for an additional 5 min. Approximately 60 μL of the emulsion was pipetted into the upper mineral oil layer in the petri dish, and droplets were allowed to descend to the interface between the two oils. Fluorescence microscopy (470 ± 20 nm ex.; 525 ± 25 nm em.) was used for spatial imaging.

#### 2.2.4.3 Droplet Monolayer Imaging in "Drop Cages"

Drop cages were prepared by spin-coating then curing PDMS onto a silicon wafer to a thickness of 150 μm. Once cured, an 8-mm diameter circular hole was punched to define the periphery of the cages. Second, 2-mm diameter circular holes were punched within the 8 mm slice in several locations, and these severed circles of PDMS were removed to define droplet imaging regions. To hold multiple cages during imaging, 11-mm diameter circular reservoirs were punched into a PDMS layer of approximately 6-mm height, and this PDMS was bonded by an air plasma treatment to a glass slide (1 mm thickness). The reservoir was filled to just less than half its volume with HFE 7500 oil containing 1.8% Krytox. Next, a drop cage (150 μm thick, 8 mm diameter, with multiple 2 mm holes) was placed on top of the more dense oil and pressed down gently with tweezers to release trapped air bubbles. Mineral oil (less dense) was then added until the drop cage was submerged, ready to accept and confine emulsion droplets. Refer to Figure 2.10 and accompanying discussion for more details.

#### 2.2.4.4 Droplet Reinjection Techniques

<u>Use of deeper channels for droplet reinjection:</u>

For reinjection into channels of 100 μm depth, emulsion droplets were loaded into the center inlet of a dual channel droplet generator [24], and the oil/surfactant mixture was loaded into the four side inlets. A syringe vacuum was applied to the outlet, and emulsion droplets were monitored as they passed by intersection of the emulsion inlet and oil inlets, providing a means for separating droplets with additional oil prior to detection.

<u>Detecting droplets using a Photomultiplier Tube (PMT):</u>

Droplets were made with a multi-channel emulsion generator using Jeffamine ED900 aqueous additive and 1.8% w/w Krytox 157 FSH in HFE 7500 oil. 3 aqueous reservoirs contained 1 μM fluorescein in PCR Buffer, 3 reservoirs contained 2x ROX dye in PCR buffer, and 2 reservoirs contained PCR Buffer (1X reaction buffer + 1% BSA). Droplets were transferred to the reinjection device for imaging in a channel of 100 μm depth.

### 2.2.5 Comparison of Droplet Size Distributions

A total of 5 devices were fabricated, each with a slightly different design. The first was the single-channel generator with varied channel lengths (7, 11 mm), channel depth of 16 μm, and a device thickness of 8 mm. Device 2 was a multi-channel generator with channel lengths of 6 and 30 mm (aqueous and oil, respectively), channel depth of 33 μm, an outlet reservoir measuring 4 mm, and a device thickness of 8 mm. Device 3 was a multi-channel generator with an O-ring adapter added to the outlet region. This device maintained the same dimensions as device 2. The outer diameter of the O-ring was 9 mm, while the inner diameter of the O-ring was 5 mm. Device 4 was a thinner multi-channel generator (3 mm thickness) with an O-ring adapter added to the outlet region. Finally, device 5 was a multi-channel generator with channel lengths of 1 and 30 mm, channel depth of 33 μm, and device thickness of 8 mm.

All emulsions were generated using 1.8% w/w Krytox 157 FSH in HFE 7500 oil and PBS buffer. Solutions were placed in proper inlets and a vacuum of 80 kPa was applied to outlet. A PDMS plug was used to interface the syringe to the device. The emulsions were then collected via pipette and imaged using the “drop cage” method. Three microliters of emulsion from each device were imaged three times and analyzed using ImageJ software to determine droplet diameters and volumes [12].

### 2.2.6 Oil/Surfactant Preparation for Use with Microfluidic Devices

The preparation of the oil/surfactant mixture used with the microfluidic devices in this chapter (1.8% w/w Krytox 157 FSH in HFE 7500 oil) is detailed in Chapter 3 (Section 3.2.2.1).

## 2.3 Results and Discussion

### 2.3.1 Single-Channel Emulsion Generator

Our PDMS/Glass, single-channel microfluidic emulsion generator (Figure 2.1) has several useful features. First, the large outlet reservoir (~350 μL) eases droplet collection and transfer. This is particularly important when generating emulsions for PCR, as additional stress placed on the droplets could cause coalescence. A pipette can easily fit into this reservoir, and droplets can be transferred directly to a PCR tube. Most microfluidic devices utilize a much smaller outlet, which allows them to simply insert vacuum-attached tubing directly into a small hole on the device. Many of these devices either are not applied to experiments that require droplet manipulation off of the chip, or they allow droplets to be collected directly into a syringe or microcentrifuge tube for incubation in a controlled environment anywhere from hours to weeks at a time before further analysis is performed [25-27]. An outlet of our size requires a method to interface the chip to the syringe vacuum. Instead of creating a small hole for tubing on the chip, we opted to place it into the center of a larger PDMS plug that fits snugly into the outlet (Figure 2.1, top right). This feature applies a steady, even pressure over the entire outlet region, allowing emulsion droplets to fill the reservoir without undergoing stress that could cause the droplets to coalesce. Another feature of the device is that the three aqueous inlets provide assay flexibility. Different reagents can be added to each inlet, allowing for on-chip mixing immediately prior to droplet formation. Finally, the device is passively controlled. Droplets were

generated using a handheld, glass syringe. Eliminating the need for mechanically-driven pumps and switches makes this device ideal for use outside of a laboratory setting. DIC images of droplets packed into the outlet region of the chip are shown in Figure 2.1 (bottom); these are the result of pulling a vacuum of ~80 kPa. HFE-7500 oil with Jeffamine-bound surfactant, (discussed in Chapter 3) was used as the carrier phase, and droplets exhibited stable packing and did not coalesce.

To further demonstrate droplet stability, while the device was still producing droplets, we added fluorescein to the central aqueous reservoir, which created a second population of droplets to be imaged in the device outlet (Figure 2.2). The fluorescent droplets are all of equal intensity, which suggests that no coalescence has occurred. If fluorescent droplets had indeed mixed with the droplets containing buffer only, the dye concentration would have been diluted, resulting in a lower visible intensity on the microscope. In addition, droplet size remained consistent, further demonstrating that none of the droplets coalesced, as this would have resulted in a population of droplets with larger diameters.

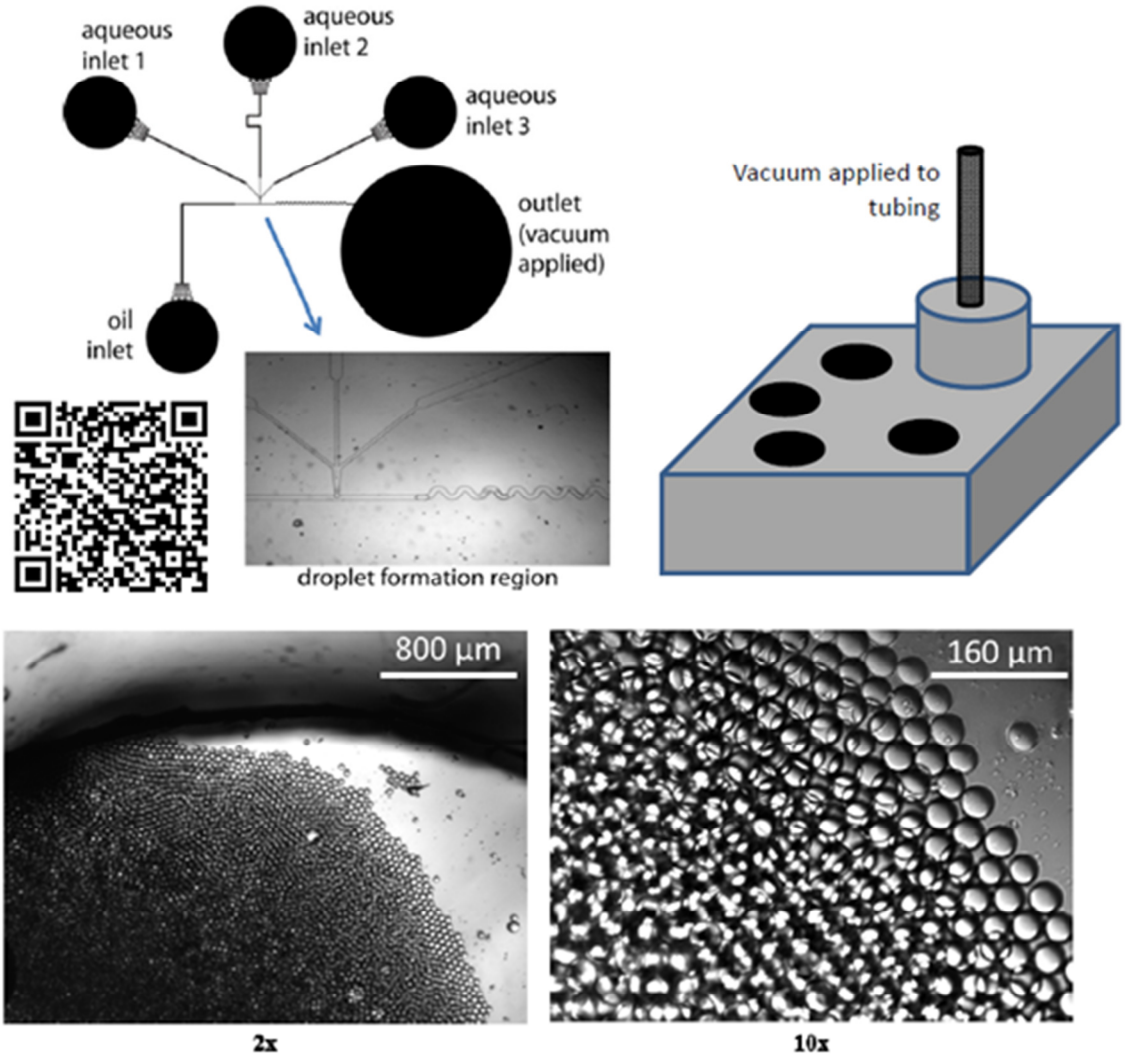


**Figure 2.1**Microfluidic droplet formation in an emulsion generating device. The passively-controlled microfluidic droplet generator with 16 µm channel depth was used to rapidly create aqueous-in-oil droplets, using Jeffamine-bound surfactants. The device has three aqueous inlets to allow for flexibility in reagent addition. The large outlet reservoir (~350 µL), interfaced to the vacuum (~ 80 kPa) via a PDMS plug that is 2 mm larger than the outlet, allows for ease of droplet collection and transfer. DIC images of droplets collected in the outlet reservoir of the device show uniform size, stable packing, and essentially no coalescence of droplets. Dimensions are: Thickness – 8 mm, Lengths – 7 and 11 mm, Depths – 16 µm, Reservoir Diameter – 8 mm.

For video of rapid droplet formation, scan the QR code with a smart phone app or visit http://www.auburn.edu/academic/cosam/faculty/chemistry/easley/research/dejournette/video001.htm

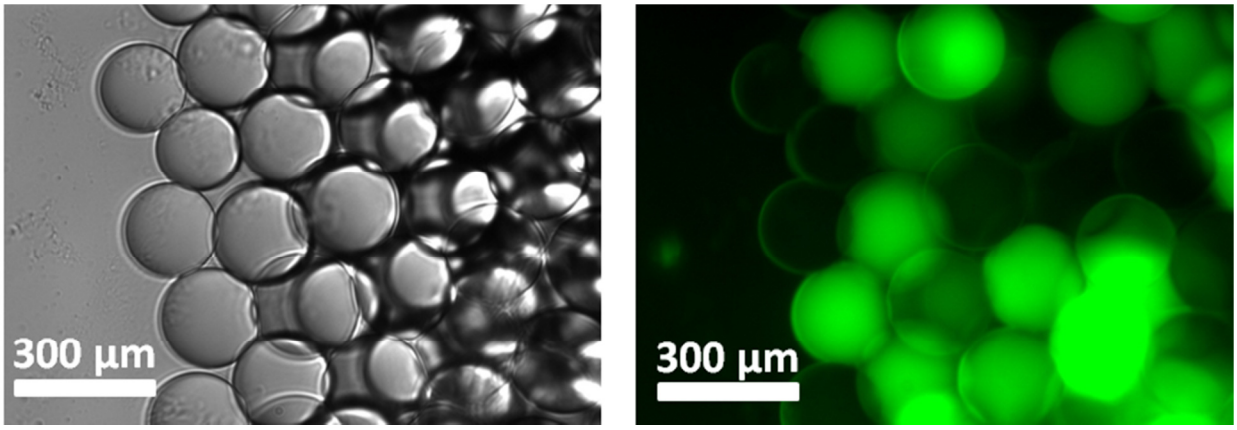


**Figure 2.2** Droplets Do Not Coalesce. While the device was running, we added ~100 µM fluorescein to the middle aqueous reservoir to further demonstrate the stability provided by this oil/surfactant combination. As fluorescent droplets were produced, the two populations were seen intact at the outlet. Above are two 20x images of the same set of droplets (DIC left, fluorescence at Ex. λ: 490 nm; Em. λ: 525 nm on right). As shown, only some droplets are fluorescent, with no evidence of coalescence.

There are several conditions that must be met in order to form water-in-oil droplets within a microfluidic device. First, the device must be hydrophobic, and the wettability of the device channels must be tailored to match that of the continuous phase. In cases where water-in-oil droplets are desired, the oil acts as the carrier phase, so channels must be hydrophobic or wetting to the oil/surfactant mixture and not to the aqueous phase [5]. It is well-documented that the plasma oxidation process used to fabricate microfluidic devices renders the surface of the PDMS hydrophilic, a property that eventually reverses on its own if the device is allowed to sit long enough [13]. Our own hydrophobicity study confirmed this result (Figure 2.3). We exposed several swatches of PDMS to an air plasma for 45 s, then tested the wettability of the surfaces with deionized water after letting the swatches sit at room temperature or at 65 °C for 0 min, 2 hours, or overnight (≈ 15 h). Our control experiments did not expose the PDMS to the air plasma at all, but tested the surface wettability under the same time constraints and temperature conditions mentioned above. The results showed that the contact angle decreases greatly immediately after exposure to the air plasma, suggesting that the surface has become hydrophilic. This contact angle then slowly increases again after two hours and even more after 24 hours. This trend was observed at both room temperature and 65 °C. If the devices sat for 43 hours, however, full recovery of surface hydrophobicity was observed, with droplet contact angles matching those of the controls. The amount of time needed for full recovery of hydrophobic surface properties is undesirable and can be improved. As a result, we use Aquapel (Pittsburgh Glass Works) to chemically treat the channels and make the devices permanently hydrophobic [1]. Aquapel is a perfluorocarbon-based glass treatment that matches the properties of our selected carrier oil, and this method has been used by other research groups as an easy way to ensure that channels and PDMS remain hydrophobic [4]. This is done by simply pulling

the solution through the channels with a syringe vacuum, immediately following with methanol, and then baking at 65 °C overnight.

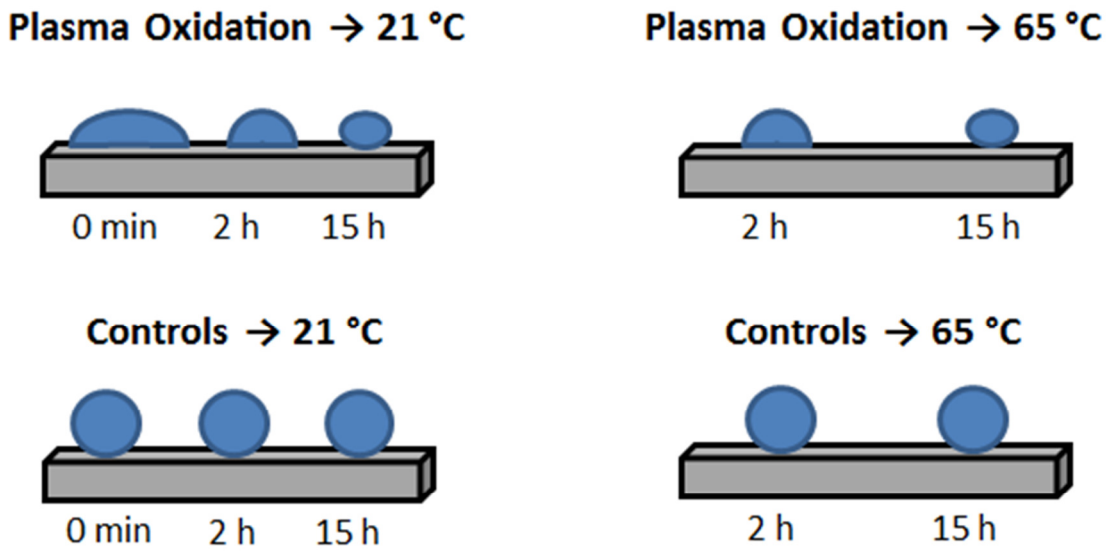


**Figure 2.3** Illustration depicting PDMS hydrophobicity study. 1 cm squares of PDMS were tested for hydrophobic recovery time after exposure to an air plasma for 45 s. 10 µL of deionized water were placed on the PDMS after sitting at room temperature (21 °C) or in an oven (65 °C) for 0 min, 2 h, or 15 h (overnight). Contact angle was greatly decreased immediately after plasma oxidation (Top Left, 0 min), but gradually increased over time at room temperature. The same trend was observed at 65 °C (Top Right). Controls at both room temperature and 65 °C (Bottom Left and Right) were not exposed to an air plasma and demonstrate that PDMS is hydrophobic in its natural state. Note: PDMS was not tested at 0 min in 65 °C due to the amount of time needed for PDMS to heat to this temperature.

Next, to form droplets we add the oil/surfactant mixture to the device first to get rid of any air bubbles that could negatively affect the flow and prevent droplet formation [1]. Because the device has been rendered hydrophobic by Aquapel, the oil is wicked into the channels without a vacuum applied. We then fill the aqueous reservoirs with solution, attach the PDMS plug, and pull the syringe plunger outward to create a vacuum and begin forming droplets. Once the aqueous phase reaches the T-junction, droplets are formed [1]. Steady flow leads to monodispersity. After formation, droplets flow into the large outlet reservoir. The PDMS plug is removed, and droplets can be collected via pipette and transferred for storage, assay performance, or analysis.

Droplet size distribution with the single-channel emulsion generator was determined by first generating emulsions with the oil/surfactant mixture and PBS Buffer. A vacuum of 80 kPa was applied to the outlet using the PDMS plug discussed previously. The emulsion was then collected and imaged to determine the diameter of each droplet and their frequencies (Figure 2.4). The device dimensions were 8 mm thickness, 7 and 11 mm channel lengths, 16 µm channel depth, and 8 mm outlet reservoir diameter. The droplets that were produced by this device were analyzed by pipetting 3 µL of emulsion into specially-made “drop cages” and imaged with a microscope, methods discussed in greater detail in Section 2.2.4.3. The average droplet diameter for this device was determined, in triplicate, to be 51 ± 14 µm. This corresponds to a droplet volume of 69 pL, which is expected based on the device dimensions.

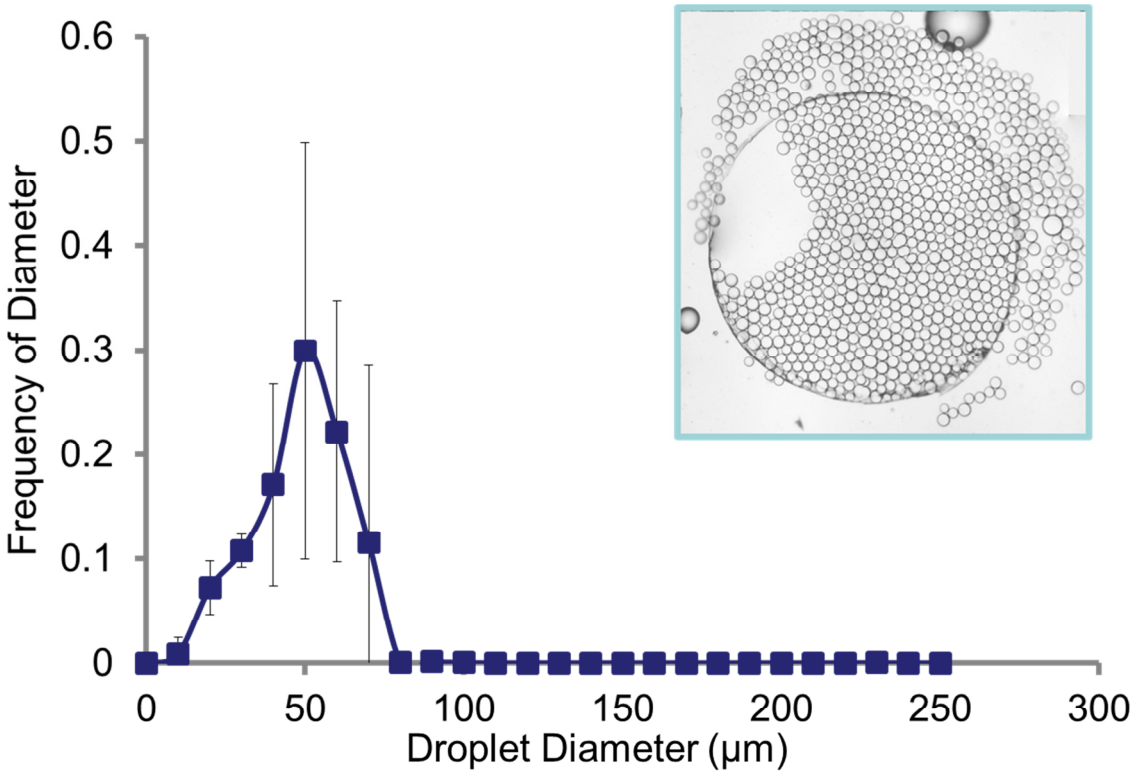


**Figure 2.4** A Monodisperse emulsion is produced by the single-channel emulsion generator. This figure shows the diameter of each droplet produced, and the frequency of these diameters. The single channel generator clearly shows a monodisperse emulsion. The majority of the droplets are 50 µm in diameter, with most droplets lying between 40-60 µm. The calculated average droplet diameter is 51 ± 14 µm. This tight distribution constitutes a monodisperse emulsion, which should serve as the standard for future devices.

### 2.3.2 Multi-Channel Emulsion Generator

The multi-channel generator was designed due to a need for increased speed of droplet production. When generating droplets for emulsion PCR (Chapter 3), the single-channel generator takes 1 hour to generate approximately 10 µL of emulsion. The minimum amount of emulsion needed to form an even layer in a standard PCR tube is 25 µL, and for added stability, we have chosen to use approximately 60 µL in our experiments. The correlation of number of droplets to droplet stability is known and demonstrated in Andrew Griffiths' use of microfine emulsions to provide added stability during emulsion PCR [14]. Our original multi-channel generator (Figure 2.5, Device 1) was able to generate emulsions for this purpose in as little as 10 min, where the droplet-generating T-junction of the single-channel device was multiplied 16 times by arranging alternating T-junctions in a circular fashion on a single device. The PDMS plug vacuum was then applied to a central outlet, and all droplets flowed into the center of the device.

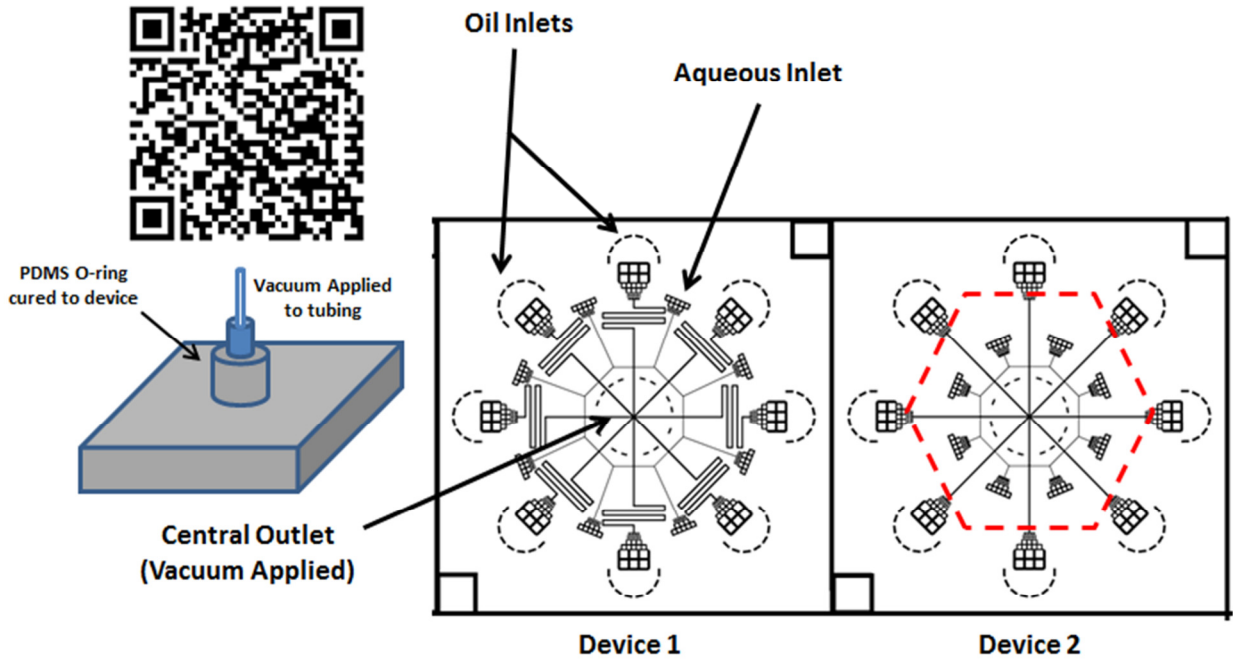


**Figure 2.5** Multi-channel microfluidic droplet generators. The passively-controlled multi-channel microfluidic droplet generator with 33 µm channel depth was used to increase droplet production speeds above the single-channel generator. The device has eight aqueous inlets and eight oil inlets that meet at alternating T-junctions to produce droplets that flow into a central outlet reservoir where the vacuum is applied. Device 1 is the standard multi-channel design, requiring individual punching and filling of all 16 inlets for droplet production. Device 2 eases fabrication by allowing the chip to be cut out in an octagonal shape (Red dashed line) that bisects all of the oil inlets. Only the 8 aqueous inlets need to be punched individually. For droplet production, the entire device is placed in an oil bath, and the aqueous reservoirs are filled individually. The central outlet reservoir is interfaced to the vacuum (~ 80 kPa) via a PDMS plug attached to an O-ring. This O-ring is cured to the device, and allows the vacuum to apply a more even pressure to the surrounding channels. Dimensions are: Thickness – 8 mm, Lengths – 6 and 30 mm, Depths – 33 µm, Reservoir Diameter – 4 mm.

For video of comparison to single-channel droplet generation speed, scan the QR code with a smart phone app or visit http://www.auburn.edu/academic/cosam/faculty/chemistry/easley/research/dejournette/video002.htm

A second design for the multi-channel emulsion generator was created to decrease the number of access holes that needed to be punched for aqueous and oil inlets. The aqueous channel lengths were shortened so that the PDMS chip could be sliced out in an octagonal shape, bisecting all of the oil/surfactant inlet channels (Figure 2.5, Device 2). Once the chip was bonded to a glass slide, the entire device could be placed in a petri dish containing oil/surfactant solution that had been poured at a level approximately half the total device height. The level of solution had to be carefully monitored to ensure that it was high enough to flow into the open channels, but low enough to prevent it from spilling over the top of the device and into the aqueous inlets. This design provided the same speed of droplet production, while allowing for easier fabrication.

This device is interfaced to the vacuum using an O-ring made from PDMS material (Figure 2.5, left). The PDMS plug is used in almost the same fashion as the single-channel generator. However, instead of inserting the plug directly into the outlet reservoir, the plug is inserted into an O-ring that was previously bonded to the chip as described in the experimental section. The multi-channel generator required an interface of this nature due to inconsistent droplet sizes. It appeared that trapped air was preventing droplets from forming. When the outlet is punched in the center of the device, if it is not perfectly centered, the vacuum will apply unequal pressure to the surrounding channels due to a difference in channel lengths, resulting in inconsistent droplet formation and size. The special, O-ring interface reduces the occurrence of these problems by moving the vacuum further away from the channels, decreasing the applied pressure. The O-ring effect is shown through a comparison study involving both multi-channel generators with and without the O-ring interface, discussed in the next section. In addition, the O-ring adapter increases the overall depth of the outlet, allowing for the collection of larger emulsion volumes.

#### 2.3.2.1 Comparison of Droplet Size Distribution

The droplet size distribution for the multi-channel emulsion generator was studied with several different variables and compared with that of the single-channel emulsion generator (Figure 2.4) to determine the best method to generate droplets quickly for different applications. Emulsions were generated on each device with surfactant/oil mixture and PBS buffered aqueous solution. A vacuum of 80 kPa was applied to the outlet using the PDMS plug discussed previously. The emulsion was then collected and imaged to determine the diameter of each droplet and their frequencies. Digital images of each device tested, along with variables and channel dimensions are shown in Figure 2.6. A single-channel generator, multi-channel generator with and without an O-ring (Device 1 in Figure 2.5), a thinner version of the multi-channel generator with an O-ring, and a new design of the multi-channel generator (Device 2 in Figure 2.5) with an O-ring were tested.

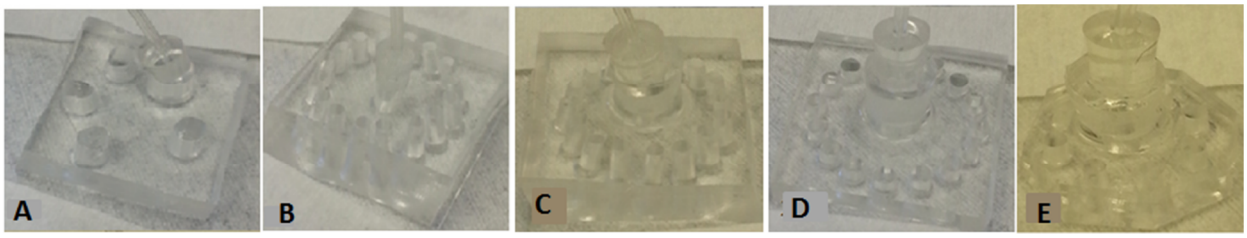


| Device | Design | Thickness | Lengths | Depths | O-ring ID-5mm OD-9mm | Reservoir Diameter |
|---|---|---|---|---|---|---|
| A | Single channel | 8mm | 7, 11 mm | 16µm | No | 8mm |
| B | Multi-channel | 8mm | 6, 30 mm | 33µm | No | 4mm |
| C | Multi-channel | 8mm | 6, 30 mm | 33µm | Yes | 3mm |
| D | Multi-channel | 3mm | 6, 30 mm | 33µm | Yes | 3mm |
| E | Multi-channel | 3mm | 1, 8 mm | 33µm | Yes | 3mm |

**Figure 2.6** Devices screened for droplet size distribution. All images show devices with vacuum plugs attached. The vacuum plug is used to create room in the chip for emulsions so they can be collected. Each plug is 2mm larger than the reservoir diameter. (A) Single- channel generator. (B) Multi-channel generator without O-ring adapter. (C) Multi-channel generator with O-ring adapter. (D) Thin multi-channel generator with O-ring adapter. (E) Newly designed multi-channel generator for "oil bath" with O-ring adapter.

For video demonstrating some of the droplet formation problems experienced with the original multi-channel generator, scan the QR code with a smart phone app or visit
http://www.auburn.edu/academic/cosam/faculty/chemistry/easley/research/dejournette/video003.htm

The droplets that were produced by these devices were imaged by pipetting 3 µL of emulsion into specially-made "drop cages", methods discussed in greater detail in Section 2.2.4.3. This process was repeated three times with each device for accurate measurement of size distribution. As shown in Figure 2.7, the single-channel emulsion generator produces a monodisperse emulsion, while the multi-channel generators do not. Based on these images, the original multi-channel device appears to produce two distinct droplet size populations. These appear to be fairly equal in the number of droplets produced. The newer device appears to produce droplets in the same manner, with a higher percentage of droplets being smaller in diameter.

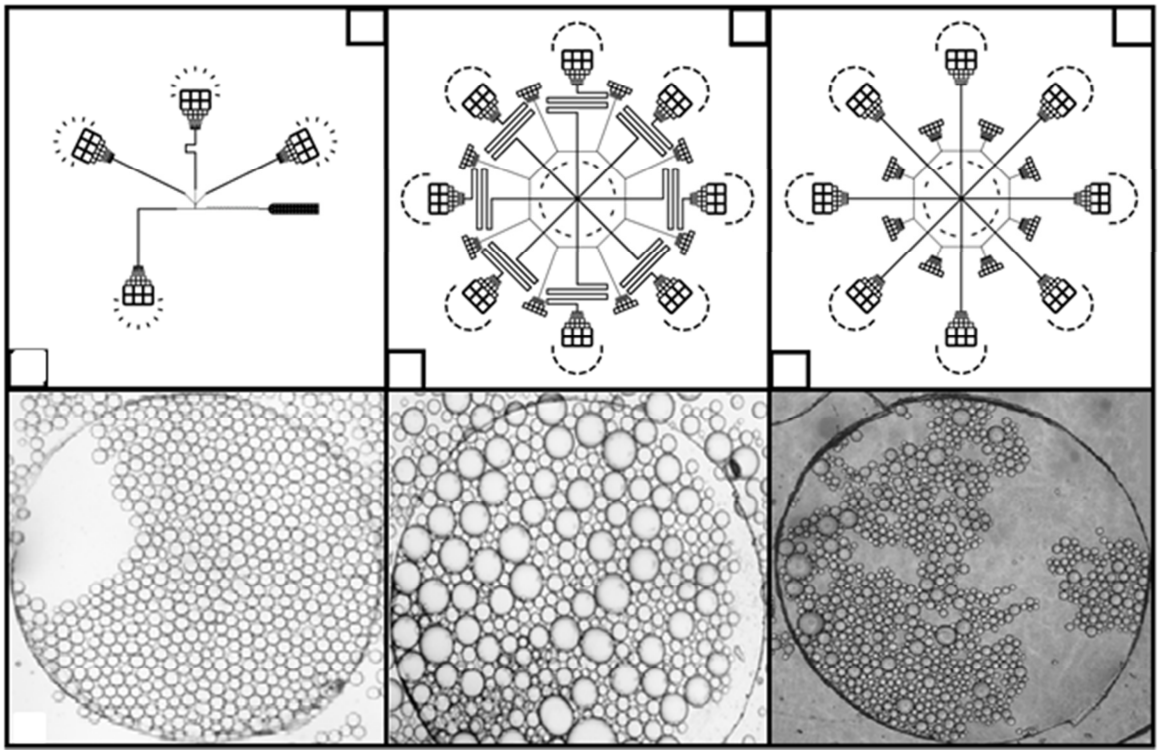

**Figure 2.7** Mask designs and resultant droplet populations trapped in "drop cages". These are the various devices tested for the droplet size distribution experiment. Droplets were generated by pulling an 80 kPa vacuum at the outlet region, and then transferred to drop cages for imaging. The single-channel generator (Left) produces a very monodisperse droplet population, while the original multi-channel generator (Center) appears to equally produce droplets of two distinct sizes. The new multi-channel generator (Right), designed for partial submersion in an oil/surfactant bath, diminishes the number of larger droplets observed, although there are still some variations in size.

A closer examination of droplet size distribution reveals that the new multi-channel generator yields a more monodisperse droplet population that is closer to the size of the single-channel generator droplets than the other ones. At first glance, the multi-channel generator appears to yield a monodisperse population around 30 µm in diameter (Figuer 2.8 A), but enlarging the range between 100 and 300 µm shows that there are a number of droplets present that are 150-200 µm in diameter. The trends observed make this device non-ideal for emulsion applications. The O-ring interface adapter eliminated these larger droplets, but it also reduced monodispersity. There is clearly a shoulder that appears next to the main droplet population, regardless of device thickness (Figure 2.8 B,C). The original multi-channel generator may have put strain on the PDMS interfaced to the channels, causing some coalescence. By adding the O-ring (Figure 2.8 B), some of the strain put on the channels by the vacuum was possibly relieved. This could lead to a reduced number of larger droplets. The majority of droplets generated showed a diameter between 20-60 µm, many of which were smaller than that from the single channel generator. The thinner device with an O-ring (Figure 2.8 C) followed the same trend. However, the distribution of droplet sizes within the population between 20 and 60 µm shifted to include more droplets of similar sizes to the single-channel generator (40-60 µm). This was an improvement over the thicker device with the O-ring.

The new multi-channel design with an O-ring (Figure 2.8 D) clearly showed that the previous issues were resolved. Droplets of larger diameter were essentially eliminated, and the main droplet population was no longer subdivided into two distinct size groups. The droplet diameters produced by this method ranged from 10 to 80 µm in diameter. The results show that the new device created a more monodisperse emulsion with an average droplet diameter of 36 ± 15 µm. The single channel device generated the majority of droplets around 50 µm in diameter,

while this device generated the majority of droplets around 30 μm in diameter. These are smaller than the single-channel generator droplets, but the two populations overlap significantly. For these reasons, this design was considered the best method thus far for rapidly generating monodisperse droplets for our applications.

In order to enhance the observed differences between droplet populations seen in Figure 2.7, the droplet diameters were plotted vs. the frequency of the area of each droplet in the image (Figure 2.8 E). In the original plot of the multi-channel generator (Figure 2.8 A), the smaller droplet population appears to occur more frequently than the larger droplet population. However, Figure 2.7 shows that the two droplet populations occur at a fairly equal rate. Therefore, Figure 2.8 E was created as a better representation of the data shown in the image (Figure 2.7). When the area of each droplet as a fraction of the total image area is taken into account, the data shows that both droplet populations occur at a fairly equal rate (Figure 2.8 E, blue trace). In addition, these results still confirm that the new multi-channel generator (green trace) produces a more monodisperse emulsion with droplets closer in size distribution to those made with the single-channel generator (red trace).

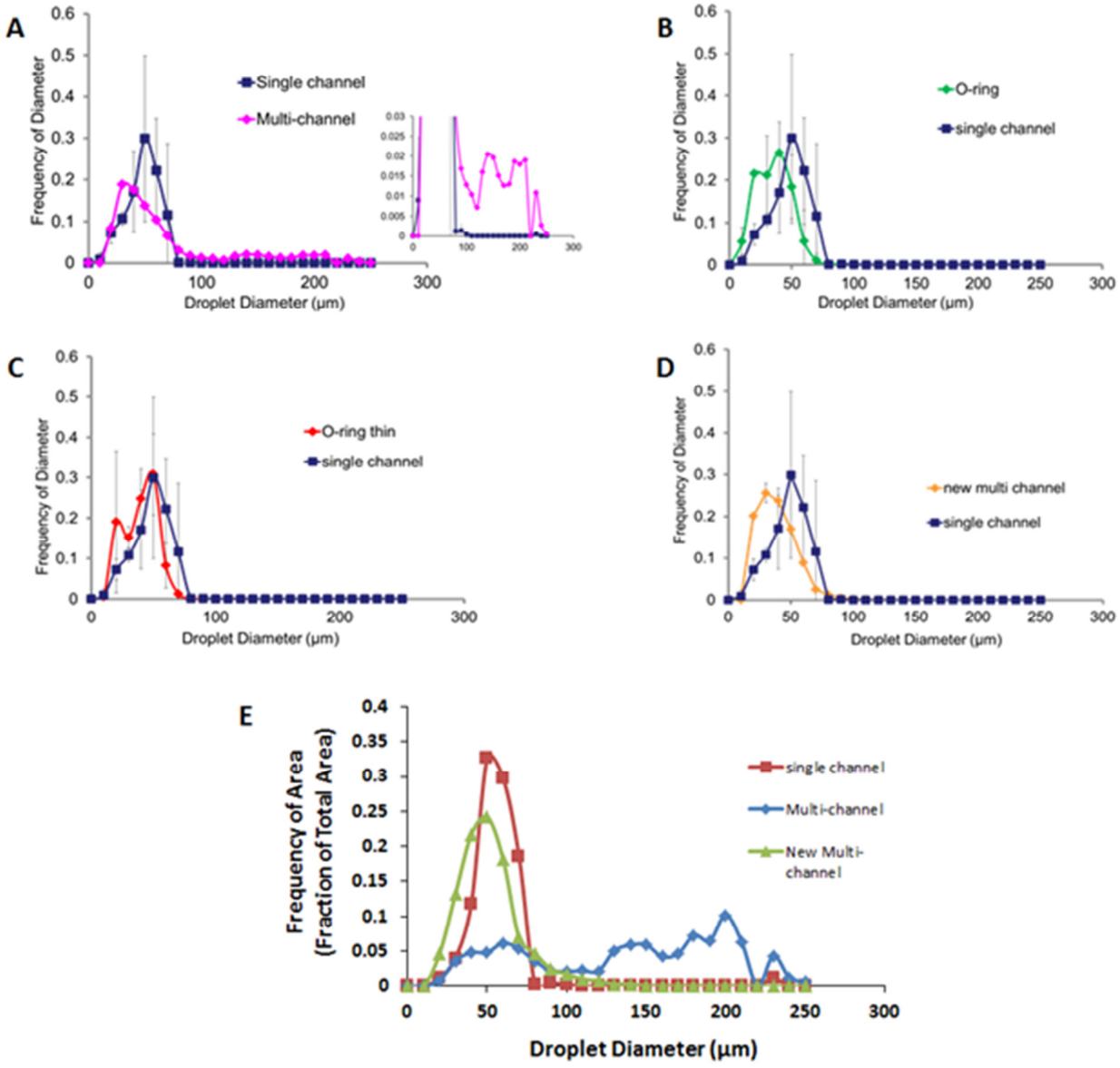


**Figure 2.8** Results of droplet size distribution experiment comparing single-channel and multi-channel generators with different variables. (A) Original multi-channel generator with PDMS plug interface to vacuum shows a population of large droplets between 100 and 250 µm in diameter that do not correlate with single-channel generator results. (B) Multi-channel generator with O-ring interface eliminates large diameter droplet population, but the main droplet population is now sub-divided into two main droplet size distributions, lacking monodispersity. (C) A thinner multi-channel emulsion generator with O-ring adapter interface still lacks monodispersity, but one droplet population is more closely correlated with the sizes produced by the single-channel generator. (D) New multi-channel generator with O-ring interface produces monodisperse emulsion with droplets that are smaller than those produced by the single-channel generator, although the peaks do overlap. (E) Single-channel, multi-channel, and new multi-channel generator diameters plotted as a function of the frequency of each droplet area in the image. Differences are enhanced here, showing that the new multi-channel generator greatly improves dispersity, with a size distribution closer to that of the single channel device.

### 2.3.3 Droplet Imaging Techniques

#### 2.3.3.1 Exploiting Density to Form Droplet Monolayers for Imaging

There are many droplet imaging methods available. Droplets are imaged for a variety of reasons, including to measure droplet size and volume, or to detect the results of reactions and assays, often via fluorescence microscopy. Flow cytometry is also used. Many of these techniques analyze one droplet at a time, which can be time consuming. Higher throughput techniques exist, such as "megapixel" detection [10] and Baret's photoresist lenses [11]. We have developed a simplified method to analyze many droplets at once by layering two different oils and using microscopy to image droplets at their interface. Several methods were utilized for droplet segregation and imaging before arriving at this point, including flattening droplets between two glass coverslips and utilizing PDMS reservoirs. Although these methods allowed droplets to flatten into a sheet for individual analysis, it was soon discovered that the fluorocarbon oil evaporated quickly, preventing imaging over long periods of time. Our latest imaging method makes the rate of oil evaporation essentially negligible by allowing the droplets to float in an abundance of oil while simultaneously forming a flat sheet.

The idea of sandwiching droplets between two layers of oil exploits the density of the water-in-oil emulsion droplets (~1.0 g/mL). The density of the fluorocarbon oil is higher at 1.6 g/mL, and the density of the mineral oil is lower at 0.8 g/mL. A petri dish was first filled halfway with fluorocarbon oil/surfactant mixture, then mineral oil was pipetted on top to form an even layer, separate from the fluorocarbon oil. 60 μL of a microfluidically generated emulsion was then pipetted into the top layer of mineral oil by first placing the tip of the pipette into the mineral oil and then releasing the droplets. The droplets which descended through the mineral

oil and stopped at the interface between the two oils. The droplets then self-assembled into a monolayer to allow analysis of many droplets at once. Figure 2.9 shows images of droplets that were prepared in this way. The figure shows that droplets were monodisperse and that many droplets could be imaged at one time, especially when using a 2X objective for imaging. In addition, the droplets maintained their original spherical shape, rather than flattening out, which allowed accurate determination of volume.

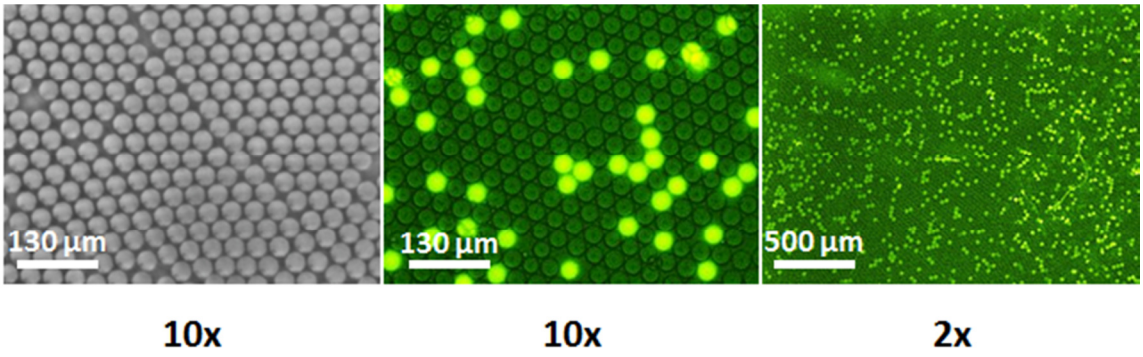


**Figure 2.9** 10X and 2X images of droplets sandwiched between two layers of oil in petri dish. A petri dish was filled halfway with 1.8% w/w Krytox 157 FSH in HFE 7500 oil. Mineral oil was then layered on top, covering the dish from wall to wall. A mixture of droplets containing either PBS buffer, or fluorescein were released into the mineral oil via pipette, and the droplets automatically settled at the interface of mineral oil (density = 0.8 g/mL) and fluorocarbon oil (density = 1.6 g/mL), due to the density of water (1 g/mL).

The main disadvantage of this technique was that the entire sheet of droplets constantly moved around in all directions. This is because the monolayer was not large enough to cover the entire petri dish from wall to wall, leaving room for the sheet to move around freely. Addition of more droplets to cover the entire dish created an alternative problem of droplet aggregation at the edges. To alleviate this problem, we constructed a solid support to trap the droplets in localized regions within the petri dish. This idea combines the PDMS reservoirs with the droplet density technique. We referred to these solid supports as "drop cages." The density of PDMS is 0.97 g/mL, which is comparable to that of water, so the cage floats at the interface between the mineral and fluorocarbon oils and traps the droplets within its borders (Figure 2.10). This technique has been used successfully for several experiments, including the droplet size distribution experiments (Figure 2.7) and for real-time monitoring of DNA amplification in droplets using recombinase polymerase amplification (RPA), detailed in Chapter 3 of this work (See Figure 3.7).

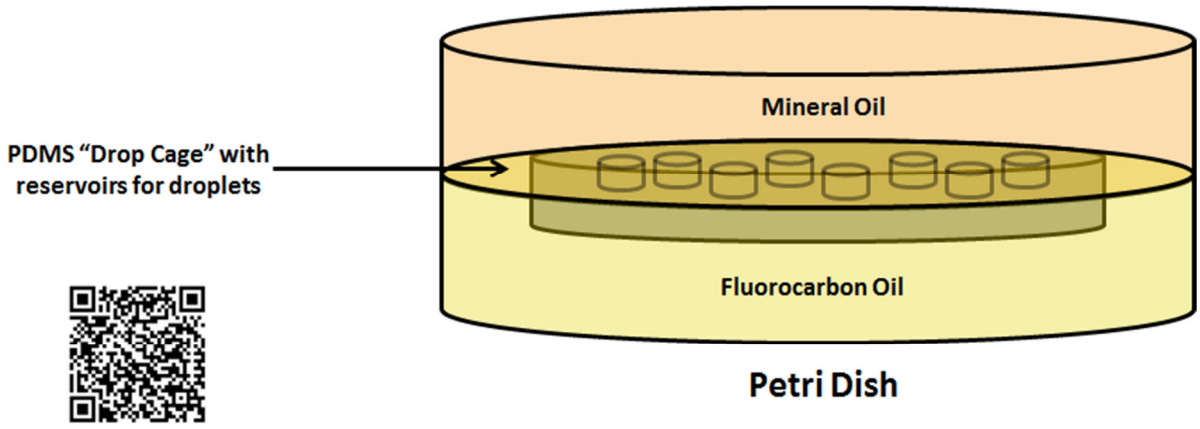


**Figure 2.10** Illustration depicting a "drop cage" inside of a petri dish. Drop cages were constructed from a thin layer of PDMS (density = 0.97 g/mL) and carefully placed at the interface between two oils. The reservoirs within the drop cage are used to entrap emulsion droplets, making imaging easier by preventing droplets from moving around the petri dish.

For video showing droplet monolayer in petri dish with and without the drop cage solid support, scan the QR code with a smart phone app or visit
http://www.auburn.edu/academic/cosam/faculty/chemistry/easley/research/dejournette/video004.htm

#### 2.3.3.2 Reinjection

Another imaging technique employed for analysis of many droplets at once involved loading droplets onto a device for imaging inside of a microfluidic channel. Compared with the double-oil method described previously, channel imaging does not allow as many droplets into the frame at one time. However, it does provide a stable support for droplets to form a monolayer, and the device can be physically moved on the microscope to image different droplets. A microfluidic chip containing a channel of 100 µm depth was frequently used for this purpose by creating only a droplet inlet hole directly at the entrance to the channel that leads to the outlet where a second, smaller hole was created for interfacing with a syringe vacuum (Figure 2.11 A). Droplets were allowed to flow into the channel and settle before imaging, providing analysis of multiple droplets at once (See Chapter 3, Figure 3.6).

For single-droplet analysis, we utilized the a droplet generating device, essentially in reverse mode, for droplet reinjection. Figure 2.11 B shows reinjection of droplets with this method as they flowed through the various parts of the design. Droplets remained intact, proving that this method can be successfully used for reinjection. Figure 2.11 C shows the device using fluorocarbon oil/surfactant from 1 inlet on each side (Left), two inlets on each side (Center), or replacing fluorocarbon oil with silicone oil (Right). This method clearly shows that injecting droplets in this way causes them to move past the droplet formation region individually with oil spacing between them. A region of interest can then be defined in a section of the channel downstream, and individual analysis of droplets can occur (Figure 2.11 C, left). Adding an additional oil inlet to each side was shown to increase the amount of space between each droplet (Figure 2.11 C, center), but it appears that this difference is not large enough to make this change necessary. Silicone oil has a higher viscosity than fluorocarbon oil and was found to have the

capability to envelop the droplets individually, further separating them from one another and reducing the chances of droplet aggregation and traveling together through the region of interest (Figure 2.11 C, right).

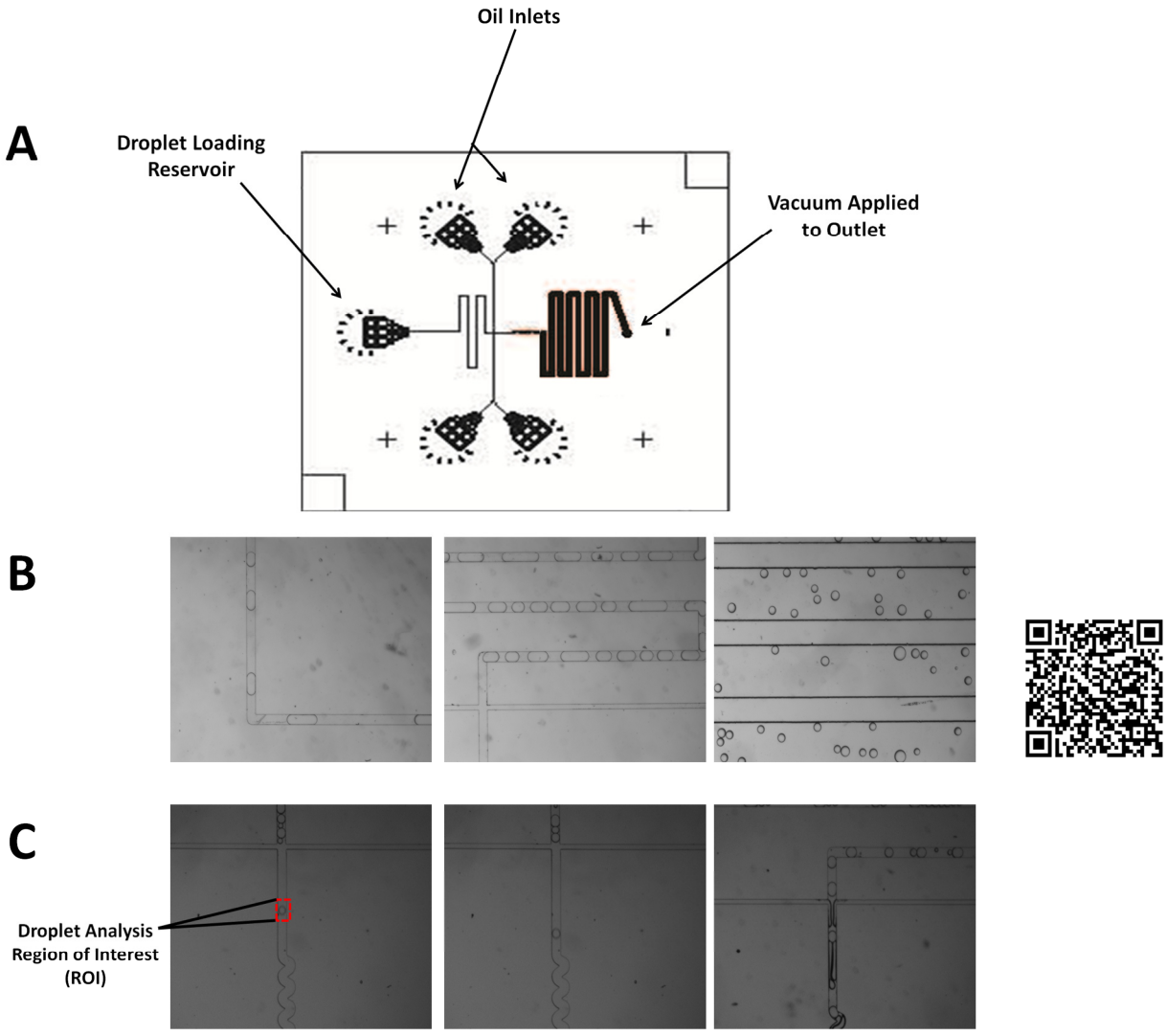


**Figure 2.11** Droplet reinjection into microfluidic device. (A) Droplet reinjection chip design. (Will depict where holes are punched for different types of reinjection.) (B) Droplets at various stages in the design after reinjection into µChopper chip. (C) Droplet spacing with 1 oil inlet on each side (left), 2 oil inlets on each side (center), or with silicone oil (right).

For video showing droplet reinjection, scan the QR code with a smart phone app or visit http://www.auburn.edu/academic/cosam/faculty/chemistry/easley/research/dejournette/video005.htm

#### 2.3.3.3 Interfacing Droplet Reinjection with a PMT

Photomultiplier tubes (PMTs) amplify photocurrents produced from the UV-Vis and near-infrared regions of the electromagnetic spectrum, allowing highly sensitive detection of light. We interfaced our droplet reinjection technique, having a defined region of interest (Figure 2.11 C, left), with fluorescence optics and a PMT for rapid, sensitive, and accurate detection of droplets in hopes of developing a method for analyzing PCR (polymerase chain reaction) products within individual droplets. Digital PCR uses Poisson statistics to estimate absolute DNA concentration by diluting DNA samples into multiple reactions of equal volume, in our case droplets, to an extent where some reactions/droplets have no template copies and others have at least one or more copies. Amplification is then allowed to take place until the plateau phase, at which point droplets are counted to obtain the fraction of positive droplets exhibiting fluorescent signal within the total droplet population [15-17]. In fact, the company Bio-Rad has acquired a system for digital PCR detection that emulsifies DNA samples, performs droplet PCR, and then individually detects fluorescent signals from each droplet with two-color capability, allowing the user to separate positive and control droplet populations [18]. With digital techniques, more droplets analyzed equate to lower levels of uncertainty within the measurements, thus Bio-Rad's system is capable of much higher precision in quantitative PCR, as much as a 1000-fold improvement. For our experiments, using the reinjection technique with PMT interfacing—as opposed to wide-field imaging of droplet monolayers—should allow for faster analysis times, provide more accurate results, and should allow us to achieve throughputs similar to those obtained by Bio-Rad.

A preliminary experiment has been performed with the PMT interface to simply determine if a signal could be obtained as droplets passed the defined region of interest. Droplets

were made with a multi-channel emulsion generator using Jeffamine ED900 aqueous additive and HFE 7500 oil with 1.8% w/w Krytox 157 FSH surfactant. 3 aqueous reservoirs contained 1 µM fluorescein in PCR Buffer, 3 reservoirs contained 2x ROX dye in PCR buffer, and 2 reservoirs contained PCR Buffer (1X reaction buffer + 1% BSA). Droplets were generated, and then the mixture of droplet populations were reinjected into a second device for analysis. The PMT was used to detect each droplet as they passed by the ROI with the following settings: 472 voltage (high); $10^{-3}$ µA/voltage – gain (High); 0.05 msec – Time (worst signal/fastest response); voltage was adjusted until a strong signal was obtained. Figure 2.12 shows that droplets are visible and pass the detector consistently, but that the fluorescent signal is the same for each droplet. This suggests that only one population of droplets generated was detected, when droplet of 3 different compositions were present. Optimization of detector settings is needed for future experiments, but this preliminary data shows that the reinjection chip can be useful for obtaining single-droplet information.

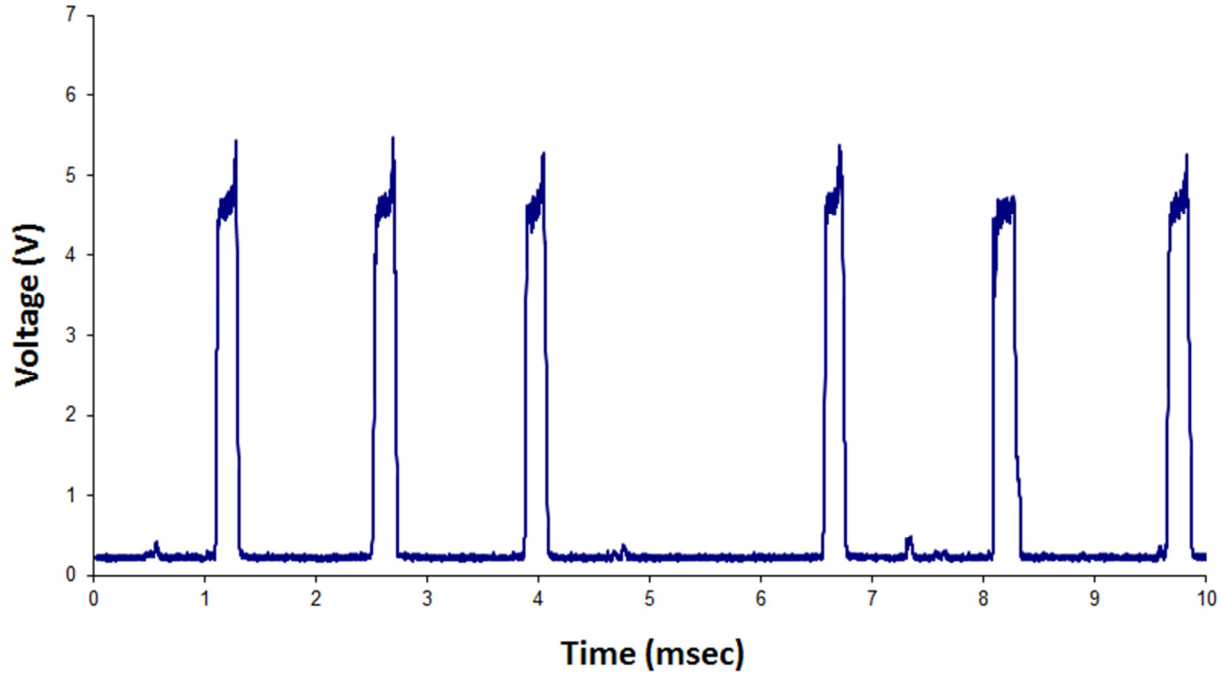


**Figure 2.12** PMT results from reinjecting droplets containing fluorescein. Droplets were made with a multi-channel emulsion generator using Jeffamine ED900 aqueous additive and HFE 7500 oil with 1.8% w/w Krytox 157 FSH surfactant, then reinjected into a second microfluidic device (Figure 2.11 A) for analysis. The PMT was used to detect each droplet as they passed by the region of interest (ROI) with the following settings: 472 voltage (high); 10-3 µA/voltage – gain (High); 0.05 msec – Time (worst signal/fastest response). The aqueous reservoirs contained either 1 µM fluorescein in PCR Buffer, 2x ROX dye in PCR buffer, or PCR Buffer (1X reaction buffer + 1% BSA), which should have resulted in detected of droplets with different intensities. However, this result was not obtained. One population of droplets was detected at a consistent rate. The beginning of the peak is the front edge of the droplet, while the end of the peak is the back edge of the droplet as it passes through the defined ROI. Although further optimization of settings is needed, these preliminary results show that the reinjection chip can be useful for obtaining single-droplet information.

## 2.4 Conclusions

We have described methods used to create two passively-controlled microfluidic devices for rapid droplet generation. The single-channel generator has three aqueous inlets, allowing for on-chip incorporation of various reagents into a single droplet. The device also has a large outlet reservoir, interfaced to a syringe vacuum through a PDMS plug, allowing for easy pipette transfer of emulsions off of the device for follow-up experiments. Droplets generated by this device are highly monodisperse and do not show signs of coalescence. A multi-channel emulsion generator was also introduced. This device greatly increased the speed of droplet generation by arranging many droplet-generating regions in a circular fashion on a single device. The multi-channel generator also utilized a PDMS plug interface to the vacuum, but was attached via an O-ring adapter bonded to the device. With these additions, emulsions could still be collected and transferred just as easily as with the single-channel generator. Several device modifications were tested to improve droplet size distribution, and these improvements in the device design led to faster production of emulsions with good monodispersity compared to those achieved with the single-channel generator.

Several droplet imaging techniques have been provided for wide-field and single-droplet analysis. For imaging of many droplets at once, monolayers were created. In one method, two layers containing oils of different densities were placed in a petri dish and used to create an interface for aqueous droplets to spread into a single layer for analysis of many droplets at one time. “Drop cage” reservoirs, which are solid supports made from PDMS, were later incorporated to trap the droplets into defined regions within the petri dish, preventing them from moving around and facilitating quantitative imaging. Another option utilized for monolayer

stability was reinjection of droplets directly into a microfluidic channel (Figure 2.10 A). Droplets were allowed to pack into this channel and settle before imaging (See Figure 3.6 C, D).

For single-droplet analysis in serial fashion, a photomultiplier tube (PMT) was interfaced with a droplet reinjection chip and used to detect droplets as they passed a defined region of interest within the channel. This proof of concept was demonstrated with emulsion droplets made using a multi-channel emulsion generator. Although droplets containing different concentrations of fluorescent material were produced, only one population of droplets was detected. Further optimization of detector settings should be performed before using this method for single-droplet analysis. With these improvements, this technique could possibly be used for droplet digital PCR (ddPCR) detection of amplified DNA sequences down to 1 copy of DNA per droplet.

## 2.5 References


1. Abate, A.R.; Weitz, D.A. *Biomicrofluidics* **2011**, 5, 1-8.
2. DeJournette, C.J.; Kim, J.; Medlen, H.; Li, X.; Vincent, L.J.; Easley, C.J. *Anal Chem* **2013**, 85, 10556-10564.
3. Holtze, C.; Rowat, A. C.; Agresti, J. J.; Hutchison, J. B.; Angilé, F. E.; Schmitz, C. H. J.; Köster, S.; Duan, H.; Humphry, K. J.; Scanga, R. A. *Lab Chip* **2008**, 8, 1632–1639.
4. Abate, A.R.; Poitzsch, A.; Hwang, Y.; Lee, J.; Czerwinska, J.; Weitz, D.A. *Phys Rev E* **2009**, 80, 026310.
5. Seemann, R.; Brinkmann, M.; Pfohl, T.; Herminghaus, S. *Rep Prog Phys* **2012**, 75, 1-41.
6. Nisisako, T.; Torii, T. *Lab Chip* **2008**, 8, 287-293.
7. Manz, A.; Miyahara, Y.; Miura, J.; Watanabe, Y.; Miyagi, H.; Sato, K. *Sensors and Actuators B* **1990**, 249-255.
8. Manz, A.; Harrison, D.J.; Verpoorte, E.M.J.; Fettinger, J.C.; Paulus, A.; Ludi, H.; Widmer, H.M. *Journal of Chromatography* **1992**, 593, 253-258.
9. Gai, H.; Li, Y.; Yeung, E.S. *Top Curr Chem* 304: 171-201, Springer-Verlag: Berlin, Heidelberg, **2011**.

10. Heyries, K.A.; Tropini, C.; VanInsberghe, M.; Doolin, C.; Petriv, O.I.; Singhal, A.; Leung, K.; Hughesman, C.B.; Hansen, C.L. *Nature Methods* **2011**, 8(8), 649-651.

11. Lim, J.; Gruner, P.; Konrad, M.; Baret, J-C. *Lab Chip* **2013**, 13, 1472-1475.

12. W.S. Rasband, ImageJ, U.S. National Institutes of Health, Bethesda, Maryland, USA, http://imagej.nih.gov/ij/, 1997–2012.

13. Vickers, J.A.; Caulum, M.M.; Henry, C.S. *Anal Chem* **2006**, 78, 7446-7452.

14. Williams, R.; Peisajovich, S.G.; Miller, O.J.; Magdassi, S.; Tawfik, D.S.; Griffiths, A.D. *Nature Methods* **2006**, 3(7), 545-550.

15. Sykes, P.J.; Neoh, S.H.; Brisco, M.J.; Hughes, E.; Condon, J.; Morley, A.A. *Biotechniques* **1992**, 13, 444-449.

16. Vogelstein, B.; Kinzler, K.W. *Proc. Natl. Acad. Sci. USA* **1999**, 96, 9236-9241.

17. Hindson, B.J.; Ness, K.D.; Masquelier, D.A.; Belgrader, P.; Heredia, N.J.; Makarewicz, A.J.; Bright, I.J.; Lucero, M.Y.; Hiddessen, A.L.; Legler, T.C.; Kitano, T.K.; Hodel, M.R.; Petersen, J.F.; Wyatt, P.W.; Steenblock, E.R.; Shah, P.H.; Bousse, L.J.; Troup, C.B.; Mellen, J.C.; Wittmann, D.K.; Erndt, N.G.; Cauley, T.H.; Koehler, R.T.; So, A.P.; Dube, S.; Rose, K.A.; Montesclaros, L.; Wang, S.; Stumbo, D.P.; Hodges, S.P.; Romine, S.; Milanovich, F.P.; White, H.e.; Regan, J.F.; Karlin-Neumann, G.A.; Hindson, C.M.; Saxonov, S.; Colston, B.W. *Anal Chem* **2011**, 83(22), 8604-8610.

18. Pinheiro, L.B.; Coleman, V.A.; Hindson, C.M.; Herrmann, J.; Hindson, B.J.; Bhat, S.; Emslie, K.R. *Anal Chem* **2012**, 84, 1003-1011.

19. Zeng, Y.; Novak, R.; Shuga, J.; Smith, M.T.; Mathies, R.A. *Anal Chem* **2010**, 82, 3183-3190.

20. Easley, C.J.; Rocheleau, J.V.; Head, S.W.; Piston, D.W. *Anal Chem* **2009**, 81, 9086-9095.

21. Easley, C.J.; Benninger, R.K.P.; Shaver, J.H.; Head, W.S.; Piston, D.W. *Lab Chip* **2009**, 9, 1119-1127.

22. Thorsen, T.; Roberts, R.W.; Arnold, F.H.; Quake, S.R. Physical Review Letters 2001, 86 (18), 4163-4166.

23. Easley, C.J.; Karlinsey, J.M.; Bienvenue, J.M.; Legendre, L.A.; Roper, M.G.; Feldman, S.H.; Hughes, M.A.; Hewlett, E.L.; Merkel, T.J.; Ferrance, J.P.; Landers, J.P. *PNAS* **2006**, 103, 19272-19277.

24. Deal, K.S.; Easley, C.J. *Anal Chem* **2012**, 84, 1510–1516.

25. Tran, T.M.; Lan, F.; Thompson, C.S.; Abate, A.R. *J. Phys. D: Appl. Phys.* **2013**, 46, 1-17.

26. Mazutis, L.; Baret, J-C.; Treacy, P.; Skhiri, Y.; Araghi, A.F.; Ryckelynck, M.; Taly, V.; Griffiths, A.D. *Lab Chip* **2009**, 9, 2902-2908.

27. Kumaresan, P.; Yang, C.J.; Cronier, S.A.; Blazej, R.G.; Mathies, R.A. *Anal. Chem.* **2008**, 80 (10), 3522-3529.

28. Kenis, P.J.A.; Ismagilov, R.F.; Takayama, S.; Whitesides, G.M. *Acc. Chem. Res*. **2000**, 33, 841-847.

29. Pompano, R.R.; Liu, W.; Du, W.; Ismagilov, R.F. *Annu. Rev. Anal. Chem.* **2011**, 4, 59-81.

# CHAPTER 3

# FORMATION AND CHARACTERIZATION OF BIOCOMPATIBLE SURFACES WITHIN PICOLITER DROPLETS

## 3.1 Introduction

On the basis of cellular compartmentalization in nature, in vitro compartmentalization (IVC) is the utilization of water-in-oil emulsion droplets of fL–nL volume to perform $>10^{10}$ reactions simultaneously in just 1 mL of sample volume [1-2]. This capability can greatly reduce assay cost and time and can open the door to a variety of high-throughput experiments, such as directed evolution of proteins and RNAs [1, 3-4], screening large libraries for rare mutations [2-3], and fluorescence-activated cell sorting (FACS) of emulsion-induced products [3, 5-6]. In recent years, droplet microfluidics has emerged to reinvigorate the IVC field, providing more flexibility, lab portability, and increased likelihood of automation [7-11].

One major advantage gained by droplet microfluidics is the ability to produce highly monodispersed emulsions. These emulsion-generating devices typically employ hydrocarbon or fluorocarbon oils for aqueous droplet encapsulation. Since emulsion formation is thermodynamically unfavorable [12], biological experiments requiring in-droplet incubation, particularly those at elevated temperature, will generally need an oil–surfactant mixture. The surfactant molecules assemble at the oil–water interface and act to lower surface tension, prevent adsorption to the surface, and counteract coalescence by creating an energy barrier [12]. The goal is to find a surfactant–oil combination that achieves the delicate balance between droplet stability and biocompatibility. Nonionic fluorosurfactants are ideal for this purpose, allowing use of hydrophobic–lipophobic fluorocarbon oils [13-15] with the biologically inert interior that

nonionic headgroups provide through minimization of charge interactions [12]. There are a few fluorosurfactants available commercially, but these either have an ionic headgroup or do not maintain maximum droplet stability for certain applications [12, 16-17].

Others have noted the apparent lack of commercially available, nonionic fluorosurfactants and opted to synthesize their own block copolymer surfactants. Currently, one of the most prominent methods used to impart biocompatibility to aqueous-in-oil droplets is to synthesize a triblock copolymer surfactant composed of perfluoropolyether and polyether blocks. After several synthetic steps, an amide bond is formed between a carboxylated, perfluorocarbon chain and a polyetherdiamine [16, 18]. The resulting perfluoropolyether-polyethylene glycol triblock copolymer (PFPE-PEG-PFPE) surfactant, termed "EA-surfactant" or "KryJeffa" in subsequent uses, has emerged as one of the most effective biocompatible surfactants for generating aqueous-in-fluorocarbon oil droplets, particularly with microfluidic emulsion generators [16, 19-20]. It allows generation of highly biocompatible droplet surfaces while maintaining the heat stability of the starting material. However, this surfactant is not commercially available, and production involves a multistep synthetic route that requires expertise in synthetic organic chemistry, creating a barrier to widespread adoption in the field. Herein, we describe a simple alternative to synthetic modification of surfactants to impart biocompatibility. We have observed that aqueous-in-oil droplet surfaces can be made biocompatible and heat stable by merely exploiting binding interactions between polyetherdiamine additives in the aqueous phase and carboxylated perfluorocarbon surfactants in the oil phase, demonstrating that synthesis of a biocompatible surfactant is unnecessary for certain biological applications.

The Weber group has thoroughly studied the noncovalent complex formation between a carboxlyated perfluoropolyether (Krytox 157 FSH) and heterocyclic, nitrogenous bases in flourous solvents [21-23]. Depending on solvent properties, the two can associate through a mixture of both hydrogen and ionic bonding. We rely on a similar property and show evidence that the carboxylated PFPE, Krytox 157 FSH (referred to herein as "Krytox"), will bind directly to primary amines in a similar fashion. A polyetherdiamine (PED), Jeffamine ED900 (referred to herein as "Jeffamine"), is shown to bind with Krytox to form a noncovalent structure similar to synthetic nonionic fluorosurfactants (PFPE/PED or PFPE/PED/PFPE), thereby imparting biocompatibility to aqueous/perfluorocarbon oil interfaces.

The binding interaction was confirmed with various methods, including FT-IR spectroscopy, NMR spectroscopy, electrospray ionization mass spectrometry (ESI-MS), and fluorescence microscopy. FT-IR and NMR spectroscopy clearly show that Jeffamine binds with Krytox. Additional electrospray ionization mass spectrometry (ESI-MS) and FT-IR evidence, akin to results from the Weber group [21-23], indicates that the binding can facilitate extraction of Jeffamine from aqueous solution into perfluorocarbon oil. Other primary amines, such as ethylenediamine or amine-labeled DNA, show evidence of binding to Krytox as well.

Using Jeffamine as an aqueous additive and Krytox in perfluorocarbon oil, biocompatible droplets of picoliter volume were formed that were stable at 95 °C and useful for DNA amplification (polymerase chain reaction (PCR) and recombinase polymerase amplification (RPA)) and homogeneous immunoassays. Droplets formed with polyetherdiamine aqueous additives are stable enough to withstand temperature cycling during PCR (30–40 cycles at 60–94 °C) while maintaining biocompatibility, and the reaction efficiency of RPA is shown to be similar to that with a covalently modified surfactant (KryJeffa). Since our approach utilizes

commercially available reagents and does not involve synthetic steps or separation/purification steps, it should allow users without expertise in synthetic chemistry to generate biocompatible droplet surfaces capable of supporting DNA and protein analysis at the subnanoliter scale.

## 3.2 Experimental

### 3.2.1 Materials

Krytox 157 FSH was obtained from DuPont, and Jeffamine ED900 and ethylenediaminetetraacetic acid (EDTA) were obtained from Sigma. $NH_4OH$, $NaH_2PO_4 \cdot H_2O$, $Na_2HPO_4 \cdot 7H_2O$, NaCl, methanol, acetone, acetone-$d_6$, 4-(2-hydroxyethyl)piperazine-1-ethanesulfonic acid (HEPES), $CaCl_2$, NaOH, HCl, NaCl, Corning plate reader assay plates (96-well, flat bottom, black polystyrene), Whatman filter papers (55-mm circles), Acrodisc syringe filters (0.2 μm HT Tuffryn), mineral oil, half-skirt 96-well PCR plates, a 100 mL glass syringe (SGE), glass slides, PCR tubes, and BSA were obtained from VWR. Novec 7500 Engineered Fluid (HFE-7500) was obtained from 3M. RPA enzyme kits and reagents were obtained from TwistDx, with probe DNA from Biosearch Technologies. Unless otherwise specified, all other DNA was obtained from Integrated DNA Technologies (IDT). Fluo-4 pentapotassium salt (cell-impermeant), Platinum *Tfi* DNA Polymerase with reaction buffer $MgCl_2$, and sulforhodamine 101 were obtained from Life Technologies.

Materials for fabrication of the microfluidic emulsion generator (See Chapter 2, Figure 2.1) are included here. SU-8 2035 photoresist was obtained from Microchem. Silicon wafers were purchased from Silicon Inc. 0.02-in I.D. Tygon tubing and blunt needles were obtained from Small Parts. Aquapel was obtained from Pittsburgh Glass Works. Polydimethylsiloxane (PDMS) precursors were obtained from Dow Corning (Sylgard 184 elastomer and curing agent).

DNA sequences are included herein. Amine-labeled DNA: 5'/5AmMC6//iSp18//iSp18//iSp18/TCA GCC ATT CGA ATC GTA CT -3' ; fluorescent complementary sequence: 5'- /56-FAM/AGT ACG ATT CGA ATG GCT GA -3'; Rox-labeled DNA for reference droplets: 5'-/56-ROXN/ CTT TCC TAC ACC TAC G, template DNA for PCR float tests (cDNA obtained by RT-PCR from mouse RNA): 5'- **AAG CAG GTC ATT GTT TCA ACA TGG** CCC TGT TGG TGC ACT TCC TAC CCC TGC TGG CCC TGC TTG CCC TCT GGG AGC CCA AAC CCA CCC AG GCT TTT GTC AAA CAG CAT CTT TGT GGT CCC CAC CTG GTA GAG GCT CTC TAC CTG GTG TGT GGG GAG CGT GGC TTC TTC TAC ACA CCC AAG TCC CGC CGT GAA GTG GAG GAC CCA CAA GTG GAA CAA CTG GAG CTG GGA GG**A AGC CCC GGG GAC CTT CAG ACC TTG GCG**-3' and corresponding double-quenched ZEN probe (Taqman format): 5'- TGT TGG TGC ACT TCC TAC CCC TG -3'; template DNA for droplet PCR: 5'-**TCC ACT CCT TTT CAT CTG CC**T TCC TTT TCT CCA TCG AGG TCC AGG TGA CCA TTG GTT TCG GCG GG**C GCA TGG TGA CAG AGG AAT**-3' and corresponding double-quenched ZEN probe (Taqman format): 5'- CCT GGA CCT CGA TGG AGA AAA GGA -3'; RPA forward primer (RPA_F-primer): 5'- GGT AAA GGT GTC GTG GAA CTA TCT AGC GGT GTA C -3' ; RPA reverse primer (RPA_R-primer) : 5'- TTT GTT TGA TAC CTT AGC CTA ATA CCC GAT T -3'; and RPA template sequence: 5'- TCG TGG AAC TAT CTA GCG GTG TAC GTG AGT GGG CAT GTA GCA AGA GGG TCA TCA TTC GAA TCG TAC TGC AAT CGG GTA TTA GGC TA -3') were obtained from Integrated DNA Technologies (IDT). RPA probe: 5'- GTA CGT GAG TGG GCA TGT AGC AAG AGG GTC A3C HT1 CGA ATC GTA CTG CAT CGT TCT CCC AGT AGT AAG -3' was obtained from Biosearch Technologies, where "3" = dT-FAM fluorescent label, "H" = tetrahydrofuran, and "1" = dT-BHQ1 quencher label.

### 3.2.2 Surfactant Optimization

#### 3.2.2.1 Krytox Preparation

Krytox 157 FSH ("Krytox") was converted to its carboxylate salt form. 20 g of Krytox and 180 g of methanol were combined in a glass dish and gently stirred. Concentrated $NH_4OH$ was then added drop wise until the solution cleared. The mixture was placed on a microplate shaker at 240 rpm for approximately 10 min then filtered by vacuum filtration to remove residual solvent, rinsed with fresh solvent, and allowed to dry over the vacuum for 5 min. The product was dissolved in pure HFE 7500 oil at a previously-determined optimal concentration of 1.8 % w/w. The mixture was passed through a 0.2 μm pore syringe filter prior to use.

#### 3.2.2.2 Optimal Krytox Concentration for Droplet Stability

Solutions of 2%, 1%, 0.1%, 0.01%, and 0.001% w/w Krytox in HFE 7500 oil were made by simply dissolving surfactant in oil. At each concentration, two separate mechanical emulsions were produced by vortexing, containing the following aqueous phases: 31 μM $CaCl_2$ and 1 μM EDTA in one emulsion, and 300 nM Fluo-4 $Ca^{2+}$ binding dye in the other emulsion. At each surfactant concentration, the two emulsions were combined, and aqueous solutions of the two were combined as a positive control. Two emulsions, made with HEPES buffer and 2% w/w oil/surfactant, were combined and used as the negative control. All emulsion combinations and controls were heated to 95 ºC for 30 min on an analog heating block (VWR), and fluorescence emission of Fluo-4 was measured at excitation/emission wavelengths of 494/506 nm on a Filter Max F5 Multimode Microplate Reader (Beckman Coulter).

### 3.2.2.3 Optimal Jeffamine Additive for Biocompatibility

Jeffamine M600 (9 PEG/4 PPG units), ED600 (9 PEG/4 PPG units), ED900 (12 PEG/5 PPG units), and ED2003 (26 PEG/11 PPG units) were investigated. A 1.8% w/w Krytox 157 FSH in HFE 7500 oil solution was prepared as mentioned previously (Section 3.2.2.1). A heat stability test was done by adding 1.8% w/w Krytox 157 FSH in HFE 7500 oil and deionized water containing 0.75% Jeffamine additive to a microcentrifuge tube at a 2:1 ratio. The solution was vortexed for 30 sec and allowed to settle for 1 min before heating to 95 °C for 10 min. The EDTA destabilization test was performed by adding 0.5 M EDTA to the Jeffamine additive solutions and generating emulsions in the same manner. Finally, an acid destabilization test was performed by adding 1 M $H_2SO_4$ to the Jeffamine additive solutions and forming emulsion in the same manner.

A real-time PCR (qPCR) "float test" was done by monitoring amplification with and without each Jeffamine additive. 20 μL of 1.8% w/w Krytox 157 FSH in HFE 7500 oil was loaded into individual PCR wells on a 96-well plate. 20 μL of amplification mixture containing 0.75% w/v Jeffamine PCR additive were carefully layered on top of this oil, avoiding emulsion generation. 30 μL of mineral oil were layered on top of the aqueous phase. The 96-well plate was covered with plastic film, and the following temperature cycling program was performed: initial denaturation at 94°C for 2 min; cycles of 94°C for 15 s and 60°C for 1 min; total of 30 cycles. Amplification without oil/surfactant present was monitored as a positive control.

### 3.2.2.4 Biocompatibility Optimization

To determine the concentration of additive needed to allow PCR biocompatibility, two PCR amplification tests were designed. Jeffamine ED 900 was used as a PCR additive at final

concentrations of 7.5% (75 mg/mL), 0.75%, 0.075%, or 0.0075% w/v by diluting in D.I. H2O and adding to the PCR amplification mixture. 20 μL of each PCR solution (D.I. H2O, Jeffamine additive, S-4 1% BSA, 42 pM template, 50 nM Taqman Probe, 0.2 μM Fwd/Rev Primer, 1.5 mM MgCl2, 1X Platinum *Tfi* Reaction Buffer, 0.2 mM dNTPs, 0.1 U/μL Platinum *Tfi* DNA Polymerase) were loaded into individual PCR wells on a 96-well plate. The 96-well plate was covered with plastic film, and the following temperature cycling program was performed: initial denaturation at 94°C for 2 min; cycles of 94°C for 15 s and 60°C for 1 min; total of 50 cycles. Amplification without Jeffamine as an additive was monitored as a positive control, and amplification without additive or template was monitored as the negative control.

The second test monitored amplification in the presence of two oil/surfactant combinations: 1.8% w/w Krytox in HFE 7500 oil, and pure HFE 7500 oil. 20 μL of each oil/surfactant combination were loaded into individual PCR wells on a 96-well plate. 20 μL of amplification mixture containing either 0.75% or 0.075% w/v Jeffamine PCR additive were carefully layered on top of this oil, avoiding emulsion generation. 30 μL of mineral oil were layered on top of the aqueous phase. The 96-well plate was covered with plastic film, and the following temperature cycling program was performed: initial denaturation at 94°C for 2 min; cycles of 94°C for 15 s and 60°C for 1 min; total of 50 cycles. Amplification without oil/surfactant present was monitored as a positive control.

#### 3.2.2.5 Synthesis of Covalently-Modified Surfactant KryJeffa

The synthetic procedure used to prepare KryJeffa follows previously reported methods [16, 18]. Briefly, thionyl chloride (2.4 mL, 33.33 mmol) was added into a solution of Krytox 157 FSH (50 g, 6.67 mmol) in HFE 7100 oil (125 mL). After the mixture was refluxed overnight under

nitrogen, the solvent and the excess $SOCl_2$ was removed under vacuum. The resulting pale yellow oil was dissolved in HFE 7100 oil (100 mL). Dimethylaminopyridine on polystyrene (2.2 g, 6.67 mmol) and a solution of Jeffamine ED 900 (2.83 mL, 3.33 mmol) in tetrahydrofuran (50 mL) was added into the solution. After stirring for 24 h, the reaction mixture was filtered through Celite and concentrated under vacuum. The residue was further dried in vacuum to yield KryJeffa (48 g, 92%) as a colorless oil. FT-IR Spectroscopy, $^{1}H$ NMR, and $^{19}F$ NMR were performed to confirm formation of the product. FT-IR ($cm^{-1}$): 1730 (CO). 1H NMR (250 MHz, Acetone-*d*6): δ 3.88(bs), 3.58 (bs), 2.22 (s), 1.41 (s). Peaks are referenced to acetone-*d*6 at 2.05.

### 3.2.3 Qualitative Testing of Emulsions

#### 3.2.3.1 Ionic Strength Test

Emulsions were generated by vortexing, using two types of oil/surfactant combinations: 1.8% w/w Krytox in HFE 7500 oil or Jeffamine-bound Krytox in HFE 7500 oil. Several dilutions of PBS were made from a stock solution (100 mM Phosphate, 150 mM NaCl). Jeffamine ED 900 was added to each dilution at a concentration of 0.75% w/v. A second set of PBS dilutions were made at the same concentrations, and 1.5 mM $MgCl_2$ was added to each solution along with 0.75% w/v Jeffamine. Emulsions were made from each PBS solution by adding 100 ・L oil/surfactant and 50 ・L of aqueous solution to a micro-centrifuge tube and vortexing for 30 s. 150 ・L of mineral oil were then added to the top of each emulsion, and the tubes were heated to 95 °C for 10 min on a heating block. Digital images of each emulsion in tubes were captured immediately before and after heating. Images were captured again after allowing emulsions to sit at room temperature overnight.

#### 3.2.3.2 pH-dependence of Interaction

Tests were performed using either pure HFE 7500 oil or 1.8% w/w Krytox in HFE 7500 oil and 75 mg/mL Jeffamine in either 0.01 M HCl (pH ≈ 2), 0.01 M NaCl (pH ≈ 7), or 0.01 M NaOH (pH ≈ 12). FT-IR spectroscopy and mass spectrometry were used to determine the extent of direct binding in different pH environments.

### 3.2.4 Analytical Techniques for Evidence of Direct Binding

#### 3.2.4.1 FT-IR Spectrometry

1.8% w/w Krytox carboxylate salt in HFE 7500 oil was added to a 50 mL centrifuge tube. Jeffamine solution (75 mg/mL in PBS) was layered onto the oil–surfactant mixture, avoiding emulsion formation. The layers were incubated and rocked overnight at RT. Then, the aqueous phase was removed, and ~400 μL of each surfactant–oil combination was added to a KBr demountable cell. After sample loading, the FT-IR system (IR Prestige-21, Shimadzu) was flushed with $N_2$ for 20 min before scanning in % transmittance mode (16 scans, 2 $cm^{-1}$ resolution, 2000–1500 $cm^{-1}$ range, square triangle apodization). Pure HFE 7500 oil was used to rinse the cell between scans and for background spectra.

#### 3.2.4.2 Mass Spectrometry

Binding of Krytox to Jeffamine was performed in pure HFE 7500 oil or 1.8% w/w Krytox in HFE 7500 oil. Each sample was diluted in acetone and then analyzed by LC/MS (Waters Acquity UPLC and Q-Tof Premier) using positive electrospray ionization.

#### 3.2.4.3 NMR Spectroscopy to Assay Binding

For $^{19}F$ NMR, Jeffamine and Krytox were mixed directly at a 1:10 ratio by weight in acetone-$d_6$, incubated overnight, and then analyzed. For proton NMR, 1.8% w/w Jeffamine-bound Krytox in HFE 7500 was dried (rotary evaporator, Heidolph) and then centrifuged for 50 min at 15 000 rcf; ~3 drops of the top layer were dissolved in acetone-$d_6$ and then analyzed. A 250 MHz NMR spectrometer (Bruker) was used, with 64 scans for proton NMR and 3500 scans for $^{19}F$ NMR.

#### 3.2.4.4 DNA/Surfactant Binding Experiment

Using microfluidics (See Chapter 2, Figure 2.1), droplets were generated with 1.8% Krytox in HFE 7500 oil and a mixture of DNA (600 nM amine-modified primer, 500 nM FAM-labeled anti-primer) as the aqueous phase. After mixing with control droplets (only FAM-labeled anti-primer), fluorescence microscopy (470 ± 20 nm ex.; 525 ± 25 nm em.) was used for spatial analysis.

### 3.2.5 Biocompatibility with Three Biochemical Assays

#### 3.2.5.1 Droplet PCR

Aqueous droplets were filled with a PCR amplification mixture (D.I. $H_2O$, 0.75% w/v Jeffamine, 1% BSA, 50 nM probe, 0.2 μM primers, 1.5 mM $MgCl_2$, 1× Platinum *Tfi* Reaction Buffer, 0.2 mM dNTPs, 0.1 U/μL Platinum *Tfi* Polymerase) and either zero, 160 fM, or 16 pM template using separate microfluidic devices (See Chapter 2, Figure 2.1). Negative controls contained 16 pM template without Jeffamine additive. Emulsion PCR was carried out on a CFX96 qPCR system (BioRad). Droplets were imaged in a microfluidic channel via confocal fluorescence

microscopy along with reference droplets (50 nM ROX-labeled DNA, 50 nM probe; 1% BSA; 1× buffer).

Droplets for performing DNA amplification by PCR were generated by pulling a vacuum of approximately 70 kPa to a single-channel emulsion generating microfluidic device (See Chapter 2, Figure 2.1), using 1.8% w/w Krytox in HFE 7500 oil as the carrier phase. The aqueous inlets were filled with amplification mix for PCR (D.I. H2O, 0.75% w/v Jeffamine, 1% BSA, template DNA, 50 nM Taqman Probe, 0.2 μM Fwd/Rev primer oligos, 1.5 mM MgCl2, 1X Platinum *Tfi* Reaction Buffer, 0.2 mM dNTPs, 0.1 U/μL Platinum *Tfi* DNA Polymerase). Solutions contained either none, 160 fM, or 16 pM template. A separate solution of amplification mix, containing 16 pM template and no Jeffamine, was also made as a negative control to show that Krytox inhibits PCR. Separate microfluidic chips (See Chapter 2, Figure 2.1) were used for each template concentration. After emulsifying all of the solution, droplets were transferred from the device outlet to individual PCR tubes. 60 μL mineral oil was layered on top of each emulsion, and PCR products were generated using a CFX1000 Thermal Cycler with CFX96 qPCR detection system (BioRad) and the following temperature cycling program: initial denaturation at 94°C for 2 min; cycling at 94°C for 15 s and at 60°C for 1 min; total of 35 cycles. An aqueous solution of amplification mixture (no oil) containing 16 pM template was used as a positive control, and a solution containing no template was used as a negative control. After thermal cycling, sample droplets were mixed with reference droplets by pipetting, and they were transferred to a single microfluidic channel for imaging via confocal microscopy. Reference droplets (50 nM ROX-labeled DNA, 50 nM Taqman probe; 1% BSA; 1X Platinum *Tfi* Reaction Buffer) were generated using a separate droplet-generating device (**Figure 3.6 B-C**).

#### 3.2.5.2 Droplet RPA

RPA solutions were prepared and used to dissolve a lyophilized enzyme mixture (TwistDx). To avoid premature reaction, sample and activation solutions were mixed on ice, and then, droplets were generated using a microfluidic device (See Chapter 2, Figure 2.1) on ice. For end-point measurements, droplets were collected for 1 h, incubated off chip at 37 °C for 30 min, and then placed back on ice prior to imaging at room temperature in a microfluidic channel.

RPA solution was prepared (700 nM Fwd & Rev primers, 200 nM RPA probe, 1.9 mg/mL BSA, and 89 ・L rehydration buffer) and used to dissolve a lyophilized enzyme mixture (TwistDx). Half of this enzyme mixture was used to make an activation solution (22.4 mM MgOAc), and the other half was used to make sample solutions containing either a reference dye (110 nM S-6 Sulforhodamine 101) with no DNA template or templates of varying concentrations (160 fM or 16 pM). The template and reference solutions were kept on ice, mixed with activation solution in a 1:1 ratio, and then again cooled on ice to avoid premature reactions at room temperature. The aqueous inlets of the microfluidic device were filled with the template/amplification mixtures for RPA. Droplets for RPA were then generated by keeping the microfluidic chip on ice and pulling a vacuum of approximately 70 kPa. 1.8% w/w Krytox in HFE 7500 oil was used as the carrier phase, and a separate chip was used for each RPA solution. For end-point measurements, droplets were collected for 1 hour then transferred to individual tubes for incubation at 37 °C. Each emulsion was incubated for 30 min on a standard PCR thermal cycler (Eppendorf). The tubes were then placed on ice to stop the reaction. After incubation, sample droplets were mixed with reference droplets in a 1:1 ratio, and they were transferred to a single microfluidic channel for imaging via fluorescence microscopy.

For stable and immobile droplet monolayer imaging during the RPA efficiency experiment, droplets were imaged inside "drop cages," in which a thin PDMS layer (density ≈ 0.97 g/mL, similar to aqueous droplets) was suspended between HFE 7500 oil (density ≈ 1.6 g/mL) and mineral oil (density ≈ 0.8 g/mL) as a simple method to trap and immobilize aqueous droplets into a monolayer between the two oils. The full assembly on the glass slide was then placed into the microscope stage-top incubator (Tokai Hit) and allowed to thermally equilibrate to 37 °C for 30 min. For imaging RPA in droplets, 0.3 μL of each microchip-generated emulsion was added into the 2 mm diameter cages by dispensing directly above the interface between the HFE 7500 and mineral oils. This approach generated a monolayer of droplets that were stable and immobile for fluorescence microscopy during RPA reactions (~10 min), serving as a measurement of reaction efficiency. A detailed protocol on constructing drop cages can be found in Chapter 2.

#### 3.2.5.3 Proximity FRET (pFRET) Protein Assay

The pFRET assay, a FRET version of the proximity ligation assay [30, 31] was conducted by combining 94 nM fluorophore- and quencher-labeled antibody oligonucleotide probes, 94 nM insulin, and 560 nM connector oligonucleotide, for a final volume of 60 μL. The assay response was measured on a Filter Max F5 Multimode Microplate Reader (Beckman Coulter and Molecular Devices). The plate wells either contained no surfactant with 110 μL HFE 7500 S-5 oil, 110 μL HFE 7500 oil with 1.8% Krytox surfactant, or 110 μL HFE 7500 with 1.8% Jeffamine-bound Krytox (**Figure 3.6A**).

### 3.2.6 Microchip Fabrication and Droplet Formation

Detailed Methods for this procedure are outlined in Chapter 2 of this text.

## 3.3 Results and Discussion

### 3.3.1 Evidence of Krytox-Diamine Binding

The proposed direct binding of a polyetherdiamine to a carboxylated perfluorocarbon surfactant is depicted in Figure 3.1. The amphipathic nature of surfactants allows them to prevent coalescence and reduce surface tension as they collect at oil–water interfaces, where their hydrophilic moiety is available to bind to aqueous additives. The water-soluble portion of Krytox is the carboxylate headgroup, and the oil-soluble portion is the perfluoropolyether backbone, having a similar structure to that of the perfluorocarbon oil. As depicted in Figure 3.1, a polyetherdiamine (PED), Jeffamine, is added to aqueous solution, and an emulsion is formed by using a microfluidic emulsion generator. Our evidence shows that the Jeffamine additive binds to the perfluoropolyether (PFPE), Krytox, at the oil–water interface, rendering the droplet surfaces biocompatible toward processes such as DNA amplification and protein sensing. Evidence shown herein and in the literature [21-23] suggests that the interaction could be taking place through a mixture of ionic and hydrogen bonding. This system is favorable in that it allows biocompatible, heat-stable droplets to be formed without requiring synthetic chemistry to modify the surfactant headgroup.

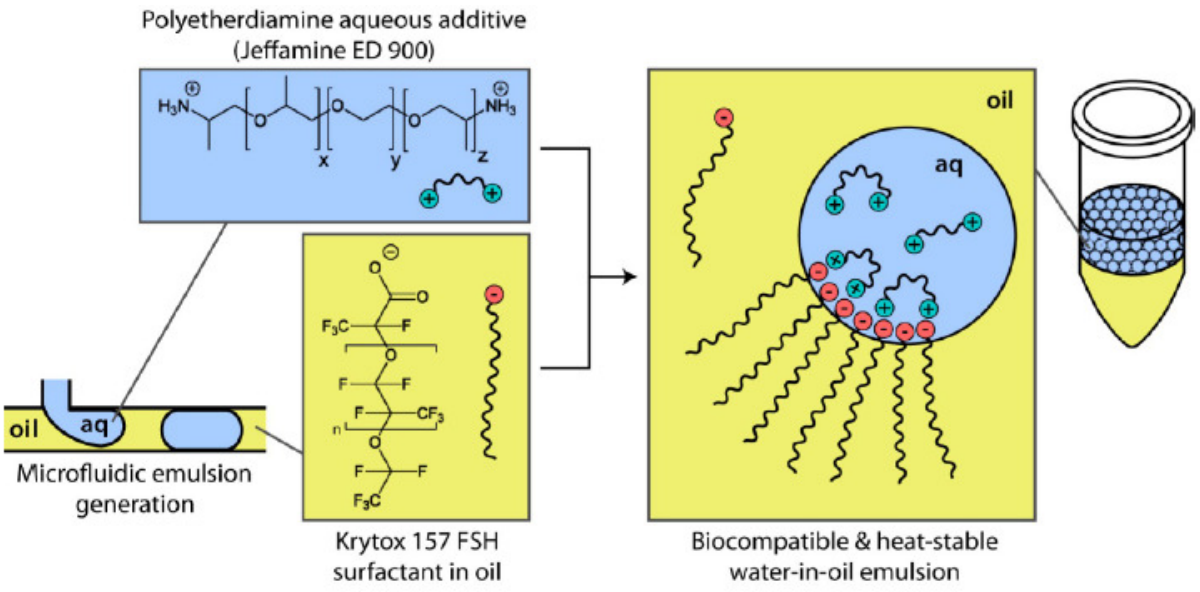


**Figure 3.1** Direct binding of surfactant to a polyetherdiamine. The unmodified surfactant, a carboxylated perfluoropolyether called Krytox, is dissolved in perfluorocarbon oil (HFE 7500). In emulsions, the anionic headgroup moves to the oil–water interface and binds to the polyetherdiamine aqueous additive (Jeffamine). This provides a biocompatible interface for biological processes and assays, without requiring synthetic chemistry.

Reprinted with permission from [42]. Copyright 2013 American Chemical Society.

Several techniques were used to show evidence of the binding interaction between Krytox and Jeffamine. Since binding likely occurs between the carboxylic acid group of Krytox and the primary amine groups of Jeffamine, we first chose FT-IR spectroscopy to monitor Krytox carbonyl stretches that would change upon binding. Figure 3.2A illustrates the changes that the carbonyl stretch undergoes upon binding of the carboxylic acid to the primary amine. Peak assignments for asymmetric $CO_2$ stretches of many carboxylic acids and carboxylates appear in the range from 1700 to 1540 $cm^{-1}$, and several studies have shown that perfluorinated carboxylic acid stretches are shifted to higher energy [24-25]. For comparison, we synthesized KryJeffa [16, 18] (covalently linked Krytox and Jeffamine), and its FT-IR spectrum (black trace) matches well with that of previous reports [24-25], showing the product peak at 1729 $cm^{-1}$ and remaining Krytox carboxylic acid at 1770 $cm^{-1}$. In contrast, the "Krytox carboxylate," which refers to the ammonium carboxylate salt of Krytox, has a carbonyl stretch that appears at 1685 $cm^{-1}$ (blue trace). With the addition of Jeffamine (blue-green trace), we observed a Krytox carbonyl peak shift to 1702 $cm^{-1}$ likely due to a binding interaction, as well as a broad signature of primary amine in the oil at 1626 $cm^{-1}$. This amine signature increased with Jeffamine concentration and was not present in the oil blank (red trace) or the Krytox-free oil exposed to Jeffamine overnight (orange trace), indicating that Jeffamine binding and extraction into the oil is dependent upon Krytox. The Jeffamine-bound Krytox sample showed a carbonyl stretch at a distinctly different energy than the Krytox or the KryJeffa product. This suggests that Krytox and Jeffamine participate in a binding interaction that is possibly ionic in nature.

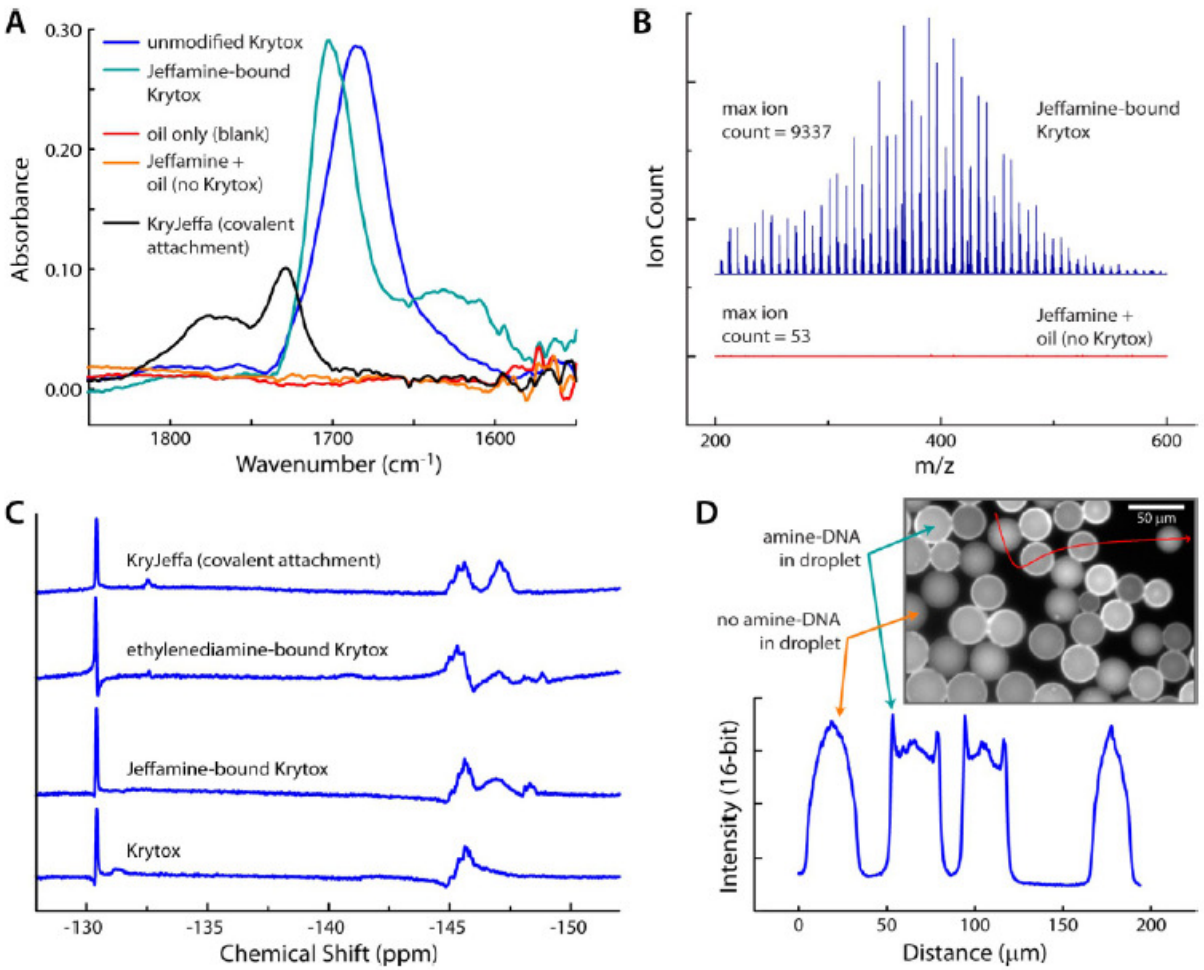


**Figure 3.2** Evidence of direct binding. (A) FT-IR evidence of Jeffamine/Krytox interaction and comparison to the covalently modified product, KryJeffa (black trace). (B) ESI-MS showed that Jeffamine extraction into HFE 7500 oil was dependent upon the presence of Krytox in the oil. (C) NMR spectra of the starting material (Krytox; bottom trace), Jeffamine-bound Krytox (second from bottom), ethylenediamine-bound Krytox (third from bottom), and the covalently modified surfactant, KryJeffa (top trace). Primary amine bound Krytox spectra show distinct patterns different from both the starting material and the covalent product. (D) Fluorescence microscopy shows that amine-labeled DNA collects at the oil–water interface, while non amine-labeled DNA is evenly dispersed.

We then used an LC/MS system with positive ESI to measure the relative amounts of Jeffamine extracted into HFE 7500 oil, in the presence or absence of Krytox surfactant (Figure 3.2B). The spectrum of oil containing Krytox (blue trace) shows strong PEG and PPG signatures from the Jeffamine with a maximum ion count of 9337, while there is no evidence of these patterns in the pure HFE 7500 oil spectrum (orange trace) with a maximum ion count of only 53. This supports the Krytox-mediated dissolution of Jeffamine into HFE 7500 oil. NMR spectroscopy also suggests a binding interaction. After mixing Jeffamine and Krytox acid at a 10:1 ratio in deuterated solvent and leaving the mixture to sit overnight, we were left with a clear solution ready for NMR analysis. $^{19}F$ was used to determine if interactions between Jeffamine and Krytox (Figure 3.2C; second trace from bottom) would show a clear spectral change compared to Krytox alone (bottom trace). The original structure of Krytox (Figure 3.1) was used to assign peaks. The NMR data shows clear changes signified by the disappearance of a peak at −132 ppm and the appearance of a sharp peak near −148 ppm. In addition, a peak at −146 ppm is changed from a singlet to a doublet. On the basis of results reported in the literature [26], these peaks can be assigned to the ~CF group in closest proximity to the carboxylic acid (−132 ppm) and its movement upfield upon the interaction of Krytox with a primary amine (−148 ppm). A peak corresponding to the ~CF group inside the repeating unit of Krytox (−146 ppm) is also changed into a doublet upon binding to a primary amine [26]. To confirm the interaction chemistry, we mixed a smaller diamine, ethylenediamine, with Krytox and collected the $^{19}F$ NMR spectrum of the mixture (Figure 3.2C; third trace from bottom). This data shows a similar signature to that of Jeffamine-bound Krytox, suggesting that the binding chemistry occurs in the same fashion for other diamines. The spectrum of the covalently modified Krytox, KryJeffa (Figure 3.2C; top trace) [16,18], showed clear differences from the starting material spectrum

(Krytox) and from the diamine-bound spectra, with the ~CF group in closest proximity to the carboxylic acid only moving slightly upfield (−133 ppm), and the appearance of the ~CF doublet peak being much sharper (−147 ppm). A peak that remains constant in all spectra is the presence of a sharp peak at −131 ppm. This corresponds to a ~$CF_2$ group along the perfluorocarbon backbone that is further away from the carboxylic acid headgroup [26]. Because of its distance away, it feels little or no effect after a binding interaction has taken place. Collectively, the FT-IR, MS, and NMR data strongly suggests that Jeffamine and Krytox participate in a binding interaction, and prior work suggests that this could be a combination of charge-based and hydrogen bonding interactions [21-23].

Fluorescence microscopy provided a final confirmation of the binding interaction. We generated emulsions containing amine-labeled ssDNA and its fluorescently labeled complementary sequence on a microfluidic device (See Chapter 2, Figure 2.1). Using fluorescence microscopy, it was possible to determine the position of the amine-DNA within the droplets using its labeled complementary sequence. Figure 3.2D shows a mixture of droplets containing the double-stranded fluorescent DNA/amine-DNA complex with droplets containing only the fluorescent complementary sequence (no amine-DNA). The control droplets (no amine-DNA) gave a spherically symmetric fluorescence image, while amine-DNA containing droplets showed clear evidence of surface fluorescence. A plot of fluorescence intensity versus distance (Figure 3.2D, lower trace) shows sharp intensity spikes at the edges of the amine-DNA containing droplets and no intensity spikes in the control droplets, suggesting again that the surfactant interacts with primary amines. This test confirms our prior findings and shows that Krytox is capable of binding to different classes of primary amines, opening the door to a variety of possibilities in surface-based biological assays within picoliter volume droplets.

### 3.3.2 Surfactant Optimization Techniques

#### 3.3.2.1 Optimal Surfactant Concentration for Droplet Stability

A calcium-sensitive fluorescent dye was used to determine droplet stability at different Krytox surfactant concentrations, with detailed methods described above. Any increase in fluorescence above the negative control was consistent with droplet coalescence, or emulsion destabilization, since this brought the $Ca^{2+}$ ions into contact with their fluorescent indicator (Fluo-4). Figure 3.3 shows the results of this test. As the concentration of Krytox decreases, the fluorescence intensity increases. This demonstrates how destabilization is preferred when there is less Krytox present. At 2% w/w, the increase is not much higher than that of the negative control (NC), and when we decrease to 1% w/w Krytox, this number essentially doubles. However, upon decreasing further, the intensity spikes to approximately five times higher than the 2% mark. This is significant destabilization, which led to the conclusion that Krytox concentration should be kept between 1 and 2% w/w in order to ensure droplet stability. A working concentration of 1.8% w/w was chosen for all future experiments, because it lies within the determined range, and was determined to be optimal by other research groups [16].

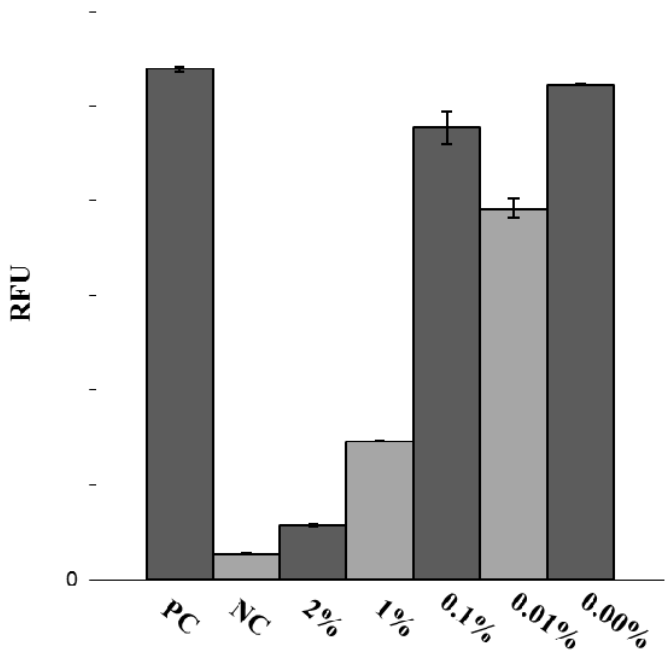


**Figure 3.3** The optimal concentration of surfactant in oil for maximum droplet stability was determined to be ~2 % w/w. After creating mechanical emulsions containing either 31 μM $CaCl_2$ and 1μM EDTA , or 300 nM $Ca^{2+}$ at each concentration, the two emulsions were mixed and heated to 95 °C for 30 min. Any increase in fluorescence above the negative control is consistent with droplet coalescence, or emulsion destabilization.

#### 3.3.2.2 How Size and Geometry of PEG Additive Affect Droplet Stability

Several additional in-house-developed tests were performed in order to optimize conditions for binding of polyetherdiamine (Jeffamine) to a carboxlyated, perfluorocarbon surfactant (Krytox). Different sizes and geometries of Jeffamine were chosen to determine which would provide the most assay biocompatibility after bonding to Krytox. Jeffamine M600 (9 PEG/4 PPG units), ED600 (9 PEG/4 PPG units), ED900 (12 PEG/5 PPG units), and ED2003 (26 PEG/11 PPG units) were investigated. A prefix of 'M' distinguishes a monoamine from a diamine, which is labeled with the prefix 'ED'. These choices allowed us to test the effects of size and geometry on droplet formation and stability. A monoamine, having a single binding group, should bind S-8 in a 1:1 ratio with surfactants. A diamine, having the ability to bind two surfactants, could form either 1:1 binding or 2:1 (Krytox:Jeffamine) binding. All of the Jeffamine groups were reacted using the same standard protocol mentioned previously. qPCR and emulsion heat stability tests were used to determine which of the polyetheramines provided both droplet stability and biocompatibility.

Jeffamine ED 900 was determined to be the best candidate for droplet stability, and Figure 3.4 is a summary of this information. A heat stability test was performed to assess each surfactant's ability to withstand PCR conditions. All of the surfactants withstood 95 °C for 10 min except for Jeffamine M600, which was slightly destabilized. This provided evidence that the polyetherdiamines participate in multivalent binding (2:1, Krytox:Jeffamine). Next, a test of emulsion destabilization using EDTA was developed. The negative effect of EDTA on PEG aqueous solubility is a well-studied process [27], thus in the presence of EDTA, Jeffamine-bound surfactant should not form an emulsion. Using 0.5 M EDTA, we found that Jeffamine was

completely destabilized, while other PEA groups were only slightly destabilized. The same solution with unmodified surfactant was not destabilized.

Next, a test of emulsion destabilization using $H_2SO_4$ was developed. In this case, the opposite effect should occur. Since the unmodified surfactant is a carboxylate, upon contact with aqueous solution, it is considered an anionic surfactant. If this group is re-protonated back to its carboxylic acid form (at very low pH), the molecule should be pushed away from the oil-water interface and lose its emulsion-forming capabilities. When using 1 M $H_2SO_4$ as the aqueous phase for an emulsion, this trend was observed. Unmodified surfactant, which the acid will re-protonate to some extent, should not form as stable of an emulsion. Conversely, Jeffamine-bound surfactant may still maintain some stability. Indeed, in Figure 3.4 we see that the unmodified surfactant is completely destabilized by the acid, while all of the modified surfactants are only partially destabilized, suggesting that Jeffamine-bound Krytox is somewhat protected from acid destabilization.

Finally, a real-time PCR float test was conducted to determine if amplification was dependent on the type of polyetheramine (PEA) group. The results demonstrate that all types of Jeffamine-bound surfactants allow for successful PCR amplification, while the unmodified surfactant showed much lower reaction efficiency. This result is likely due to the negative charge of the carboxylate group on the unmodified surfactant binding to important PCR reagents (likely enzymes) and inhibiting the reaction. Based on the results of the qualitative tests of biocompatibility, destabilization, and heat stability, we determined that the optimal PEA group for surfactant modification was Jeffamine ED 900.

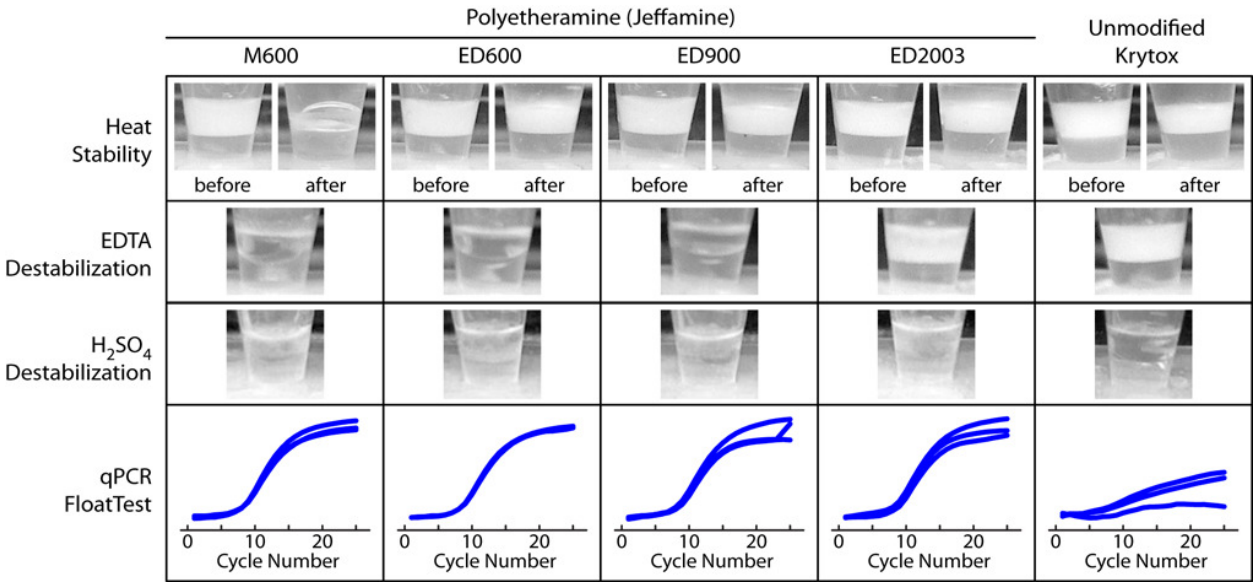


**Figure 3.4** Qualitative testing of various polyetheramines (PEA). Several sizes and geometries of PEAs were used to bind to Krytox 157 FSH and then compared to the unmodified surfactant. Jeffamines M600, ED600, ED900, and ED2003 contained 9, 9, 12, and 26 PEG units, respectively. Jeffamine M600 was the only monoamine tested. Heat stability tests were performed at 95 °C for 10 min to mimic PCR conditions. 0.5 M EDTA and 1 M $H_2SO_4$ destabilization tests were used as qualitative determinants of binding. A real-time PCR (qPCR) "float test" was used to determine surfactant biocompatibility for future applications shown in the manuscript. Jeffamine ED 900 was determined to be the most suitable PEA group, based on its heat stability and biocompatibility. Qualitative binding tests (acid and EDTA) also agreed with proposed binding that is further supported by spectroscopic results in the manuscript.

### 3.3.3 Emulsion Stability, Surface Biocompatibility, and pH Effects

Several qualitative and quantitative tests were developed to investigate the stability of Jeffamine/Krytox stabilized water-in-oil emulsions. First, a heat and ionic strength stability test was developed to mimic PCR conditions. The table in Figure 3.5A shows that emulsions made with 1.8% w/w Krytox remain stable after incubation at 95 °C when either 0.75% w/v Jeffamine or 1.5 mM $MgCl_2$ is added at all ionic strengths tested. The fact that the emulsions remain stable after incubation at 95 °C makes the Jeffamine-bound surfactant an attractive alternative for droplet PCR and digital droplet PCR. Since it could be perceived as advantageous to pre-saturate the Krytox with Jeffamine to avoid aqueous additives, the same tests were carried out on Jeffamine-saturated Krytox in oil (overnight incubation). Interestingly, we found that emulsions were destabilized at the two highest ionic strengths. Upon adding 1.5 mM $MgCl_2$, however, some (but not all) of the stability was recovered at the second-highest ionic strength; this result is reasonable since divalent cations stabilize PEG-like structures in aqueous solution [27]. We speculate that the Jeffamine-saturated Krytox, once fully dissolved in perfluorocarbon oil, is less likely to move to the interface and serve as a surfactant during droplet formation, although the system could be better understood in future studies with more quantitative measurements and a wider range of conditions. It appears that Jeffamine-saturated Krytox in oil is non-ideal for use with droplet PCR conditions, while the aqueous Jeffamine additive is promising for use in droplet PCR. Since the dynamics of surfactant mobility have not been well-studied for this particular system, determination of the time scales of adsorption to the interface for both Krytox and Jeffamine in future work could provide valuable information that could help to explain the observed trends seen in Figure 3.5A and to further optimize this system.

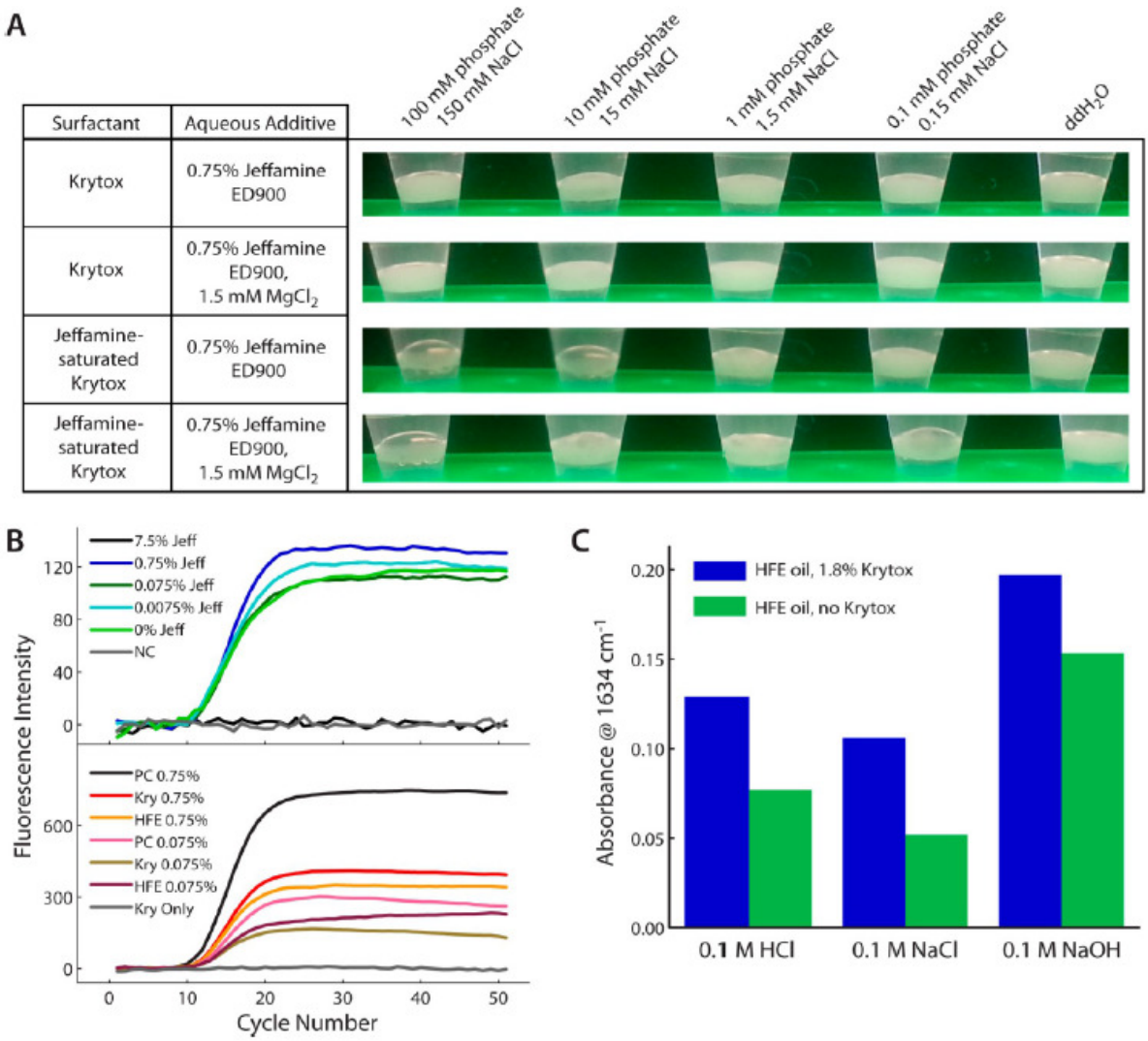


**Figure 3.5** Ionic strength, pH, and heat stability of Jeffamine-bound Krytox emulsions. (A) Heat stabilities of emulsions of varying aqueous ionic strengths with Krytox (upper 2 rows) and with Jeffamine-saturated Krytox (lower 2 rows). (B) Real-time PCR tests showed that all concentrations of Jeffamine at or below 0.75% w/v were PCR compatible. 7.5% Jeffamine (black trace) inhibited PCR (upper data set). In real-time PCR "float tests", Krytox surfactant at the oil–water interface (gray trace, lower data set) inhibited PCR, and 0.75% w/v Jeffamine additive (red trace) sufficiently rescued the biocompatibility in the presence of Krytox. (C) Jeffamine extraction into HFE 7500 oil at different aqueous pH values was monitored by FT-IR. Results are consistent with an ionic interaction between positively charged Jeffamine and negatively charged Krytox.

Since aqueous Jeffamine additives did not interfere with heat stability, it was necessary to determine the biocompatibility of this approach, for which we employed real-time PCR. First, a titration experiment was conducted to determine if any concentration of Jeffamine additive would interfere with PCR efficiency (Figure 3.5B, top). At a concentration of 7.5% (black trace), PCR is inhibited entirely, with a profile matching that of the no-template negative control (NC, gray trace). However, with Jeffamine additives at or below 0.75% w/v, the threshold cycles ($C_t$) were essentially equal to that of the positive control (0% Jeffamine, green trace). From this, we concluded that Jeffamine could be used as a PCR additive at a concentration less than or equal to 0.75% w/v.

A second PCR test was performed to determine if the Jeffamine additive could now impart biocompatibility between Krytox and the PCR assay (Figure 3.5B, bottom). In this test, the PCR amplification mixture was not formed into an emulsion, but it was thermally cycled as it floated atop HFE 7500 oil (density ~1.6 g/mL); oil was either pure or contained 1.8% w/w Krytox. The results showed that at Jeffamine additive concentrations of both 0.75% w/v (red trace) and 0.075% w/v (gold trace) PCR was successful in the presence of Krytox. Without Jeffamine additive, Krytox inhibited PCR (gray trace). Since neither oil nor surfactant were present in the positive control (PC, black trace), the real-time PCR optics registered higher fluorescence intensity for the positive control due to the difference in solution position. In emulsion PCR, there will be higher surface-area-to-volume ratios in droplets; these results suggest that for optimal droplet stability and biocompatibility, unmodified Krytox in HFE 7500 oil should be used with the highest allowable percentage (0.75% w/v) of Jeffamine as an aqueous additive.

Finally, to determine the role of ionic interactions in the Jeffamine/Krytox binding, we evaluated the pH dependence of the interaction using FT-IR (Figure 3.5C). Jeffamine was bound directly to Krytox by overnight saturation of 1.8% Krytox in HFE 7500 with Jeffamine-containing aqueous solutions of pH 2, 7, and 12 (equal ionic strengths). FT-IR spectroscopy was used to monitor the change in absorbance for the amine peak at approximately 1634 $cm^{-1}$ (see Figure 3.2A, blue-green trace), thus determining the extent of extraction of Jeffamine into HFE 7500 by Krytox. In all cases, the presence of Krytox significantly increased the amount of Jeffamine found in the oil. As expected for a charge-based interaction, the amount of extracted Jeffamine decreased from pH 2 to 7, as there will be a reduced amount of positively charged Jeffamine at pH 7. Note that the amount of negatively charged Krytox should be essentially equal at all pH values tested, since the p$K_a$ of carboxylated perfluorocarbons typically decreases as the number and proximity of fluorine atoms to the carboxylic acid increases. On the basis of its structure, Krytox should have a negative p$K_a$ [28-29]. At pH 12, the results show that more Jeffamine was extracted into the oil, even when Krytox was not present. Because Jeffamine will be predominantly neutral at this pH, the Jeffamine solubility in the oil may be increased due to the lack of charge and/or due to hydrogen bonding interactions with negatively charged Krytox [21-23]. An alternative interpretation would be that Jeffamine-bound Krytox could form micelles in the HFE-7500 oil; thus, the extraction of Jeffamine would be highly dependent upon the critical micelle concentration (CMC) of the system. Since Jeffamine was maintained at a rather high concentration in the studies in Figure 3.5, micelle formation could certainly play a role, along with charged interactions, hydrogen bonding [21-23], or other factors. This level of complexity warrants further study of the system and is beyond the scope of the current work.

### 3.3.4 Biocompatibility within Picoliter Droplets

To demonstrate biocompatibility at higher surface area-to-volume ratios, we have used the Jeffamine aqueous additive to rescue the efficiency of biochemical reactions within Krytox-stabilized picoliter droplets. One application involves our novel proximity Förster resonance energy transfer (pFRET) protein assay, which is similar in structure to the proximity ligation assay [30] and similar in readout to the molecular pincer assay [31]. Two antibody-oligonucleotide probes assemble only in the presence of the target protein (insulin), thereby quenching fluorescence in a highly selective way. As seen in Figure 3.6A, in a float test (aqueous solution floating on perfluorocarbon oil) without added surfactant in the oil phase (HFE 7500 only, blue bars), the assay responded nicely to the presence of 5.0 nM insulin (+ins). However, when exposed to 1.8% Krytox in the HFE 7500 oil, no significant assay response was observed (orange bars). Upon inclusion of the Jeffamine aqueous additive, even in the presence of 1.8% Krytox in HFE 7500, the assay performance was rescued (green bars) to a similar sensitivity level as in the control. These results support the hypothesis that Jeffamine additives can impart biocompatibility to Krytox-stabilized oil–water interfaces.

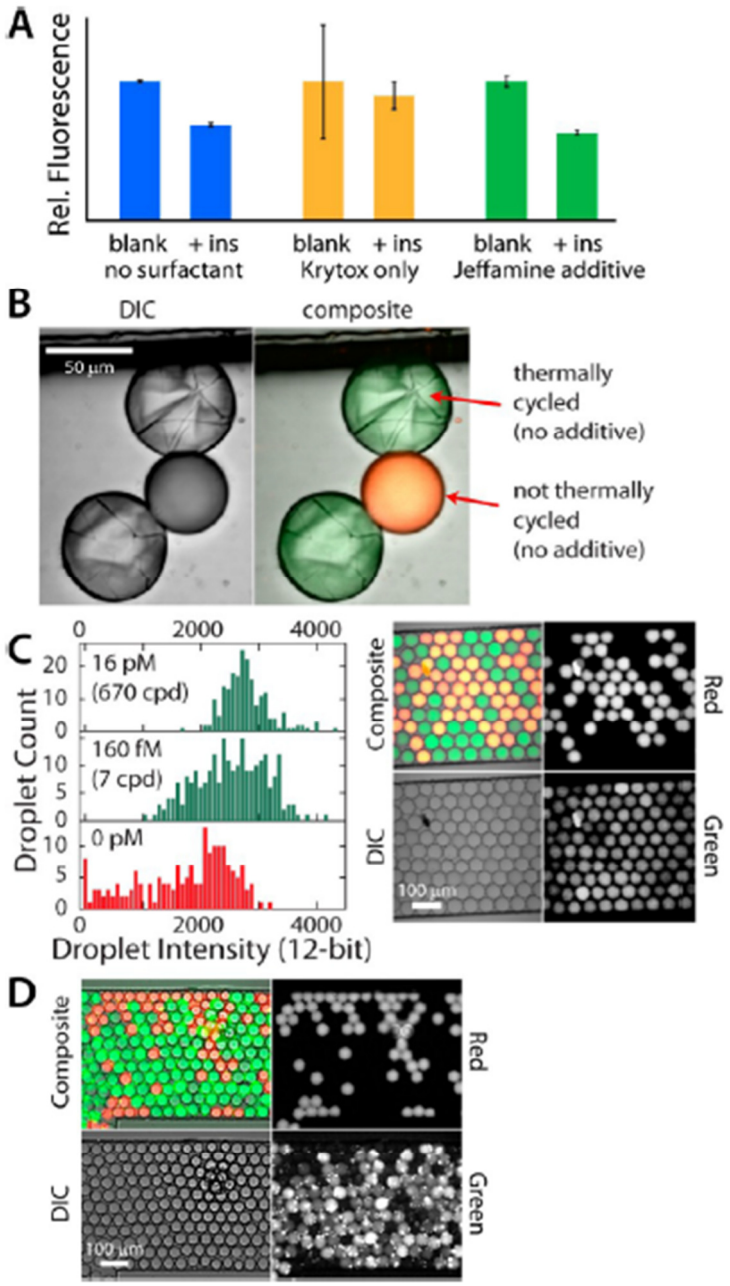


**Figure 3.6** Biocompatibility of Jeffamine-bound surfactant with three biochemical assays. (A) Homogeneous pFRET assay response to insulin (blue bars) was inhibited by Krytox (orange bars) and then rescued by the Jeffamine additive (green bars). (B) DIC and composite images of droplets made with Krytox surfactant and no Jeffamine aqueous additive. Thermally cycled droplets show evidence of reagent precipitation at the oil–water interface. (C) Droplet PCR with varying template DNA concentrations of 0, 160 fM, or 16 pM (0, 7, or 670 copies/droplet). Control droplets (red in image) contained background levels of probe and were not thermally cycled. (D) Isothermal droplet RPA with 160 fM (7 copies/droplet) template (37 °C). Control droplets (red) were subjected to incubation with RPA reagents but contained no template DNA. The abbreviation "cpd" refers to DNA copies per droplet.

A second biocompatibility test employed droplet PCR. Since digital PCR and droplet digital PCR (ddPCR) exploded onto the scene, it has been successfully used to achieve limits of detection down to only a few copies of DNA, for quantifying DNA copy number without the need for references or standards and for detecting the presence of rare mutations in a high background of other DNA [32-35]. This robust technique has seen widespread recent application, and it requires the use of a biocompatible surfactant. Working toward ddPCR, we have demonstrated successful droplet PCR using our Jeffamine aqueous additive to create heat-stable, biocompatible droplet interfaces (Figure 3.6 B,C). The importance of creating biocompatible surfaces is highlighted in Figure 3.6B. All droplets shown here were made with Krytox as the surfactant, yet they contained no Jeffamine aqueous additive. The green and red confocal fluorescence image was overlaid with the transmission image to create a composite for droplet identification. The red and green dye labeled droplet (middle droplet) was not thermally cycled, while the droplets labeled with only green dye were cycled through a typical PCR thermal program. It is clear from the laser transmission image (Figure 3.6B, left, grayscale) that thermally cycling in the presence of Krytox surfactant (without Jeffamine additive) causes PCR reagents (likely enzymes) to crash out of solution at the oil–water interface.

To perform droplet PCR at different template concentrations, we first used a passively operated microfluidic device (See Chapter 2, Figure 2.1), with 1.8% w/w Krytox surfactant as the carrier phase, to rapidly create aqueous-in-oil droplets containing 0.75% w/v Jeffamine as a PCR additive. Template DNA concentrations of 0, 160 fM, or 16 pM (0, 7, or 670 copies/droplet) were added to the inlet of the droplet generating device. After emulsions were collected and transferred to individual PCR tubes and thermally cycled, DNA products within individual droplets were identified via confocal fluorescence imaging (Figure 3.6C). As shown in

the image, droplets exhibited uniform size with no evidence of coalescence after thermally cycling and then mixing with reference droplets. The reference droplets included Taqman probes and all reagents other than enzyme. These droplets were labeled with ROX-labeled DNA ("Red"), and they exhibited lower average intensity than the sample droplets with template DNA. The histograms of droplet count versus green fluorescence intensity (left) showed a significant increase in intensity in proportion to template DNA concentration, suggesting that PCR was functional within the Jeffamine-stabilized droplets. With the current optical setup, it was not possible to image enough droplets to obtain the precision necessary for ddPCR, but positive results at only 7 copies/droplet suggest that ddPCR should be possible when using Jeffamine as an aqueous additive.

To provide a third test for biocompatibility of our approach, we successfully carried out isothermal DNA amplification using a multi-enzyme mixture for recombinase polymerase amplification (RPA) in picoliter-volume droplets. RPA allows exponential amplification of DNA, similar to PCR, but does not require an initial heating step or thermal cycling [36-37]. This method has recently been shown capable of digital nucleic acid quantitation in small, droplet-like microfluidic compartments [38] but has not been carried out in aqueous-in-oil droplets, to our knowledge. Figure 3.6D shows a mixture of test and control droplets after incubation for 30 min at 37 °C. The monodispersed emulsion was created with our passively controlled microfluidic device (See Chapter 2, Figure 2.1) and 1.8% Krytox surfactant in HFE 7500 oil. Using 160 fM template concentration (7 copies/droplet) and the Jeffamine aqueous additive, all sample droplets appeared to be positive (high green signal), while the reference droplets (red-labeled) show very little signal in the green channel. This result again supported the biocompatibility of Jeffamine-bound Krytox at the droplet surfaces.

As a final test of biocompatibility, we monitored RPA in real time within picoliter droplets to assay the efficiency of a biochemical reaction within Jeffamine/Krytox stabilized droplets (Figure 3.7). The images in Figure 3.7A show the end result of approximately 10 min of RPA-based amplification from a starting concentration of 16 pM template DNA (670 copies/droplet). The reference droplets (no template DNA) showed essentially no amplification, evidenced by the absence of yellow color in the overlaid image (R + G). Snapshots in time are shown in the rightmost three images, where a template-containing droplet is outlined in green and a control droplet (no template) is outlined in red. Within only 8 min, amplification reached >95% maximum signal, indicating that RPA was highly efficient within droplets containing the Jeffamine additive. Figure 3.7B shows a comparison of real-time RPA with "unmodified" surfactant (Krytox only, black trace), Jeffamine-bound surfactant (blue trace), and KryJeffa covalent product (orange trace). Curves depict the average of three droplets of each type, with standard deviations shown as error bars without caps (for clarity). Although the reaction was eventually functional within Krytox-stabilized droplets (no additive), the efficiency was significantly reduced by the presence of Krytox alone. The reagents specific to RPA, which differ greatly from those used in PCR, may contain molecules capable of eventually passivating the interface much like the Jeffamine additive. However, Jeffamine additive seems to preferentially migrate to the interface over these reagents, which is supported by the visible increase in efficiency once Jeffamine is added to the system. With these real-time analyses, there was no observable difference in RPA efficiency within Jeffamine-bound Krytox stabilized droplets and KryJeffa stabilized droplets. By analyzing end-point images (approximately 10 min after reaction), it appeared that KryJeffa promoted a slightly higher efficiency than Jeffamine-bound Krytox (Figure 3.7C), although both showed significantly higher RPA efficiencies than

Krytox alone. Interestingly, neither Jeffamine-bound Krytox nor KryJeffa stabilized droplets allow for 100% efficiency. This could be a result of a digital effect, where some droplets contained no template, but further investigation was deemed unwarranted. These RPA efficiency comparisons suggested that a simple polyetherdiamine aqueous additive (Jeffamine) provides a significantly simpler alternative to impart biocompatibility to droplets, compared to the synthetic modification of Krytox that is in common practice currently (e.g., EA surfactant, KryJeffa).

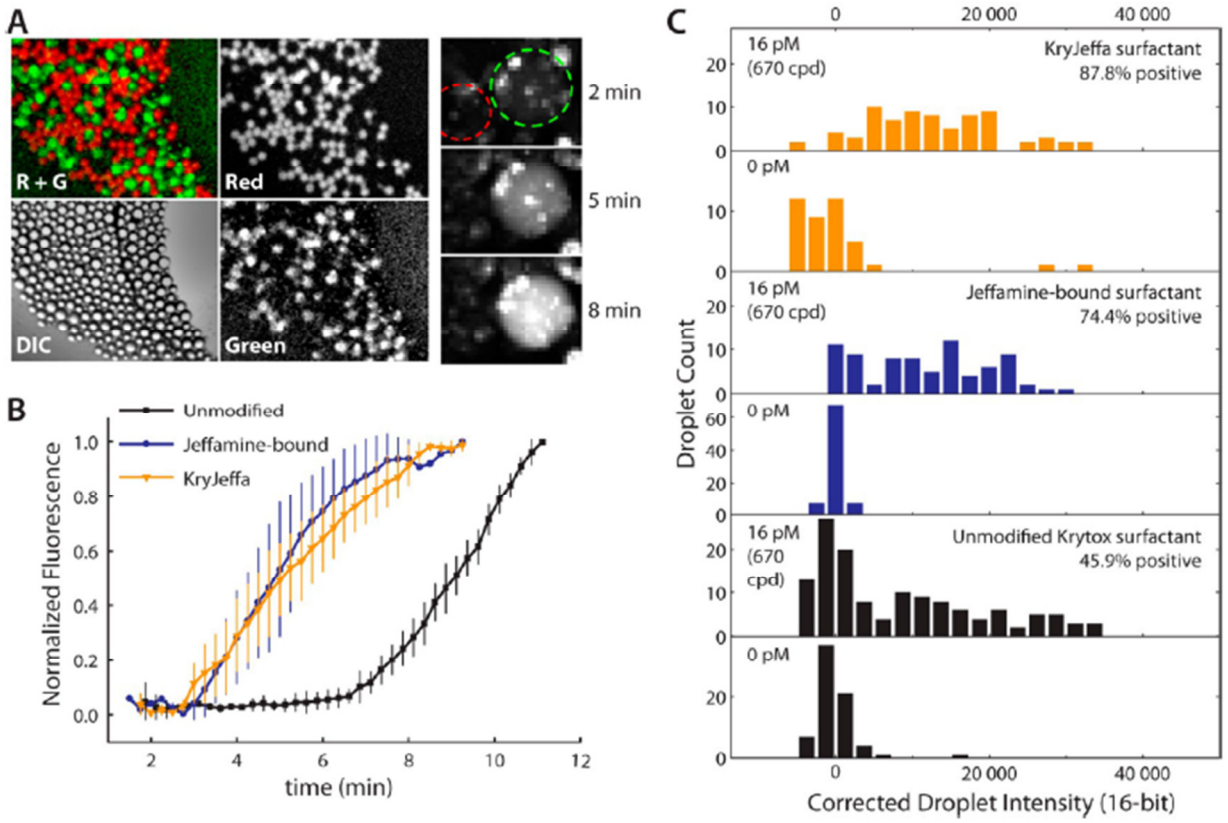


**Figure 3.7** Analysis of biological reaction efficiency in picoliter droplets. (A) Fluorescence images of droplet RPA using the Jeffamine aqueous additive with unmodified Krytox surfactant. Leftmost images show grayscale (and composite) images taken post-RPA using the red, transmission (DIC), and green imaging filters. Red droplets represent zero template controls; all other droplets contained 16 pM template (670 copies/droplet). Composite image (R + G) shows that none of the control droplets generated products. Rightmost image shows snapshots of the real-time RPA reaction; control droplet outlined in red; template-containing droplet outlined in green. (B) RPA reaction kinetics monitored in the presence of unmodified surfactant with no additive (black), Jeffamine-bound surfactant (blue), and KryJeffa surfactant (orange). Average traces from 3 representative droplets are shown with standard deviations. (C) Following droplet RPA with 0 or 16 pM template, droplet population intensities were counted with each treatment, indicating similar efficiency with KryJeffa and Jeffamine-bound surfactants. The abbreviation "cpd" refers to DNA copies per droplet.

### 3.4 Conclusions

Significant evidence was provided to support a direct binding interaction between a carboxylated perfluoropolyether (Krytox) and a polyetherdiamine (Jeffamine) at the interface of oil and aqueous solution. Evidence of the binding interaction was supported by FT-IR, mass spectrometry, fluorescence microscopy, and NMR analyses; and biocompatibility was confirmed with homogeneous protein assays, droplet PCR, and droplet RPA. For further confirmation, the efficiency of real-time RPA within Jeffamine additive stabilized droplets compared favorably with that of the KryJeffa stabilized droplets, even starting with <10 template copies per droplet.

To achieve maximum performance, it appears that Jeffamine should be added directly to the aqueous solution at a concentration of 0.75% w/v. Preparing an oil-soluble, Jeffamine-saturated surfactant in advance actually sacrifices droplet stability at higher ionic strengths; thus, this method is discouraged. To further optimize this system, future studies should involve determination of surfactant CMC and determination of the time scales of interfacial adsorption for both surfactant and aqueous additive. Overall, our current results suggest that commercially available reagents can be used to impart biocompatibility to droplet surfaces. A simple polyetherdiamine (Jeffamine) aqueous additive provides a dynamic shielding effect at droplet surfaces, an attractive alternative to covalent modification of Krytox for droplet-based biochemical reactions.

In addition, we have further improved our understanding of the binding of primary amines to Krytox. This interaction is likely a major factor in the incompatibility of Krytox with enzyme reactions, as proteins typically contain a number of primary amines, and this study should give further insight into interaction mechanisms with other additives [39-40] or

surfactants [41]. By expanding upon these studies in the future, it is feasible that one could spatially direct various biomolecules, such as DNA, to the oil–water interfaces of droplets to participate in surface-based biochemical assays.

### 3.5 References


1. Tawfik, D. S.; Griffiths, A. D. *Nat. Biotechnol.* **1998**, 16, 652– 656.
2. Williams, R.; Peisajovich, S. G.; Miller, O. J.; Magdassi, S.; Tawfik, D. S.; Griffiths, A. D.*Nat. Methods* **2006**, 3 ( 7) 545– 550.
3. Kelly, B. T.; Baret, J. C.; Taly, V.; Griffiths, A. D. *Chem. Commun.* **2007**, 1773–1788.
4. Griffiths, A. D.; Tawfik, D. S. *EMBO* **2003**, 22 ( 1) 24– 35.
5. Dressman, D.; Yan, H.; Traverso, G.; Kinzler, K. W.; Vogelstein, B. *Proc. Natl. Acad. Sci. U.S.A.* **2003**, 100 ( 15) 8817– 8822.
6. Diehl, F.; Li, M.; He, Y.; Kinzler, K. W.; Vogelstein, B.; Dresman, D. *Nat. Methods* **2006**, 3 (7) 551– 559.
7. Easley, C. J.; Rocheleau, J. V.; Head, W. S.; Piston, D. W. *Anal. Chem.* **2009**, 81, 9086–9095.
8. Sun, S.; Slaney, T. R.; Kennedy, R. T. *Anal. Chem.* **2012**, 84, 5794– 5800.
9. Abate, A. R.; Weitz, D. A. *Biomicrofluidics 5* **2011**, 014107, 1– 8.
10. Zeng, Y.; Shin, M. M.; Wang, T. Y. *Lab Chip* **2013**, 13, 267– 273.
11. Matosevic, S.; Paegel, B. M. *J. Am. Chem. Soc.* **2011**, 133, 2798– 2800.
12. Tadros, T. F. *Applied Surfactants-Principles and Applications*; Wiley-VCH: Weinheim,**2005**.
13. Curran, D. P. *Angew. Chem., Int. Ed.* **1998**, 37, 1174– 1196.
14. Hildebrand, J. H.; Cochran, D. R. F. *J. Am. Chem. Soc.* **1949**, 71, 22– 25.
15. Scott, R. L. *J. Am. Chem. Soc.* **1948**, 70, 4090– 4093.
16. Holtze, C.; Rowat, A. C.; Agresti, J. J.; Hutchison, J. B.; Angilé, F. E.; Schmitz, C. H. J.; Köster, S.; Duan, H.; Humphry, K. J.; Scanga, R. A. *Lab Chip* **2008**, 8, 1632–1639.
17. Piirma, I. *Polymeric Surfactants*; CRC Press, Marcel Dekker: New York, **1992**.
18. Skhiri, Y.; Gruner, P.; Semin, B.; Brosseau, Q.; Pekin, D.; Mazutis, L.; Goust, V.; Kleinschmidt, F.; El Harak, A.; Hutchison, J. B. *Soft Matter* **2012**, 8, 10618–10627.

19. Mazutis, L.; Araghi, A. F.; Miller, O. J.; Baret, J. C.; Frenz, L.; Janoshazi, A.; Taly, V.; Miller, B. J.; Hutchison, J. B.; Link, D.; Griffiths, A. D.; Ryckelynck, M. *Anal. Chem.* **2009**,81 ( 12) 4813– 4821.

20. Theberge, A. B.; Whyte, G.; Huck, W. T. S. *Anal. Chem.* **2010**, 82 ( 9) 3449– 3453.

21. O'Neal, K. L.; Weber, S. G. *J. Phys. Chem. B* **2009**, 113 ( 1) 149– 158.

22. O'Neal, K. L.; Geib, S.; Weber, S. G. *Anal. Chem.* **2007**, 79 ( 8) 3117– 3125.

23. O'Neal, K. L.; Zhang, H.; Yang, Y.; Hong, L.; Lu, D.; Weber, S. G. *J. Chromatogr., A* **2010**,1217 ( 16) 2287– 2295.

24. Matochko, W. L.; Ng, S.; Jafari, M. R.; Romaniuk, J.; Tang, S. K. Y.; Derda, R. *Methods***2012**, 58, 18– 27.

25. Shim, J.; Olguin, L. F.; Whyte, G.; Scott, D.; Babtie, A.; Abell, C.; Huck, W. T. S.; Hollfelder, F. *J. Am. Chem. Soc.* **2009**, 131, 15251– 15256.

26. Temtem, M.; Casimiro, T.; Santos, A. G.; Macedo, A. L.; Cabrita, E. J.; Aguiar-Ricardo, A.*J. Phys. Chem. B* **2007**, 111, 1318– 1326.

27. Jones, G. K.; McGhie, A. R.; Farrington, G. C. *Macromolecules* **1991**, 24, 3285– 3290.

28. Goss, K. *Environ. Sci. Technol.* **2008**, 42, 456– 458.

29. Henne, A. L.; Fox, C. J. *J. Am. Chem. Soc.* **1951**, 73, 2323– 2325.

30. Fredriksson, S.; Gullberg, M.; Jarvius, J.; Olsson, C.; Pietras, K.; Gustafsdottir, S. M.; Ostman, A.; Landegren, U. *Nat. Biotechnol.* **2002**, 20 ( 5) 473– 477.

31. Heyduk, E.; Dummit, B.; Chang, Y.; Heyduk, T. *Anal. Chem.* **2008**, 80 ( 13) 5152– 5159.

32. Pinheiro, L. B.; Coleman, V. A.; Hindson, C. M.; Herrmann, J.; Hindson, B. J.; Bhat, S.; Emslie, K. R. *Anal. Chem.* **2012**, 84, 1003– 101.

33. Vogelstein, B.; Kinzler, K. W. *Proc. Natl. Acad. Sci. U.S.A.* **1999**, 96, 9236– 9241.

34. Zhong, Q.; Bhattacharya, S.; Kotsopoulos, S.; Olson, J.; Taly, V.; Griffiths, A. D.; Link, D. R.; Larson, J. W. *Lab Chip* **2011**, 11, 2167– 2174.

35. Heyries, K. A.; Tropini, C.; Vanlnsberghe, M.; Doolin, C.; Petriv, O. I.; Singhal, A.; Leung,K.; Hughesman, C. B.; Hansen, C. L. *Nat. Methods* **2011**, 8 ( 8) 649– 651.

36. Piepenburg, O.; Williams, C. H.; Stemple, D. L.; Armes, N. A. *PLoS Biol.* **2006**, 4 (7), No. e204.

37. Kim, J.; Easley, C. J. *Bioanalysis* **2011**, 3 ( 2) 227– 239.

38. Shen, F.; Davydova, E. K.; Du, W.; Kreutz, J. E.; Piepenburg, O.; Ismagilov, R. F. *Anal. Chem.* **2011**, 83, 3533– 3540.

39. Brouzes, E.; Medkova, M.; Savenelli, N.; Marran, D.; Twardowski, M.; Hutchison, J. B.; Rothberg, J. M.; Link, D. R.; Perrimon, N.; Samuels, M. L. *Proc. Natl. Acad. Sci. U.S.A.***2009**, 106, 14195– 14200.

40. Courtois, F.; Olguin, L. F.; Whyte, G.; Theberge, A. B.; Huck, W. T. S.; Hollfelder, F.; Abell,C. *Anal. Chem.* **2009**, 81, 3008– 3016.

41. Baret, J. C. *Lab Chip* **2012**, 12, 422– 433.

42. DeJournette, C.J.; Kim, J.; Medlen, H.; Li, X.; Vincent, L.J.; Easley, C.J. *Anal Chem* **2013**, 85, 10556-10564.

# CHAPTER 4

# BEAD-BASED ASSAYS AS COMPLEMENTS TO DROPLET COMPARTMENTALIZATION

## 4.1 Introduction

The attachment of synthetic oligonucleotides to solid surfaces has been used to create DNA oligonucleotide arrays for a variety of molecular applications. DNA can be attached to a variety of two-dimensional and three-dimensional surfaces, such as glass slides and micro-beads [1]. Two-dimensional surfaces can sterically limit the amount of DNA that can be loaded onto the surface, which can limit signal intensity and assay dynamic range. The use of polystyrene, magnetic, and silica micro-beads as three-dimensional surfaces greatly increases the surface area per spot, allowing larger quantities of DNA to be loaded onto the surface. These beads are becoming increasingly more popular, because they are not only more cost effective than glass and silicon 2D surfaces, but also can be individually analyzed with flow cytometry and separated into different populations based on desired traits once DNA is attached. This makes them desirable for multiplexing of assays, simultaneous performance of different assays, new assay development, and rapid sample analysis [1].

The most widely used strategy for attaching DNA sequences to solid surfaces is to have the DNA sequences synthesized synthetically and then attach them to a solid support [1]. The DNA sequence is typically modified with a functional group that is designed to bond with a corresponding reactive group on the solid surface. As with any synthesis or assay, optimal reaction conditions will depend on the type of linkage being created [1]. Micro-beads can be ordered with the following reactive groups on the surface for linkage to oligonucleotides:

Carboxylic acid (-COOH), primary aliphatic amine (-$RNH_2$), aromatic amine (-$ArNH_2$), chloromethyl (vinyl benzyl chloride) (-$ArCH_2Cl$), amide (-$CONH_2$), hydrazide (-$CONHNH_2$), aldehyde (-CHO), hydroxyl (-OH), thiol (-SH), and epoxy (-COC-). A high affinity, non-covalent, biotin-streptavidin linkage can also be used by obtaining biotin-labeled DNA and avidin-coated beads. The reaction of carboxyl and amine groups is the most common, because these groups are stable over time, and their reactions have been well-studied. Amine-modified DNA has been shown to react with succinylated and PEG-modified glass beads to form a stable bond using a carbodiimide like 1-ethyl-3-[3-dimethylaminopropyl]carbodiimide (EDC) [18]. Carboxylate beads can also be reacted with an amine-modified DNA sequence in one step using EDC, or in two steps using EDC and NHS chemistry [1]. Many bioanalytical applications using DNA-modified beads require preparation of the bead surface beyond initial attachment, to cover the bead surface in a desired DNA sequence. In order to achieve this, many copies of a PCR primer are attached to the surface using one of the reactions mentioned above. The primer-modified bead, target sequence, and other necessary reagents are compartmentalized together, and once amplification takes place, many copies of the target sequence become immobilized on the bead surface [2-3]. We have used EDC/NHS chemistry on both latex and magnetic beads to attach DNA primers for PCR. In addition, a second method has been developed using “click” chemistry.

There are several applications of DNA-modified beads that are important to our research. First, beads have been used for the detection of genetic variations from individual genes by capturing and clonally populating magnetic beads with thousands of copies of a single DNA sequence from a large pool of gene sequences. Flow cytometry is then used to detect differences between the bead populations and to separate genetic variants for further testing [4]. This process

is called BEAMing (beads, emulsion, amplification, and magnetics), which is a technique that builds upon the principles of emulsion PCR [5] to amplify DNA onto magnetic beads that are compartmentalized via water-in-oil emulsion droplets. After PCR, the beads are recovered with a magnet or centrifugation and then analyzed with conventional flow cytometry [6-7]. There are several advantages to BEAMing. One advantage lies in the use of flow cytometry, which can analyze samples at a rate of up to 100,000 particles per second and detect changes or rare events at sensitivities as great as 1:1,000,000 events (Section 1.4.3.1.). A second advantage is that, as previously mentioned, by attaching the DNA to a solid support, the data becomes trapped in space and time. Because of this, bead populations can be sorted and placed in discrete locations for further analysis and manipulation. In this way beads behave much like emulsion droplets in that they can also be used to collect and store data for long periods of time [19-20]. Finally, the clonality of the bead populations accurately reflects the original DNA template pool and gives high signal to noise ratios. These positive attributes have allowed BEAMing to find application in several areas, such as the detection of cancer mutations in the blood for the development of better diagnostic tests or help with shedding light on drug resistance [7, 8-9]. It has also been used for high-throughput DNA sequencing [3, 7] and DNA methylation experiments [6, 10]. We would like to use the BEAMing technique for applications involving aptamers and aptamer selection. In Chapter 5 we will discuss the future prospect of using methods developed in our lab that could utilize BEAMing within the aptamer selection process. The current chapter will present early development of a micro-bead method to measure binding affinities of known aptamers to their targets.

Aptamers are single-stranded, ligand-binding nucleic acids that have highly selective binding affinities to a particular target and are easily amplified. Micro-beads have been utilized

with aptamers as a selection method by attaching the target of interest to the bead and incubating it with a pool of possible DNA aptamers. The sequences that do not bind to the target-bound bead can be washed away, and the bound sequences amplified by PCR for enrichment and sequencing [11]. Another micro-bead application involving aptamers clonally amplifies aptamer sequences for detection of cancer cells. In this case, the functionality is reversed, as the aptamer sequences are immobilized and incubated in a pool with the target cells [12]. Typically, aptamers are isolated from oligonucleotide libraries containing $10^{12}$ - $10^{15}$ random nucleic acid sequences. They are tested for their affinity to the target of interest during the SELEX process, where the bulk $K_d$ value should decrease as selection rounds proceed. Traditional measurements of dissociation constants involve finding the concentration of ligand at which half of the total ligand and binding sites are taken [13]. Various approaches for measuring the concentration of bound ligand can be utilized, but a simpler approach is still in demand. To measure aptamer affinities, we have used a bead-based approach. An amine-labeled forward PCR primer was immobilized onto an NHS-ester activated bead through a coupling reaction, forming a peptide bond between the carboxyl group on the bead and the amine group of the primer. The primer was then used to immobilize a known thrombin aptamer onto the beads using PCR. Real-time, quantitative PCR (qPCR) was subsequently used to validate that the aptamer was attached to the bead and to measure the amount of DNA present. After incubation with fluorescently-labeled protein target and extensive washing, flow cytometry was used to test the binding specificity. Because the amount of aptamer attached to each bead is known, $K_d$ values could be determined simply by varying the concentration of fluorescent protein incubated with the beads and monitoring their fluorescent intensity. This method is advantageous due to the automated nature of flow cytometry, significantly easing the burden of $K_d$ measurements. Tom Soh's research group at the

University of California recently demonstrated the successful use of this method for measuring binding affinities, which shows that others have also recognized the need for a bead-based method [14].

A second application of micro-beads that we have begun to develop is for the digital detection of DNA. Digital PCR, discussed in greater detail in Chapter 1 (Section 1.4.2.1.), uses the principles of limiting dilution, end-point analysis, and Poisson statistics to quantify DNA. Although originally performed in microwell plates, digital PCR has made its way into the droplet microfluidics arena for higher throughput analysis of samples [6]. Digital PCR has become commercially available in chambers and in droplets, but it has also been developed for a micro-bead format through the previously-mentioned BEAMing technique [7-8]. BEAMing has the potential to take even a complex pool of different samples, attach each sample to its own solid support using emulsion PCR, perform digital analysis with flow cytometry to determine the original DNA concentration of each sample, and then recover samples with desired traits from the pool using cell sorting technology (e.g. FACS). However, it has been said that BEAMing is limited to only a few, specialized applications due to the "specialized heterogeneous assay schemes that add complexity to the workflow" [6]. We have begun development of a bead-based method that utilizes beads and magnetics to achieve digital results. In our method, the beads themselves act as compartments, possibly eliminating the need for droplets or complex chamber-based devices. This is done by ligating the desired DNA template directly to its own solid support, rather than relying on efficient encapsulation of 1 template copy and 1 bead per droplet. In this way, beads can be amplified together in a single PCR tube, because the templates are bound and therefore spatially segregated from one another, preventing cross-contamination of PCR products onto beads. Beads can be diluted to prevent cross-talk. We have performed proof-

of-concept experiments that involve ligating template DNA to beads at various concentrations, amplifying the bead populations with PCR, and performing flow cytometry analysis of the bead products. We show that as the number of template copies per bead decreases, the C(t) value obtained during real-time PCR increases. In addition, amplified bead populations show a much higher intensity than controls in the flow cytometry histograms.

## 4.2 Experimental

### 4.2.1 Materials

For PCR forward primer attachment using EDC and NHS and preparation of aptamer-bead conjugates, 2 µm Carboxyl Latex Beads were obtained from Invitrogen. N-hydroxysuccinimide (NHS) and 1-ethyl-3-[3-dimethylaminopropyl]carbodiimide (EDC) were obtained from Fisher Scientific. 2-mercaptoethanol, MES, NaCl, Acetic Acid, Low-binding centrifuge tubes, and NaOH were obtained from VWR. Dynabeads® M-270 Carboxylic Acid were obtained from Invitrogen. DyLight™ 488 Antibody Labeling Kit was obtained from Thermo Scientific. Thrombin from human plasma was obtained from Sigma. Sso Fast™ EvaGreen® Super mix (dNTPs, Sso7d – fusion polymerase, MgCl2, EvaGreen dye, stabilizers) was obtained from BioRad. All DNA sequences were obtained from Integrated DNA Technologies (IDT). Amine-labeled forward primer : NH2 – lnkr – Fwd_P: 5- /5AmMC6//iSp18//iSp18//iSp18/TCA GCC ATT CGA ATC GTA CT -3; Native Fwd_P: 5- TCA GCC ATT CGA ATC GTA CT -3; biot – R- primer Library 01: 5- /5Biosg/TCC GTA ACT AGT CGC GTC AC-3; Thrm_apB_min5: 5- /5Phos/TCA GCC ATT CGA ATC GTA CTC GGGTAT TAG GCT AGT GACTACTGGTTG GTG AGGTTG GGT AGT CAC AAA GTG ACG CGA CTA GTT ACG GA -3; FAM_anti_NH2-lnkr-Fwd_P: 5- /56-FAM/AGT ACG ATT CGA ATG GCT GA -3.

For PCR forward primer attachment using click chemistry and preparation of aptamer-bead conjugates, Dynabeads M-270 Amine were obtained from Invitrogen. Methanol was obtained from VWR. DMF, Bromoacetyl bromide , N,N-Diisopropylethylamine (DIPEA), 4-dimethylaminopyridine (DMAP), Sodium Azide (NaN3), Triethylammonium acetate, Ascorbic Acid, Copper (II) - Tris(benzyltriazolylmethyl)amine (Cu-TBTA), DMSO, and EDTA were obtained from Sigma. All DNA sequences were obtained from Integrated DNA Technologies (IDT). Bead_fwd-p_alkyne: 5-/5Hexynyl//iSp18//iSp18//iSp18/GAA TTC CCA ACA CAC ACA ACA ACA CAT AAA GGCTA -3; Bead_anti-fwd-p: 5- TAG CCT TTATGT GTT GTT GTGTGT GTT GGG AAT TC -3; newThrm_c5_FwdPR_alkyne: 5-/5Hexynyl//iSp18//iSp18//iSp18/CGT CTA GCA GCG TAT ACC TG -3; newThrm_c3_FwdPR_alkyne: 5- /5Hexynyl//iSp18//iSp18//iSp18/AAT TCC CGC AGA ATC GTA CTC G -3; newThrm_c5_EcoRI_FwdPR: CGT CTA GCA GCG TAT ACC TGG TAG GCG TTT GGG TTG GGC GGT ATA CGC GCG CAT CGT GGA ACT ATC TAG CGG TGT ACG TG**A GTG GGC ATG TAG CAA GAG G**; newThrm_c3_EcoRI_RevPR: /5Phos/AAT TCC CGC AGA ATC GTA CTCG GGT ATT AGG CTA GTG GAT ATG CCA TGT GTG GTT GGT GTA GGT TGG **GAT GGC CAC GGT AAT TGC GA** . Reverse priming regions are bold and underlined.

For droplet PCR and RPA, mineral oil and BSA were obtained from VWR. RPA enzyme kits and reagents were obtained from TwistDx, with probe DNA from Biosearch Technologies. Platinum *Tfi* DNA Polymerase with reaction buffer $MgCl_2$, and sulforhodamine 101 were obtained from Life Technologies. Krytox 157 FSH was obtained from DuPont, and Jeffamine ED900 was obtained from Sigma. Unless otherwise specified, all DNA sequences were obtained from Integrated DNA Technologies (IDT). PLA_ZenProbe_FAM_IBQ: 5'-/56-FAM/TGT ACG

TGA/ZEN/GTG GGC AT; Template DNA for droplet PCR: 5'-**TCC ACT CCT TTT CAT CTG CC**T TCC TTT TCT CCA TCG AGG TCC AGG TGA CCA TTG GTT TCG GCG GG**C GCA TGG TGA CAG AGG AAT**-3' and corresponding double-quenched ZEN probe (Taqman format): 5'- CCT GGA CCT CGA TGG AGA AAA GGA -3'; RPA forward primer (RPA_F-primer): 5'- GGT AAA GGT GTC GTG GAA CTA TCT AGC GGT GTA C -3' ; RPA reverse primer (RPA_R-primer) : 5'- TTT GTT TGA TAC CTT AGC CTA ATA CCC GAT T -3'; RPA template sequence: 5'- TCG TGG AAC TAT CTA GCG GTG TAC GTG AGT GGG CAT GTA GCA AGA GGG TCA TCA TTC GAA TCG TAC TGC AAT CGG GTA TTA GGC TA -3'). RPA probe: 5'- GTA CGT GAG TGG GCA TGT AGC AAG AGG GTC A3C HT1 CGA ATC GTA CTG CAT CGT TCT CCC AGT AGT AAG -3' was obtained from Biosearch Technologies, where "3" = dT-FAM fluorescent label, "H" = tetrahydrofuran, and "1" = dT-BHQ1 quencher label.

For bead digital detection experiments, T4 DNA Ligase and Ligase Buffer were obtained from New England Biolabs. SYBR Green I nucleic acid stain was obtained from Invitrogen. All DNA sequences were obtained from Integrated DNA Technologies (IDT). BeadMod_phos_ThrmAptA: 5- /5Phos/CAGTCC GTG GTA GGG CAG GTT GGG GTG ACT GTG ACG AAATAA GAA GAG GAA AGA AGA GGA GAG AA -3; BeadMod_LigConn: 5- CCA CGG ACT GTA GCCTTT AT -3; BeadMod_fwd-p_native: 5- GAATTC CCA ACA CAC ACA ACA ACA CAT AAA GGCTA -3; BeadMod_rev-p: 5- TTC TCT CCT CTT CTT TCC TCT TCT TAT TTC GTC AC -3.

### 4.2.2 Methods for Aptamer Binding Affinity Measurements Using Fluorescence Based Flow Cytometry

#### 4.2.2.1 PCR Forward Primer Attachment to Beads Using EDC and NHS

Carboxyl Latex Beads of 2 µm size (Invitrogen) were suspended in Activation Buffer (0.1 M MES, 0.5 M NaCl, pH 6.0) at a final concentration of 10 mg/mL. 2.0 M 1-ethyl-3-[3-dimethylaminopropyl]carbodiimide (EDC) and 5.0 M N-hydroxysuccinimide (NHS) were added at a final concentration of 200 mM and 500 mM, respectively. The mixture (total volume 300 µL) was allowed to react at room temperature for 30 min, mixing by pipette every 5 min. A 280 mM solution of 2.0 M 2-mercaptoethanol was made in deionized water. This solution was added to the bead reaction at a final concentration of 40 mM (total volume 350 µL) and mixed well by pipette. The reaction was centrifuged at 20,000 x g for 10 min. Removed 250 µL of supernatant, leaving 100 µL behind. Washed beads 3 times with 100 µL PBS Buffer, then removed 75 µL supernatant, leaving 25 µL behind. Amine-modified forward primer was added to the reaction at a final concentration of 1000 ng/µL, using PBS buffer to adjust to a final volume of 50 µL and mixed well by pipette. The reaction proceeded for 2 hours at room temperature, mixing by pipette every 20 min. Beads were washed 6 times with 100 µL deionized water and stored at 4 °C until ready for use.

#### 4.2.2.2 Preparation of Aptamer-Bead Conjugates

Forward primer-modified beads were dried with a Savant DNA120 SpeedVac Concentrator (Thermo Scientific). Next, 26 µL of deionized water were added, and beads were mixed by pipette. For PCR, 13 µL of beads, 1 µL reverse primer, and 1 µL 8.8 nM Thrm apt B were placed in each well along with Sso FastTM EvaGreen® Super mix (dNTPs, Sso7d – fusion polymerase, MgCl2, EvaGreen dye, stabilizers). Aqueous positive control contained native forward primer, and negative control contained no template. PCR was performed on a CFX96TM qPCR Detection System and CFX1000TM Thermal Cycler (BioRad) with the following temperature program: 95°C – 5 min.; 94°C – 20 sec.; 51°C – 40 sec.; 72°C – 30 sec.; 100 cycles.

#### 4.2.2.3 Control Experiments for Aptamer-Bead Conjugates

To prove that amplification was specific to primer-labeled beads, a PCR forward primer was first attached to beads as mentioned above (Section 2.2.2.1). A bead negative control was made simultaneously by performing the same reaction without adding primer to the solution. Both the sample and the negative control beads were dried using a SpeedVac Concentrator. For PCR, 2 µL reverse primer, 2 µL deionized water, 6 µL thrombin aptamer B, and 10 µL PCR supermix (BioRad, SsoFast EvaGreen) were added to the beads. The positive control for PCR was 2 µL native forward primer, and the negative control contained everything except template. PCR was run for 100 cycles with the following temperature program: 95°C for 5 min. followed by cycles at 94°C for 20 sec.; 51°C for 40 sec.; and 72°C for 30 sec.

To demonstrate that bead presence does not affect PCR amplification, PCR mixes containing a final concentration of 0, 0.3, or 3 pM thrombin aptamer B were made with and without unmodified beads present. 2 µL native forward primer, 2 µL reverse primer, and 10 µL PCR supermix (Components listed in Materials section) were added. The positive control contained a final concentration of 13.2 pM Thrombin aptamer B, while the negative control contained no template. PCR was run for 90 cycles with the same temperature program as above.

#### 4.2.2.4 Quantifying Amount of DNA on Bead Surface

Previously-amplified beads (Section 2.2.2.2.) were combined and washed 6 times with 100 µL deionized water, centrifuging at 20,000 × g for 10 min between each wash. Beads were filtered with 20 µm pore nylon mesh filters (Spectrum Laboratories Inc.), then split into two tubes of equal volume, adding deionized water to each for a final volume of 1000 µL. These tubes were further diluted into 5 equal volumes of 1000 µL each and counted using a flow cytometer

(Accuri). 50 µL from each diluted tube were counted 3 times. The average and standard deviation of these numbers were calculated to get the final number of beads to be for quantification of DNA on the surface.

The tube of beads with the lowest standard deviation from the count was used to perform qPCR with standards to calculate the amount of DNA per bead. The bead well contained 1 µL Native Forward Primer, 1 µL Reverse Primer, 13 µL beads, and 10 µL PCR supermix. For the standards and PCR positive control, 1 µL Thrm aptamer B (various concentrations), 1 µL native forward primer, 1 µL reverse primer, 12 µL deionized water, and 10 µL PCR supermix were combined. For the PCR negative control, 15 µL water and 10 µL supermix were combined. The standards were added to solution at final concentrations of 1, 5, 10, 25, 50, 75, 100, 200, 300, and 390 pM. PCR was run for 50 cycles with the same temperature program as above.

#### 4.2.2.5 Bead Binding to Target

To prepare thrombin aptamer target (Thrombin from human plasma, Sigma) for labeling, 60 µL of buffer (0.1 M MES, pH 6.5) were added to the vial and then swirled carefully to dissolve. Next, approximately 20 µL of solution were gently pipetted into the center of the vial to wash and dissolve the maximum amount of thrombin. The full 60 µL of solution were transferred to a microcentrifuge tube. 40 µL of buffer were added to the vial to dissolve thrombin again in the same manner. Approximately 20 µL of solution were pipetted onto the walls of the vial to rinse the remainder of thrombin off. The full 40 µL of remaining solution was then transferred to a separate microcentrifuge tube. The concentration of each aliquot was measured separately.

The absorbance at 280 nm (A280) of each vial was measured at an E1% of 18.30 using a Nanodrop 1000 spectrophotometer by measuring two, 2 µL aliquots twice. 0.1 M MES buffer, pH 6.5 was used as the blank, and the concentration (µM) of each vial was calculated.

To label thrombin with AF488 fluorescent dye, a DyLight Antibody Labeling Kit was used. According to kit instructions, 500 µL of 0.05 M Borate Buffer was prepared from the 0.67 M stock provided. 400 µL of buffer were added to 1 vial of dye and vortexed gently. The dye was centrifuged then split into two microcentrifuge tubes containing 200 µL each. Thrombin was added at a final concentration of 2.5 µM in 250 µL, using borate buffer to adjust to the final volume. Thrombin was incubated at room temperature for 1 h, protected from light then purified according to kit instructions, using one column. The collected samples from each vial were combined into a single microcentrifuge tube and stored at 4 °C, protected from light, until ready for use.

The fluorescent thrombin concentration was measured on a ND1000 spectrophotometer (A280, 10 mm path length, E1% = 18.30 L/gm*cm). A small amount of labeled thrombin was diluted in 1× PBS buffer and the A280 measured at the $A_{max}$ of DyLight Dye 488, which is 493. Calculated protein concentration with the following equation:

$$\text{Protein Concentration (M)} = \frac{[A_{280} - (A_{max} \times CF)]}{\varepsilon_{thrombin}} \times \text{dilution factor}$$

- $\varepsilon_{thrombin}$ = Thrombin molar extinction coefficient (65880 L/mol*cm)
- CF = Correction factor = $\frac{A_{280} \text{ of the dye}}{A_{max} \text{ of the dye}}$ (For dye 488, this is 0.147)

Calculated the degree of labeling with the following equation:

$$\text{Moles dye per mole protein} = \frac{A_{max} \text{ of the labeled protein x dilution factor}}{\varepsilon_{dye} \text{ x protein concentration (M)}}$$

- $\varepsilon_{dye}$ = dye (Fluorophore) molar extinction coefficient at $A_{max}$ (For dye 488, this is 70,000)

Labeled thrombin was then split into 35 µL portions and stored at -20 °C, protected from light.

Beads previously amplified with thrombin aptamer B were denatured into single-stranded DNA with the following procedure: 50 µL 0.15 M NaOH, 37°C, 50 µL 0.15 M Acetic Acid wash; Twice. Aptamers were reformed by heating the beads to 95°C, then rapid cooling on ice. Beads were split into three tubes containing 50 µL of beads in each and incubated beads with 1% BSA and either 0 nM, 200 nM, or 2 µM fluorescent thrombin for four hours at room temperature, protected from light. Beads were centrifuged and supernatant was removed. Beads were washed 3 times with 100 µL 1× PBS with 1% BSA. 30 µL of fresh solution were added and beads were analyzed beads on an Accuri Flow Cytometer.

### 4.2.3 Methods for Aptamer Binding Affinity Measurements Using Magnetic Beads

#### 4.2.3.1 PCR Forward Primer Attachment Using EDC and NHS with single stranded (ss) or double-stranded (ds) DNA

Double-stranded DNA attachment (dsDNA):

First, a double-stranded DNA complex of amine-modified forward primer and its complementary sequence was made by making a 100 µL, 100 µM solution of each in STE buffer (10 mM Tris, 50 mM NaCl, 1 mM EDTA, pH 8.0), mixing well and centrifuging. The mixture was allowed to sit at room temperature for several hours.

Next, 30 µL of well-mixed magnetic beads were placed in a low-binding microcentrifuge tube and washed with 30 µL of 25 mM MES, pH 5 by mixing with pipette continuously for 10 min. The tube was placed tube on a magnet for 2 min, and then supernatant was removed. This washing process was repeated. 700 pmol (Final concentration 7.8 µM) of the double-stranded DNA complex were added to the beads after diluting the previously-made 100 µM solution to 50 µM in 25 mM MES buffer (pH 5). The mixture was rocked at room temperature on an incubating rocker (VWR) for 30 min, mixing manually by pipette at the 15 min mark. 50 mg of EDC were dissolved in 500 µL of cold, 100 mM MES (pH 5) and 9 µL of EDC solution added to the bead reaction. The reaction volume was adjusted to 90 µL using 25 mM MES, pH 5. The reaction was incubated at 4 °C for 3 hours, mixing by pipette every 30 min. Two reactions were stopped at this point, while another two reactions were left to incubate overnight at 4 °C to study the effect of time on the reaction. At the end of each reaction, whether done for 3 h or overnight, supernatant was removed, and 100 µL 50 mM Tris, pH 7.4 were added, mixing well. Reactions were incubated for 15 min at room temperature, mixing by pipette after approximately 8 min. Beads were washed 4 times with 100 µL PBS, pH 7.2 then resuspended in 100 µL PBS, pH 7.2 and stored at 4 °C, protected from light.

The second strand was removed by taking 50 µL of each batch of beads, placing in a separate microcentrifuge tube, then adding 50 µL of 0.15 M NaOH and mixing by pipette. Beads were heated to 37 °C for 20 min, and supernatant was removed. 50 µL 0.15 M Acetic Acid were added, solution was mixed, and supernatant was removed. This process was repeated with NaOH and Acetic Acid. Finally, beads were washed 2 times with 100 µL deionized water and resuspended in 50 µL deionized water.

Single-stranded DNA attachment (ssDNA):

The procedure for double-stranded DNA was repeated, but instead of using a dsDNA complex, 700 pmol of single-stranded, amine-modified forward primer were used. ssDNA was diluted to 50 µM in 25 mM MES, pH 5, and the reaction was performed in duplicate for either three hours, or overnight. At the end of each reaction, whether done for 3 hours or overnight, supernatant was removed, and 100 µL 50 mM Tris, pH 7.4 were added, mixing well. Reactions were incubated for 15 min at room temperature, mixing by pipette after approximately 8 min. Beads were washed 4 times with 100 µL PBS, pH 7.2 then resuspended in 100 µL PBS, pH 7.2 and stored at 4 °C, protected from light.

Non-specific DNA attachment (nsDNA):

The procedures for both double-stranded and single-stranded DNA were performed without adding EDC reagent. Each type of reaction was performed in duplicate for either 3 hours, or overnight.

#### 4.2.3.2 Preparation of Aptamer-Bead Conjugates

Beads were made using ss, ds, or ns DNA attachment methods (Section 2.2.3.1.) using qPCR. PCR mix (D.I. $H_2O$, 0.75% w/v Jeffamine, 1X SYBR Green, 0.2 µM primers, 1.5 mM $MgCl_2$, 1× Platinum Tfi Reaction Buffer, 0.2 mM dNTPs, 0.1 U/µL Platinum Tfi Polymerase) was combined with beads. Before adding beads made with ssDNA, 8 µL of ssDNA beads from both the 3 hour and overnight reactions were transferred to separate tubes, washed twice with 10 µL D.I. $H_2O$, and resuspended in 8 µL of D.I. $H_2O$. When beads were added in any case, no forward primer was added to solution. The PCR positive control contained all reagents and 12 pM template (Final concentration 0.6 pM). The negative control contained all reagents except for forward primer. Traditional PCR was performed for the initial 5 cycles, mixing by pipette

between each cycle with the following program: 94 ºC for 2 min, then 5 cycles of 94 ºC for 15 s; and 60 ºC for 90 s. Tubes were then transferred to a qPCR instrument with melting temperature analysis using the following program: 94 ºC for 2 min, then cycles of 94 ºC for 15 sec; 60 ºC for 1 min.

#### 4.2.3.3 Flow Cytometry Evidence of Amplification onto Beads

Batches of aptamer-modified beads from each type of bead reaction (ss, ds, or ns DNA attachment at 3 h or overnight) were combined in separate tubes. 3 h and overnight reactions with only primer attached (before PCR), along with unmodified beads at the same concentration were placed into separate tubes as well. Supernatant was removed. 20 µL 1× SYBR Green I dye were added to each batch of beads and incubated for 1 h at room temperature. 180 µL of deionized water were added, for a total volume of 200 µL. Samples were analyzed on an Accuri Flow Cytometer.

### 4.2.4. PCR Forward Primer Attachment Using "Click" Chemistry

#### 4.2.4.1 Azide-Alkyne Reaction

Beads were prepared for the reaction by aliquotting 100 µL Dynabeads M-270 Amine (~ $1\times10^8$ beads) into a centrifuge tube and placing them on a magnet for 4 min. The supernatant was carefully removed. The beads were washed with DI $H_2O$ (200 µL, 4 times), MeOH (200 µL, 4 times), and DMF (200 µL, 4 times). In each washing procedure, the beads were resuspended by vortexing for 1-2 min, and placed on the magnet for 4 min. Then supernatant was carefully removed.

For bromoacetylation, 200 µL DMF with 1% Bromoacetyl bromide, 1% N,N-Diisopropylethylamine (DIPEA), and 1% 4-dimethylaminopyridine (DMAP) was add to the beads. The beads were mixed by vortexing for 2 min and placed on a rocker overnight at room temperature. Then the beads were washed with DMF (200 µL, twice), MeOH (200 µL, twice), and DMF (200 µL, 4 times).

For the introduction of azide to the beads, 200 µL saturated Sodium Azide ($NaN_3$) solution in DMF were added, and the beads were mixed by vortexing for 2 min and placed on an Incubating Rocker (VWR) for 24 h at room temperature. The saturated $NaN_3$ solution in DMF was replaced with fresh solution after 12 h, then the beads were washed with DMF (200 µL, twice), MeOH (200 µL, twice), and DI $H_2O$ (200 µL, 4 times). The beads were stored in 100 µL $H_2O$ at 4 °C.

For the click reaction with alkyne-modified DNA, 5 µL beads, 2 M triethylammonium acetate buffer (pH 7.0, 20 µL), 5 mM Ascorbic Acid solution in $H_2O$ (20 µL), 10 M copper (II) - Tris(benzyltriazolylmethyl)amine (Cu-TBTA) in DMSO (10 µL), 5 nmol DNA-alkyne solution, and DI $H_2O$ were combined into a total volume of 200 µL. The beads were mixed by vortexing for 2 min and then placed on a rocker for 24 h at room temperature. Then the beads were washed with Tris EDTA buffer (200 µL, 4 times) and stored in Tris EDTA buffer (100 µL) at 4 °C.

#### 4.2.4.2 Proof of DNA Attachment to Beads

To demonstrate the effectiveness of the click reaction, 50 µL of beads previously modified with forward primer using the “click” reaction were placed in a microcentrifuge tube and surpernatant was removed after placing tubes on a magnet specially designed for use with microcentrifuge tubes (Invitrogen). Beads were washed twice with 50 µL deionized water, and all solution was removed. Anti-forward primer was added at a final concentration of 0.05 nmol/µL, using STE

buffer (10 mM Tris-HCl, 1 mM EDTA, 0.1 M NaCl, pH 8.0) to bring the reaction up to a final volume of 100 µL. The solution was incubated 1 h at room temperature.

Supernatant was removed from 20 µL of beads with anti-forward primer attached, 20 µL of beads without anti-forward primer, 20 µL of non-specific binding control beads, and 20 µL of azide-modified beads on a magnet, and the beads were washed 2 times with 50 µL deionized water. 20 µL 1x SYBR Green I were added to each tube, and incubated with beads for 1 hour at room temperature. Beads were washed 1 time with 50 µL deionized water and resuspended in 100 µL. Beads were analyzed using flow cytometry (Accuri flow cytometer).

#### 4.2.4.3 Amplification of DNA to Beads with Newly-selected Aptamers

Forward primer-modified beads for newly selected thrombin aptamers (selected by Dr. Joonyul Kim in the Easley laboratory), referred to as c3 and c5, were made using click chemistry as previously described (Section 4.2.4.1.). A 50 µL aliquot of beads was washed three times with 50 µL of deionized water and resuspended in 50 µL. PCR mix (D.I. H2O, 1X SYBR Green I, 0.2 µM primers, 1.5 mM MgCl2, 1× Platinum Tfi Reaction Buffer, 0.2 mM dNTPs, 0.1 U/µL Platinum Tfi Polymerase) was combined with beads. PCR solutions containing amine-labeled beads from the company, azide-modified beads, and a bead negative control (No reverse primer added to PCR solution) were also prepared. All solutions were distributed over six aliquots. This included two sets of three, in which PCR was to be stopped after 40, 60, or 80 cycles to test the effects of cycle number on amplification. One set of three contained free forward primer in solution, while the second set did not. This was done to compare results when amplification is dependent on the primer attached to the surface and when it is not. The PCR positive control contained all reagents for PCR, while the negative control contained all reagents except for

reverse primer. Real-time PCR (qPCR) was performed for 80 cycles, plus melting temperature analysis with the following program: 94 °C for 2 min, then cycles of 94 °C for 15 sec, and 55 °C for 1 min. Samples removed after 40, 60, or 80 cycles as needed. All samples were washed twice with 30 µL of deionized water, resuspended in 90 µL, and refrigerated (4 °C) until ready for use. Flow cytometry analysis was performed after adding 40 µL of 1X SYBR Green dye to bead samples.

### 4.2.5 Methods for Digital Detection

#### 4.2.5.1 Droplet Digital PCR

Experiment 1:

Emulsion droplets were generated using a multi-channel emulsion generator (Chapter 2) using Jeffamine-modified surfactant in HFE 7500 oil. The aqueous phase contained PCR mix (D.I. H2O, 1% BSA, 50 nM probe, 0.2 µM primers, 1.5 mM MgCl2, 1× Platinum Tfi Reaction Buffer, 0.2 mM dNTPs, 0.1 U/µL Platinum Tfi Polymerase) with 0, 6.6, 33.2, 66, or 1000 fM template concentration. An 85 kPa vacuum was pulled until center outlet reservoir was filled with emulsion. This was repeated 4 times until all PCR solution was converted into emulsion format. Emulsion was transferred to individual PCR tube and 60 µL mineral oil layered on top. This process was repeated, handling one concentration of template mix at a time, starting with the lowest concentration (0 fM) and ending with the highest (1 pM). Aqueous controls (not emulsified) at each DNA concentration were also prepared, and Real-time PCR was performed for 40 cycles with the following temperature program: 94 ºC for 2 min, then cycles of 94 ºC for 15 sec; 60 ºC for 1 min.

Reference droplets for imaging (1% BSA, 1X PCR Buffer, 2X ROX Reference Dye, and 50 nM Taqman Probe) were generated on a multi-channel emulsion generator. Each sample was individually wrapped in foil and stored at 4 °C until ready for use. Sample droplets were reinjected, one concentration at a time, into a microfluidic channel for imaging after mixing 5 µL sample droplets with 2 µL reference droplets by pipette in a microcentrifuge tube. Droplets were imaged with confocal microscopy.

An algorithm was created using Image J to find the droplets in each image, separate them into regions of interest, and measure their mean intensities. The data at each concentration was plotted in Excel and analyzed for digital results.

Experiment 2:

Droplets were generated by pulling a vacuum of approximately 70 kPa to a single-channel emulsion generating microfluidic device (Chapter 2), using 1.8% w/w Krytox in HFE 7500 oil as the carrier phase. The aqueous inlets were filled with amplification mix for PCR (D.I. H2O, 0.75% w/v Jeffamine ED900, 1% BSA, template DNA, 50 nM Taqman Probe, 0.2 µM Fwd/Rev primer oligos, 1.5 mM MgCl2, 1X Platinum *Tfi* Reaction Buffer, 0.2 mM dNTPs, 0.1 U/µL Platinum *Tfi* DNA Polymerase). Solutions contained either 0, 160 fM, or 16 pM template. A separate solution of amplification mix, containing 16 pM template and no Jeffamine, was also made as a negative control to show that Krytox inhibits PCR. Separate single-channel emulsion generators (Chapter 2) were used for each template concentration. After emulsifying all of the solution, droplets were transferred from the device outlet to individual PCR tubes. 60 µL mineral oil was layered on top of each emulsion, and PCR products were generated using a CFX1000 Thermal Cycler with CFX96 qPCR detection system (BioRad) and the following temperature

cycling program: initial denaturation at 94°C for 2 min; cycling at 94°C for 15 s and at 60°C for 1 min; total of 35 cycles. An aqueous solution of amplification mixture (no oil) containing 16 pM template was used as a positive control, and a solution containing no template was used as a negative control. After thermal cycling, sample droplets were mixed with reference droplets by pipetting, and they were transferred to a single microfluidic channel for imaging via confocal microscopy. Reference droplets (50 nM ROX-labeled DNA, 50 nM Taqman probe; 1% BSA; 1X Platinum *Tfi* Reaction Buffer) were generated using a separate droplet-generating device.

#### 4.2.5.2 Droplet Digital RPA

Methods used for ddRPA are identical to those included in Chapter 3, section 3.2.5.2.

#### 4.2.5.3 Bead Digital Detection

For ligation of template DNA to beads, 10 µL of 1 µM aptamer/connector ligated complex were made by first diluting both the aptamer and connector sequences to a final concentration of 10 µM in deionized water. Next, a 1 µM solution of aptamer/connector complex was made by diluting each 10 µM solution in binding buffer (50 mM Tris-HCl, 100 mM NaCl, 1 mM $MgCl_2$, pH 7.5). This solution was incubated at 16 °C for 15 min. After incubation, the 1 µM aptamer/connector complex was diluted to 11.1 pM (100 copies per bead), 1.1 pM (10 copies/bead), 0.1 pM (1 copy/bead), and 0.01 pM (0.1 copies/bead) concentrations in a final volume of 15 µL. Two additional solutions of 11.1 pM aptamer/connector complex were made for use with the positive (Native forward primer + enzyme; No beads) and negative (Native forward primer/no enzyme; No beads) controls.

Next, 40 µL of beads previously modified with PCR forward primer using click chemistry (Section 4.2.4.1.) were washed 3 times with 10 µL of binding buffer and resuspended in 5 µL of

binding buffer. The beads, along with the aptamer/connector complex dilutions, and 5 µL of 49.5 µM native Forward primer, were incubated at 16 °C for 15 min.

Next, 1 µL of incubated beads or 1 µL native forward primer were added to the aptamer/connector complex dilutions, making the total ligation volume 16 µL. These samples were allowed to incubate at 16 °C for 15 min, mixing by pipette every 5 min.

T4 DNA Ligase in 1X Ligase Buffer (New England Biolabs) was made at a final concentration of 6.7 Units/µL for all aptamer/connector complex dilutions, as well as the positive control (Native forward primer + enzyme; No beads). 4 µL were added to each sample, making the total reaction volume 20 µL. Also, 1X T4 DNA Ligase Buffer containing no enzyme was made and added to the negative control sample (Native forward primer/no enzyme; No beads) for a final reaction volume of 20 µL. All reactions were incubated at 16 °C for 20 min, mixing by pipette every 5 min. Samples were stored at 4 °C until they were ready for use.

qPCR was performed on the beads with various concentrations of aptamer now ligated to them. Beads with 100, 10, 1, and 0.1 copies of template per bead were placed on a magnet to remove the supernatant. They were then washed 1 time with 15 µL of deionized water and resuspended in 15 µL to wash away excess aptamer/connector complex. PCR mix (D.I. $H_2O$, 0.75% w/v Jeffamine, 1X SYBR Green, 0.2 µM primers, 1.5 mM $MgCl_2$, 1× Platinum Tfi Reaction Buffer, 0.2 mM dNTPs, 0.1 U/µL Platinum Tfi Polymerase) was combined with beads, and PCR was performed for 80 cycles with melting curve analysis added to the end, using the following program: 94 ºC for 2 min, then cycles of 94 ºC for 15 sec; 66 ºC for 1 min. The ligated beads and the positive and negative controls made during the ligation reaction, served as PCR templates.

No additional template was added or used. The aqueous PCR positive control contained 12 pM ligated template, and the negative control contained no template.

To prepare beads for flow Cytometry analysis, amplified beads (20 µL PCR volume) were transferred to individual 1.5 mL microcentrifuge tubes. 1 µL plain, azide-modified beads and 1 µL of forward primer-modified beads from the click reaction were each diluted to 20 µL in deionized water. 20 µL of 1X SYBR Green I nucleic acid stain were added to each sample and incubated for several hours at room temperature. Beads were analyzed via flow cytometry.

## 4.3 Results and Discussion

### 4.3.1 Toward Binding Affinity Measurements for Selected Aptamers Using Fluorescence-Based Flow Cytometry

#### 4.3.1.1 Bead Conjugation of PCR Forward Primer Using EDC and NHS

The procedure for bead modification was adapted from the Fisher Scientific Product Instructions for "NHS and Sulfo-NHS" [21]. Reaction of 2 µm-sized carboxyl latex beads (Invitrogen) were reacted with an amine-labeled PCR forward primer in the presence of 2.0 M 1-ethyl-3-[3-dimethylaminopropyl]carbodiimide (EDC) and 5.0 M N-hydroxysuccinimide (NHS) to create a stable, amide bond (Figure 4.1). This bead was later used as a forward primer during PCR to amplify a DNA aptamer sequence onto the beads.

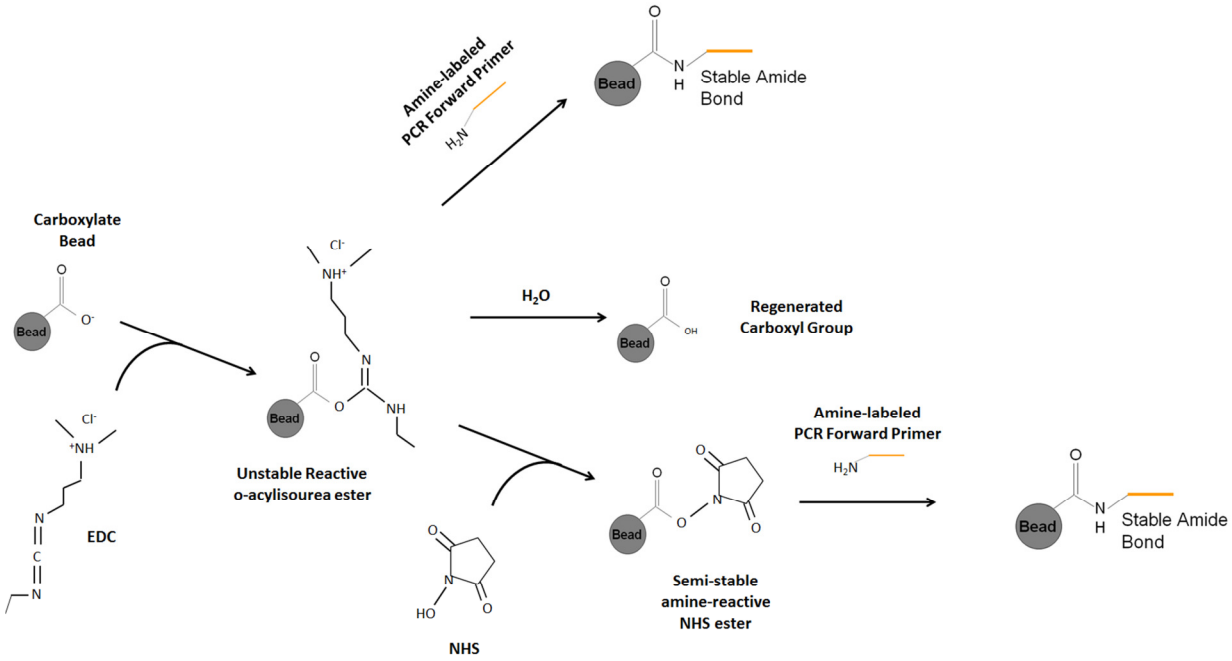


**Figure 4.1**A carboxylated bead was reacted with NHS, in the presence of EDC, to create a semi-stable, amine-reactive, NHS ester. An Amino – modified PCR forward primer was added, forming a stable amide bond.

Adapted from Fisher Scientific Product Instructions "NHS and Sulfo-NHS" (Product No. 24500, 24510, 24520, 24525), http://www.piercenet.com/instructions/2160650.pdf, Accessed May 31, 2014.

#### 4.3.1.2 Preparation of Aptamer-Bead Conjugates

In order to utilize beads for binding affinity experiments, a significant portion of the surface should be covered in a DNA aptamer sequence. Figure 4.2 A illustrates the process of transforming beads from primer-conjugated particles, to aptamer labeled particles. After amplification and second strand removal, aptamer beads were incubated with the target of interest, and binding affinity measurements were made. Preparative PCR was done on the primer-labeled beads in order to attach as many copies of thrombin aptamer B (89 nucleotides) onto the carboxyl latex beads as possible. During the primer conjugation reaction, two different concentrations of beads (1 mg/mL or 10 mg/mL) were used to optimize the reaction conditions for maximum attachment. Both of these bead concentrations were used in PCR, along with aqueous positive and negative (no template) controls, and amplification was allowed to continue for 100 cycles in order to ensure maximum amplification (Figure 4.2 B). The threshold cycle, also referred to as the C(t) value, is the cycle number at which each sample's amplification intensity increases above a defined threshold and was compared between each sample. The positive control, 1 mg/mL bead concentration, and 10 mg/mL bead concentrations all amplified with a C(t) value around 6, showing that the reaction is just as efficient with primer-labeled beads as it is when primer is added in free solution. Also, there was no contamination present in the reaction that would cause a false positive result. This was denoted by the lack of amplification by the negative control. One hundred cycles of PCR was unnecessary, as the plateau phase was reached for most reactions between 20 and 30 cycles. The plateau phase is the point in the reaction at which reagents are depleted, enzyme loses functionality, and no further amplification of product is observed. The flattening and then later return to amplification seen in the positive control and 1 mg/mL bead reaction is indicative of a second, non-specific

amplification of PCR product. However, the 10 mg/mL bead reaction appears to steadily increase without ever flattening into a plateau. In the future, amplification will be stopped between 30 and 50 cycles.

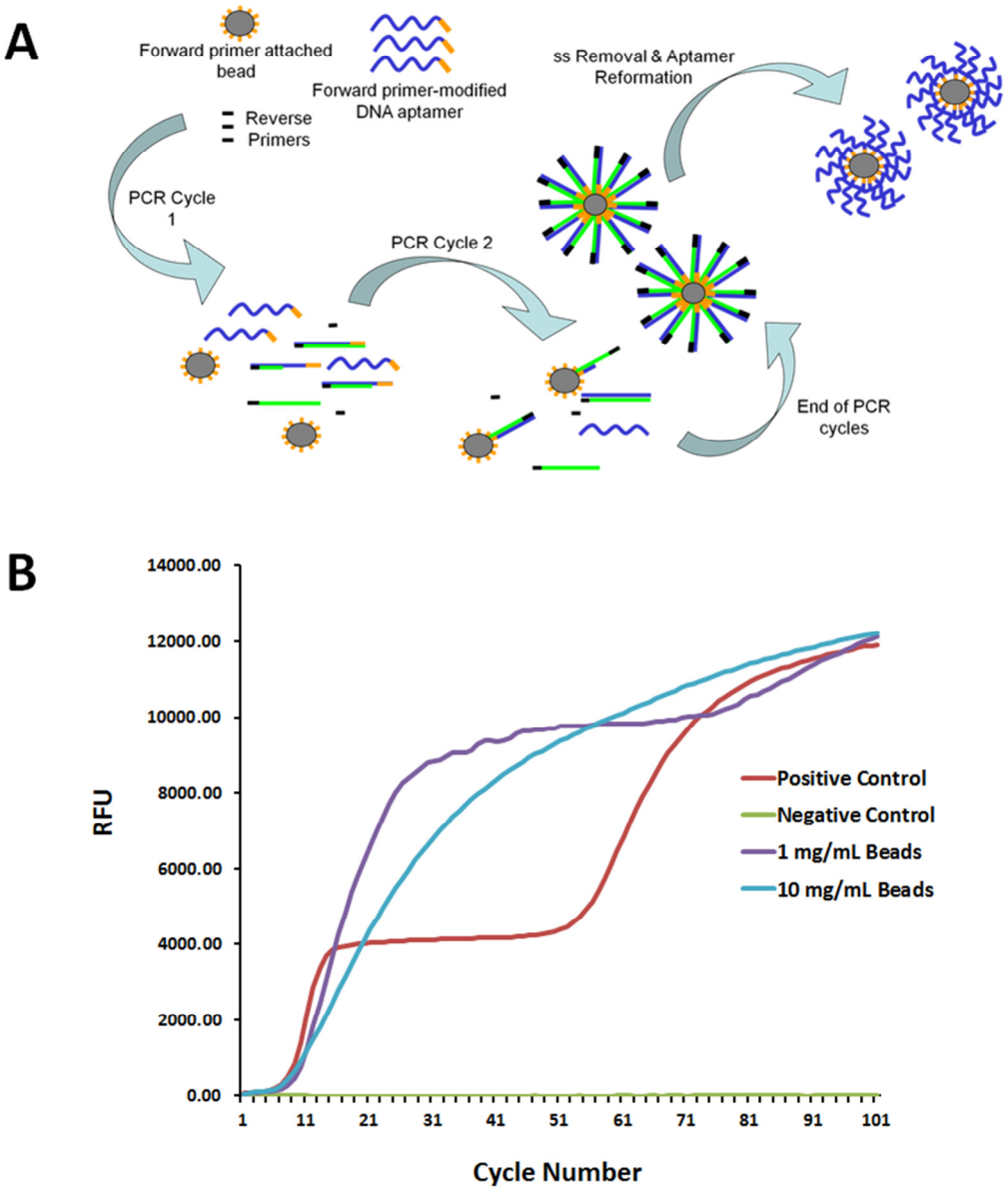


**Figure 4.2** (A) Illustration depicting the preparation of aptamer – bead conjugates. PCR is used in a preparative sense to generate many copies of dsDNA on the bead surfaces. Following PCR, aptamers are denatured to single strands and reformed for incubation with target. (B) Real-time PCR reaction amplifying thrombin aptamer B onto primer-conjugated beads. Positive control contains unbound forward primer, while negative control does not contain aptamer template sequence.

Control experiments were necessary to validate amplification results seen with primer-conjugated beads. Adding beads to PCR solution creates a different amplification environment than in aqueous solution. The bead presence could sterically hinder efficient amplification of PCR products. In order to demonstrate that bead presence does not affect PCR results, PCR mixes containing a final concentration of 0, 0.3, or 3 pM thrombin aptamer B were made with and without unmodified, carboxyl latex beads present. Amplification was allowed to occur for 50 cycles (Figure 4.3 A), and the efficiency was determined by comparing C(t) values. The C(t) value using 3 pM thrombin aptamer B (10 pM on Figure 4.3 A) is approximately 12 without beads and 13 when beads are added. For 0.3 pM aptamer, the C(t) values are approximately 16 with and without beads. Finally, for 0 pM aptamer, the C(t) values are approximately 24 without beads and 32 when beads are present. These numbers are inconsistent between trials and do not agree with each other, because the 0 pM sample should not have template present and therefore should not amplify. This indicates that there is contamination of template present in another PCR reagent, and that is what amplified at the 0 pM concentration. In the future, the reaction can be allowed to proceed for only 20 cycles to prevent amplification of the contaminant. Overall, the results from the other DNA concentrations show that bead presence does not affect PCR efficiency.

To obtain qPCR evidence that amplification is specific to primer-labeled beads, forward primer-conjugated beads, created as previously described (Section 4.2.2.1), was amplified with 350 pM thrombin aptamer B. This was compared with amplification using beads without forward primer attached to them. These beads were made during the same reaction by not adding forward primer to the solution. No additional forward primer was added to the PCR solution, and amplification proceeded for 100 cycles (Figure 4.3 B). Amplification of primer-conjugated beads

occurs around 30 cycles, while beads without primer do not amplify. As expected, the aqueous PCR positive control showed successful amplification, while the negative control (no template) did not.

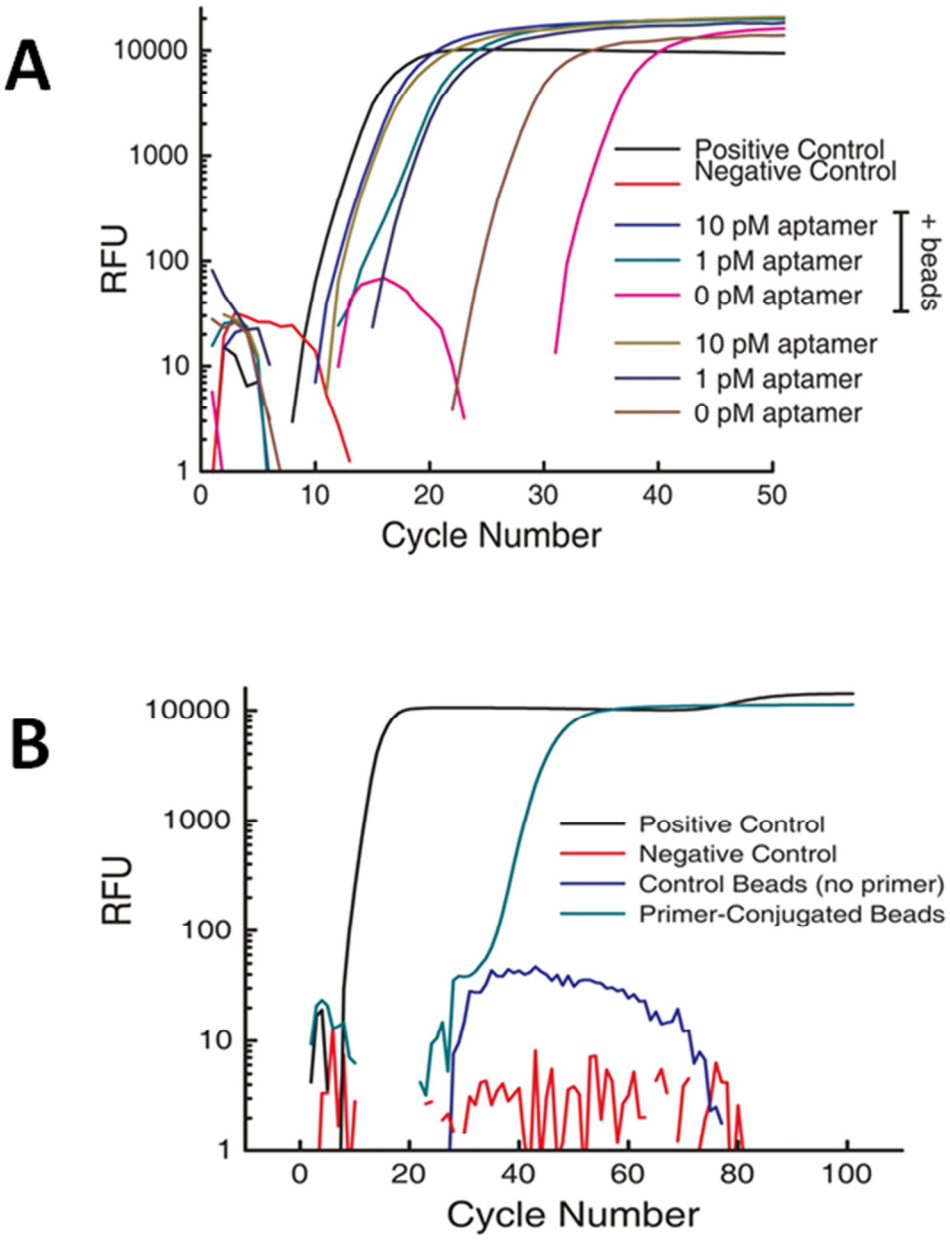


**Figure 4.3** (A) Bead presence does not affect PCR. Three concentrations of thrombin aptamer were amplified with and without beads present (qPCR), and no significant difference in Ct was seen between the two groups. (No primer-conjugated beads used) (B) Thrombin aptamer amplification is specific to modified beads. qPCR was performed on both primer-conjugated and unconjugated beads using 352 pM of aptamer. PCR product was only observed with primer-conjugated beads present.

#### 4.3.1.3 Aptamer-Bead Conjugate Functionality

The concentration of DNA amplified onto the surface of each bead was calculated by first counting aliquots of aptamer-modified beads using flow cytometry. Next, a known number of aptamer-modified beads were used as PCR templates and amplified alongside a standard curve of reactions containing template at varying concentrations. Standard solutions were made at final aptamer template concentrations of 1, 5, 10, 25, 50, 75, 100, 200, 300, and 390 pM. Each standard was analyzed in duplicate, and the log of the C(t) values for all of the standard solutions were then plotted versus concentration to make the curve (Figure 4.4, Top). Four different aliquots containing a known amount of beads were analyzed, and the log of the C(t) values did not fall within the standard curve. Nonetheless, extrapolation was used to predict that the average concentration of DNA in all four aliquots was 800 ± 300 pM. This information, combined with the number of beads counted, was used to calculate the concentration of DNA per bead as 0.2 attomoles per bead. This number agrees with other groups attaching DNA in a similar manner [2]. In the future, the amount of beads should be decreased so that the C(t) value will fall within the standard curve range.

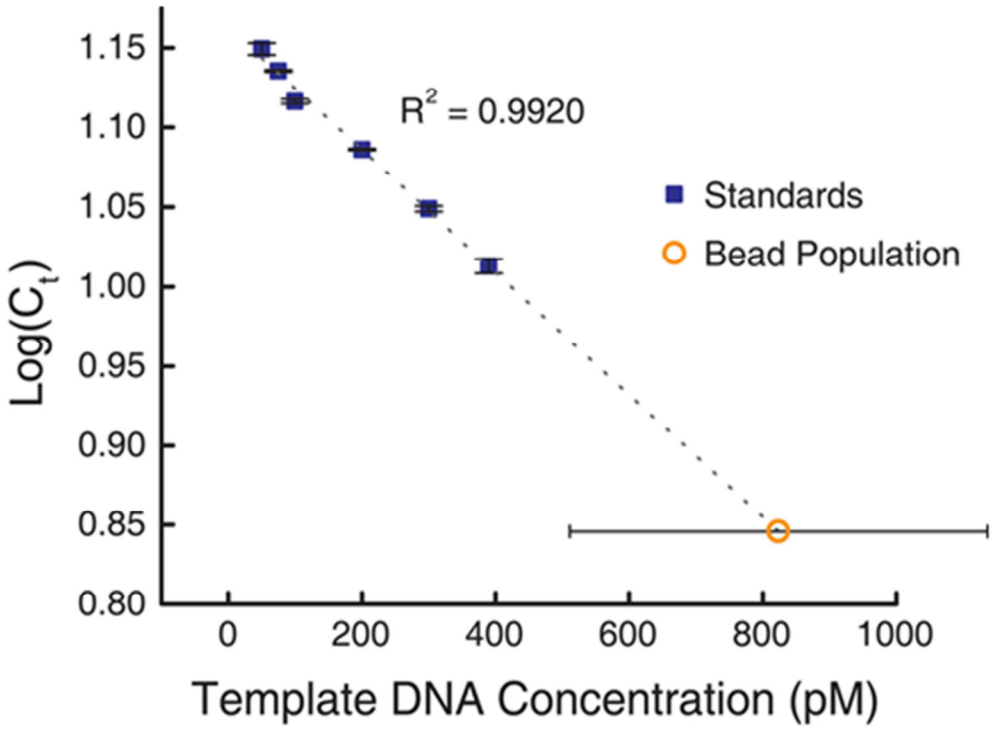


| Moles DNA | # DNA strands | # beads in qPCR volume | # DNA strands per bead | moles DNA per bead | Attomoles DNA per bead |
|---|---|---|---|---|---|
| 2E-14 | 1E+10 | 9E+04 | **1E+05** | 2E-19 | **0.2** |

**Figure 4.4** Preliminary study determining the amount of aptamer conjugated to each bead. A 6-point standard curve was created ([aptamer] from 1 to 390 pM) for qPCR. Four equal aliquots of aptamer-modified beads were analyzed, and extrapolation was used to determine that the average concentration of DNA in all four aliquots was 800 ± 300 pM. qPCR volume = 25 µL; The table shows the calculated amount of DNA per bead. The bead count was 6.73 x $10^9$ ± 0.07 beads/L. 50-µL aliquots were counted in triplicate (Accuri flow cytometer). Attomole amounts of conjugated DNA per bead is comparable to values previously reported [2].

Aptamer-modified beads were tested for binding to thrombin from human plasma. Thrombin was handled very carefully during the process to ensure that it retained its functionality. For example, when dissolving the thrombin, solution was swirled instead of pipetted to avoid creating air bubbles and denaturing the protein. Also, thrombin was dissolved over several aliquots of solution, totaling 100 µL, in order to dissolve the maximum amount of protein. The thrombin was labeled with Alex Fluor 488 dye (Ex: 498 nm; Em: 518 nm) so that binding could be detected from a fluorescent signal during flow cytometry. After labeling with dye, thrombin concentration was determined from the A280 signal at an E1% of 18.30 using a Nanodrop 1000 spectrophotometer. The second strand was removed from beads previously modified with thrombin aptamer B via PCR, in order to transform them into single-stranded aptamer sequences. The beads were cooled rapidly to promote folding of aptamers into well-defined tertiary structures that are known to bind to specific sites on the thrombin molecule. Using a variety of methods, the $K_d$ of thrombin aptamer B has been determined to fall within the range of 100-300 nM at room temperature [22], so beads were incubated with 1% BSA and either 0 nM, 200 nM, or 2 µM fluorescent thrombin. The BSA was added to block sites for non-specific adsorption of thrombin to the bead surface, which would result in a false positive signal. Unmodified beads were also incubated with fluorescent thrombin as a negative control. Figure 4.5 shows the flow cytometry histogram comparing the negative control bead population to modified beads incubated with 200 nM fluorescent thrombin. The modified beads not incubated with thrombin (0 nM fluorescent thrombin) showed similar intensity to the control bead population. A significant shift in intensity is seen after incubating functionalized beads with 200 nM thrombin. However, there was no further shift in intensity when beads were incubated with 2 µM thrombin. This suggests that the $K_d$ for thrombin aptamer B lies between 0 and 200 nM, as

expected. Further experiments using concentrations in this range are necessary in order to determine an exact $K_d$ for the aptamer with this method. Also, the aptamer-conjugated bead peak in figure 4.5 represents two droplet populations, denoted by the presence of a shoulder at a slightly higher intensity than the main peak. These beads are most likely doublets, or two beads stuck together, which gives a higher signal than the singlet bead population. Careful gating of the data is necessary in future experiments to eliminate peak shoulders. In addition, surfactants such as Tween 20 can be added to bead solutions to prevent bead aggregation [1]. This could be added to PCR solution or immediately before flow Cytometry to prevent aggregation of beads.

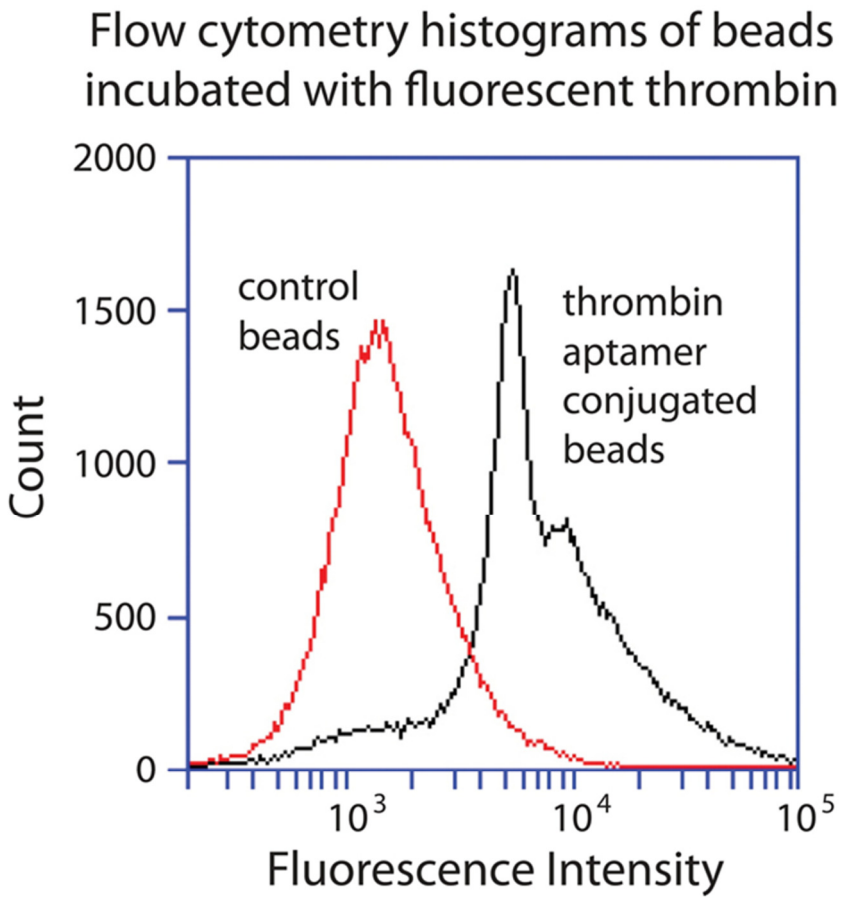


**Figure 4.5** Target binds aptamer-modified beads with high specificity. Aptamer-modified beads were incubated with 200 nM fluorescent thrombin and 0.1% BSA for 4 hours. Beads were washed thoroughly and analyzed via flow cytometry with a control population of unmodified beads. A significant shift in intensity was seen from 0 nM to 200 nM in the aptamer-conjugated population, but 2 µM fluorescent thrombin resulted in no further significant shift, suggesting that the $K_d$ for thrombin aptamer to thrombin lies between 0 nM and 200 nM.

#### 4.3.1.4 Bead Conjugation of PCR Forward Primer to Magnetic Beads

##### 4.3.1.4.1 EDC Reaction

Due to the difficulty of handling latex beads, the EDC/NHS method of primer attachment was developed using carboxylic acid-modified magnetic beads. Magnetic beads ease the washing process, as beads in a centrifuge tube can simply be placed on a magnet to remove supernatant. One of the challenges presented with latex beads was that washing the beads required pelleting them through centrifugation. Pelleting efficiency was not 100%, which led to loss of beads during the washing process.

While exploring DNA attachment with magnetic beads, two methods were used. The reaction was performed with either single-stranded or double-stranded DNA. The single-stranded, amine-labeled forward primer was shown to successfully attach to carboxyl latex beads, but some of the sequences may have bonded with internal amines found within the individual nucleotide structures, which is a caveat found in the bead protocol [23]. These improperly attached DNA strands could lead to steric hindrance and formation of incorrect products. In theory, using a double-stranded DNA complex would ensure that all bases were paired, leaving only the primary amine exposed and available for reaction. After the reaction, the second strand could be removed, exposing the covalently-bound PCR primer.

The double-stranded DNA complex was made using amine-modified forward primer and its complementary sequence. The two were allowed to anneal in STE buffer (10 mM Tris, 50 mM NaCl, 1 mM EDTA, pH 8.0), which is often used for annealing DNA. The complex was simply allowed to sit at room temperature for several hours to promote annealing. Often, DNA sequences are heated and then cooled slowly to prevent formation of secondary structures during

the annealing process. This was unnecessary in this case, because the primer only contains 20 base pairs and no secondary structures should form.

The reaction used to attach DNA to the beads only required the use of EDC during a one-step coating procedure. The procedure was performed with both single-stranded and double-stranded DNA for either 3 hours or overnight. This was done to simultaneously test the effects of time on reaction efficiency. A non-specific binding study was also performed alongside the reaction. This involved performing the same reactions with the same variables but omitting EDC reagent from the process. Without EDC, the carboxyl groups should remain inactivated and therefore not react with amine-labeled DNA. After the reactions involving double-stranded DNA, the second strand was removed. All beads, regardless of attachment method, were washed and refrigerated (4 °C) until ready for further use.

#### 4.3.1.4.2 Preparation of Aptamer-Bead Conjugates

Magnetic beads previously modified through EDC chemistry were amplified with PCR to cover the bead surface in thrombin aptamer B. Figure 4.6 shows the real-time PCR traces for amplification with beads reacted with double-stranded (Figure 4.6 A) or single-stranded (Figure 4.6 B) PCR forward primer for both 3 hours and overnight. Beads from a non-specific adsorption study with ss or ds DNA were also amplified (Figure 4.6 C). Traditional PCR was performed on the beads for 5 cycles. The thermal cycler was stopped, and solutions were mixed by pipetting between each cycle. The assumption was that if forward primer was attached to the beads, the initial 5 cycles should have been enough to copy and amplify some template DNA into free solution. As a result, these copies should now amplify properly during qPCR and give a strong

signal. Tubes were transferred to a qPCR instrument, along with aqueous positive (primer in aqueous solution) and negative (no forward primer) controls for amplification.

Figure 4.6 A shows the dsDNA trace. The positive control amplified, while the negative control did not, meaning that there was no contamination present. Beads were placed in the PCR reaction at two different concentrations to determine the number of cycles needed for amplification in future experiments. The higher bead concentration amplified with a C(t) of approximately 35, while the lower bead population amplified with a C(t) of approximately 45. A set of control beads (unmodified) were also analyzed, and no amplification was observed. All beads amplified, regardless of the amount of time they were reacted with primer. In addition, when beads were added, no forward primer was added to free solution, making amplification dependent solely on the bead surface. This demonstrates that primer was successfully attached to beads during the EDC reaction. In addition, the final RFU for bead reactions (< 200) is much lower than that of the positive control ( ≈1 500 ). This is because beads settle to the bottom of the PCR tube during thermal cycling, causing the detector to register a lower fluorescence signal due to optical settings. This result further confirms that PCR products are bound to the beads. Figure 4.6 B shows the ssDNA trace. Much like the dsDNA results, positive and negative controls results were expected, and primer-modified beads showed amplification with a C(t) of approximately 25, regardless of whether the reaction was performed for 3 h or overnight. Finally, the non-specific adsorption study is shown in Figure 4.6 C. This study was done to ensure that amplification of ss and ds DNA beads was not due to non-specific attachment of DNA to the bead surface. The results showed no amplification when beads were reacted (No EDC) with ss or ds primer for 3 h or overnight. None of the bead populations amplified. Based on all of the results in Figure 4.6, a 3 h reaction is sufficient to modify beads for this purpose. Also, the

results show that single-stranded DNA should be used, because the results obtained were comparable to ds DNA results, and ds DNA bead preparation is more complex.

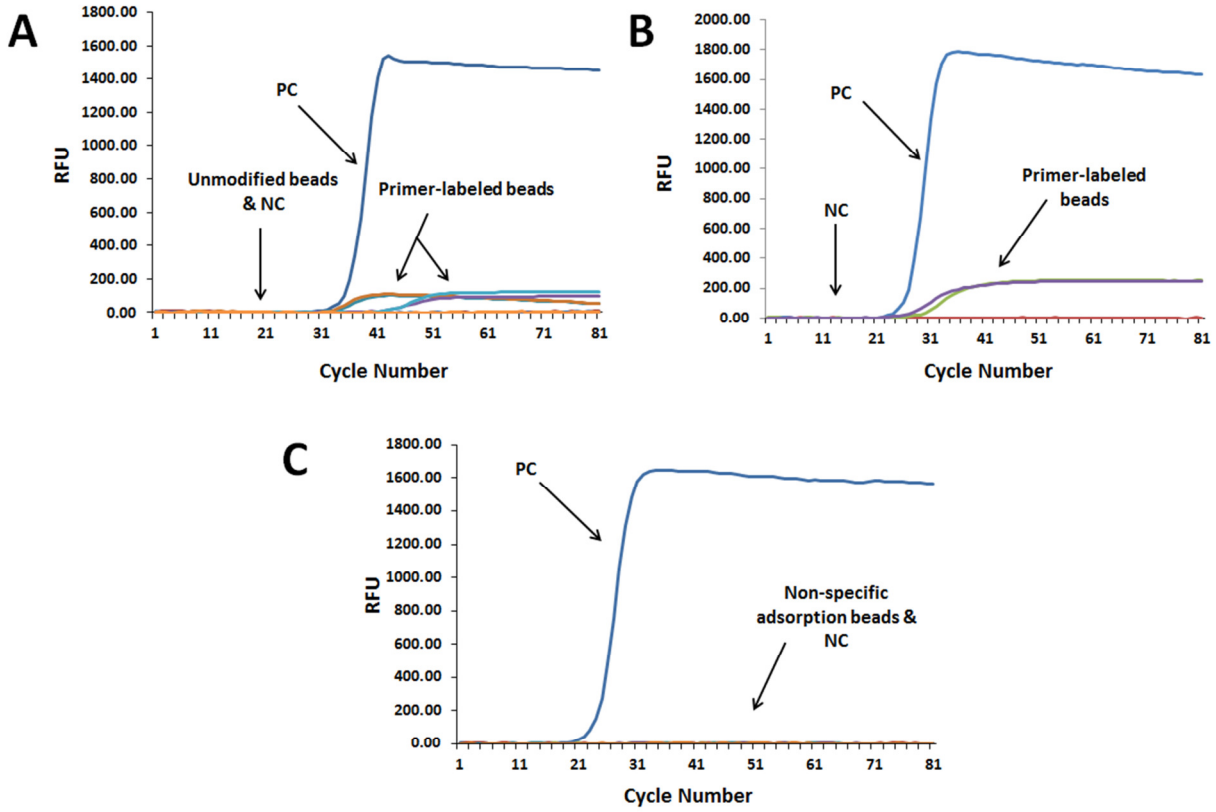


**Figure 4.6** Real-time PCR amplification of magnetic beads modified with forward primer using two different methods. (A) Carboxylated, magnetic beads were modified with amine-labeled dsDNA forward primer by reacting in the presence of EDC for either 3 hours or overnight (≈15 h). Beads were added to PCR reactions at two different concentrations in order to determine the number of cycles needed for amplification. PC = All reagents + 12 pM template. NC = All reagents except forward primer. In each instance where beads are included in the reaction, no additional forward primer was added in free solution. Results show that amplification is dependent on forward primer attached to the bead surface. (B) Beads were modified with ssDNA forward primer and tested in the same manner as dsDNA beads, and similar results were obtained. Only one concentration of beads were added to this reaction. (C) Beads were tested for non-specific adsorption of DNA by incubating with both ssDNA and dsDNA (no EDC present) for either 3 hours or overnight (≈15 h). Real-time PCR results show no amplification of either bead population, meaning that non-specific adsorption does not occur.

#### 4.3.1.4.3 Flow Cytometry Results for Aptamer-Bead Conjugates

Flow cytometry was used as further confirmation of DNA attachment and successful bead amplification. Beads made via ss or ds DNA attachment for 3 h or overnight, as well as beads from the non-specific adsorption study were analyzed before and after PCR amplification. In addition, unmodified beads were analyzed as a control. A dsDNA intercalating dye, SYBR Green I, was used to stain the beads, and fluorescent intensity was obtained using flow cytometry (Figure 4.7). Because SYBR green has some affinity for ssDNA, an intensity shift should be seen after attachment of forward primer to the beads. Upon amplification, an even greater shift should be observed, because the surface converts from a 20 nt primer sequence to an 80 bp aptamer sequence. Not only is the sequence longer, but also the dye has a higher affinity for double-stranded DNA.

Figure 4.7 A shows results obtained from ds DNA attachment. The 3 h reaction (Figure 4.7A, Left) showed a shift in intensity units from approximately 17 000 to 67 000 after reacting with primer. However, after amplification, the peak shifted to a lower intensity. The average intensity after amplification was approximately 60 000, and the peaks overlapped significantly. When the reaction was allowed to proceed overnight (4.7A, Right) a better result was obtained. Primer modification caused the peak to shift to 94 000, while PCR causes an even greater shift to 104 000. Although not baseline-resolved, the aptamer peak is now at a higher intensity than the primer-labeled peak as expected. Results from ss DNA attachment showed the opposite trend (Figure 4.7 B). In this case, it is the overnight reaction that shows no separation in intensity after PCR (Figure 4.7 B, Right). The 3 h reaction did show separation, and peaks were baseline-resolved (Figure 4.7 B, Left). In this instance, primer attachment yielded a fluorescence intensity of approximately 50 000, and PCR amplification caused the peak to shift to 90 000. This trend

could be the result of improper attachment or binding of ss DNA sequences through amines found internally within the structure of individual nucleotides. The longer the reaction was allowed to proceed, the more this anomaly could occur. Therefore, when ss DNA is used, it is best to perform the reaction for only 3 h. The ss DNA method may have resulted in better PCR amplification, as denoted by the greater increase in intensity after PCR, if the second strand was not completely removed from the ds DNA complex after the reaction. If still present, the second strand would compete with the aptamer template for annealing during PCR, resulting in fewer amplified products formed. The non-specific adsorption study performed as expected, further confirming that DNA does not attach to the beads without EDC reagent (Figure 4.7 C,D). In each case, primer-modified beads remained at the same intensity as control (unmodified) beads. One interesting observation, however, is that fluorescence intensity decreased after amplification. The PCR thermal cycle may have caused denaturation or removal of materials inherently present on the bead surface as manufactured, which may have some affinity to the fluorescent dye, causing a decrease in signal.

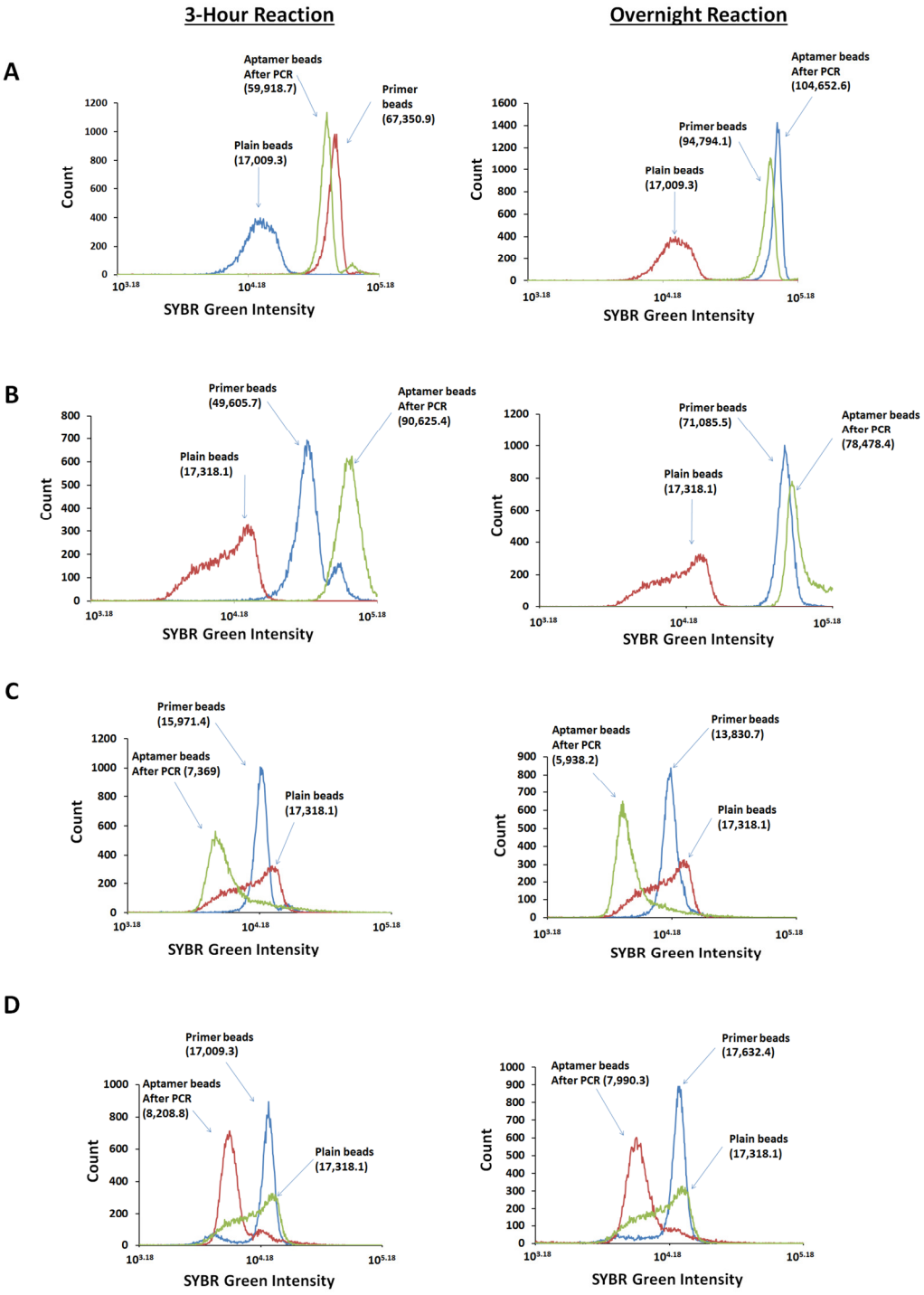


**Figure 4.7** Flow cytometry histograms of beads modified with forward primer during a 3 h or overnight (≈15 h) reaction. Beads were analyzed before and after PCR amplification by staining with a double-stranded DNA intercalating dye (SYBR Green I). Results are plotted on a log scale, and the average intensity of each peak is included in parentheses. (A) Beads were modified using the dsDNA method (Section 4.2.3.1). (B) Beads were modified using ssDNA. (C) Beads were tested for non-specific adsorption by incubating with ds DNA. EDC activating reagent was not added. (D) Non-specific adsorption study was also performed with ssDNA.

#### 4.3.1.5 DNA Attachment Using Click Chemistry

##### 4.3.1.5.1 Click Chemistry Reaction

Another method developed for attaching DNA to magnetic beads involved the use of click chemistry. "Click Chemistry" was first described by K. B. Sharpless in 2001 as a type of reaction that produces high yields, has many applications, has byproducts that are easily removed, is stereospecific, is easily carried out, and uses solvents that are either easily removed or whose presence does not negatively impact the reaction [15-16]. Click chemistry has become popular and has been applied to several areas of research, including polymer chemistry, bioconjugation, and drug discovery. There are several types of click reactions in circulation, such as “nucleophilic ring opening reactions of epoxides and aziridines, formation of hydrazones and heterocycles, oxidative formation of epoxides and Michael Additions, and cycloaddition reactions” [16]. These reactions match the criteria, because they are thermodynamically favorable and form only one product [16].

The click reaction used in our experiments is the well-studied Huisgen copper(I)-catalyzed azide-alkyne 1,3-dipolar cycloaddition (CuAAC) (Figure 4.8). The product of this reaction is a 1,4-disubstituted, five-membered 1,2,3-triazole ring. The azide-alkyne reaction is a high-yielding reaction that occurs between two functional groups that can be incorporated onto polymers, fluorophores, and small molecules. In addition, azides and alkynes are unreactive toward most biological materials, making these functional groups suitable for use in a wide variety of experiments [17]. We have performed this reaction by using magnetic, azide beads with an alkyne-modified PCR forward primer for thrombin aptamer A ($K_d$ = 25.6 nM at 30 °C) [22]. Amine-labels on commercially available beads were converted into azide groups in

preparation for reaction with the alkyne functional group on the DNA (details in methods section).

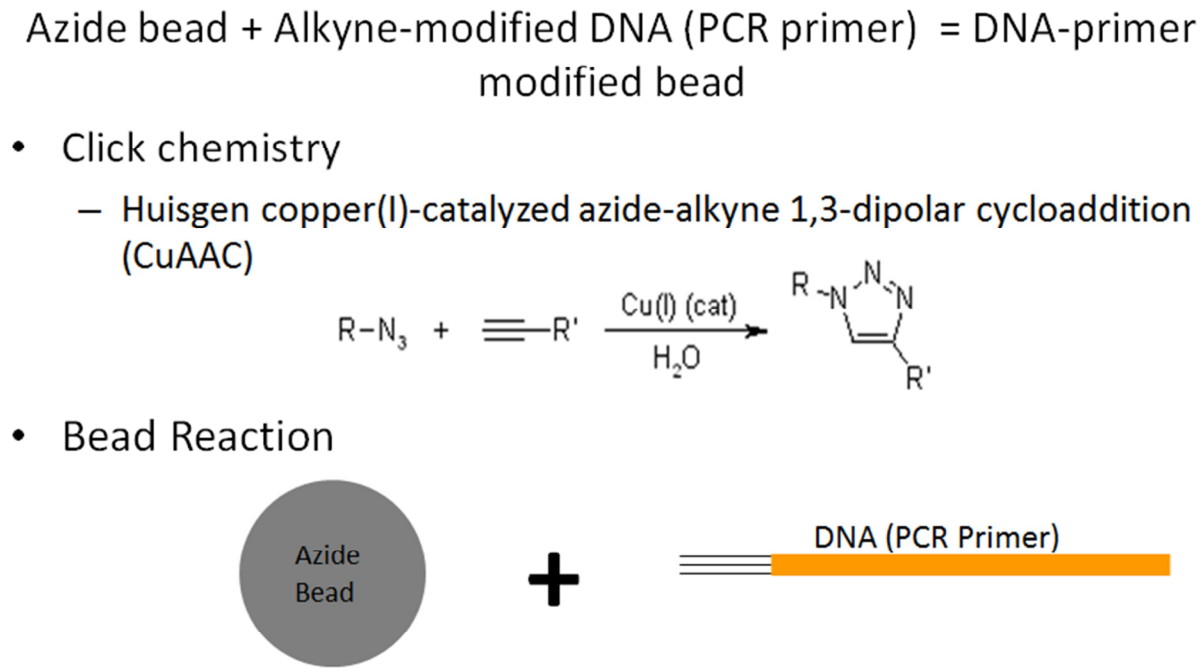


**Figure 4.8** An Overview of the click chemistry reaction: Huisgen copper(I)-catalyzed azide-alkyne 1,3-dipolar cycloaddition (CuAAC). Azide-modified beads are reacted with alkyne-modified PCR forward primer in the presence of a copper catalyst to form a 1,4-disubstituted, five-membered 1,2,3-triazole ring. Click chemistry reactions are easily performed with high yields and minimal side products [15-16].

After using click chemistry to attach forward primer sequences to the beads, the reaction was assessed for completion by incubating forward primer labeled beads with the complementary sequence in STE buffer. Beads were then stained with SYBR Green I and fluorescence was analyzed with flow cytometry. These results were compared to primer-conjugated beads not incubated with the complementary sequence, beads created to test non-specific binding, and azide-modified beads, which were also stained with SYBR Green I (Figure 4.9). The non-specific binding beads were created by performing the click reaction without the addition of Ascorbic Acid solution or the copper (II) - Tris(benzyltriazolylmethyl)amine (Cu-TBTA) catalyst. Without these reagents, reaction cannot occur between the two functional groups. Therefore, a fluorescent signal from this bead population would indicate that primer attaches to the beads non-specifically. Azide-modified beads were also analyzed in order to determine if the first step of azide modification of the beads causes non-specific interaction with DNA primers.

Figure 4.9 shows that the click chemistry reaction was successful. Azide-modified beads showed a fluorescent signal of approximately 1 700. The non-specific binding population was slightly higher at approximately 1 900. After attachment of forward primer, fluorescence shifted to 2 100. This shift was expected, because, although SYBR green is a double-strand DNA intercalating dye, it does have some affinity for single strands. After adding the complementary sequence, however, fluorescence intensity shifted to over 80 000. This demonstrated that forward primer was, in fact, attached to the beads.

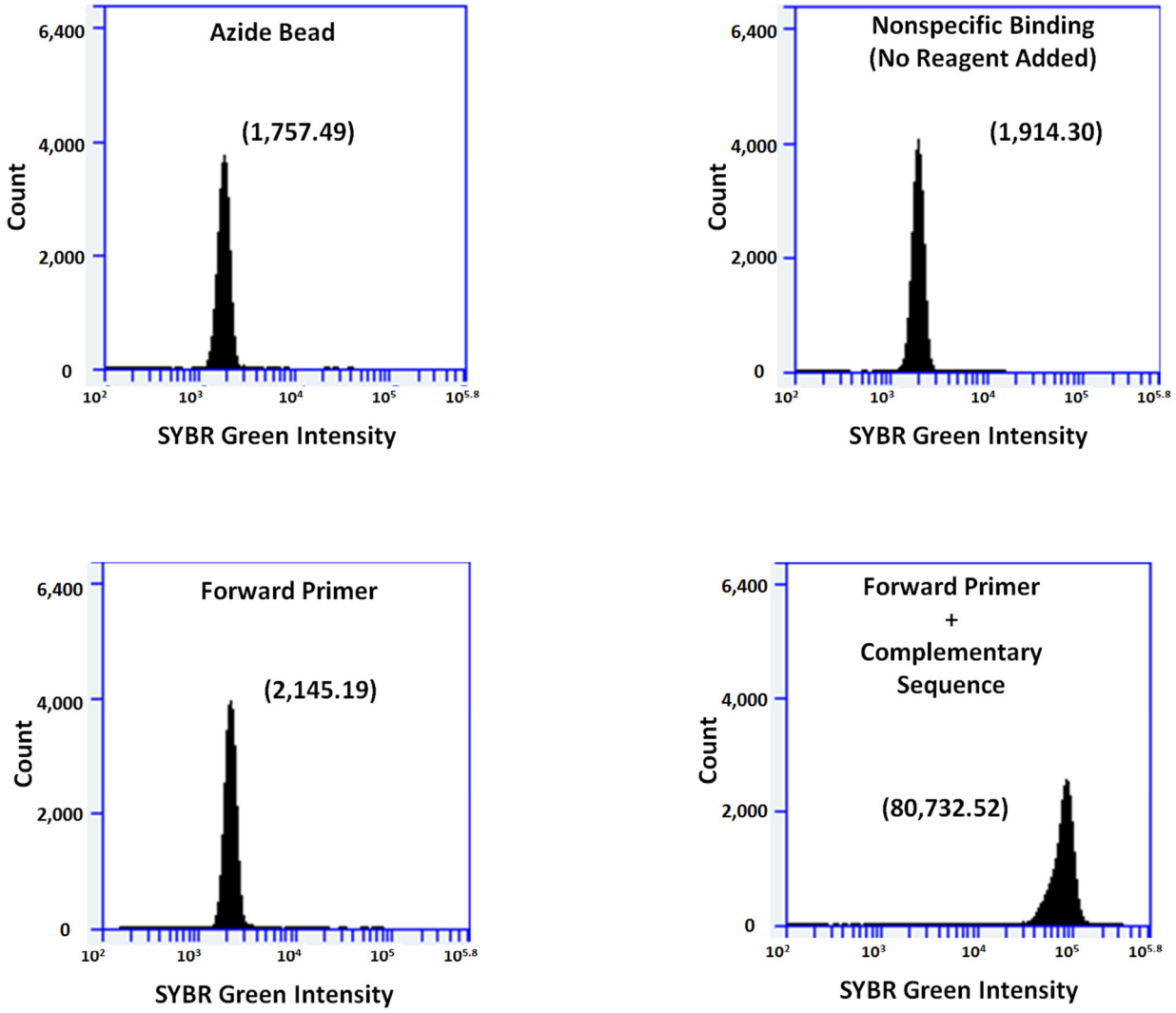


**Figure 4.9** Evidence of forward primer attachment after using click chemistry. Magnetic beads modified with a PCR forward primer sequence using click chemistry (Section 4.2.4.1) were analyzed for attachment by incubating modified beads with the complementary sequence. After staining beads with a double-stranded DNA intercalating dye (SYBR Green I), beads were analyzed via flow cytometry (Average intensities in parentheses). These results were compared with azide-modified beads, beads tested for nonspecific binding (no catalyst added during reaction), and forward primer-labeled beads. Results show successful attachment of forward primer to the beads.

#### 4.3.1.5.2 Amplification of DNA to Beads with Newly-selected Aptamers

Forward primer-modified beads for a newly-selected thrombin aptamer (c5; selected by Dr. Joonyul Kim) were tested for functionality by first amplifying beads in the presence of template to cover the surface. Beads were then analyzed via flow cytometry and compared to controls to confirm successful amplification. During PCR, beads were tested with and without c5 forward primer in free solution, for varying numbers of cycles. The effect of free forward primer on bead saturation is of interest, because allowing amplification to solely depend on DNA attached to the bead surface could delay the reaction. The number of cycles needed to saturate the beads was determined by reacting aliquots for 40, 60, or 80 PCR cycles. When the flow cytometry histogram no longer shifts to higher fluorescence intensity, the minimum number of cycles needed to saturate the beads has been reached. All of these variables were applied to primer-labeled beads, amine-modified beads from the company, azide-modified beads, and forward primer beads without reverse primer in solution (NC). These controls were designed to reveal if there was any non-specific binding of PCR product to the beads.

Figure 4.10 shows the flow cytometry results for this experiment. The plots show that increasing the number of cycles had no effect on bead saturation. Fluorescence intensity after 40, 60, or 80 cycles remained at between approximately 4 000 and 6 000 for primer-labeled beads. Adding forward primer in free solution did affect the intensity slightly, pushing the result up to 6 300 after 80 cycles under these conditions. These results could be taken as positive, but the controls tell a different story. Negative control beads (no reverse primer in solution) are slightly higher in intensity than the positive samples. For instance, after 40, 60, and 80 cycles the negative beads are 6 600, 6 900, and 7 400 respectively. This indicates that either there was

contamination of reverse primer in the PCR solution, or amplification did not occur properly on the primer-labeled beads. Because the aqueous negative control for PCR did not amplify, we must assume that no contamination was present in the PCR solutions. Results obtained from the other controls do suggest that non-specific adsorption of DNA does not play a factor. For instance, unmodified amine-labeled beads from the company register an intensity of 3 900 after 40 cycles. However, when forward primer is added in free solution the intensity shifts to 117 000. For this control, having forward primer in solution is the only way that amplification can occur, since there are no primers on the bead surface. The trend continues regardless of cycle number and indicates that unmodified beads adsorb PCR products from solution. Upon azide modification, however, the fluorescence intensity no longer shifts. For example, after 40 cycles, azide beads shifted from 4 500 to only 5 400 when forward primer was added in free solution. This trend continues, regardless of cycle number. Since azide-modified beads were used in the attachment of forward primer via click chemistry, we know that non-specific adsorption of DNA will not occur. Therefore, the result obtained from primer-labeled beads must be due to failure of PCR to efficiently amplify DNA onto the bead surface. Some aspect of the click chemistry could have rendered the DNA on the surface unable to amplify efficiently. Further experimentation must be done to address this issue if click chemistry is to be used in the future. Favorable results obtained in the study of digital bead detection (Section 4.3.2) may present a solution to this problem.

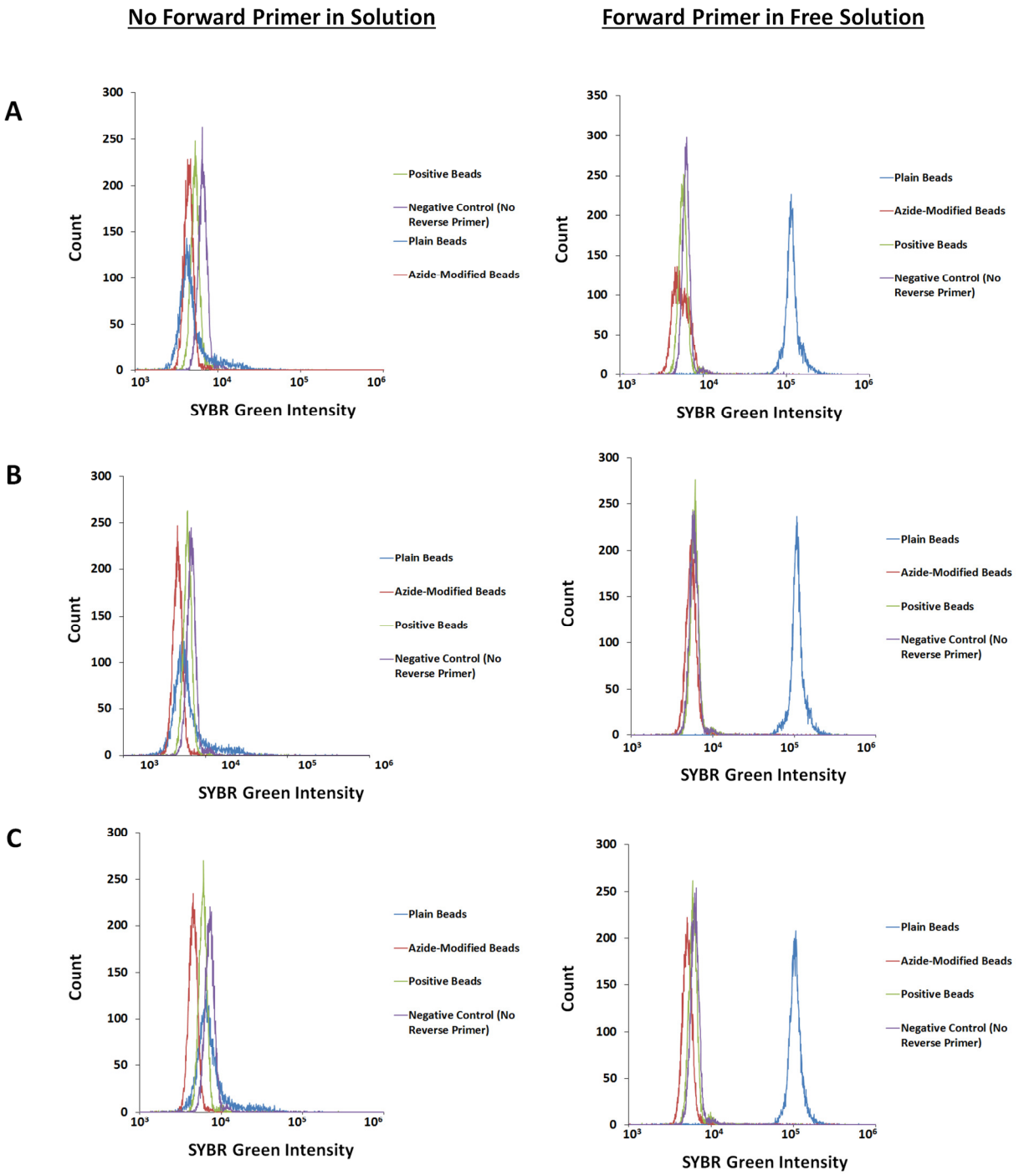


**Figure 4.10** Flow cytometry histograms of beads modified with forward primer (click chemistry) for amplification of a selected aptamer sequence. Beads were analyzed before and after PCR amplification in the presence of aptamer template sequence, by staining with a double-stranded DNA intercalating dye (SYBR Green I). PCR was performed for varying numbers of cycles with and without forward primer in free solution to assess the effect on amplification efficiency. Results are plotted on a log scale. Controls include unmodified amine beads, azide-modified beads, and primer-labeled beads with no reverse primer in solution. "Positive Beads" denotes primer-labeled beads with all necessary reagents for successful amplification. (A) 40 cycles of PCR. (B) 60 cycles of PCR. (C) 80 cycles of PCR.

### 4.3.2 Toward Digital Analyte Detection with Micro-beads

Initially, digital PCR was attempted by using template concentrations of 0, 6.6, 33.2, 66, or 1 000 fM in droplets. This translates to 1 copy in every 5 droplets, 1 copy per droplet, 3 copies per droplet, and 40 copies per droplet, respectively. Droplets were generated with a multi-channel emulsion generator (See Chapter 2, Figure 2.5), and PCR amplification was performed. After PCR, droplets were imaged on a confocal microscope to determine how the frequency of positive droplets changed with template concentration. An algorithm was created using Image J to find the droplets in each image, separate them into regions of interest, and measure their mean intensities. The data at each concentration was plotted in Excel and analyzed for digital results. The results obtained were inconsistent and did not show a clear difference between concentrations. It was later discovered that PCR reagents, including DNA, can interact with surfactants at the droplet oil-water interface (Figure 3.6 B), and a biocompatible surfactant was designed to address this issue (Chapter 3).

Using biocompatible surfactants, both the polymerase chain reaction (PCR) and recombinase polymerase amplification (RPA) have been performed in droplets at low template concentrations, as described in Chapter 3 (Section 3.3.4). PCR was performed at 0, 7, and 670 copies per droplet (Figure 3.6 C) and showed promise for application to digital detection. Analysis of droplet populations with confocal microscopy showed a clear difference in droplet intensities and the number of positive droplets. Because there was more than 1 copy per droplet present at the two concentrations tested (160 fM and 16 pM), there is no separation in intensity between the two, as all droplets should be positive. Reduction of template copy number to 1 copy per droplet or less should yield digital results. Isothermal amplification, RPA, also shows

promise for digital amplification, by allowing successful detection of as few as 7 DNA copies per droplet as well (Figure 3.6 D).

As introduced at the beginning of this chapter, droplet digital detection has been shown to be a highly efficient method for quantifying DNA samples using Poisson statistics. It has recently been transformed into commercially-available workflows with sample-in/answer-out capabilities [6]. Performing digital analysis with beads, however, could further increase throughput by harnessing the power of flow cytometry to rapidly analyze PCR products. Once information is obtained, DNA can easily be recovered for additional purposes—a capability that is possible yet more complex using only droplet-based confinement and amplification.

#### 4.3.2.1 Toward Digital Detection via Ligation of Template to Beads

Thrombin aptamer A was used as a template for attempting digital detection of PCR products through ligation. The aptamer template to be ligated to the beads was hybridized with a partially complementary DNA connector sequence, where one half was complementary to the aptamer, and the other half was complementary to the forward primer already attached to the beads. Once all three were hybridized, the aptamer and forward primer were brought into close enough proximity to connect via a ligation enzyme (Figure 4.11 A). Varying concentrations of hybridized aptamer/connector DNA sequence were added to equal concentrations of primer-modified beads in order to ligate different concentrations of thrombin aptamer A. Beads were then amplified with PCR, and flow cytometry was used to count the number of fluorescent beads. The expectation was that only beads with ligated template would amplify. Therefore, all beads should amplify when 1 or more copies of DNA are ligated per bead. As concentration is decreased to less than 1 copy per bead, the flow cytometry distribution should split into two

populations of positive and negative beads. The PCR protocol was carefully considered and adjusted to an extension temp of 66 °C to prevent annealing of the excess connector sequence to either the forward primer or aptamer sequence during amplification. This could cause artifactual PCR amplification products to build up in the reaction. Beads were washed several times before PCR in order to remove excess aptamer/ connector, but remaining above the melting temperature ($T_M$) of the connector should greatly reduce the chances of nonspecific products from any connector that may be left over.

Figure 4.11 B shows the real-time PCR trace for beads ligated with 100, 10, 1, or 0.1 template copies per bead. During ligation, controls were made in free solution without beads to test enzyme efficiency. The negative control (NC) consisted of forward primer and template, while the positive control (PC) contained forward primer with template and ligation enzyme. These controls were used as templates during PCR, along with aliquots of the ligated beads. No additional template was added to beads for the reaction, ensuring that amplification was strictly dependent on the amount of DNA ligated to the bead surface. Aqueous PCR positive and negative (no template) controls were also analyzed. Amplification was expected only in the wells where ligase was added. The PCR results clearly showed that different concentrations of DNA were ligated to the beads (Figure 4.11 B). The bead populations of 100, 10, 1, and 0.1 copies per bead showed C(t) values of 25, 30, 35, and 40, respectively.

Flow cytometry results (Figure 4.11 C) showed that azide-modified beads had a fluorescence of 2 034, and forward primer-labeled beads had an average intensity of 4 345. Sample beads were observed to split into multiple populations of different intensities, and gating of the data allowed for determination of the percentage of total counted beads that were represented by each intensity. When 100 copies of template were ligated per bead, the average

intensities were 23 546 (17.23%), 77 906 (68.57%), and 613 239 (5.18%), where the percentage in parenthesis represents the amount of beads of that particular intensity on the plot. At a ligation concentration of 10 copies per bead, the intensity of the majority of the beads shifted to 91 918 (67.43%) and 734 246 (23.31%). This could be due to steric crowding of the beads at 100 copies per bead. Reducing the amount of DNA on the surface may lead to more efficient amplification. The same trend is observed after decreasing to 1 copy per bead, yielding results of 104 305 (83.99%) and 727 833 (5.80%). Finally, 1 copy in every 10 beads showed average intensities of 513 (5.40%), 63 657 (56.51%), and 421 146 (31.90%), which are lower than previous results.

The results obtained are not entirely as expected, meaning that all beads were positive regardless of the concentration of DNA ligated. Once PCR amplification begins, the second DNA strand created from the ligated template is free to leave the proximity of the original bead and anneal with other primer-labeled beads. This will eventually result in the amplification of all beads, especially after 60 cycles of PCR. In order to obtain digital results, this technique must be combined with droplet encapsulation to ensure that amplified DNA only remains in contact with the bead to which it was originally ligated. In addition, the number of PCR cycles can be decreased, as droplet encapsulation increases the surface area-to-volume ratio, which should result in more efficient amplification.

The results of the ligation experiment were positive, however, in that they demonstrate how amplification can work when beads are modified with forward primer using click chemistry. Thus far, the only indication of DNA amplification has been obtained using beads modified via EDC and NHS chemistry. Each amplified bead population from the ligation experiment shows a flow cytometry intensity of at least 15 times higher than that of the primer-labeled beads (Figure 4.11 C). Therefore, when click chemistry is used, template should be ligated to the bead to

ensure successful amplification. This technique should also be applied when attempting to amplify aptamer sequences for the purpose of obtaining binding affinity measurements (Section 4.3.1.5.2).

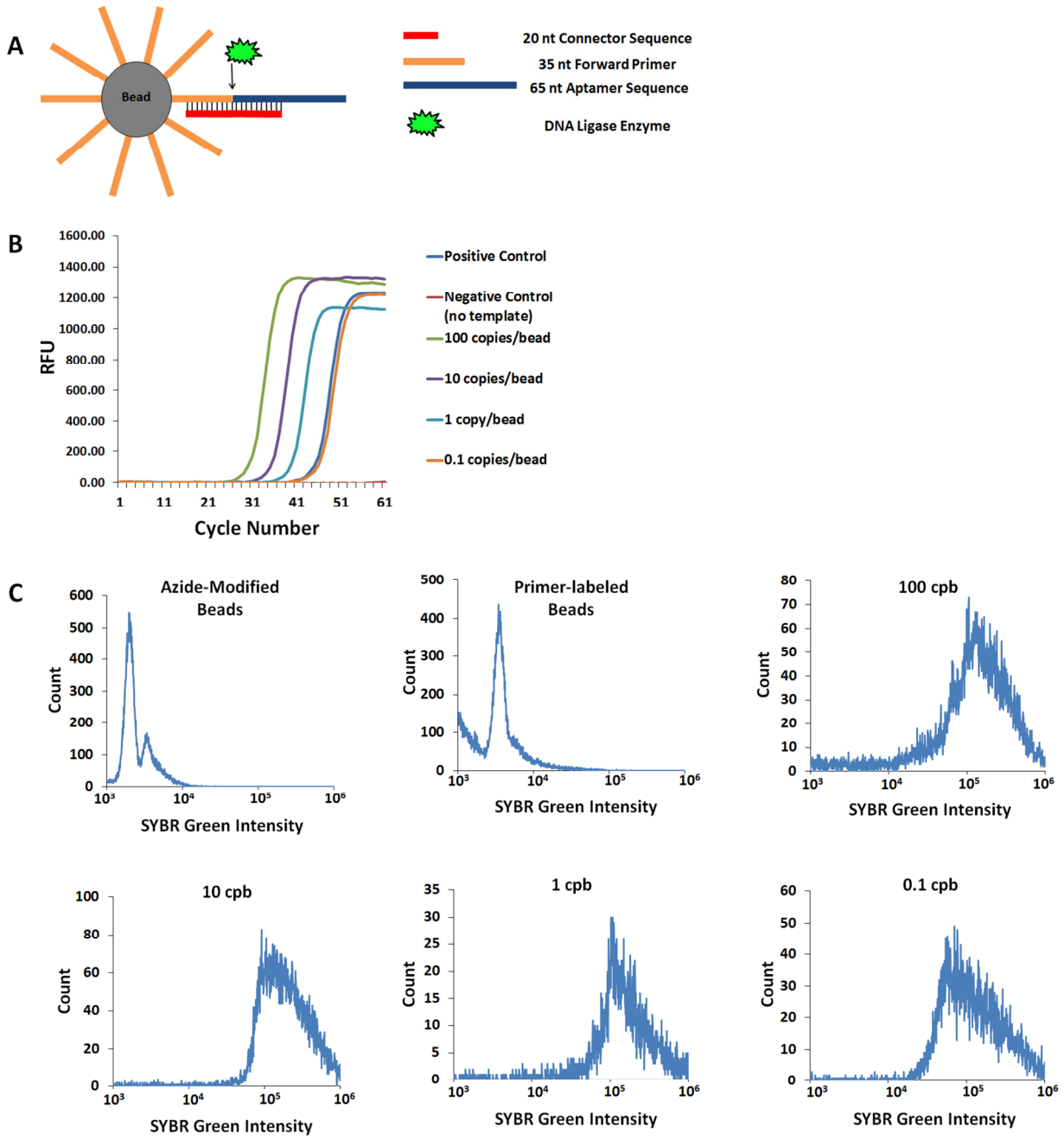


**Figure 4.11** Amplification and detection of template ligated beads. (A) The desired DNA template sequence (Thrombin aptamer A) is hybridized with a partially complementary DNA connector sequence, where one half is complementary to the template, and the other half is complementary to the forward primer already attached to the beads. Once all three are hybridized, the aptamer and forward primer are in close enough proximity to connect via a ligation enzyme. (B) Real-time PCR trace for amplification of beads ligated with 100, 10, 1, or 0.1 copies of thrombin aptamer A per bead. Aqueous positive control contains all reagents for amplification, while negative control does not contain template sequence. Beads amplify at different C(t) values proportional to the amount of template present. (C) Flow cytometry histograms of beads amplified with 100, 10, 1, or 0.1 template copies per bead (cpb). Beads were stained with a double-stranded DNA intercalating dye (SYBR Green I). Azide-modified beads and primer-labeled beads are used as controls.

## 4.4 Conclusions

DNA-coated beads were created to use for aptamer binding affinity measurements. Several methods of DNA attachment were explored. A PCR forward primer for thrombin aptamer B was successfully attached to carboxyl latex beads using EDC and NHS conjugation to bind the beads to an amine-labeled DNA sequence. DNA aptamers were specifically produced onto primer-conjugated bead surfaces using PCR. Thrombin protein bound specifically to thrombin aptamer-conjugated beads, and flow cytometry suggested that the $K_d$ is no higher than 200 nM, in agreement with prior studies. Results and calculations revealed that attomole amounts of DNA were attached to the bead surface, which agrees with previously-published data gathered by similar methods [2].

EDC was also used to successfully attach a forward primer for thrombin aptamer B to magnetic beads, which were found to be easier to handle than latex beads. Both single-stranded and double-stranded DNA were used in the reaction to determine the best method of attachment, and reacting with ss DNA for a shorter amount of time was found to give the best result. Real-time PCR and flow cytometry were used to confirm that amplification successfully occurs on beads made in this manner. The next step in experimentation will be to incubate aptamer-modified beads with fluorescent thrombin and analyze them with flow cytometry.

Another method of attachment developed simultaneously involved the use of click chemistry. An azide-modified bead and an alkyne-forward primer were reacted using standard "click" chemistry. Annealing of the primer's complementary sequence proved successful attachment after staining the beads with a double-stranded DNA intercalating dye, solidifying this method as another option for attaching PCR primers to magnetic beads for amplification of

target sequences. The click chemistry attachment method was used to bind PCR primers for newly-selected aptamers c3 and c5, and beads were amplified by PCR to cover the bead surface in the aptamer sequences. However, flow cytometry of bead-confined PCR products was inconclusive, because the negative control (no reverse primer in solution) and sample beads registered at the same fluorescent intensity. This suggests that either amplification did not work properly at the bead surface, or there is contamination that amplified the negative control. Amine-labeled beads from the company non-specifically bound to DNA, but azide modification of beads prevented adsorption from occurring. Further development of the click chemistry method, mainly in achieving successful PCR amplification, is needed before it can be used for binding affinity measurements.

Beads were also used to begin development of a method for digital detection of PCR products. This method should allow detection of rare events from a pool of DNA sequences through ligation, amplification, and flow cytometry analysis. qPCR, as well as flow cytometry, were used to show successful ligation of DNA to beads. Flow cytometry histograms showed traces of a digital result, which could be improved by further diluting beads before amplification. If desired, droplet encapsulation could still be used with this technique. One benefit of template ligation when utilizing droplets is that template sequences are trapped within the droplet and do not interact with surfactants at the oil-water interface. DNA has been demonstrated to have some interaction with surfactants, especially if they are charged. In some cases the interaction can cause the DNA to migrate from the droplets and into the oil phase, negatively impacting amplification results. A second benefit would be to further prevent cross-talk between beads and ensure efficient amplification. This is an aspect that is particularly important when attempting to simultaneously amplify unique sequences much like the process used during aptamer selection.

With the bead ligation method, sequences from a library of potential aptamers could be individually ligated to beads, encapsulated in droplets, and amplified in a single PCR tube. The potential for aptamer selection is discussed in greater detail in Chapter 5.

## 4.5 References


1. "Strategies for Attaching Oligonucleotides to Solid Supports", 2014, v5, Integrated DNA Technologies.
2. Kumaresan, P.; Yang, C.J.; Cronier, S.A.; Blazej, R.G.; Mathies, R.A. *Anal. Chem.* **2008**, 80 (10), 3522-3529.
3. Margulies, M. et al. *Nature* **2005**, 437, 376-380.
4. Dressman, D.; Yan, H.; Traverso, G.; Kinzler, K.W.; Vogelstein, B. *Proc. Natl. Acad. Sci.* **2003**, 100 (15), 8817-8822.
5. Williams, R.; Peisajovich, S.G.; Miller, O.J.; Magdassi, S.; Tawfik, D.S.; Griffiths, A.D. *Nature Methods* **2006**, 3(7), 545-550.
6. Hindson, B.J. et. al., *Anal Chem* **2011**, 83(22), 8604-8610.
7. Diehl, F.; Li, M.; He, Y.; Kinzler, K.W.; Vogelstein, B.; Dressman, D. *Nature Methods* **2006**, 3 (7), 551-559.
8. Chen, W.W.; Balaj, L.; Liau, L.M.; Samuels, M.L.; Kotsopoulos, S.K.; Maguire, C.A.; LoGuidice, L.; Soto, H.; Garrett, M.; Zhu, L.D.; Sivaraman, S.; Chen, C.; Wong, E.T.; Carter, B.S.; Hochberg, F.H.; Breakefield, X.O.; Skog, J. *Molecular Therapy – Nucleic Acids* **2013**, 2, e109.
9. Lauring, J.; Park, B.H. *Clin Cancer Res* **2011**, 17 (24), 7508-7510.
10. Li, M.; Chen, W.; Papadopoulos, N.; Goodman, S.N.; Bjerregarrd, N.C.; Laurberg, S.; Levin, B.; Juhl, H.; Arber, N.; Moinova, H.; Durkee, K.; Schmidt, K.; He, Y.; Diehl, F.; Velculescu, V.E.; Zhou, S.; Diaz, L.A.; Kinzler, K.W.; Markowitz, S.D.; Vogelstein, B. *Nat Biotechnol* **2009**, 27(9), 858-863.
11. Tok, J.B-H.; Fischer, N.O. *Chem Commun* **2008**, 1883-1885.
12. Smith, J.E.; Medley, C.D.; Tang, Z.; Shangguan, D.; Lofton, C.; Tan, W. *Anal Chem* **2007**, 79, 3075-3082.
13. Nelson, David L.; Cox, Michael M. Lehninger *Principles of Biochemistry, 5th ed.*; W.H. Freeman and Company: New York, 2008.
14. Wang, J.; Gong, Q.; Maheshwari, N.; Eisenstein, M.; Arcila, M.L.; Kosik, K.S.; Soh, H.T. *Angew. Chem. Int. Ed.* **2014**, 53, 1-6.

15. Kolb, H.C.; Finn, M.G.; Sharpless, K.B. *Angew. Chem. Int. Ed.* **2001**, 40, 2004-2021.

16. http://www.organic-chemistry.org/namedreactions/click-chemistry.shtm, Accessed May 17, 2014

17. http://www.sigmaaldrich.com/chemistry/chemistry-products.html?TablePage=18413131, Accessed May 18, 2014.

18. Walsh, M.K.; Wang, X.; Weimer, B.C. *J. Biochem. Biophys. Methods* **2001**, 47, 221-231.

19. Tran, T.M.; Lan, F.; Thompson, C.S.; Abate, A.R. *J. Phys. D: Appl. Phys.* **2013**, 46, 1-17.

20. Mazutis, L.; Baret, J-C.; Treacy, P.; Skhiri, Y.; Araghi, A.F.; Ryckelynck, M.; Taly, V.; Griffiths, A.D. *Lab Chip* **2009**, 9, 2902-2908.

21. Fisher Scientific Product Instructions "NHS and Sulfo-NHS" (Product No. 24500, 24510, 24520, 24525), http://www.piercenet.com/instructions/2160650.pdf, Accessed May 31, 2014.

22. Hu, J.; Easley, C.J. *Analyst* **2011**, 136, 3461-3468.

23. Invitrogen™ by Life Technologies™ Instructions "Dynabeads® M-270 Carboxylic Acid" (Product No. 14305D, 14306D).

# CHAPTER 5

# CONCLUSIONS AND FUTURE EXPERIMENTS

## 5.1 Conclusions

### 5.1.1 Passively-Controlled Droplet Generators and Imaging Techniques

A major component of this dissertation work was related to the successful formation and passivation of sub-nanoliter droplets for high throughput biological assay platforms. First, we described methods used to create two passively-controlled microfluidic devices for rapid droplet generation: a single-channel generator for steady and monodisperse droplet formation, and a multi-channel generator for increased speed of production. Both devices allowed for assay flexibility through on-chip mixing of various reagents into a single droplet. Emulsion droplets were collected in a larger outlet reservoir that was interfaced to a syringe vacuum through a PDMS plug, which was ideal for easy pipette transfer of emulsions to other devices for experimentation. The multi-channel generator also utilized a custom-made PDMS O-ring adapter, which was bonded directly to the device and used as an interface between the outlet and the PDMS plug. Several changes made to the design and fabrication of the multi-channel generator allowed for the rapid production of emulsion droplets of similar monodispersity to those created by the single-channel generator. The number of aqueous inlets on the multi-channel emulsion generator allowed for the simultaneous production of droplets with up to 4 different compositions. In the future, the speed of production and the increased number of inlet reservoirs provided by the multi-channel chip could allow for the testing of different sample concentrations, or performance of high-throughput experiments with samples and calibration curve points all produced on a single device for quantitative analysis.

In addition to successful droplet generation, we also presented several methods for droplet imaging. Density differences between aqueous solutions and oils were exploited to create an aqueous monolayer at the interface of the two different oils and obtain data from many droplets in a single image. A solid support called a "drop cage" was created to stabilize the monolayer and to keep droplets from moving during imaging. These methods were used to obtain data from droplets during real-time RPA experiments presented in Chapter 3 (Figure 3.7). Another imaging method used frequently was the reinjection of droplets directly into a 100 µm-deep microfluidic channel. Droplets were allowed to pack into this channel and settle before imaging (See Figure 3.6 C, D). Finally, single-droplet analysis was made possible through the use of single-point detection with a photomultiplier tube (PMT). The PMT was focused on a defined region of interest (ROI) along a microfluidic channel on the droplet reinjection chip, and data was obtained from each droplet as they passed through the ROI. This technique should be useful for detecting PCR products in droplets containing various starting template concentrations. These droplet reinjection and optical detection methods hold significant promise for droplet digital PCR (ddPCR) applications, which would be a powerful asset to the laboratory and a cost-effective alternative to commercially available platforms of this nature [1-2].

### 5.1.2 Formation and Characterization of Biocompatible Surfaces within Picoliter Droplets

Additionally, we have shown that commercially available reagents can be used to impart biocompatibility to droplet surfaces. A direct binding interaction between a carboxylated perfluoropolyether (Krytox) and a polyetherdiamine (Jeffamine) at the interface of oil and aqueous solution—supported by FT-IR, mass spectrometry, fluorescence microscopy, and NMR data—was harnessed to create biocompatible aqueous droplets for homogeneous protein assays,

droplet PCR, and droplet RPA. Furthermore, the efficiency of real-time RPA within droplets passivated by the "Jeffamine" additive was compared with that of KryJeffa-stabilized droplets at concentrations of <10 template copies per droplet and shown to be just as effective. Maximum biocompatibility was achieved when Jeffamine was added directly to aqueous solution at a concentration of 0.75% w/v, but additional optimization can be achieved in the future by determining the surfactant critical micelle concentration (CMC) and the time scales of interfacial adsorption for both surfactant and aqueous additive. Overall, our current results suggest that this simple polyetherdiamine (Jeffamine) aqueous additive provides a dynamic shielding effect at droplet surfaces and is an attractive alternative to covalent modification of Krytox for droplet-based biochemical reactions.

This interaction between Krytox carboxylate and primary amines is likely a major factor in the incompatibility of unbound Krytox with many biochemical reactions, as enzymes and proteins typically contain a number of primary amines that could be attracted to the interface and lead to the failure of the reaction. This study should also give further insight into interaction mechanisms with other additives [3-4] or surfactants [5]. Finally this type of interaction could be used for various future applications, such as the attraction of biomolecules like DNA to the oil–water interfaces of droplets to participate in surface-based biochemical assays.

### 5.1.3 Bead-based Assays as Complements to Droplet Compartmentalization

We have utilized DNA-covered beads for a variety of applications, including for the creation of methodology for making aptamer binding affinity measurements ($K_d$). Several methods of DNA attachment were used to attach a PCR forward primer to both latex and magnetic micro-beads, and DNA amplification was used to cover the bead surfaces with

aptamers. After incubation of aptamer-modified beads with target protein (human thrombin), flow cytometry analysis showed specific binding and allowed accurate estimation of the $K_d$ (≤ 200 nM). In addition, qPCR was used to determine that the amount of aptamer bound to the beads was in the attomole range, a figure that agrees with other reports [6].

A method using EDC and NHS attachment was also developed to successfully attach a forward primer for aptamer introduction onto magnetic beads, which were found to be easier to handle than latex beads. Two methods of attachment involving either single-stranded, amine-modified primer, or a double-stranded complex with the primer and its complementary sequence, were used in the reaction to determine the best method of attachment. It was found that reacting with ss DNA for a shorter amount of time gave the best result. qPCR and flow cytometry results confirmed that amplification successfully occurs on beads made in this manner. The next step in experimentation will be to incubate aptamer-modified beads with fluorescent thrombin and analyze them with flow cytometry to reproduce the results obtained with latex beads.

Click chemistry was also developed as an alternative method of attaching forward primer to beads due to the nature of the reaction, which easily forms stereospecific products in benign solvents at high yields [7-8]. A popular click chemistry reaction named the Huisgen copper (I)-catalyzed azide-alkyne 1,3-dipolar cycloaddition (CuAAC) reaction was used to bond an azide-modified bead to an alkyne-forward primer. The reaction was shown to be complete by incubating the reacted beads with the primer's complementary sequence and then detecting fluorescence via flow cytometry after staining the beads with a double-stranded DNA intercalating dye. To use this method for aptamer binding affinity measurements, click chemistry was used to bind PCR primers for newly-selected aptamers c3 and c5, and beads were amplified by PCR to cover the bead surface in the aptamer sequences. Flow cytometry of bead PCR

products was inconclusive, however, because the negative control (no reverse primer in solution) and sample beads registered at the same fluorescent intensity, suggesting that amplification does not work properly at the bead surface and that further development of the method is needed before click chemistry can be used as a viable option.

A second application for DNA-covered beads in the future is the digital detection of PCR products through ligation, amplification, and flow cytometry analysis. Traditionally, digital PCR is performed by diluting template to no more than one copy per chamber or droplet, amplifying to end point, and then counting the fraction of positive chambers/droplets from the total number of chambers/droplets in order to determine the starting DNA concentration. One of our goals is to use beads as the "compartments" for dilution and rapid flow cytometry analysis of end-point PCR products to determine DNA concentration. Thus far, real-time PCR, as well as flow cytometry, have been used to show successful ligation of DNA to beads at 100, 10, 1, and 0.1 template copies per bead. Flow cytometry histograms showed traces of a digital result, which could be improved by further diluting beads before amplification. If desired, droplet encapsulation could still be used with this technique to further prevent cross-talk between beads and ensure efficient amplification.

## 5.2 Future Experiments

### 5.2.1 Toward Aptamer Selection

#### 5.2.1.1 Introduction to Aptamer Selection

Aptamers are single-stranded, ligand-binding nucleic acids that bind to targets with high affinity. The name aptamer is derived from the Latin root words "aptus meros," meaning fitting particle. Aptamers exist for many different targets, including peptides, proteins, viruses, drugs,

and cells, and they are so specific that they can easily distinguish between closely-related targets [9]. As shown in Figure 5.1, aptamers bind to their targets by folding into well-defined tertiary structures. Some of the parameters that encourage binding are electrostatic and Van der Waals attractions, hydrogen bonding, aromatic ring stacking, that contribute to overall compatibility of the aptamer and target [10]. In many ways, aptamers are similar to antibodies in their binding affinity, but they provide several advantages over antibodies. These advantages include ease of synthesis and modification due to their lower molecular weights, lower cost, resistance to changes in assay conditions, and ease of reproduction [10]. Aptamers are becoming increasingly popular for biomarker recognition, and they could eventually replace antibodies. Although a general lack of numbers in selected aptamers and aptamer pairs continues to limit application toward medical research, recently there have been significant increases in interest and investments in aptamer-selection technology in the commercial sector, and multiple aptamer based drugs are in late stages of clinical trials.

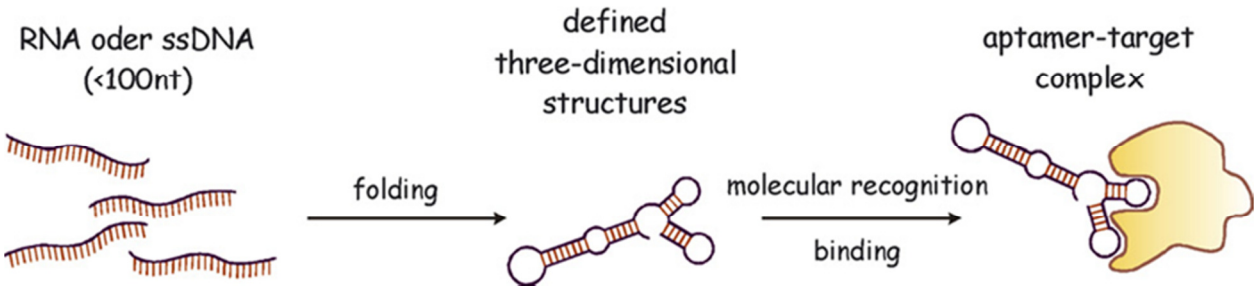


**Figure 5.1** Schematic representation of the functionality of aptamers. After folding into three-dimensional structures, aptamers (RNA or DNA) can recognize and bind to their target.

Reprinted from [10]. Copyright 2007 with permission from Elsevier.

A given aptamer is discovered through a process called SELEX, which stands for the systematic evolution of ligands by exponential enrichment, and is illustrated in Figure 5.2. Using an In Vitro, Darwininan-like selection, this process allows complex, synthetic libraries of $10^{12}$ – $10^{15}$ different nucleotide sequences to be reduced to populations consisting of just a few of the strongest binding aptamer sequences. The main steps involved in the SELEX process are binding, partitioning, elution, amplification (PCR), and conditioning [10]. In short, the process must include methods to create a random oligonucleotide library, incubate it with the target of interest, discard non-binding sequences, elute the bound sequences, amplify these sequences to enrich the pool, and then condition them to return to single-stranded DNA and begin the cycle again. If RNA aptamers are desired, appropriate in vitro transcription steps will need to be inserted as necessary to convert the DNA pool to RNA. According to Stoltenburg et al, SELEX is generally finished when an enrichment of target-specific oligonucleotides is observed with no further increase in affinity. This can take anywhere from 6-20 rounds to complete [10]. The end of the process must also include a method to characterize selected aptamers, such as sequencing and measuring binding affinity.

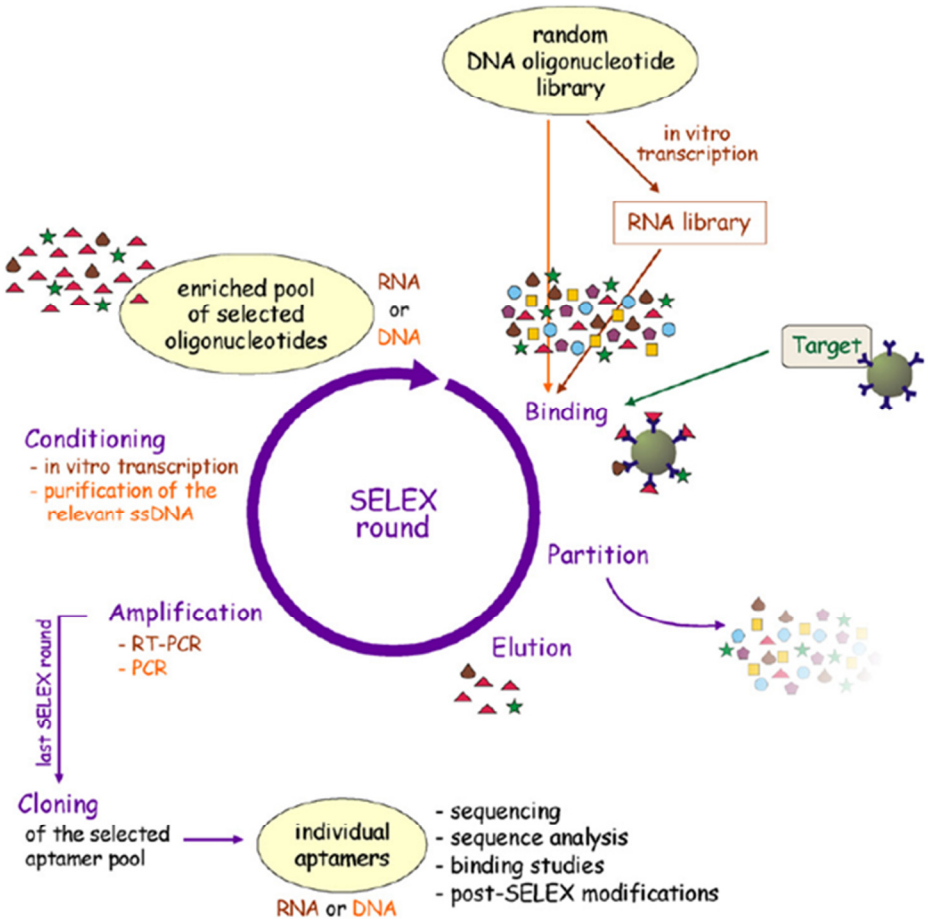


**Figure 5.2** In vitro selection of target-specific aptamers using SELEX technology. Starting point of each SELEX process is a synthetic random DNA oligonucleotide library consisting of a multitude of ssDNA fragments with different sequences (1015). This library is used directly for the selection of DNA aptamers. For the selection of RNA aptamers the library has to be transferred into an RNA library. The SELEX procedure is characterized by the repetition of successive steps consisting of selection (binding, partition, and elution), amplification and conditioning. In the first SELEX round the library and the target molecules are incubated for binding. Unbound oligonucleotides are removed by several stringent washing steps of the binding complexes. The target-bound oligonucleotides are eluted and subsequently amplified by PCR or RT-PCR. A new enriched pool of selected oligonucleotides is generated by preparation of the relevant ssDNA from the PCR products (DNA SELEX) or by in vitro transcription (RNA SELEX). This selected oligonucleotide pool is then used for the next selection round. In general, 6 to 20 SELEX rounds are needed for the selection of highly affine, target-specific aptamers. The last SELEX round is finished after the amplification step. The enriched aptamer pool is cloned and several individual aptamers have to be characterized.

Most aspects of the SELEX process, excluding amplification, will depend on the type of target and the desired application in mind for the aptamer [10]. Some common selection methods include capillary electrophoresis, magnetic beads, affinity chromatography, and flow cytometry [10-11]. This is an advantage, because the selected aptamer is already suited for the application, as if it were custom-made for it. Therefore, there is no need to worry about whether or not the DNA will perform under the assay conditions. Another benefit lies in the DNA library complexity. Utilizing a synthetic DNA library of such large complexity ($10^{12}$ – $10^{15}$ sequences) opens the door to select DNA sequences that do not exist in nature, which may bind even better [9]. In addition, several groups have shown that chemical modification of nucleotides may encourage even tighter binding [10, 12, 21-22].

#### 5.2.1.2 Toward Aptamer Selection Using Beads and In Vitro Compartmentalization

Currently, there is no standardized SELEX protocol for any target. The majority of published aptamers were manually selected with widely differing methodology, which is a time-consuming and inefficient process. In addition, because the PCR amplification is not specific and is done in free solution, it is easy for sequences that do not bind the target to be enriched alongside the wanted aptamers [10]. One of the major goals of the Easley laboratory is to create a standard protocol for aptamer selection that addresses these issues and incorporates all of the methodology developed in this dissertation work, including microfluidic emulsion generators (Chapter 2), biocompatible surfactants (Chapter 3), and bead-based PCR (Chapter 4).

To begin this process, an aptamer library will be diluted to a concentration that incorporates only 1 DNA sequence per droplet using an emulsion generator. Segregating the DNA sequences in this manner allows for each droplet to act as its own miniature reaction compartment,

preventing recombination of DNA sequences and build-up of shorter, artifactual products that often occurs when amplification is done in free solution [13]. In addition to a single library template sequence, 1 forward primer-modified micro-bead, and PCR reagents will also be incorporated into a single droplet. Emulsion PCR will follow. After PCR, droplets will be broken, and magnetics used to recover DNA-covered beads for aptamer preparation. This portion of the selection method is taken from BEAMing, which was discussed in detail in Chapter 4 [14-15]. As mentioned in Chapter 4, in order to create functional aptamer beads, the second DNA strand must be removed, and aptamers must be cooled rapidly to encourage folding into well-defined tertiary structures. Aptamer-labeled beads can then be incubated with the fluorescently-labeled target of interest (e.g. thrombin, insulin) and separated into binding and non-binding populations using fluorescence-activated cell sorting (FACS). When analyzing histogram plots of number of events vs. intensity, the beads with the best aptamers should have high intensity and a low number of events. DNA sequences can then be cleaved and taken through the selection process again. This process would continue until the majority of events detected are of high intensity. The recovered aptamers will then be sequenced and analyzed for binding affinity.

Another research group has recently performed this bead-based aptamer selection method using polydispersed emulsion droplets generated by stir bar. The technology, which they named "particle display," was used to select high-affinity DNA aptamers for four different proteins in just three rounds of the SELEX process by screening the binding affinities of $>10^8$ aptamer micro-beads [19]. Their research supports the usefulness and necessity of micro-beads for rapid and cost-effective analysis of large libraries of sequences. Our research group would like to streamline the process further by using droplet microfluidics, which would provide greater

control over the number of beads and template sequences encapsulated through the generation of monodispersed droplet populations.

One change that can be incorporated to improve this method is template ligation. As discussed in Chapter 4, PCR templates were ligated to beads in order to facilitate digital amplification and detection. Droplets were not used for that method, but there are benefits to incorporating them when needed. For instance, DNA has been demonstrated to interact with charged surfactants at the oil-water interface, which can negatively impact assays contained within the droplet (Chapter 3). At such low concentrations of 1 template sequence per droplet needed for SELEX, the entire experiment could be ruined by this effect. Herein, biocompatible surfactants have been shown to reduce interaction of reagents with the interface (Chapter 3), but ligating 1 template sequence per bead would further ensure that DNA will remain encapsulated within the droplet and ensure efficient, unbiased amplification of library sequences.

#### 5.2.1.2.1 Incorporating Beads Into Droplets on Emulsion Generator

Thus far we have demonstrated rapid formation of monodisperse droplet populations using microfluidic devices. We have also utilized biocompatible surfactants to successfully perform emulsion PCR and successfully performed PCR on bead populations. The next step in realizing a bead-based aptamer selection method is the incorporation of micro-beads into emulsion droplets.

Stir bar emulsions were used as a preliminary experiment to demonstrate how beads can become encapsulated within water-in-oil emulsion droplets. A flat-bottomed microcentrifuge tube containing “Griffith’s mix” (4.5% v/v Span 80, 0.4% v/v Tween 80, 0.05% v/v Triton X-100, Mineral oil), an oil/surfactant combination shown to work with emulsion PCR [13], was

placed on a magnetic stir plate and stirred at 1 000 rpm. An aqueous solution containing 2 μm latex beads was prepared and added to the stirring oil/surfactant mixture dropwise over a period of 1.5 min. Once all of the solution was added, the mixture was allowed to continue stirring for an additional 5 min. Emulsion droplets were transferred to a PDMS/glass reservoir and imaged via confocal microscopy. Figure 5.3 shows a confocal image of beads in droplets. Many droplets contain more than one bead due to the polydispersity of droplet sizes created when using the stir bar method. Videos of the beads in droplet demonstrated that droplets were stable and that beads remained encapsulated.

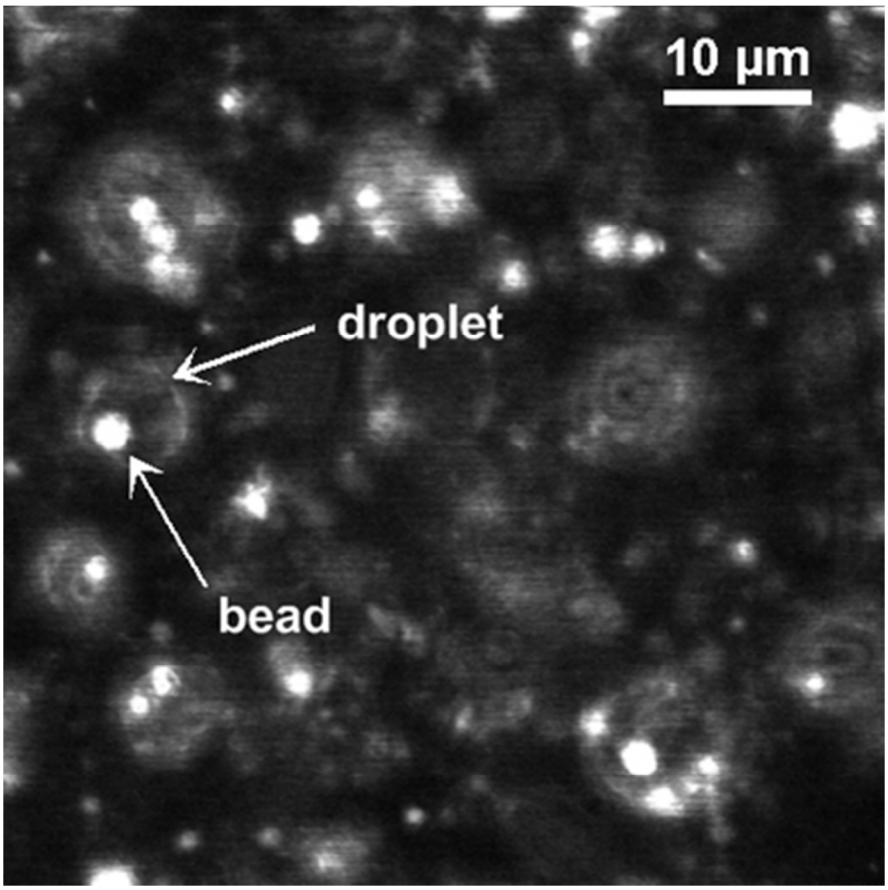


**Figure 5.3** Confocal reflectance image of 2 μm beads inside of water-in-oil emulsion droplets. Emulsion was made via stir bar by adding an aqueous solution containing 2 μm latex beads dropwise to a solution of "Griffith's mix" (4.5% v/v Span 80, 0.4% v/v Tween 80, 0.05% v/v Triton X-100, Mineral oil), an oil/surfactant combination shown to work with emulsion PCR [13]. The solution was stirred on a magnetic stir plate at 1 000 rpm. The resulting emulsion was transferred to a PDMS reservoir (See Chapter 2, Section 2.2.4.1) for imaging.

In order to create monodisperse droplets and better control the number of beads incorporated per droplet, microfluidic droplet generators were introduced. Because PDMS devices are used, the Griffith's mixture of oil and surfactant, which contains mineral oil, could no longer be used. Instead, fluorocarbon oils and surfactants were incorporated (See Chapter 3). A single-channel emulsion generator (Chapter 2, Figure 2.1) was prepared for this purpose. Droplets were generated using our standard fluorocarbon oil/surfactant mixture as the carrier phase and PCR buffer as the aqueous phase. 1 µL of Dynabeads® M-270 Carboxylic Acid (Invitrogen) were added to the center reservoir, which equates to 2 x $10^6$ beads total. Beads were mixed into the PCR buffer by pipetting, and droplets were formed by pulling an 80 kPa vacuum. Images and videos of beads were taken using microscopy. Figure 5.4 shows images of these droplets after being reinjected into a microfluidic channel. As shown, many droplets contain only one bead. There are some droplets that contain two beads, but this can be addressed by adjusting the bead concentration.

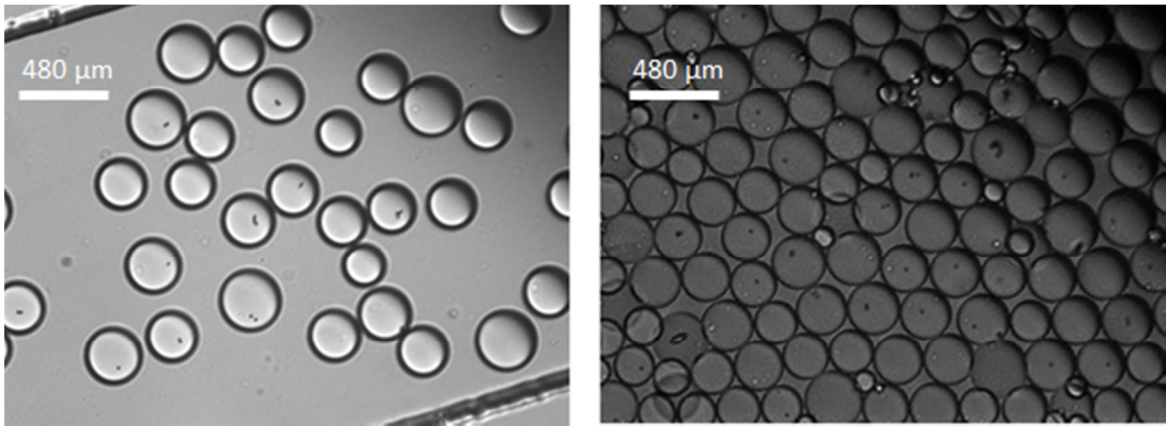


**Figure 5.4** Bead-containing emulsion droplets reinjected and packed into a microfluidic channel. A single-channel emulsion generator (Chapter 2, Figure 2.1) was used to generate droplets containing beads of 2.8 µm size using a fluorocarbon oil/surfactant mixture as the carrier phase and PCR buffer as the aqueous phase. Droplets were formed by pulling an 80 kPa vacuum. Droplets were then transferred so a second microfluidic device for reinjection (Chapter 2, Figure 2.11 A) and imaged via microscopy after packing into a microfluidic channel. Many droplets contain only 1 bead.

Future work for the aptamer selection experiment includes the combination of all of the elements presented here and in the preceding chapters of this dissertation work. Before using a large aptamer pool, a simple starting point in combining beads with emulsion PCR would be to encapsulate one forward primer-modified bead per droplet along with two different aptamer sequences containing two different fluorescent tags. After PCR, droplets could be broken and beads recovered and sorted into the two populations. Another proof of concept experiment would be to encapsulate one bead per droplet and perform emulsion PCR with two different aptamers. One aptamer would be for a specific target (e.g. thrombin), while the second aptamer would be for another target (e.g. leptin). After PCR and bead recovery, all beads would be incubated with one of the fluorescent targets, and flow cytometry used to sort binding from non-binding beads. Both of these experiments can be done with and without ligating the aptamer template sequences directly to the beads, providing a means for comparing the effectiveness of each method.

#### 5.2.1.2.2 Methods for Breaking Emulsions

The last element needed to make the aptamer selection project successful is an efficient method for breaking emulsions to recover beads after amplification. Several methods have been demonstrated to be useful for breaking emulsions made with Krytox (perfluoropolyether) surfactant bound to Jeffamine (polyetheramine) aqueous additive at the oil-water interface. Two of these methods, previously discussed in Chapter 3, were the use of EDTA or $H_2SO_4$ for emulsion destabilization. EDTA has been shown to destabilize PEG groups by binding and removing divalent ions from solution [16]. Since the Jeffamine additive used for biocompatibility is composed of polyethylene glycol (PEG) and polypropylene glycol (PPG) chains, we hypothesized that Jeffamine-bound surfactant would be destabilized in the presence of EDTA. Adding 0.5 M EDTA caused Jeffamine-bound surfactants to become destabilized,

while unmodified Krytox surfactant remained intact (Chapter 3, Figure 3.4). This method could be useful in the future for controlled emulsion breakage.

An even simpler method can be used when beads are included in the droplets, as they will be for the aptamer selection experiments. We made an emulsion containing PCR buffer, Jeffamine additive, and 2 μm magnetic beads by vortexing for 30 seconds in the presence of the oil/surfactant mixture. The emulsion was centrifuged at 19 000 rcf for 45 min, and the emulsion was observed to separate into two distinct layers. Beads remained at the water-oil interface, because they have a density of 1.6 g/mL, which is less than that of the fluorocarbon oil (1.91 g/mL). Further experimentation is needed in order to optimize the amount of time needed to break the emulsion. This is a simple and effective method for recovering beads from emulsion droplets.

### 5.2.2 Surface-Based Assays in Droplets via Direct Interaction with Surfactants

In Chapter 3 we introduced an interaction between Krytox carboxylate Perfluoropolyether surfactant and primary amines, which we believe to be a combination of ionic and hydrogen bonding. This interaction was demonstrated through the use of FT-IR, NMR, and MS, and it could open the door for exploration of other interactions between surfactants and reagents in aqueous solutions to perform a variety of assays. For instance, amine-labeled DNA was shown to be capable of participating in the primary amine interaction through the fluorescent detection of a complex containing amine-labeled DNA and its fluorescent complementary sequence at the oil-water interface of Krytox-stabilized droplets. Attracting DNA to the oil-water interface could provide a vehicle for detection of proteins with high signal-to-noise ratios using techniques similar to previously-developed electrochemical proximity assays (ECPA) [17, 20].

Since ECPA is a surface-based assay using DNA to recruit probes and target protein, our discovery of direct interactions between Krytox carboxylate surfactants and amine-terminated DNA could allow for a droplet surface-based assay similar to ECPA to be used in droplets, if the experimental read-out is converted to a fluorescence format. Two possibilities are illustrated in Figure 5.5. If the target protein is fluorescent, migration to the interface should cause a measurable increase in signal at the droplet edges and a decrease at the droplet center (Figure 5.5 A). As a second option, probes could be reconfigured into a "turn-on" format by including a short DNA probe that is complementary to the thiolated DNA present at the interface. When the aptamer complex forms with the target, this short sequence could be displaced and fluorescent signal released into the center of the droplet (Figure 5.5 B).

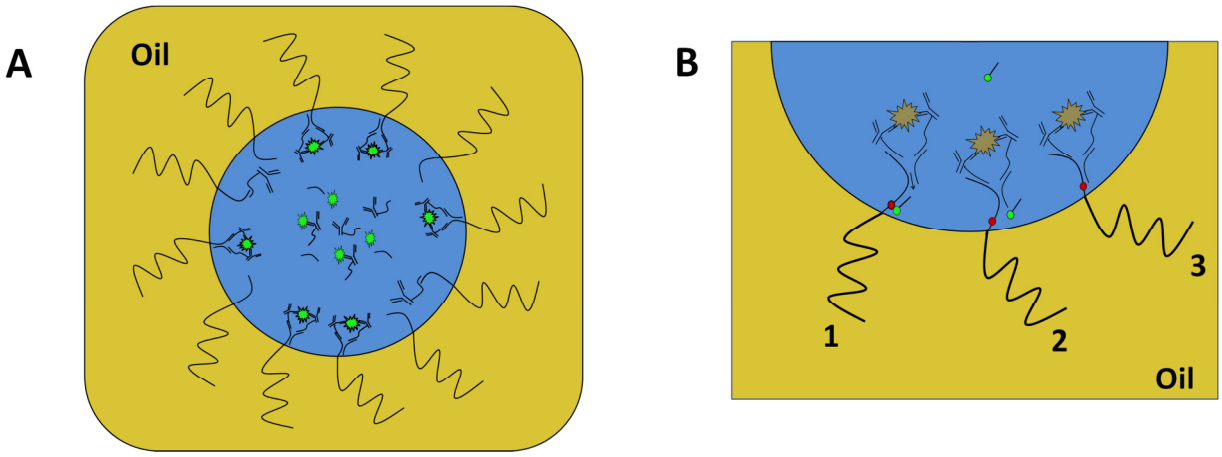


**Figure 5.5** Proposed droplet surface-based proximity assays. (A) An interaction between a DNA sequence and surfactant causes DNA to assemble at the inner oil-water interface. Next, encapsulated fluorescent target and antibody-oligo pairs form a complex that drives fluorescent target to the interface, causing a decrease in intensity at the droplet center and an increase at the droplet edges. Results should be quantitative if droplets containing known amounts of target are analyzed alongside samples of unknown concentration to generate a standard curve. (B) The droplet surface based assay could also be converted to a "turn-on" format. 1 – The DNA assembled at the interface now contains a quencher and is annealed to a shorter segment of DNA containing a fluorophore, to form a FRET pair. 2 – When the target/antibody-oligo complex forms, the short segment of DNA is displaced, causing an increase in fluorescence at the droplet center. 3 – The fully-formed complex is assembled at the interface. Note: Target is not fluorescently-labeled in this method.

Additional experiments confirming the effectiveness of the DNA-Krytox interaction need to be performed before utilizing this method. Thus far, internal amines within the DNA strand have been shown to interact with Krytox as well, which may present a problem. However, utilizing a double-stranded complex of DNA should resolve this issue. If this option is to be used, the proposed system would have to be redesigned in a way in which the assay will cause displacement of the second strand. If DNA cannot successfully interact directly with Krytox, it can be attached to another primary-amine modified molecule that would in turn serve as a linker between the Krytox and the DNA, so that assembly at the interface can still occur. Other interactions also been explored. We have begun development of a method that involves synthesis of biotin-modified Krytox for use with streptavidin-coated materials in order to make droplet-based surface assays a reality.

### 5.2.3 Multi-Islet Secretion Measurements with pFRET Assay

Our research group is interested in performing continuous monitoring of hormone secretions from pancreatic islets in order to further understand the effects of diabetes and obesity on glucose regulation in the body. The use of a passively-controlled microfluidic device that traps and measures secretions from up to 8 murine islets at once was previously demonstrated [18]. This technique utilized enzyme-linked immunosorbent assays (ELISA) to measure insulin secreted from each islet after basal (3 mM) and stimulatory (11 mM) levels of glucose were applied, which yielded results comparable to conventional methods performed in bulk solution [18]. This method not only simplified stimulation and sampling through the use of a passively-controlled device, but also provided a platform for obtaining information from single islets.

We would like to simplify these measurements even further by replacing ELISA techniques with our highly-sensitive proximity FRET (pFRET) assays. Quantitative information could be obtained by simply using fluorescence microscopy to detect signals directly from droplets containing islet secretions, eliminating the need for post sampling analysis involving transfer of material to external devices for measurement and read-out. Instead, the hormone secretions will be trapped within individual droplets already containing probes for pFRET and allowed to incubate on a specially-designed microfluidic device that allows droplets to remain on the device for up to 5-6 min from the point of formation to the point of reaching the outlet, providing the desired measurement of concentration over time. These devices also contain chambers where droplets can be stored and incubated further if the vacuum is stopped. This dissertation work will contribute to the realization of this goal by providing a biocompatible surfactant that allows for droplet stability and optimal assay performance. As mentioned in Chapter 3, the pFRET assay for measurement of insulin concentration did not work in the presence of unmodified, Krytox carboxylate surfactant. However, when Jeffamine aqueous additive is included, assay performance was recovered (Chapter 3, Figure 3.6 A). Therefore, the realization of a passively-controlled method for continuous monitoring of hormone secretions from multiple islets directly on chip will require the combination of previously-reported techniques and our method to generate biocompatible droplet surfaces.

### 5.3 References


1. Pinheiro, L.B.; Coleman, V.A.; Hindson, C.M.; Herrmann, J.; Hindson, B.J.; Bhat, S.; Emslie, K.R. *Anal. Chem.* **2012**, 84, 1003-1011.

2. Hindson, B.J.; Ness, K.D.; Masquelier, D.A.; Belgrader, P.; Heredia, N.J.; Makarewicz, A.J.; Bright, I.J.; Lucero, M.Y.; Hiddessen, A.L.; Legler, T.C.; Kitano, T.K.; Hodel, M.R.; Petersen, J.F.; Wyatt, P.W.; Steenblock, E.R.; Shah, P.H.; Bousse, L.J.; Troup, C.B.; Mellen, J.C.; Wittmann, D.K.; Erndt, N.G.; Cauley, T.H.; Koehler, R.T.; So, A.P.; Dube, S.; Rose, K.A.; Montesclaros, L.; Wang, S.; Stumbo, D.P.; Hodges, S.P.; Romine,

S.; Milanovich, F.P.; White, H.e.; Regan, J.F.; Karlin-Neumann, G.A.; Hindson, C.M.; Saxonov, S.; Colston, B.W. *Anal. Chem.* **2011**, 83(22), 8604-8610.

3. Brouzes, E.; Medkova, M.; Savenelli, N.; Marran, D.; Twardowski, M.; Hutchison, J. B.; Rothberg, J. M.; Link, D. R.; Perrimon, N.; Samuels, M. L. *Proc. Natl. Acad. Sci. U.S.A.***2009**, 106, 14195– 14200.
4. Courtois, F.; Olguin, L. F.; Whyte, G.; Theberge, A. B.; Huck, W. T. S.; Hollfelder, F.; Abell,C. *Anal. Chem.* **2009**, 81, 3008– 3016.
5. Baret, J. C. *Lab Chip* **2012**, 12, 422– 433.
6. Kumaresan, P.; Yang, C.J.; Cronier, S.A.; Blazej, R.G.; Mathies, R.A. *Anal. Chem.* **2008**, 80 (10), 3522-3529.
7. Kolb, H.C.; Finn, M.G.; Sharpless, K.B. *Angew. Chem. Int. Ed.* **2001**, 40, 2004-2021.
8. http://www.organic-chemistry.org/namedreactions/click-chemistry.shtm, Accessed May 17, 2014
9. Cho, E.J.; Lee, J-W.; Ellington, A.D. *Annu. Rev. Anal. Chem.* **2009**, 2, 241-264.
10. Stoltenburg, R.; Reinemann, C.; Strehlitz, B. *Biomolecular Eng* **2007**, 24, 381-403.
11. Mendonsa, S.D.; Bowser, M.T. *J. Am. Chem. Soc.* **2004**, 126(1), 20-21.
12. Ruff, K.M.; Snyder, T.M.; Liu, D.R. *J Am Chem Soc.* **2010**, 132, 9453-9464.
13. Williams, R.; Peisajovich, S.G.; Miller, O.J.; Magdassi, S.; Tawfik, D.S.; Griffiths, A.D. *Nature Methods* **2006**, 3(7), 545-550.
14. Diehl, F.; Li, M.; He, Y.; Kinzler, K.W.; Vogelstein, B.; Dressman, D. *Nature Methods* **2006**, 3 (7), 551-559.
15. Dressman, D.; Yan, H.; Traverso, G.; Kinzler, K.W.; Vogelstein, B. *Proc. Natl. Acad. Sci.* **2003**, 100 (15), 8817-8822.
16. Jones, G. K.; McGhie, A. R.; Farrington, G. C. *Macromolecules* **1991**, 24, 3285– 3290.
17. Hu, J.; Wang, T.; Kim, J.; Shannon, C.; Easley, C.J. *J. Am. Chem. Soc.* **2012**, 134, 7066-7072.
18. Godwin, L.A.; Pilkerton, M.A.; Deal, K.S.; Wanders, D.; Judd, R.L.; Easley, C.J. *Anal. Chem.* **2011**, 83, 7166-7172.
19. Wang, J.; Gong, Q.; Maheshwari, N.; Eisenstein, M.; Arcila, M.L.; Kosik, K.S.; Soh, H.T. *Angew. Chem. Int. Ed*. **2014**, 53, 1-6.
20. Hu, J.; Yu, Y.; Brooks, J.C.; Godwin, L.A.; Somasundaram, S.; Torabinejad, F.; Kim, J.; Shannon, C.; Easley, C.J. *J. Am. Chem. Soc.* **2014**, DOI: 10.1021/ja503679q.

21. Gold, L.; Ayers, D.; Bertino, J.; Bock, C.; Bock, A. et al. *PLoS ONE* **2010**, 5(12): e15004. doi:10.1371/journal.pone.0015004.

22. Kimoto, M.; Yamashige, R.; Matsunaga, K-I. Yokoyama, S.; Hirao, I. Nature Biotech. 2013. doi:10.1038/nbt.2556.

Appendix 1: Copyright Permissions

1. Figures 1.3 and 1.4 were reprinted from *TRENDS in Biotechnology*, 24(9), Griffiths, A.D.; Tawfik D.S., "Miniaturising the laboratory in emulsion droplets," 395-402, Copyright **2006** with permission from Elsevier.

2. Figure 1.5 was reprinted by permission from Macmillan Publishers Ltd: *Nature Methods*, Williams, R.; Peisajovich, S. G.; Miller, O. J.; Magdassi, S.; Tawfik, D. S.; Griffiths, A. D. *Nature Methods* **2006**, 3 ( 7) 545– 550, Copyright 2006.

3. Figure 1.6 was reprinted with permission from Easley, C. J.; Rocheleau, J. V.; Head, W. S.; Piston, D. W. *Anal. Chem.* **2009**, 81, 9086–9095. Copyright **2009** American Chemical Society.

4. Figure 1.8 A was reprinted from *Journal of Chromatography A*, 593, Manz, A.; Harrison, D.J.; Verpoorte, E.M.J.; Fettinger, J.C.; Paulus, A.; Ludi, H.; Widmer, H.M., "Planar chips technology for miniaturization and integration of separation techniques into monitoring systems: Capillary electrophoresis on a chip," 253-258, Copyright **1992**, with permission from Elsevier.

5. Figures 1.8 B and 1.9 were reprinted by permission from IOP Publishing Ltd: *Reports on Progress in Physics*, Seemann, R.; Brinkmann, M.; Pfohl, T.; Herminghaus, S. *Rep Prog Phys* **2012**, 75, 1-41, Copyright **2012**.

6. Figure 1.10 was reprinted from Utada, A.S.; Lorenceau, E.; Link, D.R.; Kaplan, P.D.; Stone, H.A.; Weitz, D.A. *SCIENCE* **2005**, 308, 537-541 with permission from AAAS.

7. Figure 1.15 was reprinted with permission from Pinheiro, L.B.; Coleman, V.A.; Hindson, C.M.; Herrmann, J.; Hindson, B.J.; Bhat, S.; Emslie, K.R. *Anal. Chem* **2012**, 84, 1003-1011. Copyright **2012** American Chemical Society.

8. Figure 2.1 was adapted with permission from DeJournette, C.J.; Kim, J.; Medlen, H.; Li, X.; Vincent, L.J.; Easley, C.J. *Anal Chem* **2013**, 85, 10556-10564. Copyright **2013** American Chemical Society.

9. Chapter 3 was reprinted with permission from DeJournette, C.J.; Kim, J.; Medlen, H.; Li, X.; Vincent, L.J.; Easley, C.J. *Anal Chem* **2013**, 85, 10556-10564. Copyright **2013** American Chemical Society.

10. Figures 5.1 and 5.2 were reprinted from *Biomolecular Engineering*, 24, Stoltenburg, R.; Reinemann, C.; Strehlitz, B., "SELEX – A (r)evolutionary method to generate high-affinity nucleic acid ligands," 381-403, Copyright **2007**, with permission from Elsevier.

# Review Order

Jun 04, 2014

This is a License Agreement between Cheryl J DeJournette ("You") and Elsevier ("Elsevier") provided by Copyright Clearance Center ("CCC"). The license consists of your order details, the terms and conditions provided by Elsevier, and the payment terms and conditions.

**All payments must be made in full to CCC. For payment instructions, please see information listed at the bottom of this form.**

| | |
|---|---|
| Supplier | Elsevier Limited<br>The Boulevard,Langford Lane<br>Kidlington,Oxford,OX5 1GB,UK |
| Registered Company Number | 1982084 |
| Customer name | Cheryl J DeJournette |
| Customer address | 179 Chemistry Building<br>AUBURN UNIVERSITY, AL 36849 |
| License number | 3401990594069 |
| License date | Jun 04, 2014 |
| Licensed content publisher | Elsevier |
| Licensed content publication | Trends in Biotechnology |
| Licensed content title | Miniaturising the laboratory in emulsion droplets |
| Licensed content author | Andrew D. Griffiths,Dan S. Tawfik |
| Licensed content date | September 2006 |
| Licensed content volume number | 24 |
| Licensed content issue number | 9 |
| Number of pages | 8 |
| Start Page | 395 |
| End Page | 402 |
| Type of Use | reuse in a thesis/dissertation |
| Intended publisher of new work | other |
| Portion | figures/tables/illustrations |
| Number of figures/tables/illustrations | 2 |
| Format | both print and electronic |
| Are you the author of this Elsevier article? | No |
| Will you be translating? | No |
| Order reference number | 1.3-1.4 |
| Title of your thesis/dissertation | Formation and Passivation of Sub-Nanoliter Droplets for High Throughput Biological Assay Platforms |
| Expected completion date | Aug 2014 |

| | |
|---|---|
| Estimated size (number of pages) | 200 |
| Elsevier VAT number | GB 494 6272 12 |
| Price | 0.00 USD |
| VAT/Local Sales Tax | 0.00 USD / 0.00 GBP |
| **Total** | **0.00 USD** |

Terms and Conditions

**INTRODUCTION**

1. The publisher for this copyrighted material is Elsevier. By clicking "accept" in connection with completing this licensing transaction, you agree that the following terms and conditions apply to this transaction (along with the Billing and Payment terms and conditions established by Copyright Clearance Center, Inc. ("CCC"), at the time that you opened your Rightslink account and that are available at any time at http://myaccount.copyright.com).

**GENERAL TERMS**

2. Elsevier hereby grants you permission to reproduce the aforementioned material subject to the terms and conditions indicated.

3. Acknowledgement: If any part of the material to be used (for example, figures) has appeared in our publication with credit or acknowledgement to another source, permission must also be sought from that source. If such permission is not obtained then that material may not be included in your publication/copies. Suitable acknowledgement to the source must be made, either as a footnote or in a reference list at the end of your publication, as follows:
"Reprinted from Publication title, Vol /edition number, Author(s), Title of article / title of chapter, Pages No., Copyright (Year), with permission from Elsevier [OR APPLICABLE SOCIETY COPYRIGHT OWNER]." Also Lancet special credit - "Reprinted from The Lancet, Vol. number, Author(s), Title of article, Pages No., Copyright (Year), with permission from Elsevier."

4. Reproduction of this material is confined to the purpose and/or media for which permission is hereby given.

5. Altering/Modifying Material: Not Permitted. However figures and illustrations may be altered/adapted minimally to serve your work. Any other abbreviations, additions, deletions and/or any other alterations shall be made only with prior written authorization of Elsevier Ltd. (Please contact Elsevier at permissions@elsevier.com)

6. If the permission fee for the requested use of our material is waived in this instance, please be advised that your future requests for Elsevier materials may attract a fee.

7. Reservation of Rights: Publisher reserves all rights not specifically granted in the combination of (i) the license details provided by you and accepted in the course of this licensing transaction, (ii) these terms and conditions and (iii) CCC's Billing and Payment terms and conditions.

8. License Contingent Upon Payment: While you may exercise the rights licensed immediately upon issuance of the license at the end of the licensing process for the transaction, provided that you have disclosed complete and accurate details of your proposed use, no license is finally effective unless and until full payment is received from you (either by publisher or by CCC) as provided in CCC's Billing and Payment terms and conditions. If full payment is not received on a timely basis, then any license preliminarily granted shall be deemed automatically revoked and shall be void as if never granted. Further, in the event that you breach any of these terms and conditions or any of CCC's Billing and Payment terms and conditions, the license is automatically revoked and shall be void as if never granted. Use of materials as described in a revoked license, as well as any use of the materials beyond the scope of an unrevoked license, may constitute copyright infringement and publisher reserves the right to take any and all action to protect its copyright in the materials.

9. Warranties: Publisher makes no representations or warranties with respect to the licensed material.

10. Indemnity: You hereby indemnify and agree to hold harmless publisher and CCC, and their respective officers, directors, employees and agents, from and against any and all claims arising out of your use of the licensed material other than as specifically authorized pursuant to this license.

11. No Transfer of License: This license is personal to you and may not be sublicensed, assigned, or transferred by you to any other person without publisher's written permission.

12. No Amendment Except in Writing: This license may not be amended except in a writing signed by both parties (or, in the case of publisher, by CCC on publisher's behalf).

13. Objection to Contrary Terms: Publisher hereby objects to any terms contained in any purchase order, acknowledgment, check endorsement or other writing prepared by you, which terms are inconsistent with these terms and conditions or CCC's Billing and Payment terms and conditions. These terms and conditions, together with CCC's Billing and Payment terms and conditions (which are incorporated herein), comprise the entire agreement between you and publisher (and CCC) concerning this licensing transaction. In the event of any conflict between your obligations established by these terms and conditions and those established by CCC's Billing and Payment terms and conditions,

these terms and conditions shall control.

14. Revocation: Elsevier or Copyright Clearance Center may deny the permissions described in this License at their sole discretion, for any reason or no reason, with a full refund payable to you. Notice of such denial will be made using the contact information provided by you. Failure to receive such notice will not alter or invalidate the denial. In no event will Elsevier or Copyright Clearance Center be responsible or liable for any costs, expenses or damage incurred by you as a result of a denial of your permission request, other than a refund of the amount(s) paid by you to Elsevier and/or Copyright Clearance Center for denied permissions.

**LIMITED LICENSE**

The following terms and conditions apply only to specific license types:

15. **Translation**: This permission is granted for non-exclusive world **English** rights only unless your license was granted for translation rights. If you licensed translation rights you may only translate this content into the languages you requested. A professional translator must perform all translations and reproduce the content word for word preserving the integrity of the article. If this license is to re-use 1 or 2 figures then permission is granted for non-exclusive world rights in all languages.

16. **Posting licensed content on any Website**: The following terms and conditions apply as follows: Licensing material from an Elsevier journal: All content posted to the web site must maintain the copyright information line on the bottom of each image; A hyper-text must be included to the Homepage of the journal from which you are licensing at http://www.sciencedirect.com/science/journal/xxxx or the Elsevier homepage for books at http://www.elsevier.com; Central Storage: This license does not include permission for a scanned version of the material to be stored in a central repository such as that provided by Heron/XanEdu.

Licensing material from an Elsevier book: A hyper-text link must be included to the Elsevier homepage at http://www.elsevier.com . All content posted to the web site must maintain the copyright information line on the bottom of each image.

**Posting licensed content on Electronic reserve**: In addition to the above the following clauses are applicable: The web site must be password-protected and made available only to bona fide students registered on a relevant course. This permission is granted for 1 year only. You may obtain a new license for future website posting.

**For journal authors:** the following clauses are applicable in addition to the above: Permission granted is limited to the author accepted manuscript version* of your paper.

***Accepted Author Manuscript (AAM) Definition:** An accepted author manuscript (AAM) is the author's version of the manuscript of an article that has been accepted for publication and which may include any author-incorporated changes suggested through the processes of submission processing, peer review, and editor-author communications. AAMs do not include other publisher value-added contributions such as copy-editing, formatting, technical enhancements and (if relevant) pagination.

You are not allowed to download and post the published journal article (whether PDF or HTML, proof or final version), nor may you scan the printed edition to create an electronic version. A hyper-text must be included to the Homepage of the journal from which you are licensing at http://www.sciencedirect.com/science/journal/xxxxx. As part of our normal production process, you will receive an e-mail notice when your article appears on Elsevier's online service ScienceDirect (www.sciencedirect.com). That e-mail will include the article's Digital Object Identifier (DOI). This number provides the electronic link to the published article and should be included in the posting of your personal version. We ask that you wait until you receive this e-mail and have the DOI to do any posting.

**Posting to a repository:** Authors may post their AAM immediately to their employer's institutional repository for internal use only and may make their manuscript publically available after the journal-specific embargo period has ended. Please also refer to Elsevier's Article Posting Policy for further information.

18. **For book authors** the following clauses are applicable in addition to the above: Authors are permitted to place a brief summary of their work online only.. You are not allowed to download and post the published electronic version of your chapter, nor may you scan the printed edition to create an electronic version. **Posting to a repository:** Authors are permitted to post a summary of their chapter only in their institution's repository.

20. **Thesis/Dissertation**: If your license is for use in a thesis/dissertation your thesis may be submitted to your institution in either print or electronic form. Should your thesis be published commercially, please reapply for permission. These requirements include permission for the Library and Archives of Canada to supply single copies, on demand, of the complete thesis and include permission for UMI to supply single copies, on demand, of the complete thesis. Should your thesis be published commercially, please reapply for permission.

**Elsevier Open Access Terms and Conditions**

Elsevier publishes Open Access articles in both its Open Access journals and via its Open Access articles option in subscription journals.

Authors publishing in an Open Access journal or who choose to make their article Open Access in an Elsevier subscription journal select one of the following Creative Commons user licenses, which define how a reader may reuse their work: Creative Commons Attribution License (CC BY), Creative Commons Attribution – Non Commercial - ShareAlike (CC BY NC SA) and Creative Commons Attribution – Non Commercial – No Derivatives (CC BY NC ND)

**Terms & Conditions applicable to all Elsevier Open Access articles:**

Any reuse of the article must not represent the author as endorsing the adaptation of the article nor should the article be modified in such a way as to damage the author's honour or reputation.

The author(s) must be appropriately credited.

If any part of the material to be used (for example, figures) has appeared in our publication with credit or acknowledgement to another source it is the responsibility of the user to ensure their reuse complies with the terms and conditions determined by the rights holder.

**Additional Terms & Conditions applicable to each Creative Commons user license:**

**CC BY:** You may distribute and copy the article, create extracts, abstracts, and other revised versions, adaptations or derivative works of or from an article (such as a translation), to include in a collective work (such as an anthology), to text or data mine the article, including for commercial purposes without permission from Elsevier

**CC BY NC SA:** For non-commercial purposes you may distribute and copy the article, create extracts, abstracts and other revised versions, adaptations or derivative works of or from an article (such as a translation), to include in a collective work (such as an anthology), to text and data mine the article and license new adaptations or creations under identical terms without permission from Elsevier

**CC BY NC ND:** For non-commercial purposes you may distribute and copy the article and include it in a collective work (such as an anthology), provided you do not alter or modify the article, without permission from Elsevier

Any commercial reuse of Open Access articles published with a CC BY NC SA or CC BY NC ND license requires permission from Elsevier and will be subject to a fee.

Commercial reuse includes:

- Promotional purposes (advertising or marketing)
- Commercial exploitation ( e.g. a product for sale or loan)
- Systematic distribution (for a fee or free of charge)

Please refer to Elsevier's Open Access Policy for further information.

21. **Other Conditions:**

v1.7

**If you would like to pay for this license now, please remit this license along with your payment made payable to "COPYRIGHT CLEARANCE CENTER" otherwise you will be invoiced within 48 hours of the license date. Payment should be in the form of a check or money order referencing your account number and this invoice number None501319851. Once you receive your invoice for this order, you may pay your invoice by credit card. Please follow instructions provided at that time.**

**Make Payment To:**
**Copyright Clearance Center**
**Dept 001**
**P.O. Box 843006**
**Boston, MA 02284-3006**

**For suggestions or comments regarding this order, contact RightsLink Customer Support:**
customercare@copyright.com **or +1-877-622-5543 (toll free in the US) or +1-978-646-2777.**

**Gratis licenses (referencing $0 in the Total field) are free. Please retain this printable license for your reference. No payment is required.**

# Review Order

Jun 04, 2014

This is a License Agreement between Cheryl J DeJournette ("You") and Nature Publishing Group ("Nature Publishing Group") provided by Copyright Clearance Center ("CCC"). The license consists of your order details, the terms and conditions provided by Nature Publishing Group, and the payment terms and conditions.

**All payments must be made in full to CCC. For payment instructions, please see information listed at the bottom of this form.**

| | |
|---|---|
| License Number | 3401471356376 |
| License date | Jun 03, 2014 |
| Order Content Publisher | Nature Publishing Group |
| Order Content Publication | Nature Methods |
| Order Content Title | Amplification of complex gene libraries by emulsion PCR |
| Order Content Author | Richard Williams,Sergio G Peisajovich,Oliver J Miller,Shlomo Magdassi,Dan S Tawfik et al. |
| Order Content Date | Jul 1, 2006 |
| Volume number | 3 |
| Issue number | 7 |
| Type of Use | reuse in a dissertation / thesis |
| Requestor type | academic/educational |
| Format | print and electronic |
| Portion | figures/tables/illustrations |
| Number of figures/tables/illustrations | 1 |
| High-res required | no |
| Figures | Amplification of complex gene libraries by conventional PCR and emulsion PCR. |
| Author of this NPG article | no |
| Your reference number | 1.5 |
| Title of your thesis / dissertation | Formation and Passivation of Sub-Nanoliter Droplets for High Throughput Biological Assay Platforms |
| Expected completion date | Aug 2014 |
| Estimated size (number of pages) | 200 |
| **Total** | **0.00 USD** |
| Terms and Conditions | |

Terms and Conditions for Permissions

Nature Publishing Group hereby grants you a non-exclusive license to reproduce this material for this purpose, and for no other use,subject to the conditions below:

1. NPG warrants that it has, to the best of its knowledge, the rights to license reuse of this material. However, you should ensure that the material you are requesting is original to Nature Publishing Group and does not carry the copyright of another entity (as credited in the published version). If the credit line on any part of the material you have requested indicates that it was reprinted or adapted by NPG with permission from another source, then you should also seek permission from that source to reuse the material.

2. Permission granted free of charge for material in print is also usually granted for any electronic version of that work, provided that the material is incidental to the work as a whole and that the electronic version is essentially

equivalent to, or substitutes for, the print version.Where print permission has been granted for a fee, separate permission must be obtained for any additional, electronic re-use (unless, as in the case of a full paper, this has already been accounted for during your initial request in the calculation of a print run).NB: In all cases, web-based use of full-text articles must be authorized separately through the 'Use on a Web Site' option when requesting permission.

3. Permission granted for a first edition does not apply to second and subsequent editions and for editions in other languages (except for signatories to the STM Permissions Guidelines, or where the first edition permission was granted for free).

4. Nature Publishing Group's permission must be acknowledged next to the figure, table or abstract in print. In electronic form, this acknowledgement must be visible at the same time as the figure/table/abstract, and must be hyperlinked to the journal's homepage.

5. The credit line should read:
   Reprinted by permission from Macmillan Publishers Ltd: [JOURNAL NAME] (reference citation), copyright (year of publication)
   For AOP papers, the credit line should read:
   Reprinted by permission from Macmillan Publishers Ltd: [JOURNAL NAME], advance online publication, day month year (doi: 10.1038/sj.[JOURNAL ACRONYM].XXXXX)

   **Note: For republication from the *British Journal of Cancer*, the following credit lines apply.**
   Reprinted by permission from Macmillan Publishers Ltd on behalf of Cancer Research UK: [JOURNAL NAME] (reference citation), copyright (year of publication)For AOP papers, the credit line should read:
   Reprinted by permission from Macmillan Publishers Ltd on behalf of Cancer Research UK: [JOURNAL NAME], advance online publication, day month year (doi: 10.1038/sj.[JOURNAL ACRONYM].XXXXX)

6. Adaptations of single figures do not require NPG approval. However, the adaptation should be credited as follows:

   Adapted by permission from Macmillan Publishers Ltd: [JOURNAL NAME] (reference citation), copyright (year of publication)

   **Note: For adaptation from the *British Journal of Cancer*, the following credit line applies.**
   Adapted by permission from Macmillan Publishers Ltd on behalf of Cancer Research UK: [JOURNAL NAME] (reference citation), copyright (year of publication)

7. Translations of 401 words up to a whole article require NPG approval. Please visit http://www.macmillanmedicalcommunications.com for more information.Translations of up to a 400 words do not require NPG approval. The translation should be credited as follows:

   Translated by permission from Macmillan Publishers Ltd: [JOURNAL NAME] (reference citation), copyright (year of publication).

   **Note: For translation from the *British Journal of Cancer*, the following credit line applies.**
   Translated by permission from Macmillan Publishers Ltd on behalf of Cancer Research UK: [JOURNAL NAME] (reference citation), copyright (year of publication)

We are certain that all parties will benefit from this agreement and wish you the best in the use of this material. Thank you.
Special Terms:
v1.1

**If you would like to pay for this license now, please remit this license along with your payment made payable to "COPYRIGHT CLEARANCE CENTER" otherwise you will be invoiced within 48 hours of the license date. Payment should be in the form of a check or money order referencing your account number and this invoice number None501318941. Once you receive your invoice for this order, you may pay your invoice by credit card. Please follow instructions**

**provided at that time.**

**Make Payment To:**
**Copyright Clearance Center**
**Dept 001**
**P.O. Box 843006**
**Boston, MA 02284-3006**

**For suggestions or comments regarding this order, contact RightsLink Customer Support:** customercare@copyright.com **or +1-877-622-5543 (toll free in the US) or +1-978-646-2777.**

**Gratis licenses (referencing $0 in the Total field) are free. Please retain this printable license for your reference. No payment is required.**

# Review Order

Jun 12, 2014

This is a License Agreement between Cheryl J DeJournette ("You") and Elsevier ("Elsevier") provided by Copyright Clearance Center ("CCC"). The license consists of your order details, the terms and conditions provided by Elsevier, and the payment terms and conditions.

**All payments must be made in full to CCC. For payment instructions, please see information listed at the bottom of this form.**

| | |
|---|---|
| Supplier | Elsevier Limited<br>The Boulevard,Langford Lane<br>Kidlington,Oxford,OX5 1GB,UK |
| Registered Company Number | 1982084 |
| Customer name | Cheryl J DeJournette |
| Customer address | 179 Chemistry Building<br>AUBURN UNIVERSITY, AL 36849 |
| License number | 3403100733469 |
| License date | Jun 06, 2014 |
| Licensed content publisher | Elsevier |
| Licensed content publication | Journal of Chromatography A |
| Licensed content title | Planar chips technology for miniaturization and integration of separation techniques into monitoring systems: Capillary electrophoresis on a chip |
| Licensed content author | Andreas Manz,D.Jed Harrison,Elisabeth M.J. Verpoorte,James.C. Fettinger,Aran Paulus,Hans Lüdi,H.Michael Widmer |
| Licensed content date | 28 February 1992 |
| Licensed content volume number | 593 |
| Licensed content issue number | 1–2 |
| Number of pages | 6 |
| Start Page | 253 |
| End Page | 258 |
| Type of Use | reuse in a thesis/dissertation |
| Intended publisher of new work | other |
| Portion | figures/tables/illustrations |
| Number of figures/tables/illustrations | 1 |
| Format | both print and electronic |
| Are you the author of this Elsevier article? | No |
| Will you be translating? | No |
| Order reference number | 1.8A |
| Title of your thesis/dissertation | Formation and Passivation of Sub-Nanoliter Droplets for High Throughput Biological Assay Platforms |

| | |
|---|---|
| Expected completion date | Aug 2014 |
| Estimated size (number of pages) | 200 |
| Elsevier VAT number | GB 494 6272 12 |
| Price | 0.00 USD |
| VAT/Local Sales Tax | 0.00 USD / 0.00 GBP |
| **Total** | **0.00 USD** |

Terms and Conditions

**INTRODUCTION**

1. The publisher for this copyrighted material is Elsevier. By clicking "accept" in connection with completing this licensing transaction, you agree that the following terms and conditions apply to this transaction (along with the Billing and Payment terms and conditions established by Copyright Clearance Center, Inc. ("CCC"), at the time that you opened your Rightslink account and that are available at any time at http://myaccount.copyright.com).

**GENERAL TERMS**

2. Elsevier hereby grants you permission to reproduce the aforementioned material subject to the terms and conditions indicated.

3. Acknowledgement: If any part of the material to be used (for example, figures) has appeared in our publication with credit or acknowledgement to another source, permission must also be sought from that source. If such permission is not obtained then that material may not be included in your publication/copies. Suitable acknowledgement to the source must be made, either as a footnote or in a reference list at the end of your publication, as follows:
"Reprinted from Publication title, Vol /edition number, Author(s), Title of article / title of chapter, Pages No., Copyright (Year), with permission from Elsevier [OR APPLICABLE SOCIETY COPYRIGHT OWNER]." Also Lancet special credit - "Reprinted from The Lancet, Vol. number, Author(s), Title of article, Pages No., Copyright (Year), with permission from Elsevier."

4. Reproduction of this material is confined to the purpose and/or media for which permission is hereby given.

5. Altering/Modifying Material: Not Permitted. However figures and illustrations may be altered/adapted minimally to serve your work. Any other abbreviations, additions, deletions and/or any other alterations shall be made only with prior written authorization of Elsevier Ltd. (Please contact Elsevier at permissions@elsevier.com)

6. If the permission fee for the requested use of our material is waived in this instance, please be advised that your future requests for Elsevier materials may attract a fee.

7. Reservation of Rights: Publisher reserves all rights not specifically granted in the combination of (i) the license details provided by you and accepted in the course of this licensing transaction, (ii) these terms and conditions and (iii) CCC's Billing and Payment terms and conditions.

8. License Contingent Upon Payment: While you may exercise the rights licensed immediately upon issuance of the license at the end of the licensing process for the transaction, provided that you have disclosed complete and accurate details of your proposed use, no license is finally effective unless and until full payment is received from you (either by publisher or by CCC) as provided in CCC's Billing and Payment terms and conditions. If full payment is not received on a timely basis, then any license preliminarily granted shall be deemed automatically revoked and shall be void as if never granted. Further, in the event that you breach any of these terms and conditions or any of CCC's Billing and Payment terms and conditions, the license is automatically revoked and shall be void as if never granted. Use of materials as described in a revoked license, as well as any use of the materials beyond the scope of an unrevoked license, may constitute copyright infringement and publisher reserves the right to take any and all action to protect its copyright in the materials.

9. Warranties: Publisher makes no representations or warranties with respect to the licensed material.

10. Indemnity: You hereby indemnify and agree to hold harmless publisher and CCC, and their respective officers, directors, employees and agents, from and against any and all claims arising out of your use of the licensed material other than as specifically authorized pursuant to this license.

11. No Transfer of License: This license is personal to you and may not be sublicensed, assigned, or transferred by you to any other person without publisher's written permission.

12. No Amendment Except in Writing: This license may not be amended except in a writing signed by both parties (or, in the case of publisher, by CCC on publisher's behalf).

13. Objection to Contrary Terms: Publisher hereby objects to any terms contained in any purchase order, acknowledgment, check endorsement or other writing prepared by you, which terms are inconsistent with these terms and conditions or CCC's Billing and Payment terms and conditions. These terms and conditions, together with CCC's Billing and Payment terms and conditions (which are incorporated herein), comprise the entire agreement between you

and publisher (and CCC) concerning this licensing transaction. In the event of any conflict between your obligations established by these terms and conditions and those established by CCC's Billing and Payment terms and conditions, these terms and conditions shall control.

14. Revocation: Elsevier or Copyright Clearance Center may deny the permissions described in this License at their sole discretion, for any reason or no reason, with a full refund payable to you. Notice of such denial will be made using the contact information provided by you. Failure to receive such notice will not alter or invalidate the denial. In no event will Elsevier or Copyright Clearance Center be responsible or liable for any costs, expenses or damage incurred by you as a result of a denial of your permission request, other than a refund of the amount(s) paid by you to Elsevier and/or Copyright Clearance Center for denied permissions.

**LIMITED LICENSE**

The following terms and conditions apply only to specific license types:

15. **Translation**: This permission is granted for non-exclusive world **English** rights only unless your license was granted for translation rights. If you licensed translation rights you may only translate this content into the languages you requested. A professional translator must perform all translations and reproduce the content word for word preserving the integrity of the article. If this license is to re-use 1 or 2 figures then permission is granted for non-exclusive world rights in all languages.

16. **Posting licensed content on any Website**: The following terms and conditions apply as follows: Licensing material from an Elsevier journal: All content posted to the web site must maintain the copyright information line on the bottom of each image; A hyper-text must be included to the Homepage of the journal from which you are licensing at http://www.sciencedirect.com/science/journal/xxxxx or the Elsevier homepage for books at http://www.elsevier.com; Central Storage: This license does not include permission for a scanned version of the material to be stored in a central repository such as that provided by Heron/XanEdu.

Licensing material from an Elsevier book: A hyper-text link must be included to the Elsevier homepage at http://www.elsevier.com . All content posted to the web site must maintain the copyright information line on the bottom of each image.

**Posting licensed content on Electronic reserve**: In addition to the above the following clauses are applicable: The web site must be password-protected and made available only to bona fide students registered on a relevant course. This permission is granted for 1 year only. You may obtain a new license for future website posting.

**For journal authors:** the following clauses are applicable in addition to the above: Permission granted is limited to the author accepted manuscript version* of your paper.

***Accepted Author Manuscript (AAM) Definition:** An accepted author manuscript (AAM) is the author's version of the manuscript of an article that has been accepted for publication and which may include any author-incorporated changes suggested through the processes of submission processing, peer review, and editor-author communications. AAMs do not include other publisher value-added contributions such as copy-editing, formatting, technical enhancements and (if relevant) pagination.

You are not allowed to download and post the published journal article (whether PDF or HTML, proof or final version), nor may you scan the printed edition to create an electronic version. A hyper-text must be included to the Homepage of the journal from which you are licensing at http://www.sciencedirect.com/science/journal/xxxxx. As part of our normal production process, you will receive an e-mail notice when your article appears on Elsevier's online service ScienceDirect (www.sciencedirect.com). That e-mail will include the article's Digital Object Identifier (DOI). This number provides the electronic link to the published article and should be included in the posting of your personal version. We ask that you wait until you receive this e-mail and have the DOI to do any posting.

**Posting to a repository:** Authors may post their AAM immediately to their employer's institutional repository for internal use only and may make their manuscript publically available after the journal-specific embargo period has ended. Please also refer to Elsevier's Article Posting Policy for further information.

18. **For book authors** the following clauses are applicable in addition to the above: Authors are permitted to place a brief summary of their work online only.. You are not allowed to download and post the published electronic version of your chapter, nor may you scan the printed edition to create an electronic version. **Posting to a repository:** Authors are permitted to post a summary of their chapter only in their institution's repository.

20. **Thesis/Dissertation**: If your license is for use in a thesis/dissertation your thesis may be submitted to your institution in either print or electronic form. Should your thesis be published commercially, please reapply for permission. These requirements include permission for the Library and Archives of Canada to supply single copies, on demand, of the complete thesis and include permission for UMI to supply single copies, on demand, of the complete thesis. Should your thesis be published commercially, please reapply for permission.

**Elsevier Open Access Terms and Conditions**

Elsevier publishes Open Access articles in both its Open Access journals and via its Open Access articles option in subscription journals.

Authors publishing in an Open Access journal or who choose to make their article Open Access in an Elsevier subscription journal select one of the following Creative Commons user licenses, which define how a reader may reuse their work: Creative Commons Attribution License (CC BY), Creative Commons Attribution – Non Commercial - ShareAlike (CC BY NC SA) and Creative Commons Attribution – Non Commercial – No Derivatives (CC BY NC ND)

**Terms & Conditions applicable to all Elsevier Open Access articles:**

Any reuse of the article must not represent the author as endorsing the adaptation of the article nor should the article be modified in such a way as to damage the author's honour or reputation.

The author(s) must be appropriately credited.

If any part of the material to be used (for example, figures) has appeared in our publication with credit or acknowledgement to another source it is the responsibility of the user to ensure their reuse complies with the terms and conditions determined by the rights holder.

**Additional Terms & Conditions applicable to each Creative Commons user license:**

**CC BY:** You may distribute and copy the article, create extracts, abstracts, and other revised versions, adaptations or derivative works of or from an article (such as a translation), to include in a collective work (such as an anthology), to text or data mine the article, including for commercial purposes without permission from Elsevier

**CC BY NC SA:** For non-commercial purposes you may distribute and copy the article, create extracts, abstracts and other revised versions, adaptations or derivative works of or from an article (such as a translation), to include in a collective work (such as an anthology), to text and data mine the article and license new adaptations or creations under identical terms without permission from Elsevier

**CC BY NC ND:** For non-commercial purposes you may distribute and copy the article and include it in a collective work (such as an anthology), provided you do not alter or modify the article, without permission from Elsevier

Any commercial reuse of Open Access articles published with a CC BY NC SA or CC BY NC ND license requires permission from Elsevier and will be subject to a fee.

Commercial reuse includes:

- Promotional purposes (advertising or marketing)
- Commercial exploitation ( e.g. a product for sale or loan)
- Systematic distribution (for a fee or free of charge)

Please refer to Elsevier's Open Access Policy for further information.

21. **Other Conditions:**

v1.7

**If you would like to pay for this license now, please remit this license along with your payment made payable to "COPYRIGHT CLEARANCE CENTER" otherwise you will be invoiced within 48 hours of the license date. Payment should be in the form of a check or money order referencing your account number and this invoice number None501321961. Once you receive your invoice for this order, you may pay your invoice by credit card. Please follow instructions provided at that time.**

**Make Payment To:**
**Copyright Clearance Center**
**Dept 001**
**P.O. Box 843006**
**Boston, MA 02284-3006**

**For suggestions or comments regarding this order, contact RightsLink Customer Support:**
customercare@copyright.com **or +1-877-622-5543 (toll free in the US) or +1-978-646-2777.**

**Gratis licenses (referencing $0 in the Total field) are free. Please retain this printable license for your reference. No payment is required.**

**Note:** Copyright.com supplies permission but not the copyrighted content itself.

## Get Copyright Permission

**Get permission for a different publication**
**Copyright FAQs**

Copyright.com makes it easy for you to get permission to use copyrighted materials. Simply review the permission types that are available below. If you don't have an Annual License, you can select "Price & Order" below and purchase permission now.

Your session has expired.
Please choose a type of use for this title or return to search to find another title

### Reports on Progress in Physics

**ISSN:** 1361-6633
**Publication year(s):** 1934 - present
**Publication type:** e-Journal
**Publisher:** IOP Publishing

**Language:** English
**Country of publication:** United Kingdom of Great Britain and Northern Ireland

**Rightsholder:** IOP PUBLISHING, LTD

**Pay Per Use Options** **Annual License Options**

## Business

*Don't have an annual business license? Not sure? Find out more.*

| Permission type | Coverage |
|---|---|
| **Photocopy and share with co-workers More...** | Covered by CCC Annual License - Business |
| **E-mail to co-workers or post to an intranet More...** | Covered by CCC Annual License - Business<br>Digital Responsive Rights |

Multinational exceptions to our annual license agreement

## Academic

*Don't have an annual academic license? Not sure? Find out more.*

| Permission type | Coverage |
|---|---|
| **Photocopy or share content electronically More...** | Covered by CCC Annual License - Academic |

# Review Order

Jun 12, 2014

This is a License Agreement between Cheryl J DeJournette ("You") and The American Association for the Advancement of Science ("The American Association for the Advancement of Science") provided by Copyright Clearance Center ("CCC"). The license consists of your order details, the terms and conditions provided by The American Association for the Advancement of Science, and the payment terms and conditions.

**All payments must be made in full to CCC. For payment instructions, please see information listed at the bottom of this form.**

| | |
|---|---|
| License Number | 3403121477218 |
| License date | Jun 06, 2014 |
| Order Content Publisher | The American Association for the Advancement of Science |
| Order Content Publication | Science |
| Order Content Title | Monodisperse Double Emulsions Generated from a Microcapillary Device |
| Order Content Author | A. S. Utada, E. Lorenceau, D. R. Link, P. D. Kaplan, H. A. Stone, D. A. Weitz |
| Order Content Date | Apr 22, 2005 |
| Volume number | 308 |
| Issue number | 5721 |
| Type of Use | Thesis / Dissertation |
| Requestor type | Scientist/individual at a research institution |
| Format | Print and electronic |
| Portion | Figure |
| Number of figures/tables | 1 |
| Order reference number | 1.10 |
| Title of your thesis / dissertation | Formation and Passivation of Sub-Nanoliter Droplets for High Throughput Biological Assay Platforms |
| Expected completion date | Aug 2014 |
| Estimated size(pages) | 200 |
| **Total** | **0.00 USD** |

Terms and Conditions

American Association for the Advancement of Science TERMS AND CONDITIONS
Regarding your request, we are pleased to grant you non-exclusive, non-transferable permission, to republish the AAAS material identified above in your work identified above, subject to the terms and conditions herein. We must be contacted for permission for any uses other than those specifically identified in your request above.
The following credit line must be printed along with the AAAS material: "From [Full Reference Citation]. Reprinted with permission from AAAS."
All required credit lines and notices must be visible any time a user accesses any part of the AAAS material and must appear on any printed copies and authorized user might make.
This permission does not apply to figures / photos / artwork or any other content or materials included in your work that are credited to non-AAAS sources. If the requested material is sourced to or references non-AAAS sources, you must obtain authorization from that source as well before using that material. You agree to hold harmless and indemnify AAAS against any claims arising from your use of any content in your work that is credited to non-AAAS sources.
If the AAAS material covered by this permission was published in Science during the years 1974 - 1994, you must also obtain permission from the author, who may grant or withhold permission, and who may or may not charge a fee if permission is granted. See original article for author's address. This condition does not apply to news articles.

The AAAS material may not be modified or altered except that figures and tables may be modified with permission from the author. Author permission for any such changes must be secured prior to your use.
Whenever possible, we ask that electronic uses of the AAAS material permitted herein include a hyperlink to the original work on AAAS's website (hyperlink may be embedded in the reference citation).
AAAS material reproduced in your work identified herein must not account for more than 30% of the total contents of that work.
AAAS must publish the full paper prior to use of any text.
AAAS material must not imply any endorsement by the American Association for the Advancement of Science.
This permission is not valid for the use of the AAAS and/or Science logos.
AAAS makes no representations or warranties as to the accuracy of any information contained in the AAAS material covered by this permission, including any warranties of
merchantability or fitness for a particular purpose.
If permission fees for this use are waived, please note that AAAS reserves the right to charge for reproduction of this material in the future.
Permission is not valid unless payment is received within sixty (60) days of the issuance of this permission. If payment is not received within this time period then all rights granted herein shall be revoked and this permission will be considered null and void.
In the event of breach of any of the terms and conditions herein or any of CCC's Billing and Payment terms and conditions, all rights granted herein shall be revoked and this permission will be considered null and void.
AAAS reserves the right to terminate this permission and all rights granted herein at its discretion, for any purpose, at any time. In the event that AAAS elects to terminate this permission, you will have no further right to publish, publicly perform, publicly display, distribute or otherwise use any matter in which the AAAS content had been included, and all fees paid hereunder shall be fully refunded to you. Notification of termination will be sent to the contact information as supplied by you during the request process and termination shall be immediate upon sending the notice. Neither AAAS nor CCC shall be liable for any costs, expenses, or damages you may incur as a result of the termination of this permission, beyond the refund noted above.
This Permission may not be amended except by written document signed by both parties.
The terms above are applicable to all permissions granted for the use of AAAS material. Below you will find additional conditions that apply to your particular type of use.

**FOR A THESIS OR DISSERTATION**

If you are using figure(s)/table(s), permission is granted for use in print and electronic versions of your dissertation or thesis. A full text article may be used in print versions only of a dissertation or thesis.
Permission covers the distribution of your dissertation or thesis on demand by ProQuest / UMI, provided the AAAS material covered by this permission remains in situ.
If you are an Original Author on the AAAS article being reproduced, please refer to your License to Publish for rules on reproducing your paper in a dissertation or thesis.

**FOR JOURNALS:**

Permission covers both print and electronic versions of your journal article, however the AAAS material may not be used in any manner other than within the context of your article.

**FOR BOOKS/TEXTBOOKS:**

If this license is to reuse figures/tables, then permission is granted for non-exclusive world rights in all languages in both print and electronic formats (electronic formats are defined below).
If this license is to reuse a text excerpt or a full text article, then permission is granted for non-exclusive world rights in English only. You have the option of securing either print or electronic rights or both, but electronic rights are not automatically granted and do garner additional fees. Permission for translations of text excerpts or full text articles into other languages must be obtained separately.
Licenses granted for use of AAAS material in electronic format books/textbooks are valid only in cases where the electronic version is equivalent to or substitutes for the print version of the book/textbook. The AAAS material reproduced as permitted herein must remain in situ and must not be exploited separately (for example, if permission covers the use of a full text article, the article may not be offered for access or for purchase as a stand-alone unit), except in the case of permitted textbook companions as noted below.
You must include the following notice in any electronic versions, either adjacent to the reprinted AAAS material or in the terms and conditions for use of your electronic products: "Readers may view, browse, and/or download material for temporary copying purposes only, provided these uses are for noncommercial personal purposes. Except as provided by law, this material may not be further reproduced, distributed, transmitted, modified, adapted, performed, displayed, published, or sold in whole or in part, without prior written permission from the publisher."
If your book is an academic textbook, permission covers the following companions to your textbook, provided such

companions are distributed only in conjunction with your textbook at no additional cost to the user:

- Password-protected website
- Instructor's image CD/DVD and/or PowerPoint resource
- Student CD/DVD

All companions must contain instructions to users that the AAAS material may be used for non-commercial, classroom purposes only. Any other uses require the prior written permission from AAAS.

If your license is for the use of AAAS Figures/Tables, then the electronic rights granted herein permit use of the Licensed Material in any Custom Databases that you distribute the electronic versions of your textbook through, so long as the Licensed Material remains within the context of a chapter of the title identified in your request and cannot be downloaded by a user as an independent image file.

Rights also extend to copies/files of your Work (as described above) that you are required to provide for use by the visually and/or print disabled in compliance with state and federal laws.

This permission only covers a single edition of your work as identified in your request.

**FOR NEWSLETTERS:**

Permission covers print and/or electronic versions, provided the AAAS material reproduced as permitted herein remains in situ and is not exploited separately (for example, if permission covers the use of a full text article, the article may not be offered for access or for purchase as a stand-alone unit)

**FOR ANNUAL REPORTS:**

Permission covers print and electronic versions provided the AAAS material reproduced as permitted herein remains in situ and is not exploited separately (for example, if permission covers the use of a full text article, the article may not be offered for access or for purchase as a stand-alone unit)

**FOR PROMOTIONAL/MARKETING USES:**

Permission covers the use of AAAS material in promotional or marketing pieces such as information packets, media kits, product slide kits, brochures, or flyers limited to a single print run. The AAAS Material may not be used in any manner which implies endorsement or promotion by the American Association for the Advancement of Science (AAAS) or Science of any product or service. AAAS does not permit the reproduction of its name, logo or text on promotional literature.

If permission to use a full text article is permitted, The Science article covered by this permission must not be altered in any way. No additional printing may be set onto an article copy other than the copyright credit line required above. Any alterations must be approved in advance and in writing by AAAS. This includes, but is not limited to, the placement of sponsorship identifiers, trademarks, logos, rubber stamping or self-adhesive stickers onto the article copies.

Additionally, article copies must be a freestanding part of any information package (i.e. media kit) into which they are inserted. They may not be physically attached to anything, such as an advertising insert, or have anything attached to them, such as a sample product. Article copies must be easily removable from any kits or informational packages in which they are used. The only exception is that article copies may be inserted into three-ring binders.

**FOR CORPORATE INTERNAL USE:**

The AAAS material covered by this permission may not be altered in any way. No additional printing may be set onto an article copy other than the required credit line. Any alterations must be approved in advance and in writing by AAAS. This includes, but is not limited to the placement of sponsorship identifiers, trademarks, logos, rubber stamping or self-adhesive stickers onto article copies.

If you are making article copies, copies are restricted to the number indicated in your request and must be distributed only to internal employees for internal use.

If you are using AAAS Material in Presentation Slides, the required credit line must be visible on the slide where the AAAS material will be reprinted

If you are using AAAS Material on a CD, DVD, Flash Drive, or the World Wide Web, you must include the following notice in any electronic versions, either adjacent to the reprinted AAAS material or in the terms and conditions for use of your electronic products: "Readers may view, browse, and/or download material for temporary copying purposes only, provided these uses are for noncommercial personal purposes. Except as provided by law, this material may not be further reproduced, distributed, transmitted, modified, adapted, performed, displayed, published, or sold in whole or in part, without prior written permission from the publisher." Access to any such CD, DVD, Flash Drive or Web page must be restricted to your organization's employees only.

**FOR CME COURSE and SCIENTIFIC SOCIETY MEETINGS:**

Permission is restricted to the particular Course, Seminar, Conference, or Meeting indicated in your request. If this license covers a text excerpt or a Full Text Article, access to the reprinted AAAS material must be restricted to attendees of your event only (if you have been granted electronic rights for use of a full text article on your website, your website must be password protected, or access restricted so that only attendees can access the content on your site).

If you are using AAAS Material on a CD, DVD, Flash Drive, or the World Wide Web, you must include the following notice in

any electronic versions, either adjacent to the reprinted AAAS material or in the terms and conditions for use of your electronic products: "Readers may view, browse, and/or download material for temporary copying purposes only, provided these uses are for noncommercial personal purposes. Except as provided by law, this material may not be further reproduced, distributed, transmitted, modified, adapted, performed, displayed, published, or sold in whole or in part, without prior written permission from the publisher."

**FOR POLICY REPORTS:**

These rights are granted only to non-profit organizations and/or government agencies. Permission covers print and electronic versions of a report, provided the required credit line appears in both versions and provided the AAAS material reproduced as permitted herein remains in situ and is not exploited separately.

**FOR CLASSROOM PHOTOCOPIES:**

Permission covers distribution in print copy format only. Article copies must be freestanding and not part of a course pack. They may not be physically attached to anything or have anything attached to them.

**FOR COURSEPACKS OR COURSE WEBSITES:**

These rights cover use of the AAAS material in one class at one institution. Permission is valid only for a single semester after which the AAAS material must be removed from the Electronic Course website, unless new permission is obtained for an additional semester. If the material is to be distributed online, access must be restricted to students and instructors enrolled in that particular course by some means of password or access control.

**FOR WEBSITES:**

You must include the following notice in any electronic versions, either adjacent to the reprinted AAAS material or in the terms and conditions for use of your electronic products: "Readers may view, browse, and/or download material for temporary copying purposes only, provided these uses are for noncommercial personal purposes. Except as provided by law, this material may not be further reproduced, distributed, transmitted, modified, adapted, performed, displayed, published, or sold in whole or in part, without prior written permission from the publisher."

Permissions for the use of Full Text articles on third party websites are granted on a case by case basis and only in cases where access to the AAAS Material is restricted by some means of password or access control. Alternately, an E-Print may be purchased through our reprints department (brocheleau@rockwaterinc.com).

REGARDING FULL TEXT ARTICLE USE ON THE WORLD WIDE WEB IF YOU ARE AN 'ORIGINAL AUTHOR' OF A SCIENCE PAPER

If you chose "Original Author" as the Requestor Type, you are warranting that you are one of authors listed on the License Agreement as a "Licensed content author" or that you are acting on that author's behalf to use the Licensed content in a new work that one of the authors listed on the License Agreement as a "Licensed content author" has written.

Original Authors may post the 'Accepted Version' of their full text article on their personal or on their University website and not on any other website. The 'Accepted Version' is the version of the paper accepted for publication by AAAS including changes resulting from peer review but prior to AAAS's copy editing and production (in other words not the AAAS published version).

**FOR MOVIES / FILM / TELEVISION:**

Permission is granted to use, record, film, photograph, and/or tape the AAAS material in connection with your program/film and in any medium your program/film may be shown or heard, including but not limited to broadcast and cable television, radio, print, world wide web, and videocassette.

The required credit line should run in the program/film's end credits.

**FOR MUSEUM EXHIBITIONS:**

Permission is granted to use the AAAS material as part of a single exhibition for the duration of that exhibit. Permission for use of the material in promotional materials for the exhibit must be cleared separately with AAAS (please contact us at permissions@aaas.org).

**FOR TRANSLATIONS:**

Translation rights apply only to the language identified in your request summary above.

The following disclaimer must appear with your translation, on the first page of the article, after the credit line: "This translation is not an official translation by AAAS staff, nor is it endorsed by AAAS as accurate. In crucial matters, please refer to the official English-language version originally published by AAAS."

**FOR USE ON A COVER:**

Permission is granted to use the AAAS material on the cover of a journal issue, newsletter issue, book, textbook, or annual report in print and electronic formats provided the AAAS material reproduced as permitted herein remains in situ and is not exploited separately

By using the AAAS Material identified in your request, you agree to abide by all the terms and conditions herein.

Questions about these terms can be directed to the AAAS Permissions department permissions@aaas.org.

Other Terms and Conditions:

v 2

**If you would like to pay for this license now, please remit this license along with your payment made payable to "COPYRIGHT CLEARANCE CENTER" otherwise you will be invoiced within 48 hours of the license date. Payment should be in the form of a check or money order referencing your account number and this invoice number None501322033. Once you receive your invoice for this order, you may pay your invoice by credit card. Please follow instructions provided at that time.**

**Make Payment To:**
**Copyright Clearance Center**
**Dept 001**
**P.O. Box 843006**
**Boston, MA 02284-3006**

**For suggestions or comments regarding this order, contact RightsLink Customer Support:**
customercare@copyright.com **or +1-877-622-5543 (toll free in the US) or +1-978-646-2777.**

**Gratis licenses (referencing $0 in the Total field) are free. Please retain this printable license for your reference. No payment is required.**

# Standard *ACS AuthorChoice/Editors' Choice* Usage Agreement

Back to ACS Publishing Policies

## Standard *ACS AuthorChoice/Editors' Choice* Usage Agreement

This ACS article is provided to You under the terms of this Standard *ACS AuthorChoice/Editors' Choice* usage agreement between You and the American Chemical Society ("ACS"), a federally-chartered nonprofit located at 1155 16th Street NW, Washington DC 20036. Your access and use of this ACS article means that you have accepted and agreed to the Terms and Conditions of this Agreement. ACS and You are collectively referred to in this Agreement as "the Parties").

### 1. SCOPE OF GRANT

ACS grants You non-exclusive and nontransferable permission to access and use this ACS article subject to the terms and conditions set forth in this Agreement.

### 2. PERMITTED USES

a. For non-commercial research and education purposes only, You may access, download, copy, display and redistribute articles as well as adapt, translate, text and data mine content contained in articles, subject to the following conditions:

i. The authors' moral right to the integrity of their work under the Berne Convention (Article 6bis) is not compromised.

ii. Where content in the article is identified as belonging to a third party, it is your responsibility to ensure that any reuse complies with copyright policies of the owner.

iii. Copyright notices or the display of unique Digital Object Identifiers (DOI's), ACS or journal logos, bibliographic (e.g. authors, journal, article title, volume, issue, page numbers) or other references to ACS journal titles, web links, and any other journal-specific "branding" or notices that are included in the article or that are provided by the ACS with instructions that such should accompany its display, should not be removed or tampered with in any way. The display of *ACS AuthorChoice* or *ACS Editors' Choice* articles on non-ACS websites must be accompanied by prominently displayed links to the definitive published versions of those articles on the ACS website.

iv. Any adaptations for non-commercial purposes must prominently link to the definitive published version on the ACS website and prominently display the statement: "This is an unofficial adaptation of an article that appeared in an ACS publication. ACS has not endorsed the content of this adaptation or the context of its use."

v. Any translations for non-commercial purposes, for which a prior translation agreement with ACS has not been established, must prominently link to the definitive published version on the ACS website and prominently display the statement: "This is an unofficial translation of an article that appeared in an ACS publication. ACS has not endorsed the content of this translation or the context of its use."

b. Each time You distribute this ACS article or an adaptation, ACS offers to the recipient a license to this ACS article on the same terms and conditions as the license granted to You under this License.

c. For permission to use ACS copyrighted articles beyond that permitted here, visit: http://pubs.acs.org/copyright/permissions.html

### 3. PROHIBITED USES

a. Use of this ACS article for commercial purposes is prohibited. Examples of such prohibited commercial purposes include but are not limited to:

i. Copying or downloading of articles, or linking to such postings, for further distribution, sale or licensing, for a fee;

ii. Copying, downloading or posting by a site or service that incorporates advertising with such content;

iii. The inclusion or incorporation of article content in other works or services (other than normal quotations with an appropriate citation) that is then available for sale or licensing, for a fee;

iv. Use of articles or article content (other than normal quotations with appropriate citation) by a for-profit organizations for promotional purposes, whether for a fee or otherwise;

v. Sale of translated versions of the article that have not been authorized by license or other permission from the ACS

### 4. TERMINATION

ACS reserves the right to limit, suspend, or terminate your access to and use of the ACS Publications Division website and/or all ACS articles immediately upon detecting a breach of this License.

### 5. COPYRIGHTS; OTHER INTELLECTUAL PROPERTY RIGHTS

Except as otherwise specifically noted, ACS is the owner of all right, title and interest in the content of this ACS article, including, without limitations, graphs, charts, tables illustrations, and copyrightable supporting information. This ACS article is protected under the Copyright Laws of the United States Codified in Title 17 of the U.S. Code and subject to the Universal Copyright Convention and the Berne Copyright Convention. You agree not to remove or obscure copyright notices. You acknowledge that You have no claim to ownership of any part of this ACS article or other proprietary information accessed under this Agreement.

The names "American Chemical Society," "ACS" and the titles of the journals and other ACS products are trademarks of ACS.

### 6. DISCLAIMER OF WARRANTIES; LIMITATION OF LIABILITY

ACS warrants that it is entitled to grant this Agreement.

EXCEPT AS SET FORTH IN THE PRECEDING SENTENCE, ACS MAKES NO WARRANTY OR REPRESENTATION OF ANY KIND, EXPRESS OR IMPLIED, WITH RESPECT TO THIS ACS ARTICLE INCLUDING, BUT NOT LIMITED TO WARRANTIES AS TO THE ACCURACY OR COMPLETENESS OF THE ACS ARTICLE, ITS QUALITY, ORIGINALITY, SUITABILITY, SEARCHABILITY, OPERATION, PERFORMANCE, COMPLIANCE WITH ANY COMPUTATIONAL PROCESS, MERCHANTABILITY OR FITNESS FOR A PARTICULAR PURPOSE.

ACS SHALL NOT BE LIABLE FOR: EXEMPLARY, SPECIAL, INDIRECT, INCIDENTAL, CONSEQUENTIAL OR OTHER DAMAGES ARISING OUT OF OR IN CONNECTION WITH THE AGREEMENT GRANTED HEREUNDER, THE USE OR INABILITY TO USE ANY ACS PRODUCT, ACS'S PERFORMANCE UNDER THIS AGREEMENT, TERMINATION OF THIS AGREEMENT BY ACS OR THE LOSS OF DATA, BUSINESS OR GOODWILL EVEN IF ACS IS ADVISED OR AWARE OF THE POSSIBILITY OF SUCH DAMAGES. IN NO EVENT SHALL THE TOTAL AGGREGATE LIABILITY OF ACS OUT OF ANY BREACH OR TERMINATION OF THIS AGREEMENT EXCEED THE TOTAL AMOUNT PAID BY YOU TO ACS FOR ACCESS TO THIS ACS ARTICLE FOR THE CURRENT YEAR IN WHICH SUCH CLAIM, LOSS OR DAMAGE OCCURRED, WHETHER IN CONTRACT, TORT OR OTHERWISE, INCLUDING, WITHOUT LIMITATION, DUE TO NEGLIGENCE.

The foregoing limitations and exclusions of certain damages shall apply regardless of the success or effectiveness of other remedies. No claim may be made against ACS unless suit is filed within one (1) year after the event giving rise to the claim.

### 7. GENERAL

This Agreement sets forth the entire understanding of the Parties. The validity, construction and performance of this Agreement shall be governed by and construed in accordance with the laws of the District of Columbia, USA without reference to its conflicts of laws principles. You acknowledge that the delivery of the ACS article will occur in the District of Columbia, USA. You shall pay any taxes lawfully due from it, other than taxes on ACS's net income, arising out of your use of this ACS article and/or other rights granted under this Agreement. You may not assign or transfer its rights under this Agreement without the express written consent of ACS.

### 8. ACCEPTANCE

You warrant that You have read, understand, and accept the terms and conditions of this Agreement. ACS reserves the right to modify this Agreement at any time by posting the modified terms and conditions on the ACS Publications Web site. Any use of this ACS article after such posting shall constitute acceptance of the terms and conditions as modified.

*Posted: 03/06/2014*

1155 Sixteenth Street NW,
Washington, DC 20036
(800) 333-9511

Copyright Clearance Center RightsLink®

Home | Account Info | Help

ACS Publications
MOST TRUSTED. MOST CITED. MOST READ.

**Title:** Creating Biocompatible Oil–Water Interfaces without Synthesis: Direct Interactions between Primary Amines and Carboxylated Perfluorocarbon Surfactants

**Author:** Cheryl J. DeJournette, Joonyul Kim, Haley Medlen, Xiangpeng Li, Luke J. Vincent, and Christopher J. Easley

**Publication:** Analytical Chemistry

**Publisher:** American Chemical Society

**Date:** Nov 1, 2013



Logged in as:
Cheryl DeJournette
Account #:
3000795420

LOGOUT

## Quick Price Estimate

**Permission for this particular request is granted for print and electronic formats, and translations, at no charge. Figures and tables may be modified. Appropriate credit should be given. Please print this page for your records and provide a copy to your publisher. Requests for up to 4 figures require only this record. Five or more figures will generate a printout of additional terms and conditions. Appropriate credit should read: "Reprinted with permission from {COMPLETE REFERENCE CITATION}. Copyright {YEAR} American Chemical Society." Insert appropriate information in place of the capitalized words.**

| | |
|---|---|
| **I would like to...** | reuse in a Thesis/Dissertation |
| **Requestor Type** | Author (original work) |
| **Portion** | Full article |
| **Format** | Print |
| **Will you be translating?** | No |
| **Select your currency** | USD - $ |
| **Quick Price** | Click Quick Price |

This service provides permission for reuse only. If you do not have a copy of the article you are using, you may copy and paste the content and reuse according to the terms of your agreement. Please be advised that obtaining the content you license is a separate transaction not involving Rightslink.

QUICK PRICE CONTINUE

To request permission for a type of use not listed, please contact the publisher directly.

# Review Order

May 29, 2014

This is a License Agreement between Cheryl J DeJournette ("You") and Elsevier ("Elsevier") provided by Copyright Clearance Center ("CCC"). The license consists of your order details, the terms and conditions provided by Elsevier, and the payment terms and conditions.

**All payments must be made in full to CCC. For payment instructions, please see information listed at the bottom of this form.**

| | |
|---|---|
| Supplier | Elsevier Limited<br>The Boulevard,Langford Lane<br>Kidlington,Oxford,OX5 1GB,UK |
| Registered Company Number | 1982084 |
| Customer name | Cheryl J DeJournette |
| Customer address | 179 Chemistry Building<br>AUBURN UNIVERSITY, AL 36849 |
| License number | 3397681220794 |
| License date | May 28, 2014 |
| Licensed content publisher | Elsevier |
| Licensed content publication | Biomolecular Engineering |
| Licensed content title | SELEX—A (r)evolutionary method to generate high-affinity nucleic acid ligands |
| Licensed content author | Regina Stoltenburg,Christine Reinemann,Beate Strehlitz |
| Licensed content date | October 2007 |
| Licensed content volume number | 24 |
| Licensed content issue number | 4 |
| Number of pages | 23 |
| Start Page | 381 |
| End Page | 403 |
| Type of Use | reuse in a thesis/dissertation |
| Portion | figures/tables/illustrations |
| Number of figures/tables/illustrations | 2 |
| Format | both print and electronic |
| Are you the author of this Elsevier article? | No |
| Will you be translating? | No |
| Order reference number | 5.1-5.2 |
| Title of your thesis/dissertation | Formation and Passivation of Sub-Nanoliter Droplets for High Throughput Biological Assay Platforms |
| Expected completion date | Aug 2014 |
| Estimated size (number of pages) | 200 |

| | |
|---|---|
| Elsevier VAT number | GB 494 6272 12 |
| Price | 0.00 USD |
| VAT/Local Sales Tax | 0.00 USD / 0.00 GBP |
| **Total** | **0.00 USD** |

Terms and Conditions

**INTRODUCTION**

1. The publisher for this copyrighted material is Elsevier. By clicking "accept" in connection with completing this licensing transaction, you agree that the following terms and conditions apply to this transaction (along with the Billing and Payment terms and conditions established by Copyright Clearance Center, Inc. ("CCC"), at the time that you opened your Rightslink account and that are available at any time at http://myaccount.copyright.com).

**GENERAL TERMS**

2. Elsevier hereby grants you permission to reproduce the aforementioned material subject to the terms and conditions indicated.

3. Acknowledgement: If any part of the material to be used (for example, figures) has appeared in our publication with credit or acknowledgement to another source, permission must also be sought from that source. If such permission is not obtained then that material may not be included in your publication/copies. Suitable acknowledgement to the source must be made, either as a footnote or in a reference list at the end of your publication, as follows:
"Reprinted from Publication title, Vol /edition number, Author(s), Title of article / title of chapter, Pages No., Copyright (Year), with permission from Elsevier [OR APPLICABLE SOCIETY COPYRIGHT OWNER]." Also Lancet special credit - "Reprinted from The Lancet, Vol. number, Author(s), Title of article, Pages No., Copyright (Year), with permission from Elsevier."

4. Reproduction of this material is confined to the purpose and/or media for which permission is hereby given.

5. Altering/Modifying Material: Not Permitted. However figures and illustrations may be altered/adapted minimally to serve your work. Any other abbreviations, additions, deletions and/or any other alterations shall be made only with prior written authorization of Elsevier Ltd. (Please contact Elsevier at permissions@elsevier.com)

6. If the permission fee for the requested use of our material is waived in this instance, please be advised that your future requests for Elsevier materials may attract a fee.

7. Reservation of Rights: Publisher reserves all rights not specifically granted in the combination of (i) the license details provided by you and accepted in the course of this licensing transaction, (ii) these terms and conditions and (iii) CCC's Billing and Payment terms and conditions.

8. License Contingent Upon Payment: While you may exercise the rights licensed immediately upon issuance of the license at the end of the licensing process for the transaction, provided that you have disclosed complete and accurate details of your proposed use, no license is finally effective unless and until full payment is received from you (either by publisher or by CCC) as provided in CCC's Billing and Payment terms and conditions. If full payment is not received on a timely basis, then any license preliminarily granted shall be deemed automatically revoked and shall be void as if never granted. Further, in the event that you breach any of these terms and conditions or any of CCC's Billing and Payment terms and conditions, the license is automatically revoked and shall be void as if never granted. Use of materials as described in a revoked license, as well as any use of the materials beyond the scope of an unrevoked license, may constitute copyright infringement and publisher reserves the right to take any and all action to protect its copyright in the materials.

9. Warranties: Publisher makes no representations or warranties with respect to the licensed material.

10. Indemnity: You hereby indemnify and agree to hold harmless publisher and CCC, and their respective officers, directors, employees and agents, from and against any and all claims arising out of your use of the licensed material other than as specifically authorized pursuant to this license.

11. No Transfer of License: This license is personal to you and may not be sublicensed, assigned, or transferred by you to any other person without publisher's written permission.

12. No Amendment Except in Writing: This license may not be amended except in a writing signed by both parties (or, in the case of publisher, by CCC on publisher's behalf).

13. Objection to Contrary Terms: Publisher hereby objects to any terms contained in any purchase order, acknowledgment, check endorsement or other writing prepared by you, which terms are inconsistent with these terms and conditions or CCC's Billing and Payment terms and conditions. These terms and conditions, together with CCC's Billing and Payment terms and conditions (which are incorporated herein), comprise the entire agreement between you and publisher (and CCC) concerning this licensing transaction. In the event of any conflict between your obligations established by these terms and conditions and those established by CCC's Billing and Payment terms and conditions, these terms and conditions shall control.

14. Revocation: Elsevier or Copyright Clearance Center may deny the permissions described in this License at their sole discretion, for any reason or no reason, with a full refund payable to you. Notice of such denial will be made using the contact information provided by you. Failure to receive such notice will not alter or invalidate the denial. In no event will Elsevier or Copyright Clearance Center be responsible or liable for any costs, expenses or damage incurred by you as a result of a denial of your permission request, other than a refund of the amount(s) paid by you to Elsevier and/or Copyright Clearance Center for denied permissions.

**LIMITED LICENSE**

The following terms and conditions apply only to specific license types:

15. **Translation**: This permission is granted for non-exclusive world **English** rights only unless your license was granted for translation rights. If you licensed translation rights you may only translate this content into the languages you requested. A professional translator must perform all translations and reproduce the content word for word preserving the integrity of the article. If this license is to re-use 1 or 2 figures then permission is granted for non-exclusive world rights in all languages.

16. **Posting licensed content on any Website**: The following terms and conditions apply as follows: Licensing material from an Elsevier journal: All content posted to the web site must maintain the copyright information line on the bottom of each image; A hyper-text must be included to the Homepage of the journal from which you are licensing at http://www.sciencedirect.com/science/journal/xxxxx or the Elsevier homepage for books at http://www.elsevier.com; Central Storage: This license does not include permission for a scanned version of the material to be stored in a central repository such as that provided by Heron/XanEdu.

Licensing material from an Elsevier book: A hyper-text link must be included to the Elsevier homepage at http://www.elsevier.com . All content posted to the web site must maintain the copyright information line on the bottom of each image.

**Posting licensed content on Electronic reserve**: In addition to the above the following clauses are applicable: The web site must be password-protected and made available only to bona fide students registered on a relevant course. This permission is granted for 1 year only. You may obtain a new license for future website posting.

**For journal authors:** the following clauses are applicable in addition to the above: Permission granted is limited to the author accepted manuscript version* of your paper.

***Accepted Author Manuscript (AAM) Definition:** An accepted author manuscript (AAM) is the author's version of the manuscript of an article that has been accepted for publication and which may include any author-incorporated changes suggested through the processes of submission processing, peer review, and editor-author communications. AAMs do not include other publisher value-added contributions such as copy-editing, formatting, technical enhancements and (if relevant) pagination.

You are not allowed to download and post the published journal article (whether PDF or HTML, proof or final version), nor may you scan the printed edition to create an electronic version. A hyper-text must be included to the Homepage of the journal from which you are licensing at http://www.sciencedirect.com/science/journal/xxxxx. As part of our normal production process, you will receive an e-mail notice when your article appears on Elsevier's online service ScienceDirect (www.sciencedirect.com). That e-mail will include the article's Digital Object Identifier (DOI). This number provides the electronic link to the published article and should be included in the posting of your personal version. We ask that you wait until you receive this e-mail and have the DOI to do any posting.

**Posting to a repository:** Authors may post their AAM immediately to their employer's institutional repository for internal use only and may make their manuscript publically available after the journal-specific embargo period has ended. Please also refer to Elsevier's Article Posting Policy for further information.

18. **For book authors** the following clauses are applicable in addition to the above: Authors are permitted to place a brief summary of their work online only.. You are not allowed to download and post the published electronic version of your chapter, nor may you scan the printed edition to create an electronic version. **Posting to a repository:** Authors are permitted to post a summary of their chapter only in their institution's repository.

20. **Thesis/Dissertation**: If your license is for use in a thesis/dissertation your thesis may be submitted to your institution in either print or electronic form. Should your thesis be published commercially, please reapply for permission. These requirements include permission for the Library and Archives of Canada to supply single copies, on demand, of the complete thesis and include permission for UMI to supply single copies, on demand, of the complete thesis. Should your thesis be published commercially, please reapply for permission.

**Elsevier Open Access Terms and Conditions**

Elsevier publishes Open Access articles in both its Open Access journals and via its Open Access articles option in subscription journals.

Authors publishing in an Open Access journal or who choose to make their article Open Access in an Elsevier

subscription journal select one of the following Creative Commons user licenses, which define how a reader may reuse their work: Creative Commons Attribution License (CC BY), Creative Commons Attribution – Non Commercial - ShareAlike (CC BY NC SA) and Creative Commons Attribution – Non Commercial – No Derivatives (CC BY NC ND)

**Terms & Conditions applicable to all Elsevier Open Access articles:**

Any reuse of the article must not represent the author as endorsing the adaptation of the article nor should the article be modified in such a way as to damage the author's honour or reputation.

The author(s) must be appropriately credited.

If any part of the material to be used (for example, figures) has appeared in our publication with credit or acknowledgement to another source it is the responsibility of the user to ensure their reuse complies with the terms and conditions determined by the rights holder.

**Additional Terms & Conditions applicable to each Creative Commons user license:**

**CC BY:** You may distribute and copy the article, create extracts, abstracts, and other revised versions, adaptations or derivative works of or from an article (such as a translation), to include in a collective work (such as an anthology), to text or data mine the article, including for commercial purposes without permission from Elsevier

**CC BY NC SA:** For non-commercial purposes you may distribute and copy the article, create extracts, abstracts and other revised versions, adaptations or derivative works of or from an article (such as a translation), to include in a collective work (such as an anthology), to text and data mine the article and license new adaptations or creations under identical terms without permission from Elsevier

**CC BY NC ND:** For non-commercial purposes you may distribute and copy the article and include it in a collective work (such as an anthology), provided you do not alter or modify the article, without permission from Elsevier

Any commercial reuse of Open Access articles published with a CC BY NC SA or CC BY NC ND license requires permission from Elsevier and will be subject to a fee.

Commercial reuse includes:

- Promotional purposes (advertising or marketing)
- Commercial exploitation ( e.g. a product for sale or loan)
- Systematic distribution (for a fee or free of charge)

Please refer to Elsevier's Open Access Policy for further information.

21. **Other Conditions**:

v1.7

**If you would like to pay for this license now, please remit this license along with your payment made payable to "COPYRIGHT CLEARANCE CENTER" otherwise you will be invoiced within 48 hours of the license date. Payment should be in the form of a check or money order referencing your account number and this invoice number None501314419. Once you receive your invoice for this order, you may pay your invoice by credit card. Please follow instructions provided at that time.**

**Make Payment To:**
**Copyright Clearance Center**
**Dept 001**
**P.O. Box 843006**
**Boston, MA 02284-3006**

**For suggestions or comments regarding this order, contact RightsLink Customer Support:**
customercare@copyright.com **or +1-877-622-5543 (toll free in the US) or +1-978-646-2777.**

**Gratis licenses (referencing $0 in the Total field) are free. Please retain this printable license for your reference. No payment is required.**